

SOCIETÀ NAZIONALE DI SCIENZE LETTERE E ARTI IN NAPOLI

RENDICONTO
DELL'ACADEMIA DELLE SCIENZE
FISICHE E MATEMATICHE

SERIE IV - VOL. LXXXIX - ANNO CLXI

(2022)



GIANNINI EDITORE

SOCIETÀ NAZIONALE DI SCIENZE LETTERE E ARTI IN NAPOLI

RENDICONTO
DELL'ACADEMIA DELLE SCIENZE
FISICHE E MATEMATICHE

SERIE IV - VOL. LXXXIX - ANNO CLXI

(2022)



GIANNINI EDITORE

La pubblicazione è stata resa possibile grazie ai contributi

- della Regione Campania



(Progetto finanziato con la L.R. n. 7/2003, contributi per la promozione culturale anno 2022)

- dell'Università degli Studi di Napoli "Federico II"



- del Ministero per i Beni Culturali



Si ringrazia l'Associazione "Amici della Società Nazionale di Scienze Lettere e Arti in Napoli" per la collaborazione e il supporto.

N. 89 - Dicembre 2022

ISSN 0370-3568

Nessuna parte di questa pubblicazione può essere tradotta, riprodotta, copiata o trasmessa senza l'autorizzazione scritta dell'Editore.

Fotocopie per uso personale del lettore possono essere effettuate nei limiti del 15% di ciascuna pubblicazione. Le riproduzioni ad uso differente da quello personale potranno avvenire, per un numero di pagine non superiore al 15% per pubblicazione, solo a seguito di specifica autorizzazione rilasciata da AIDRO, via delle Erbe, n. 2, 20121 Milano, telefax 02 809506, e-mail segreteria@aidro.org

Direttore responsabile: Carlo Sbordone

Volume a cura di Marco Napolitano

© 2022 by Accademia delle Scienze Fisiche e Matematiche

Tutti i diritti sono riservati

Prima edizione italiana

Finito di stampare in Italia nel mese di maggio 2023

da Officine Grafiche Francesco Giannini & figli S.p.A. - Napoli

Autorizzazione del Tribunale di Napoli n. 780 del 14/08/1954

ISBN 978-88-6906-272-8

Indice

PARTE A – Scienze Naturali	5
V. Ghini – <i>Application of NMR-based Metabolomics in Biomedical Research</i>	7
S. Magni, R. Sbarberi – <i>Plastic Detection in the Sediments of Lambro River (North Italy): a Preliminary Study</i>	15
F. Mensitieri – <i>Microbial Enzymes and Systems: a Tool Box for Every Biotechnological Process</i>	25
G. Geraci – <i>Epigenetica e complessità biologica. Correlazioni con lo sviluppo e l'evoluzione?</i>	49
 PARTE B – Scienze Matematiche	 63
G. Cimmino – <i>Approximate Computation of the Solutions of Systems of Linear Equations</i>	65
M. Benzi – <i>Gianfranco Cimmino's Contributions to Numerical Mathematics</i>	73
 PARTE C – Vita dell'Accademia	 99
Nota del Segretario M. Napolitano	101
 APPENDICE	 109
N. Scafetta, R. Di Cristo, R. Viola, A. Mazzarella – <i>L'Osservatorio Meteorologico di San Marcellino Napoli Centro: i dati dell'anno 2022</i>	111
 ISTRUZIONI E MODELLO	 161

PARTE A
Scienze Naturali

Application of NMR-based Metabolomics in biomedical research

Nota di Veronica Ghini¹

Presentata dal socio Alberto Di Donato
(Adunanza del 17 giugno 2022)

Keywords: Metabolomics, Nuclear Magnetic Resonance.

Abstract – Metabolomics represents a powerful tool to approach biomedical issues and precision medicine, with the final aim of obtaining disease characterization, early diagnosis, prognosis and monitoring the individual response to pharmacological treatments, thus improving patient stratification and management. In this framework, a series of case studies drawn on the research activities of Dr. Veronica Ghini based on nuclear magnetic resonance spectroscopy (NMR) are described.

Riassunto – La metabolomica rappresenta un potente strumento per affrontare le problematiche biomediche e la medicina di precisione, con l'obiettivo finale di ottenere la caratterizzazione della malattia, la diagnosi precoce, la prognosi e il monitoraggio della risposta individuale ai trattamenti farmacologici, migliorando così la classificazione e la gestione dei pazienti. In questo quadro, vengono descritti una serie di casi di studio tratti dalle attività di ricerca della Dott.ssa Veronica Ghini e basati sulla spettroscopia di risonanza magnetica nucleare (NMR).

1 - INTRODUCTION

Metabolomics is the -omics discipline that allows to achieve a comprehensive and simultaneous determination of a large fraction of the small metabolites, referred as “metabolome”, present in biological samples such as body fluids (urine,

¹ Vincitrice del Premio “Lisa De Conciliis” per il 2021. Centro di Risonanze Magnetiche (CERM), Università degli Studi di Firenze.

blood, saliva etc.), cells and tissues (Nicholson *et al.*, 2008). With respect to the other -omics (genomics, transcriptomics, and proteomics), this approach shifts the focus onto small-molecular-weight molecules that link biochemical processes in biological matrices. Metabolites in fact represent the direct signature of biochemical activity during metabolism and therefore closely reflect the current phenotype (Figure 1).

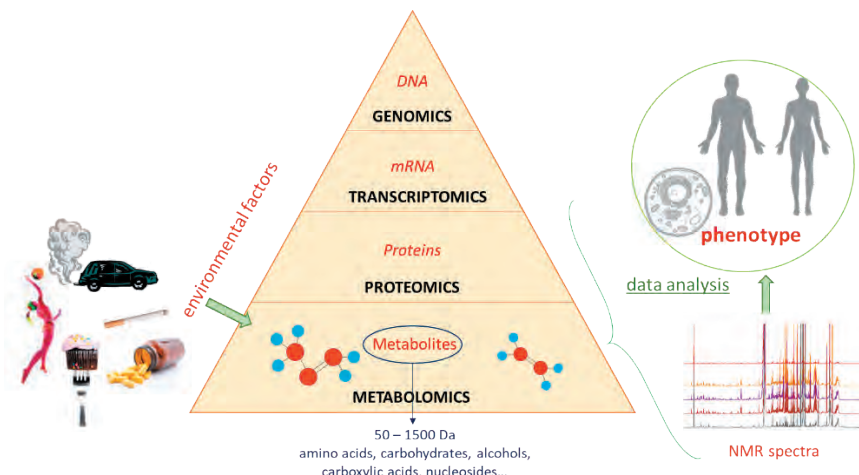


Figure 1 The flow of information in systems biology from the genome to the metabolome.

The field of metabolomics is rapidly expanding driven by advances in the two main analytical platforms i.e., high-resolution nuclear magnetic resonance (NMR) spectroscopy and mass spectrometry (MS) (Pan *et al.*, 2007). My research activities are based on NMR-based metabolomics in biomedicine field (Vignoli *et al.*, 2019; Takis *et al.*, 2019). Precisely, NMR technique offers a window into unbiased systematic studies of the metabolic fingerprints by observing and rigorously quantifying the most abundant small molecules present in the samples analyzed. ^1H NMR is routinely used because of its simplicity, rapidity, high reproducibility and minimal sample handling. At the present stage of instrumental development, metabolites $>1 \mu\text{M}$ can be detected in solution ^1H NMR spectra acquired for 5-15 min at 600 MHz, thus ensuring sample stability during acquisition. The resulting spectra are full of chemical information, containing qualitative information about tens of molecules as well as quantitative information about their concentrations; thus, constituting sample-specific and global fingerprints of the NMR-detectable portion of the whole metabolome (Vignoli *et al.*, 2019; Takis *et al.*, 2019). Due to its characteristics and potentialities, there are many possible applications for NMR-based metabolomics in the context of biomedical research

(Nicholson *et al.*, 2003). The main application is in disease diagnosis and characterization. In this framework, metabolomic profiling can also be used to identify biomarkers, or metabolic profiles, whose concentrations are altered due to a certain type of pathology. In the past years, metabolomics has already helped to characterise several important chronic and complex diseases using samples from human origins, affirming its powerful role to obtain easy and fast discriminations between patients and healthy people, patient stratification, indication of the mode and efficacy of therapeutics and of the disease occurrence risk. NMR-based metabolomics is also well suited to approach precision medicine, with the final aim of designing personalized health care solution.

2 – NMR-BASED METABOLOMICS IN THE FIGHT AGAINST CANCER-FROM CELLS TO BIOFLUIDS

Cell cultures: NMR-based metabolomics studies of cell cultures and measurement of intra- and extracellular metabolites constitute ideal tools to assess tumour response to drugs and provide insights into the mechanisms of action and resistance, in an accessible, manageable, and practical biological setup (Zhang *et al.*, 2013). Importantly, such approaches are perfectly applicable using a variety of cell lines, obtaining information about tens of metabolites participating in the main cellular metabolic pathways. Thus, variations in the levels of intracellular metabolites (endo-metabolome) induced by treatment with drugs can be directly related to the up- or down- regulation of specific pathways involved in the anti-tumor action and/or resistance development. Moreover, for a comprehensive picture of the biochemistry of cells, the analysis of growth media (exo-metabolome) provides complementary information. Thus, the integrated analysis of the endo- and exo-metabolome offers the possibility of identifying specific markers for monitoring tumour responsiveness to anticancer treatments and characterizing the major metabolic alterations (D'Alessandro *et al.*, 2019; Bernacchioni *et al.*, 2017).

Auranofin, a gold(I)-based compound, is one of the most promising gold-based metallodrugs for cancer treatment. Despite several mechanistic studies demonstrated that the gold compounds possess mechanisms of action that are distinct from those of the well-known anticancer platinum-drugs (DNA binding), their precise mechanisms of action remain to be elucidated to a large extent (Marzo *et al.*, 2018). Accordingly, AF interacts very weakly with DNA while manifesting high affinity and selectivity for proteins with free cysteines and selenocysteines. The selenoenzyme Thioredoxin reductase, a key protein governing the intracellular redox balance, is believed to be its primary target.

In this framework, in 2021, ¹H NMR-spectroscopy was used as an efficient and highly reproducible platform for the analysis of A2780 ovarian cancer cells after auranofin treatment (Ghini *et al.*, 2021). A2780 cells were treated with Auranofin 0.7 µM and 4 different time points were tested, i.e., 3, 6, 12, and 24 h.

At each time point, cell lysates and the culture media were obtained for treated and control cells. Then, cell lysates and their respective culture media were analysed by ¹H NMR. 33 and 29 metabolites were identified and quantified in all the spectra of the cell lysates and growth media, respectively. The analysis of the changes of the metabolite concentration levels between controls and treated cells, at the different time points allowed us to characterize the cellular effects induced by Auranofin treatment. The most striking change is a large increase in intracellular glutathione concentration upon Auranofin treatment; this alteration is observed starting from 6 h but it becomes more evident at 12 h and 24 h. The increase in glutathione is accompanied by intra- and extra-cellular changes in the concentration of its amino acid constituents (i.e., glutamate, glycine and cysteine). The observed biochemical alteration can be interpreted in terms of the crosstalk between the thioredoxin and glutathione redox systems. Auranofin-induced Thioredoxin reductase inhibition might promote a compensatory glutathione biosynthesis. The induction of GSH biosynthesis would represent a primary cellular defence mechanism that is not effective in protecting cancer cells from auranofin damage (Ghini *et al.*, 2021).

More in general, this study demonstrated that NMR metabolomics is an excellent, direct and relatively easy tool to investigate and characterize the cellular mode of action of metal-based drugs according to an untargeted approach.

Biofluids: In the context oncology, metabolomics of biofluids has shown immense potential for early diagnosis, prognosis, individual monitoring and drug therapy design. NMR is an efficient and highly reproducible platform for the analysis of biofluids that can be collected non-invasively. Metabolomics could reveal novel cancer biomarkers that might expand our current understanding of cancer diagnosis, prognosis, and treatment, i.e., can predict disease aggressiveness as well as its likelihood of responding to the given treatment. Similarly, markers can also be used to determine the most effective treatment regime for a particular patient, paving the path for development of personalized cancer care.

In this framework, thanks to the fellowships received from Fondazione Veronesi and AIRC, two important Italian associations supporting biomedical and oncological research, metabolomic analysis of serum samples was used with the final aim to predict the outcome of immunotherapy treatment in non-single cell lung cancer (NSCLC) patients.

Almost 80% of lung cancer cases are classified as NSCLC. Among all the therapeutic strategies, immunotherapy drugs (like the Immune Checkpoint Inhibitor agents (ICIs)) have become attractive treatments for advanced solid tumours (Postow *et al.*, 2015). As most cancer cell types, NSCLC cells have the ability to evade the body immune system by expressing on their membranes some “immune checkpoint” molecules such as the programmed cell death protein 1 (PD-

1) and its ligand (PDL-1), that normally have the role to protect against autoimmunity and inflammation. ICIs, such as the monoclonal antibodies nivolumab and pembrolizumab, can reactivate the immune response against the cancer cells by blocking the immune checkpoint molecules (Brahmer *et al.*, 2014; Hamada *et al.*, 2018) and these have been shown to improve survival in various cancer types, including advanced NSCLC.

Unfortunately, not all patients respond to these treatments with a response rate of approximately 30% or less. True predictive markers of treatment efficacy do not exist, and the associated costs are very high. Thus, the identification of biomarkers that can identify the patients that are most likely to respond to, and benefit from, ICIs treatment is of pivotal importance (Brahmer *et al.*, 2014). In this framework, metabolomic fingerprinting of biofluids may represent a timely tool of crucial importance to define metabolomic signatures that might inform on treatment outcomes.

This methodological approach was used in a retrospective pilot study to predict the outcome of immunotherapy in advanced NSCLC patients. A total of 53 patients were enrolled; thirty-four patients were treated with nivolumab (monoclonal antibody against PD-1) and 19 patients were treated with pembrolizumab (monoclonal antibody against PDL-1). From all the patients, serum samples were collected before the beginning of the treatment with the aim to a-priori identify responder and non-responder subjects. Significantly, we showed that the metabolomic fingerprint of serum acts as a predictive biomarker of ICIs response, being able to predict individual therapy outcome with > 80% accuracy (Ghini *et al.*, 2020). The strength of our study relies on the uniqueness of the ¹H NMR fingerprinting, which takes advantage of its intrinsically untargeted nature and high reproducibility. This approach allowed us to identify metabolomic signatures that are independent of metabolite assignment and act as stronger “collective” biomarkers with respect to a single molecule or to a panel of a few molecules.

3 – NMR-BASED METABOLOMICS IN THE FIGHT AGAINST COVID-19

From the beginning of the pandemic, NMR profiling has been used to define the biochemical alterations induced by COVID-19 disease and to highlight the presence of a strong metabolomic/lipoproteomic signature of the acute infection (Meoni *et al.*, 2021; Masuda *et al.*, 2021).

The COMETA project (funded by Regione Toscana) aimed at the metabolomic characterization of the biochemical alterations induced by COVID-19 disease. In this framework, ¹H NMR spectra were acquired on the EDTA-plasma samples from hospitalized COVID-19 positive patients with various disease severity and at different stages of the disease’s course and recovered subjects after 3-6 months from SARS-CoV-2 eradication.

The whole NMR spectrum, which embeds the metabolome and lipoproteome information, has a high discriminatory power between the two groups, with an accuracy higher than 93%. The differences originate from significant alterations in the concentrations of 16 metabolites and 74 lipoprotein-related parameters. Within the acute phase patients, characteristic trends in metabolite levels are observed as a function of the disease severity (Ghini, Meoni *et al.*, 2022). The metabolites found altered in COVID-19 patients with respect to recovered individuals overlap with the acute infection biomarkers identified in the comparison with healthy subjects (Meoni *et al.*, 2021), indicating the substantial metabolic healing of recovered COVID-19 subjects. We also observed that during the healing process, the restoration of the “healthy” values for the metabolites and lipoproteins does not occur at the same rate. In particular, both during spontaneous recovery and after pharmacological treatments, the alterations in lipoproteins persist in the subjects much longer than those in metabolites. The latter could therefore provide the timeliest sign of the individual response to clinical treatment or spontaneous healing from the infection (Ghini, Meoni *et al.*, 2022).

¹H NMR spectra of sera have been also used to define the changes induced by vaccination with Pfizer-BioNTech vaccine in a small group of healthy subjects ((Ghini, Maggi *et al.*, 2022). Ten COVID-19-recovered subjects and ten COVID-19-naïve subjects were enrolled for the study and their serum samples were collected at different time points, starting from before the first injection (first dose), then weekly until 7 days after the second vaccine injection (second dose) and finally 1 month after the second dose. Our data show that vaccination does not induce any significant variation in the metabolome, whereas it causes changes at the level of lipoproteins. Interestingly, the effects are different for COVID-19-recovered subjects with respect to naïve subjects, suggesting that a previous infection reduces the vaccine modulation of the lipoproteome composition.

REFERENCES

- Bernacchioni C, Ghini V, Cencetti F, et al (2017) NMR metabolomics highlights sphingosine kinase-1 as a new molecular switch in the orchestration of aberrant metabolic phenotype in cancer cells. Mol Oncol 11:517–533.
<https://doi.org/10.1002/1878-0261.12048>
- Bizkarguenaga M, Bruzzone C, Gil-Redondo R, et al (2021) Uneven metabolic and lipidomic profiles in recovered COVID-19 patients as investigated by plasma NMR metabolomics. NMR Biomed e4637. <https://doi.org/10.1002/nbm.4637>
- Brahmer JR (2014) Immune checkpoint blockade: the hope for immunotherapy as a treatment of lung cancer? Semin Oncol 41:126–132. <https://doi.org/10.1053/j.seminonc.2013.12.014>
- D’Alessandro G, Quaglio D, Monaco L, et al (2019) 1H-NMR metabolomics reveals the Glabrescione B exacerbation of glycolytic metabolism beside the cell growth inhibitory effect in glioma. Cell Commun Signal 17:108.

- <https://doi.org/10.1186/s12964-019-0421-8>
- Ghini V, Senzacqua T, Massai L, et al (2021) NMR reveals the metabolic changes induced by auranofin in A2780 cancer cells: evidence for glutathione dysregulation. *Dalton Trans* 50:6349–6355. <https://doi.org/10.1039/D1DT00750E>
- Ghini V, Laera L, Fantechi B, et al (2020) Metabolomics to Assess Response to Immune Checkpoint Inhibitors in Patients with Non-Small-Cell Lung Cancer. *Cancers* 12:3574. <https://doi.org/10.3390/cancers12123574>
- Ghini V, Maggi L, Mazzoni A, et al (2022) Serum NMR Profiling Reveals Differential Alterations in the Lipoproteome Induced by Pfizer-BioNTech Vaccine in COVID-19 Recovered Subjects and Naïve Subjects. *Frontiers in Molecular Biosciences* 9:. <https://doi.org/10.3389/fmbo.2022.839809>
- Ghini V, Meoni G, Pelagatti L, et al (2022) Profiling metabolites and lipoproteins in COMETA, an Italian cohort of COVID-19 patients. *PLOS Pathogens* 18:e1010443. <https://doi.org/10.1371/journal.ppat.1010443>
- Hamada T, Kosumi K, Nakai Y, Koike K (2018) Surrogate study endpoints in the era of cancer immunotherapy. *Ann Transl Med* 6:S27. <https://doi.org/10.21037/atm.2018.09.31>
- Marzo T, Cirri D, Pollini S, et al (2018) Auranofin and its Analogues Show Potent Antimicrobial Activity against Multidrug-Resistant Pathogens: Structure–Activity Relationships. *ChemMedChem* 13:2448–2454. <https://doi.org/10.1002/cmdc.201800498>
- Masuda R, Lodge S, Nitschke P, et al (2021) Integrative Modeling of Plasma Metabolic and Lipoprotein Biomarkers of SARS-CoV-2 Infection in Spanish and Australian COVID-19 Patient Cohorts. *J Proteome Res* 20:4139–4152. <https://doi.org/10.1021/acs.jproteome.1c00458>
- Meoni G, Ghini V, Maggi L, et al (2021) Metabolomic/lipidomic profiling of COVID-19 and individual response to tocilizumab. *PLoS Pathog* 17:e1009243. <https://doi.org/10.1371/journal.ppat.1009243>
- Nicholson JK, Lindon JC (2008) Systems biology: Metabonomics. *Nature* 455:1054–1056
- Nicholson JK, Wilson ID (2003) Understanding “Global” Systems Biology: Metabonomics and the Continuum of Metabolism. *Nat Rev Drug Discov* 2:668–676. <https://doi.org/10.1038/nrd1157>
- Pan Z, Raftery D (2007) Comparing and combining NMR spectroscopy and mass spectrometry in metabolomics. *Anal Bioanal Chem* 387:525–527. <https://doi.org/10.1007/s00216-006-0687-8>
- Postow MA, Callahan MK, Wolchok JD (2015) Immune Checkpoint Blockade in Cancer Therapy. *JCO* 33:1974–1982. <https://doi.org/10.1200/JCO.2014.59.4358>
- Takis PG, Ghini V, Tenori L, et al (2019) Uniqueness of the NMR approach to metabolomics. *TRAC Trends in Analytical Chemistry* 120:115300. <https://doi.org/10.1016/j.trac.2018.10.036>
- Vignoli A, Ghini V, Meoni G, et al (2019) High-Throughput Metabolomics by 1D NMR. *Angew Chem Int Ed* 58:968–994. <https://doi.org/10.1002/anie.201804736>
- Zhang A, Sun H, Xu H, et al (2013) Cell metabolomics. *OMICS* 17:495–501. <https://doi.org/10.1089/omi.2012.0090>

Plastic detection in the sediments of Lambro River (North Italy): a preliminary study

Nota di Stefano Magni¹ e di Riccardo Sbarberi²

Presentata dal socio Lelio Mazzarella
(Adunanza del 18 novembre 2022)

Keywords: plastic pollution, monitoring, sediments, freshwaters.

Abstract – Plastic pollution represents an emerging global problem, and freshwaters massively contribute to the ocean plastic contamination. For this reason, the aim of this preliminary study was the evaluation of the plastic presence in the sediments of Lambro River, a tributary of the Po River, which crosses one of the main industrialized areas of North Italy. Sediments were collected using a Van Veen grab and plastics were separated from this complex matrix through a density extraction. In particular, we compared the extraction efficiency of two hypersaline solutions of sodium chloride (NaCl; density of 1.2 g/cm³) and zinc chloride (ZnCl₂; density of 1.6 g/cm³). Obtained results highlighted the presence of plastics in the Lambro sediments, as well as a significant difference ($p < 0.05$) in the extraction performance of selected solutions, with 8.3 ± 10.4 number of plastics/Kg sediments wet weight (w.w.), extracted by NaCl solution, and 53.3 ± 16.1 number of plastics/Kg sediments w.w. extracted by ZnCl₂ solution. This preliminary study represents the first evidence of plastics in the Lambro River sediments and highlights the importance to use high-density solutions, as ZnCl₂, in the plastic extraction protocol. Other studies are needed to deeply characterize this type of pollution in a matrix, as sediments, still poorly investigated.

¹Vincitore del Premio “Lisa De Conciliis” per il 2021. Ricercatore presso il Dipartimento di Bioscienze, Università degli Studi di Milano, Via Celoria 26, 20133 Milano, Italia.

²Dottorando presso il Dipartimento di Bioscienze, Università degli Studi di Milano, Via Celoria 26, 20133 Milano, Italia.

Riassunto – L'inquinamento da plastica rappresenta un problema globale emergente e le acque dolci contribuiscono in modo massiccio alla contaminazione da plastica a livello oceanico. Per questo motivo, l'obiettivo del presente studio preliminare è stata la valutazione della presenza di plastiche nei sedimenti del fiume Lambro, un affluente del fiume Po che attraversa una delle principali aree industrializzate del Nord Italia. I sedimenti sono stati raccolti utilizzando una benna Van Veen e le plastiche sono state separate da questa matrice complessa attraverso un'estrazione densimetrica. In particolare, abbiamo confrontato l'efficienza di estrazione di due soluzioni ipersaline di cloruro di sodio (NaCl ; densità di $1,2 \text{ g/cm}^3$) e cloruro di zinco (ZnCl_2 ; densità di $1,6 \text{ g/cm}^3$). I risultati ottenuti hanno evidenziato la presenza di plastiche nei sedimenti del Lambro e una differenza statisticamente significativa ($p < 0,05$) nella capacità di estrazione delle soluzioni considerate, con $8,3 \pm 10,4$ plastiche/Kg di sedimenti *wet weight* (w.w.), estratti dalla soluzione di NaCl , e $53,3 \pm 16,1$ plastiche/Kg sedimenti w.w. estratti con ZnCl_2 . Questo studio preliminare rappresenta la prima evidenza di plastiche nei sedimenti del fiume Lambro e mette in risalto l'importanza di utilizzare soluzioni ad alta densità, come ZnCl_2 , nel protocollo di estrazione della plastica. Altri studi sono necessari per confermare questa evidenza e per caratterizzare a fondo questo tipo di inquinamento in una matrice, come i sedimenti, ancora poco indagata.

1 – INTRODUCTION

Plastic pollution is one of the main ecological problems in modern society. In 1950, which represents the starting point of the massive production of plastics, the global production was 1.5 million tons (Crawford and Quinn, 2017). The actual scenario is completely different. Indeed, as reported by the last report of Plastics Europe (2021), the worldwide plastic production follows a positive trend, moving from 335 million tons in 2016 to 368 million tons in 2019. In this context, a slight reduction in plastic production was observed in 2020, due to COVID-19 pandemic. China is the largest plastic producer (32 %), followed by North America Free Trade Agreement (NAFTA; 19 %), while Europe is responsible of the 15 % of the total plastic production. This situation is complicated by the presence of the *non-conventional* plastics, as tire rubbers and water-soluble polymers, which increase the number of synthetic materials reversed in the environment (Magni *et al.*, 2022a; Nigro *et al.*, 2022).

Consequently, the continuous increase in the plastic synthesis, associated to its incorrected disposal, re-use and recycling, led to an accumulation of this material in the aquatic ecosystems (Talbot and Chang, 2022) and Oceans represent the final compartment of plastic accumulation (for instance the Great Pacific Garbage Patch). However, despite the continental area is the main source of plastic pollution towards Oceans, only few studies, compared to those conducted on marine ecosystem, concern freshwaters. For example, it was estimated that Rhine and Danube Rivers transport, respectively, about 20.4 tons and 532.4 tons of plastics/year to the sea (Van Der Wal *et al.*, 2015). On the other hand, Po River, the

main Italian water course, contributes annually with 145 tons of plastics towards Mediterranean Sea (Munari *et al.* 2021). Among the Po tributaries there is Lambro River, which, with its 130 Km, crosses one of the main industrialized areas of North Italy. Some studies reported the presence of floating plastics along the Lambro River course, with an important impact on plastics release into the Po River. In particular, after sampling by a plankton net with a 300 µm mesh, a number of plastics/m³ was found ranging from 0.5 ± 0.3 at the source of the Lambro (Merone) to 14.3 ± 11.0 at its entrance in the Po River (Graffignana).

In this context, an estimation of 6 million/plastics daily released in Po waters by Lambro River was performed (Magni *et al.*, 2021). The amount of plastics changed dramatically reducing the mesh of plankton net.

Indeed, two other studies conducted on Lambro River, sampling plastics by a plankton net of 100 µm mesh, detected a number of plastics/m³ from 71 to 2070 (Binelli *et al.*, 2022; Magni *et al.*, 2022b).

Between the possible sources of these pollutants toward freshwaters could be the Wastewater Treatment Plants (WWTPs), which are not engineered to remove emerging contaminants, as plastics, to the treated effluents (Magni *et al.*, 2019). Considering these aspects, the monitoring of plastic contamination in freshwater environment constitutes a pivotal approach to characterize, and subsequently mitigate, the eventual pollution induced by these contaminants.

Despite the plastic presence in the aqueous matrices begins to be well known, few information is available about the deposition of these contaminants in the water body bottom, contaminating the sediments. Indeed, if some plastics can float on water surface, other polymers can settle based on their density or after the fouling phenomenon induced by microorganisms or organic matter (Lobelle and Cunliffe, 2011; Woodall *et al.*, 2014).

Based on these considerations, the aim of this preliminary study was to define the method setting for extracting plastics from the sediments, using Lambro River as reference site.

In order to analyze the plastic abundance in river sediments, it is essential to process the samples for the density separation, and some salt solutions can be used for this purpose. The most widely used solution is composed by sodium chloride (NaCl), presenting a density of 1.2 g/cm³. However, this solution is not indicated in the separation of high-density plastics such as polyvinyl chloride (PVC, density 1.15 - 1.70 g/cm³) or some polyesters, as polyethylene terephthalate (PET, density 1.40 - 1.50 g/cm³), which could be found in sediments. To overcome this problem, solutions with higher densities, such as zinc chloride (ZnCl₂, density of 1.6 g/cm³) and sodium iodide (NaI, density of 1.8 g/cm³), can be used despite their high costs and toxicity compared to NaCl (Crawford and Quinn, 2017). Given the lack of standardized methods about all steps of plastic monitoring, this preliminary study evaluated, for the first time, the presence of plastics in the Lambro River sediments comparing the separation performance of

two hypersaline solutions.

2 – MATERIALS AND METHODS

2.1 – SEDIMENT COLLECTION AND PLASTIC EXTRACTION

Lambro River was chosen as sampling site due to its course along some of the most industrialized and urbanized areas of North Italy, as well as due to the overt presence of plastics in its aqueous matrix (Binelli *et al.*, 2022; Magni *et al.* 2021, 2022b). This feature made Lambro River an excellent sampling site to compare the plastic extraction performance of NaCl and ZnCl₂ hypersaline solutions. The sediments were collected at the Lambro Park (Figure 1), in the city of Milan, using a Van Veen grab (sampling area of 200 cm²; Scubla, Italy). Due to the sediment nature, mainly constituted by coarse materials, we collected the samples in two points near the riverbank, in the deposition zones (two samples for each of the two sampling points).



Figure 1 Lambro River course in the City of Milan with the two sampling sites (red points) in the Lambro Park

After sampling, the sediments were placed in two glass bottles of 0.5 L *per* sampling point and stored at 4 °C until analysis. Before processing the sample, the collected sediments were pooled and analyzed in triplicate (3 samples from the same pool). Subsequently, the two hypersaline solutions of NaCl and ZnCl₂ were used to separate the plastics from the sediments and their efficiency was compared. Before using them, the solutions were filtered using a vacuum pump on glass fiber filters with 1.2 µm mesh (Whatman GF/C 47 mm) to eliminate the possible interfering material. The sediments (200 g *per* replicate) were placed in

200 mL of hypersaline solution, stirred for 5 min by a magnetic stirrer, and decanted overnight.

The supernatant was filtered through nitrate cellulose membrane filters with 8 µm mesh (Sartorius™ 50 mm), using a vacuum pump, and digested with hydrogen peroxide (H_2O_2 , 15 % v/v) to remove the traces of organic matter. The filters were then dried under a laminar flow hood, to avoid the atmospheric contamination by eventual plastics. For each of the two different hypersaline solutions 3 replicates were performed. In order to avoid a contamination of samples, filters were kept covered when possible and lab cotton coats were worn both during samplings and sample treatments. In addition, two filters were processed as blanks, maintaining the filters exposed to the air, near the working zone, to monitor the eventual atmospheric contamination by plastics (Magni *et al.*, 2019).

2.2 – PLASTICS QUANTIFICATION AND CHARACTERIZATION

Filters were observed at the stereomicroscope and the particles with a suspected plastic nature were transferred on clean filters; this step is called visual sorting. The material collected in this way was quantified and characterized using the Fourier Transform Infrared Microscope System (μ FTIR; Spotlight 200i equipped with Spectrum Two, Perkin Elmer). As regards the analysis of the polymer composition, the obtained μ FT-IR spectra were acquired in attenuated total reflectance (ATR) with 32 scans in the wavelength range between 600 and 4,000 cm^{-1} . Subsequently, the spectra were analyzed using Spectrum 10 software and compared with standard libraries. Similarity of measured sample and reference spectrum was accepted only after visual examination of spectrum peaks and considering a matching score ≥ 0.70 (Magni *et al.*, 2019). Based on their shape, we classified the detected particles as fragments, films, pellets and fibers. On the other hand, about the size measurement we used the ImageJ software, categorizing the particles, based on Hartmann classification (Hartman *et al.*, 2019), as micro- (1 to $< 1000 \mu m$), meso- (1 to $< 10 mm$) and macroplastics ($> 1 cm$). Lastly, also the color of detected plastics was registered.

The values of plastic quantification, after the extraction with the two hypersaline solutions, were compared using the one-way analysis of variance (one-way ANOVA), followed by Bonferroni post-hoc test, to evaluate the eventual significant differences between the different treatments.

3 – RESULTS AND DISCUSSIONS

The obtained results showed the presence of plastics in the sediments of Lambro River. This aspect is not surprisingly, considering the detection of these contaminants in the Lambro aqueous matrix (Binelli *et al.*, 2022; Magni *et al.*, 2021, 2022b). In particular, in the 3 replicates of samples treated with NaCl hypersaline solution we detected, respectively, 0 plastics and 12 particles with a natural-based

origin (in all samples the majority of particles with a natural origin were fibers of cellulose), 4 plastics and 34 particles with a natural origin, and 1 plastic and 7 particles with a natural origin in the last sample. This situation changed in the sediments treated with ZnCl₂ hypersaline solution. Indeed, we detected 12 plastics in the first replicate, with 19 particles with a natural-based origin, 7 plastics in the second replicate, with 23 particles with a natural origin, and 13 plastics in the third replicate, with 13 particles with a natural origin. All these data, for each replicate, were referred to 200 g of analyzed sediments, for a total of 145 analyzed particles through the μFT-IR (Figure 2). On the other hand, in the blanks we detected 19 particles with a natural origin and only 1 orange fiber of polyacrylate (PAK). Since no orange fibers of PAK were detected in the samples, we considered reliable the data we presented on the preliminary characterization of plastics in Lambro River sediments, excluding any type of external plastic contamination.

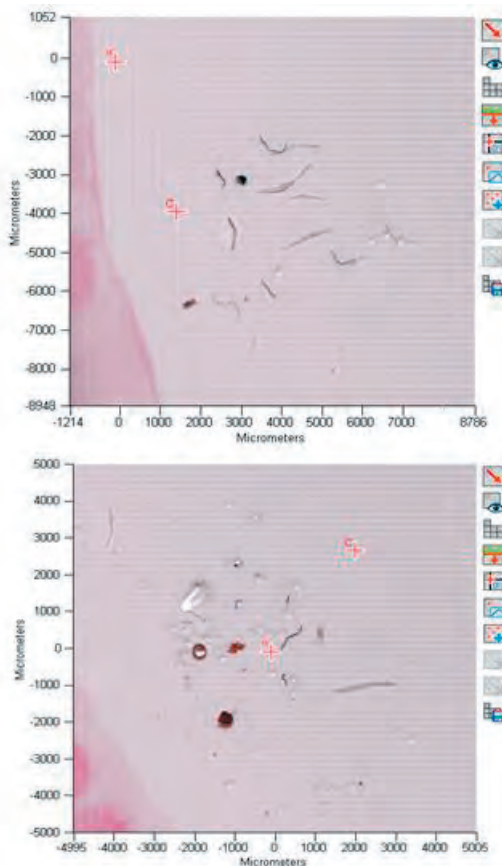


Figure 2 μFT-IR scans of filter surface with detected plastic fibers, pellets and fragments

Moving on the discussion of obtained data, we converted the plastic amount from number of plastics/200 g sediments wet weight (w.w.) to number of plastics/Kg sediments w.w., to facilitate the comparison with other studies that may be found in scientific literature. We detected 8.3 ± 10.4 number of plastics/Kg sediments w.w. in the sediments of Lambro River treated with NaCl hypersaline solution. This value increased significantly ($F_{1,4}=16.56818$; $p < 0.05$) to 53.3 ± 16.1 number of plastics/Kg sediments w.w. when the samples were treated with the ZnCl₂ hypersaline solution.

About the characterization of the plastics, we observed, once again, some differences between the two treatments (Figure 3). In particular, we detected a high percentage of mesoplastics (60 %), followed by microplastics (40 %), in the samples treated with NaCl. In these sediments the shape was mainly represented by fibers (80 %) of polyester (PEST; 60 %). This ratio changed considering the samples treated with ZnCl₂. Indeed, in these sediments the number of recovered plastics increased and other types of these contaminants, in terms of size, shape and polymer composition, were detected. We observed mainly microplastics (78 %) in these matrices, followed by meso- (14 %) and macroplastics (9 %). Once again,

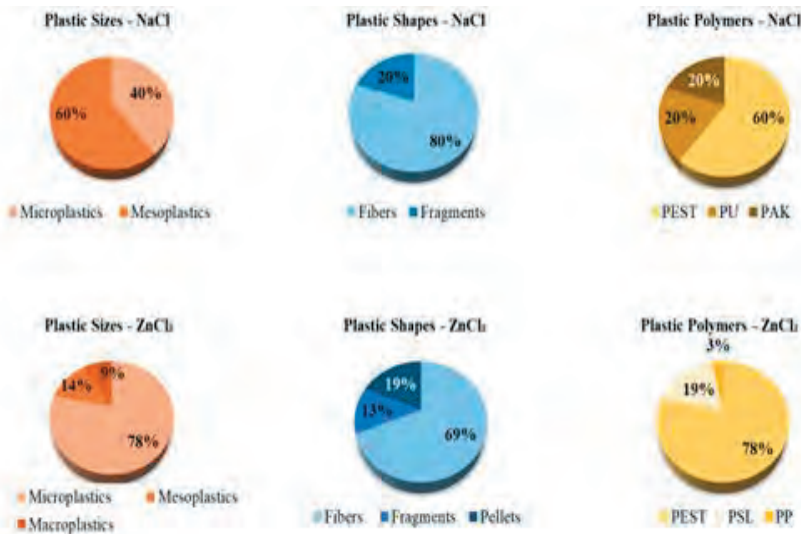


Figure 3 Plastic characterization. Physical parameters of detected plastics in Lambro River sediments extracted with NaCl and ZnCl₂ hypersaline solutions. In the pie charts are reported the percentages of detected sizes (micro-, meso- and macroplastics), shapes (fibers, fragments and pellets) and polymer composition (polyester - PEST, polyurethane - PU, polyacrylate - PAK, polystyrene sulfonate - PSL and polypropylene - PP) of extracted plastics.

fibers were the main detected shape (69 %), but it is important to note that in these samples appeared the pellets (19 %) of polystyrene sulfonate (PSL), which constituted the 19 % of the total polymer composition. Despite Lambro River is highly impacted by polystyrene (PS) pellets, a typical example of plastics with a primary industrial origin (Magni *et al.*, 2021, 2022b), the PSL, also detected in Canadian Lake Ontario in form of smooth, spherics and beads (Ballent *et al.*, 2016), was not previously observed in the Lambro. For this reason, more investigations and confirmations are required about the PLS presence.

In addition, it is important to note that no high-density plastics, as polyvinyl chloride (PVC), were detected in Lambro River sediments and the observed polymers, except for PSL, are those normally found in freshwater aqueous matrices (Talbot and Chang, 2022). Detected plastics, in all samples, were characterized mainly by synthetic fibers of PEST. These plastics represent the typical secondary origin contamination, probably associated to the release by WWTPs. Lambro River receives the water from more than 30 WWTPs during its course, and the PEST fibers, derived by synthetic clothes washing, can reach the river trough the WWTP effluents (Magni *et al.*, 2019). However, another important source of synthetic fibers could be associated to their direct release by synthetic clothes during the walking or sport activity, as observed by De Falco *et al.* (2020). Other detected synthetic particles in Lambro sediments were made by polyurethane (PU) and polypropylene (PP). This last polymer, in particular, represents one of the main used plastics to produce common objects (Figure 3). Lastly, in all samples, regardless of the extraction protocol, the main colors of detected plastics were blue and black (40 % for both colors in the NaCl extraction and 31 % and 22 %, respectively, in the ZnCl₂ extraction).

Despite we performed this preliminary plastic monitoring to set the extraction methods in only one sampling point of Lambro River (Lambro Park), it is possible to compare the observed level of contamination with other Italian water courses. For example, the study of Winkler *et al.* (2022), conducted on Ticino River (North Italy), reported a sediment contamination, after an extraction with NaCl, of 11.0 ± 7.8 plastics/Kg sediments dry weight (d.w.). This value is partially comparable with our result of 8.3 ± 10.4 number of plastics/Kg sediments w.w., observed with the same NaCl extraction protocol. However, the contamination values increase up to 1,540 plastics/Kg sediments d.w. in Mugnone Creek (Central Italy), an Arno River tributary (Rimondi *et al.*, 2022), and in other rivers of Tuscany as Albegna, Osa and Ombrone with an amount from 45 to 1,069 plastics/Kg sediments d.w. (Guerranti *et al.*, 2017). These heterogeneous data, in our national context, suggest the importance to develop a common standardized protocol for plastic monitoring/extraction, as well as of data expression (dry or wet weight), to facilitate the comparison of results and delineate a clear scenario of plastic contamination in freshwater environments.

4 – CONCLUSIONS

Considering that ZnCl₂ allows to obtain a denser solution of 1.6 g/cm³, compared to NaCl (1.2 g/cm³), our results showed the ability of this substance to extract the highest number of plastics from the sediments, avoiding a pollution underestimation. The use of ZnCl₂ allowed five times the extraction than NaCl solution, so it is recommended, in future studies, to use this high-density solution to monitoring plastics in sediments.

Our preliminary results indicated the presence of plastics in Lambro River sediments, despite other sampling activities along all river course are needed to characterize in an exhaustive manner this type of anthropic contamination.

5 – REFERENCES

- Ballent A., Corcoran P.L., Madden O., Helm P.A., Longstaffe F.J. (2016). Sources and sinks of microplastics in Canadian Lake Ontario nearshore, tributary and beach sediments. *Marine Pollution Bulletin*. **110**, 383-395.
- Binelli A., Della Torre C., Nigro L., Riccardi N., Magni S. (2022). A realistic approach for the assessment of plastic contamination and its ecotoxicological consequences: A case study in the metropolitan city of Milan (N. Italy). *Science of the Total Environment*. **806**, 150574.
- Crawford C.B., Quinn B. (2017). Microplastic pollutants. Elsevier Limited.
- De Falco F., Cocca M., Avella M., Thompson R.C. (2020). Microfiber release to water, via laundering, and to air, via everyday use: a comparison between polyester clothing with differing textile parameters. *Science of the Total Environment*. **54**, 3288-3296.
- Guerranti C., Cannas S., Scopetani C., Fastelli P., Cincinelli A., Renzi M. (2017). Plastic litter in aquatic environments of Maremma Regional Park (Tyrrhenian Sea, Italy): Contribution by the Ombrone river and levels in marine sediments. *Marine Pollution Bulletin*. **117**, 366-370.
- Hartmann N.B., Huffer T., Thompson R.C., Hassellöv M., Verschoor A., Daugaard A.E., Rist S., Karlsson T., Brennholt N., Cole M., Herrling M.P., Hess M.C., Ivleva M.P., Lusher A.L., Wagner M. (2019). Are we speaking the same language? Recommendations for a definition and categorization framework for plastic debris. *Environmental Science & Technology*. **53**, 1039-1047.
- Lobelle D., Cunliffe M. (2011). Early microbial biofilm formation on marine plastic debris. *Marine Pollution Bulletin*. **62**, 197-200.
- Magni S., Binelli A., Pittura L., Avio C.G., Della Torre C., Parenti CC., Gorbi S., Regoli F. (2019). The fate of microplastics in an Italian Wastewater Treatment Plant. *Science of the Total Environment*. **652**, 602-610.
- Magni S., Della Torre C., Nigro L., Binelli, A. (2022b). Can COVID-19 pandemic change plastic contamination? The Case study of seven watercourses in the metropolitan city of Milan (N. Italy). *Science of The Total Environment*. **831**, 154923.
- Magni S., Nigro L., Della Torre C., Binelli, A. (2021). Characterization of plastics and their ecotoxicological effects in the Lambro River (N. Italy). *Journal of Hazardous Materials*. **412**, 125204.

- Magni S., Tediosi E., Maggioni D., Sbarberi R., Noé F., Rossetti F., Fornai D., Persici V., Neri M.C. (2022a). Ecological Impact of End-of-Life-Tire (ELT)-Derived Rubbers: Acute and Chronic Effects at Organism and Population Levels. *Toxics*. **10**, 201.
- Munari C., Scoponi M., Sfriso A. A., Sfriso A., Aiello J., Casoni E., Mistri M. (2021). Temporal variation of floatable plastic particles in the largest Italian river, the Po. *Marine Pollution Bulletin*. **171**, 112805.
- Nigro L., Magni S., Ortenzi M.A., Gazzotti S., Della Torre C., Binelli A. (2022). Are “liquid plastics” a new environmental threat? The case of polyvinyl alcohol. *Aquatic Toxicology*. **248**, 106200.
- Plastics Europe (2021). Plastics-the Facts.
- Rimondi V., Monnanni A., De Beni E., Bicocchi G., Chelazzi D., Cincinelli A., Fratini S., Martellini T., Morelli G., Venturi S., Lattanzi P., Costagliola, P. (2022). Occurrence and Quantification of Natural and Microplastic Items in Urban Streams: The Case of Mugnone Creek (Florence, Italy). *Toxics*. **10**, 159.
- Talbot R., Chang H. (2022). Microplastics in freshwater: a global review of factors affecting spatial and temporal variations. *Environmental Pollution*. **292**, 118393.
- Van der Wal M., Van der Meulen M., Tweehuijsen G., Peterlin M., Palatinus A., Virsek M.K., Coscia L., Krsan A. (2015). Identification and assessment of riverine input of (marine) litter. Final report for the European Commission DG Environment under Framework Contract No ENV. D. 25. 208.
- Winkler A., Antonioli D., Masseroni A., Chiarcos R., Laus M., Tremolada P. (2022). Following the fate of microplastic in four abiotic and biotic matrices along the Ticino River (North Italy). *Science of the Total Environment*. **823**, 153638.
- Woodall L.C., Sanchez-Vidal A., Canals M., Paterson G.L.J., Coppock R., Sleight V., Calafat A., Rogers A.D., Narayanaswamy B.E., Thompson R.C. (2014). The deep sea is a major sink for microplastic. *Royal Society Open Science*. **1**, 140317.

Microbial Enzymes and Systems: a toolbox for every biotechnological process.

Nota di Francesca Mensitieri¹

Presentata dal socio Alberto Di Donato
(Adunanza del 18 novembre 2022)

Keywords: biocatalysis, enzymes, microorganisms, protein engineering.

Abstract – “Bacteria don't build cities and don't have a very interesting social life, that's true, but when the sun will explode, they'll still be here. This is their planet, and we only inhabit it because they let us. Bacteria, let's not forget, have lived for billions of years without us; we, on the contrary, would not be able to survive a single day without them” (A Short History of Nearly Everything, Bill Bryson, 2003). To briefly introduce my work, described in the following paper, I borrow these thoughts from the American journalist and writer Bill Bryson. With the irony that distinguishes his words, in fact, he explains in a few lines the enormous importance that microorganisms have in our ecosystem, in which they have the leading role. Their very long life on the planet has made them capable of transforming any organic compound and thus to adapt themselves to any environmental condition. On the other side, their striking abilities allow us to use them as a source of useful macromolecules to exploit for our clinical and industrial applications. The operators of bacteria unique features are indeed the microbial enzymes. My work was focused on the identification and characterization of different enzymes isolated from microbiome and environmental- derived bacteria. In particular, the bioprospecting of different glycosyl hydrolases and oxygenases from different microbial sources was carried out for the development and/or the optimization of novel biocatalytic processes. Our studies attempted to use these biocatalysts to produce high value-added products or in light of a clinical biotechnological application. The enzymes catalytic activities were also evaluated in a whole-cell bioreactor approach that allowed obtaining a good biocatalysis efficiency overcoming complex purification steps.

¹ Vincitrice del Premio “Umberto Pierantoni” per il 2021. Department of Medicine, Surgery and Dentistry “Scuola Medica Salernitana”, University of Salerno, Baronissi (SA) Italy. Email: fmensitieri@unisa.it

Riassunto – “I batteri non costruiscono città e non hanno una vita sociale molto interessante, questo è vero, ma quando il Sole esploderà, saranno ancora qui. Questo è il loro pianeta, e noi lo abitiamo solo perché loro ce lo consentono. I batteri, non dimentichiamolo, hanno vissuto per miliardi di anni senza di noi; noi, al contrario, non riusciremmo a sopravvivere un solo giorno senza di loro” (Breve storia di (quasi) tutto. Bill Bryson, 2003). Per introdurre brevemente il lavoro descritto nel seguente elaborato, prendo in prestito queste parole dallo scrittore e divulgatore americano Bill Bryson. Con l’ironia che lo contraddistingue infatti egli ci espone in poche righe l’enorme importanza che i microorganismi hanno nel nostro ecosistema, di cui sono, di fatto, protagonisti molto più di noi. La loro lunghissima vita sul pianeta, li ha resi capaci di trasformare qualsiasi composto organico consentendogli di adattarsi a qualsiasi condizione ambientale. D’altra parte, le loro straordinarie capacità ci consentono di utilizzarli come fonte di utili macromolecole da sfruttare per le nostre applicazioni cliniche e industriali. Gli operatori straordinari che rendono possibile questo adattamento sono gli enzimi micobici. Il mio lavoro si è concentrato sull’identificazione e caratterizzazione di diversi enzimi isolati da batteri del microbioma ed ambientali. In particolare, l’attenzione è stata focalizzata sull’attività di bioprospecting (identificazione e valutazione dell’utilizzo biotecnologico) di differenti ossigenasi e glicosil idrolasi provenienti da diverse fonti micobiche. Successivamente, questi enzimi sono stati utilizzati in diversi approcci di biocatalisi. I nostri studi hanno previsto l’utilizzo di questi biocatalizzatori per produrre prodotti ad alto valore aggiunto o in previsione di una loro applicazione clinica. Lo sfruttamento delle attività catalitiche degli enzimi è stato anche valutato in un approccio di bioreattore a cellula intera che ha dato buoni risultati in termini di efficienza della biocatalisi, superando così fasi complesse di purificazione dei prodotti.

1 – INTRODUCTION

“For every naturally occurring organic compound, there exists a microbe or enzyme system capable of its degradation” – E.F. Gale (1952).

Ernest Frederick Gale was a British microbiologist. In 1952, Dr. Gale developed the microbial infallibility hypothesis, which states that “the build-up of compounds initially resistant to biodegradation exerts a strong selective pressure on nearby microbes to evolve to consume them” (Reynolds, 2007). This concept could be simply considered a consequence of the Darwinian evolutionary theory. A sufficiently strong selective pressure in the environment, sooner or later will lead to the evolution of the living organisms in a direction that allows them to maximize their fitness. In this context, bacteria are the first and most efficient organisms to react to environmental changes and selective pressure. Their genomic plasticity through mechanisms of conjugation and transformation renders them the most suited organisms to exert genetic exchanges and to differentiate mutations that would confer them significant advantages to survive and proliferate even in the harshest environments. These unique features in the microbial

world are put in place through the rise of ideally any type of enzymatic machinery able to degrade the different organic compounds present in the environment as either nutrients or xenobiotic or pollutant compounds. Environmental bioremediation has its roots in this unique metabolic plasticity of bacteria along with the huge variety of enzymatic activities found in these organisms.

In this framework, in the following lines a summary of works devoted to exploring the elegant efficiency of microbial metabolism and the unique features and applicability of microbial enzymes is presented.

In the first period of my Master degree at the University of Naples ‘Federico II’, I had the occasion to have some insights into the bioremediation field by working with a microorganism isolated from surface seawater samples, collected from a closed bay in the harbour of Pozzuoli (Naples, Italy). *Novosphingobium* sp. PP1Y was isolated and characterized as a Sphingomonas Gram negative bacterium able to use fuels and aromatic hydrocarbons as its sole carbon and energy source. Strain PP1Y not only degraded a surprisingly large number of mono and polycyclic aromatic compounds but it also showed a very interesting and effective adaptation to grow on complex mixtures of aromatic compounds dissolved in oil phases such as diesel oil and gasoline (Notomista *et al.* 2011) (Figure 1).

Later, during my PhD in Biotechnology at the University Federico II in Naples (Italy), I focused my attention on the enzymatic activities expressed by this peculiar, oil-degrading microorganism. In particular, the characterization of different enzymes isolated from *Novosphingobium*. sp. PP1Y was carried out and these enzymes were used for different biocatalysis purposes. In the following paragraphs the study of glycosyl hydrolases and dioxygenases that was carried out, is detailed. Then, our studies attempted to use these different enzymes as biocatalysts to produce high value-added products. The exploiting of the enzymes catalytic activities was also evaluated in a whole-cell bioreactor approach that yielded promising results in terms of biocatalysis efficiency, thus overcoming complex product compounds and enzymes purification steps.

In the last paragraph, some insights are presented about a current protein engineering project focused on chimeric proteins production and functionalization of bacterial vesicles.

2 – EXTRADIOL RING - CLEAVAGE DIOXYGENASES OF BIOTECHNOLOGICAL RELEVANCE FROM *NOVOSPHINGOBIUM* SP. PP1Y

Due to the spreading of chemical pollution in the environment, several bacterial strains able to use pollutants as carbon and energy sources were studied for their ecological role and for their possible use in bioremediation processes (Timmis *et al.* 1999). The need to activate and degrade xenobiotic compounds has

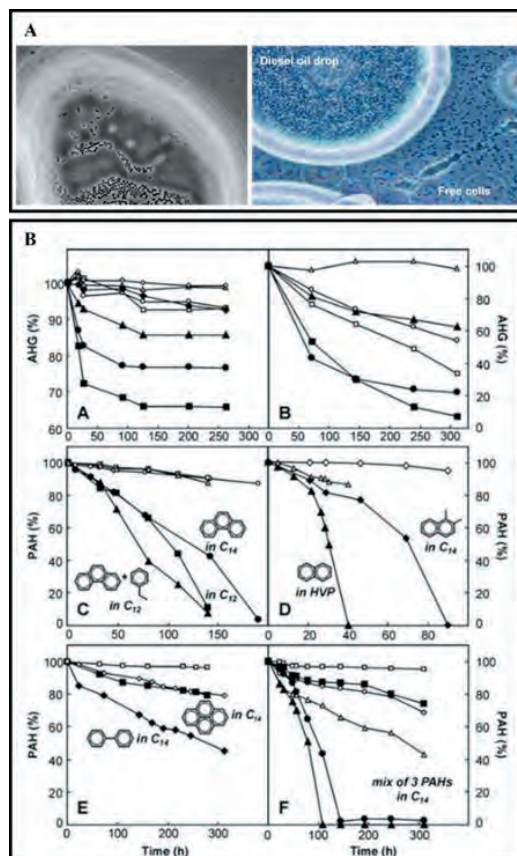


Figure 1 *Novosphingobium* sp. PP1Y aromatic compounds degradation features.

Panel A: Phase contrast microscopy analysis of diesel oil drops coated with the bacterium. Coated diesel oil drops after 10 days of incubation (right) and coated drops of emulsions produced by cultures grown using C14-dissolved 1% p-xylene (left). **Panel B:** Removal by strain PP1Y of aromatic hydrocarbons from fuel and paraffin oil drops. A and B = removal of hydrocarbons containing one (filled squares), two (filled circles), or three aromatic rings (filled triangles) and of (alkyl)pyrenes (filled diamonds) from diesel oil and gasoline, respectively. C = Phenanthrene removal from C14 containing 0.1% phenanthrene (filled circles), C12 containing 0.1% phenanthrene (filled squares), C12 containing 0.1% phenanthrene and 0.1% ethylbenzene (filled triangles). D = removal of 0.1% naphthalene from HVP (filled triangles) and of 0.1% 1,2-dimethylnaphthalene from C14 (filled diamonds). E = Removal of 0.1% biphenyl (filled diamonds) and 0.1% pyrene (filled squares) from C14. F = Removal of 0.2% naphthalene (filled triangles), 0.1% phenanthrene (filled circles) and 0.1% pyrene (filled squares) from C14 containing a mix of the three PAH and 0.1% p-xylene. In all panels empty symbols show the amount of PAHs in control samples lacking cells (Adapted from Notomista *et. al.* 2011).

been the driving force in these microorganisms to develop enzymes able to catalyze chemical reactions for the degradation of peculiar compounds. Therefore, these strains, such as *Novosphingobium* sp. PP1Y, could be exploited as a source of interesting metabolic activities and unusual biocatalysts, which can be used to synthesize pharmacologically active molecules and compounds of industrial interest.

Among the main enzymes involved in the biodegradation processes of xenobiotic compounds we find monooxygenases and dioxygenases, dehydrogenases, and hydrolases. The principal task achieved by these enzymes, both in aerobic and anaerobic conditions, is the catalysis of redox reactions in a site- and stereospecific mode. In aerobic conditions, mono and dioxygenases typically use molecular oxygen (O_2) as the oxygen donor and most of them require reduction counterparts, usually NADH or NADPH. Most oxygenases are cofactor-dependent enzymes requiring metal-ions (e.g., copper or iron), metal-ion complexes (e.g., heme, Fe-S cluster) or coenzymes (e.g., flavin, pterin, pyrroloquinoline quinone) (Torres *et al.* 2010). The polycyclic aromatic hydrocarbons (PAHs) degradation in bacteria is often carried out with an initial “ring activation” through hydroxylation in specific positions, followed by ring cleavage, a reaction catalyzed by specialized dioxygenases. These latter are divided in intra- and extradiol dioxygenases, indicated as IRCD and ERCD respectively (Harayama *et al.* 1989), leading to the conversion of dihydroxylated aromatic molecules into intermediates of the tricarboxylic acid cycle (TCA), which are readily metabolized by any type of organism. Oxygenases are attractive biocatalysts as they carry out the regio-, stereo- and chemio-selective introduction of oxygen in a wide range of organic molecules, in contrast to the poor selectivity of the traditional organic chemical synthesis, which use strong reducing agents. (Cirino *et al.* 2002). Therefore, oxygenases hold a great potential for new applications in many fields, such as: food, environment (biodegradation and bioremediation), biosensors, organic synthesis (chiral and asymmetric synthesis, pharmaceuticals), and biofuels (Bühler *et al.* 2004). However, the practical use of oxygenases compared with other industrial enzymes such as hydrolases, lyases and isomerases, is still limited by many factors. Many oxygenases, indeed, have poor stability in non-native environments as most of them are multicomponent complexes. In addition, in many cases their function depends on the presence of cofactors that need to be regenerated or on the oxidation state of a metal cofactor that tends to be unstable in an outside cell environment. In most cases, whole cell systems for oxygenase-catalyzed biotransformation were used to bypass the need for co-factor regeneration and some industrial processes involving oxygenases are carried out as batch or fed-batch fermentations (Drora *et al.* 2012). In our studies we focused our attention on the characterization of different ERCDs, which catalyze the incorporation of O_2 oxygen into catechol derivatives, resulting in ring-opening and formation

of corresponding muconic semialdehyde compounds. These dioxygenases are often enzymes with one or two subunits and work using a Fe (II) ion as a cofactor that modulates an electron transfer from the catechol substrate to an O₂ molecule, in order to cleave the aromatic ring forming a reduced product (Vaillancourt *et al.* 2006). Among the potential substrates of the ERCDs, the steroids and steroid like molecules (estrogens, 17 β -estradiol, estron, catecholestrogens) are of primary interest for pharmaceutical applications. Their site-specific cleavage and modification could be useful both for biosynthetic pathways and for biodegradation purposes. In fact, these compounds represent nowadays important environmental water pollutants, mainly derived from livestock farming activity (Gonçalves *et al.* 2020).

The analysis of *Novosphingobium* sp. PP1Y genome revealed the presence of hypothetical orfs coding for 7 ERCDs and several IRCDs, which constitute an impressive reservoir of oxygenase activities that enable PP1Y to degrade a wide range of mono-, bi-, tri-, tetra- and penta-cyclic aromatic compounds (D'Argenio, *et al.* 2014). Four ERCDs were cloned, recombinantly expressed in active form in *E. coli* purified and characterized. The kinetic parameters of purified ERCDs on four catecholic substrates selected, 2,3-dihydroxybiphenyl (2,3-DHBP), 3-methylcatechol (3MC), 4-methylcatechol (4MC) and catechol (CAT), were determined. The screening of the enzymes activity showed that the ERCD proteins, bearing the smaller active sites, are more effective towards monoaromatic catechols, with the most active protein, PP00124, preferentially recognizing biphenyl compounds. The other two proteins resulted to be more active towards polycyclic structures, probably due to the presence of wider active site pockets, as a preliminary molecular docking analysis has highlighted (Figure 2A). Therefore, the four enzymes from PP1Y represent a potential subset of enzymes that could be used for the bioconversion of different aromatic compounds. Finally, the most efficient enzyme PP00124 was used in the biodegradation of 4-hydroxyestradiol (4-OHE2), a carcinogenic hydroxylated derivate of 17- β estradiol. 4-OHE2 complete cleavage was obtained using PP00124 both in soluble form and recombinantly expressed in whole *E. coli* cells (Figure 2B and C). LC-MS/MS analyses confirmed the generation of a semialdehyde product, through A-ring meta cleavage, supporting the expected catalytic mechanism of ERCDs, mediating the insertion of an O₂ molecule in the substrate (Figure 2B). To the best of our knowledge, PP00124 is the first characterized enzyme able to directly degrade 4-OHE2 via meta cleavage. Several works reported estrogen biodegradation using different environmental strains or consortia (Li *et al.* 2018). Even though this approach could be highly beneficial in bioremediation purposes, our studies have highlighted the advantages of using recombinant strains to improve the biodegradation of specific compounds. In fact, *E. coli* whole cells in which the recombinant expression of PP00124 was induced were able to effectively degrade 4-OHE2

with high efficiency and in short time, thus suggesting that the whole cells bioconversion protocol might be foreseen as an efficient approach to avoid the time and cost consuming steps of protein purification. Moreover, a similar approach could be hypothesized for the degradation of different recalcitrant compounds which are still poorly metabolized from wild-type environmental strains and consortia.

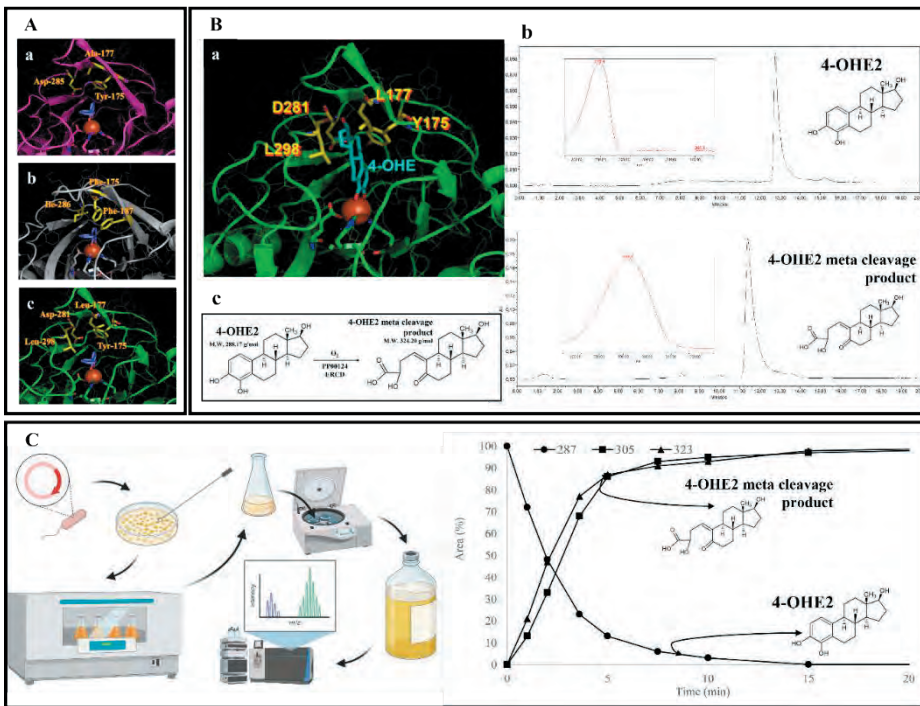


Figure 2 ERCDs from *Novosphingobium* sp. PP1Y for the bioconversion of catechol estrogens. **Panel A:** Homology models of PP1Y ERCDs. In yellow the amino acids participating in the interaction with the substrate, and 2,3-DHBP in violet. **a** = PP28735 **b** = PP26077 **c** = PP00124 (adapted from D'Argenio *et al.* 2014). **Panel B:** PP00124 bioconversion **a** = Homology model of PP00124 ERCD with 4-OHE2 (light blue) (adapted from D'Argenio *et al.* 2014). **b** = HPLC analysis of 4-OHE cleavage performed by PP00124 protein. In the upper panel the HPLC chromatogram (280 nm) and UV-vis spectrum of 4-OHE blank reaction is shown. In the lower panel, HPLC chromatogram (280 nm) and UV-vis spectrum of 4-OHE reaction: meta cleavage reaction product generation. **c** = 4-OHE2 hypothesized degradation mechanism and reaction product. **Panel C:** Whole cells bioconversion of 4-OHE2 with *E. coli* recombinantly expressing PP00124. A representation of the experimental flow through is shown on the left. The LC-MS/MS analysis of 4-OHE2 degradation and product generation in the exhaust medium registered over time is reported on the right.

3 – NOVEL GLYCOSYL HYDROLASES FROM *NOVOSPHINGOBIUM* SP. PP1Y AND *BACTEROIDES FINEGOLDII* AND THEIR BIOTECHNOLOGICAL POTENTIAL.

The second class of enzymatic activities examined during our studies were the Glycosyl Hydrolases. Simple and complex carbohydrates are ubiquitous in nature where they play a multitude of functions, ranging from simple sources of energy to molecular recognition scaffolds critical to the interactions/communication among a wide array of biomolecules, cells, tissues and organisms. The synthesis and degradation of carbohydrates in the form of di-, oligo-, and polysaccharides, is crucial in all living organisms. Two main classes of biocatalysts are involved in the modification of carbohydrates in nature and are involved in a wide spectrum of biological processes: Glycosyl Hydrolases (GHs) and Glycosyl Transferases (GTs), which are responsible for the hydrolysis and the synthesis of sugars, respectively. GHs hydrolyse the glycosidic linkage between two or more carbohydrates or between a carbohydrate and a non-carbohydrate moiety, leading to the formation of a sugar hemiacetal or hemiketal and the corresponding free aglycon (McCarter *et al.* 1994). GHs are indeed the most important classes of biocatalysts currently used in biotechnological applications. Their applicability as biocatalysts is increased by their general stability and the absence of renewable cofactors needed for catalysis. Classical examples include baking processes (amylases), detergent formulations (cellulases and amylases), fabrics treatment (amylases and xylanases), pulp and paper bleaching (xylanases); production of soft drinks and saccharification. Fruit juice processing, and lignocellulosic plant biomass conversion into bioethanol, are also well-known applications. In general, the use of glycosyl hydrolases and glycosyl transferases allow a stereospecific glycosylation of a wide range of substrates. This feature is of interest for the production of functional foods and drugs, whose characteristics might be specifically improved by either the addition or removal of specific glycan moieties (Cobucci-Ponzano *et al.* 2012).

As for oxygenase activities, also in the case of GHs biocatalysts, natural selection allowed some bacteria living in peculiar environments to evolve a great abundance of enzymes able to degrade a wide range of complex polysaccharides. Among them, the most representative polysaccharide specialized degraders are the ones of the human gut microbiome (HGM). These bacteria are primary targets for the enzyme bioprospecting of novel GHs activities. Three main bacterial phyla dominate the HGM, Bacteroidetes, Firmicutes and Actinobacteria. Bacteroidetes, largely represented from the genus *Bacteroides*, account for the major capability to degrade an extensive array of plant, animal, and host complex carbohydrates (Flint *et al.* 2012). The main operators of these degradation systems are indeed the GHs enzymes. Another group of microorganisms often specialized for the production and metabolism of complex extracellular polysaccharides is

the Sphingomonadales order. In these bacteria the production of exopolysaccharides, known in some cases as sphingans, seems to be part of a specific adaptation strategy aimed at producing a biofilm that functions as a barrier to protect bacteria from environmental pollutants and to prevent nutrient diffusion. (Hui *et al.* 2016). In this framework, the study of *Novosphingobium* sp. PP1Y genome revealed that, again, this strain is a source of new promising GHs activities. More in depth, a great number of genes encoding for both GHs (53 orfs) and GTs (57 orfs) were identified in this microorganism. These features make both *Bacteroides* species and *Novosphingobium* sp. PP1Y optimal candidates for the isolation and characterization of novel GHs activities, appealing for biotechnological applications.

In this regard, a project focused on the identification, in HGM microorganisms, of novel GHs able to degrade the Arabinogalactan (AG) polysaccharide of *Mycobacterium tuberculosis* cell wall, was developed at the Newcastle University (Newcastle upon Tyne (UK), in the laboratory of Prof. Henry J. Gilbert. In his career Prof. Gilbert has contributed to the understanding of GH catalytic mechanism and dissected the role of non-catalytic carbohydrate binding modules (CBMs) to these enzymes substrate specificity (Boraston *et al.* 2004; Gilbert 2003). In his laboratory, mechanisms of glycans utilisation by gut bacteria, in the human microbiota are investigated. Moreover, using structure-based strategies, this research group engineered novel GHs catalytic functions (Codera *et al.* 2015).

Novel GHs were identified to be used as a therapeutic agent towards *M. tuberculosis* infection. Mycobacteria share a complex cell wall structure, peculiar when compared to other prokaryotes. They are Gram positive microorganisms showing a pseudo-outer membrane region. Mycobacteria are notoriously difficult to treat, and they are naturally resistant to regular antibiotic treatment, due to the peculiar structure of their cell wall (Zuber *et al.* 2008; Brown *et al.* 2015). This cell wall architecture, defined as mAGP (mycolyl-arabinogalactan-peptidoglycan), is therefore the most common target for antituberculosis drugs. The mAGP structure is composed of three distinct layers formed by different macromolecules - peptidoglycan, arabinogalactan and mycolic acids - surrounded by a non-covalently linked capsule of polysaccharides, proteins and mycolic acids. Core of this structure is the arabinogalactan heteropolysaccharide (AG), with a galactan and an arabinan domain, in which both arabinose and galactose are found in their rare furanoid ring conformations (Figure 3).

Among the therapeutics currently used against *M. tuberculosis*, molecules such as ethambutol (EMB) hinder the arabinan domains and AG formation (Mikusova' *et al.* 1995). Nevertheless, in recent years a multidrug resistance towards these compounds was observed, which boosted the research for novel and more effective therapeutic agents including GHs endowed with the ability to degrade the complex arabinogalactan polysaccharide. In addition to their potential use as therapeutic agents, enzymes that cleave specific linkages in AG molecules

are still not well characterized in literature and they would be of great biotechnological interest for their biosynthetic value.

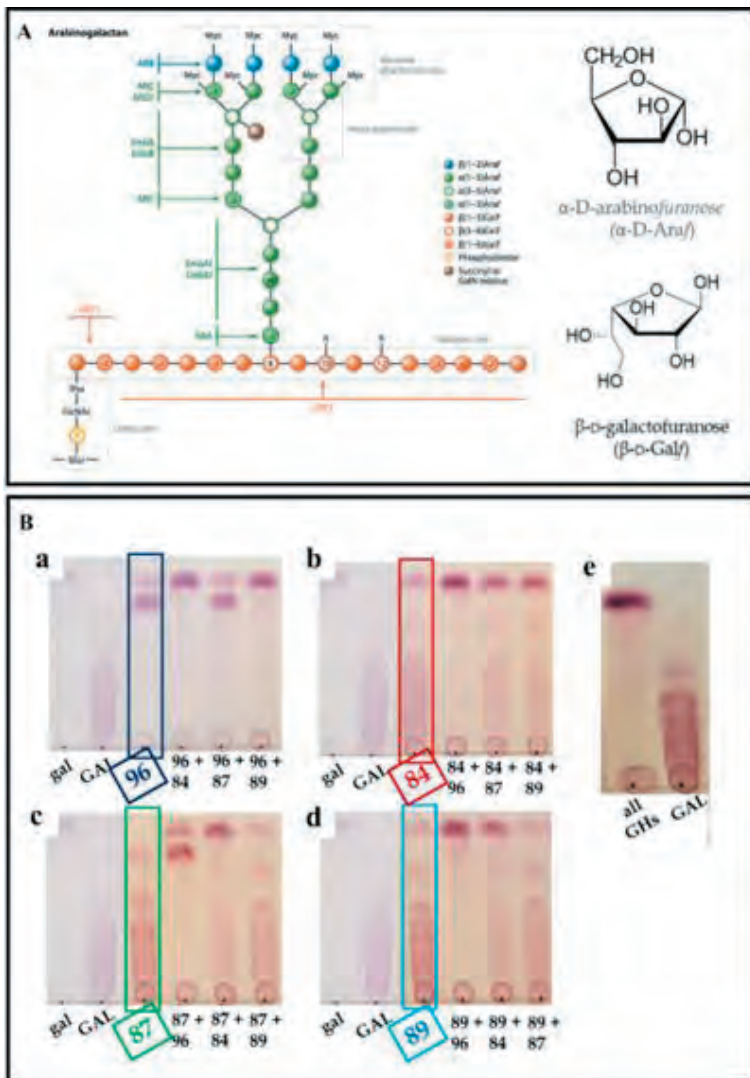


Figure 3 Arabinofuranosidases from *Bacteroides finegoldii* (BF) activity characterization on the arabinogalactan (AG) polysaccharide. **Panel A:** Detail of the mycobacteria AG. The arabinan and galactan moiety are shown in green and orange, respectively (adapted from Brown *et al.* 2015). The arabinofuranose and galactofuranose main sugar components are reported. **Panel B:** TLC analysis of combination assays with BF proteins and galactose (gal) or galactan (GAL) as substrate. The single reactions are highlighted in the coloured box. gal = galactose; GAL = galactan

The degradation of *M. tuberculosis* arabinogalactan was initially observed after the incubation of this polysaccharide in the growth media of different HGM bacteria. RNA-seq data obtained from these *Bacteroides* strains, allowed to identify the upregulation of different genes corresponding to GH enzymes. Particularly interesting results were the ones observed for AG degradation in *Bacteroidetes finegoldii* DSM 17565. Therefore, all the GH and unknown proteins found upregulated in this strain were selected for the characterization. Cloning, recombinant expression in *E. coli* BL21(DE3) and purification of 9 proteins from *B. finegoldii* DSM 17565 was performed. To investigate substrate specificity of the purified proteins, their hydrolytic activity was screened on different sugars (α - and β -D-glucose, α -L-arabinose, α -L-rhamnose, α - and β -D-xylose, α -D-mannose, β -L-fucose, β -D-N-Acetylglucosamine, α - and β -D-galactose, α -L-arabinofuranose, β -D-galactofuranose) using the synthetic substrates conjugated to *para*-nitrophenol (pNP). The enzymatic hydrolysis of pNP-sugars releases pNP which displays a λ_{max} at 404 nm. Four among the nine proteins were only active towards pNP- β -D- galactofuranose. Their high specificity for galactose in its furanosic conformation suggested their possible role in the degradation of AG polysaccharide and these proteins were further characterized. Their enzymatic activity was screened on different polysaccharidic subunits of AG by thin layer chromatography (TLC) and high-performance anion-exchange chromatography, with pulsed amperometric detector (HPAEC-PAD) (TLC data are shown in Figure 3). In particular, the conversion of the galactan moiety to galactofuranose was observed. The four enzymes revealed different substrate specificity towards the different glycosidic linkages of the galactan backbone (β -1,5 and β -1,6 linkages). In fact, the release of galactose and oligosaccharidic products of different nature was observed when the four enzymes are incubated in presence of galactan. However, the four galactofuranosidases were able to completely degrade the complex polysaccharide to galactose units, when acting together (Figure 3B). The enzymatic activity of the four GH was further characterized with combined assays leading to the identification of their exo- or endo- activity (hydrolysis of terminal or internal glycosidic linkages) and their preference for β -1,5 or β -1,6 bonds (Figure 3B). In particular, the galactofuranosidases named BF03696 and BF04084 were selected for a more detailed characterization of their enzymatic behavior, being able to completely hydrolyze galactan when used together. Substrate specificity of BF03696 and BF04084 towards β -1,5 and β -1,6 glycosidic linkages, was determined using synthetic galactobiose residues with either β -1,5 or β -1,6 linkages, bound to an aromatic ANS molecule (1-diazo-2-naphthol-4-sulfonic acid) which absorbs UV light. Results identified BF03696 as able to hydrolyze only β -1,5 glycosidic linkages with high specificity and acting as an exo- glycosidase active on terminal residues. Conversely, BF04084 protein was able to hydrolyze both β -1,5 and β -1,6 linkages with high efficiency (Figure 4). This latter

was also not annotated in any known GH class, suggesting that BF04084 could be a member of a new GH family. The activity of this protein was characterized in terms of optimal reaction conditions, pH and kinetic parameters on pNP- β -D-Galf and on β (1,6)-galactofuranose disaccharide(Figure 5).

In conclusion, this work allowed to identify and characterize 2 enzymes able together to completely degrade the galactan backbone of mycobacteria cell wall. Afterwards, different enzymatic candidates able to degrade the other main component of AG, the arabinan polysaccharide, were identified. To this purpose, the identified enzymes were used to completely degrade the galactan backbone in the AG polysaccharide from *M. tuberculosis*. The remaining arabinan moiety was then purified and used as energy source for the growth of other HGM microorganisms, to identify microorganisms able to grow degrading arabinan. Data revealed that the microorganism *D. gadai* was able to grow on arabinan and is therefore endowed with enzymatic activities able to cleave the arabinan backbone.

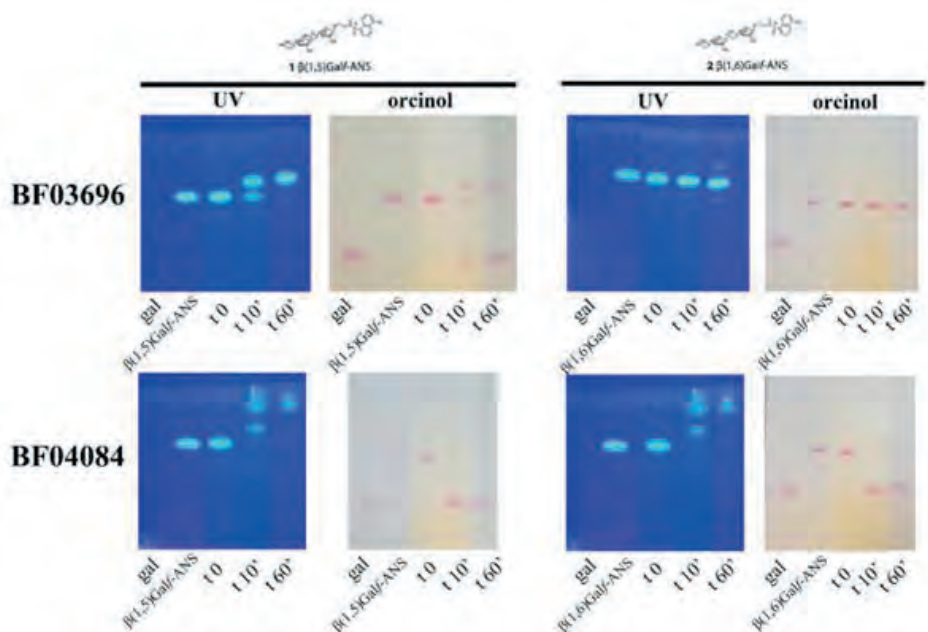


Figure 4 TLC analysis of substrate specificity determination assays with proteins BF03696 and BF04084. The chemical structure of the galactofuranose-containing synthetic substrates β (1,5)GalF-ANS and β (1,6)GalF-ANS is shown. TLC plate of the reactions carried out for the two proteins with the two substrates are reported. Both UV light (ANS moiety) and orcinol (sugar) staining are shown.

The same bioprospecting process will be followed on *D. gadai* in Prof. Gilbert laboratory in order to identify catalysts able to be used for the complete degradation also of the second part of the AG polysaccharide. Altogether, these results pave the way to obtain recombinant enzymes able to efficiently degrade one of the main cell wall components of mycobacteria and appealing to be characterized in view of their biotechnological use for the treatment of tuberculosis disease.

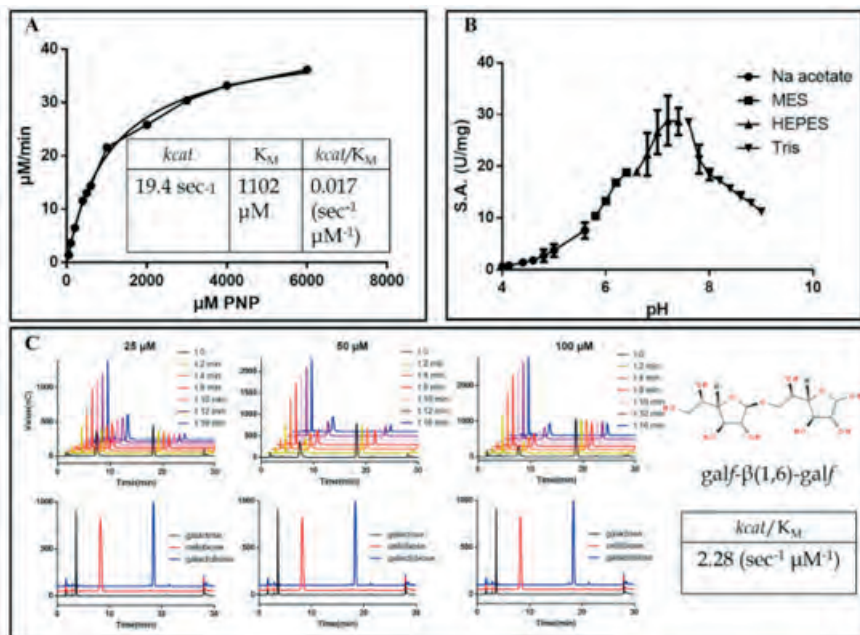


Figure 5 Characterization of BF04084 catalytic activity on pNPR and galactobiose. **Panel A:** Kinetic constants and behaviour of BF04084 on pNP- β -D-Galf substrate. **Panel B:** BF04084 pH optimum curve determined on pNP- β -D-Galf. **Panel C:** HPAEC-PAD analysis of BF04084 substrate depletion experiment using galactobiose as substrate. Three substrate concentration are shown. Galactose (black line), purified galactobiose (red line) and cellobiose (blue line) are shown as standards. The chemical structure of the $\beta(1,6)$ -galactofuranose disaccharide and the catalytic constant measured, are shown.

The second GH enzyme bioprospecting project was centred on the structural and functional characterization of a novel α -L-rhamnosidase from *Novosphingobium* sp. PP1Y. α -L-Rhamnosidases (α -RHAs) are a subset of GHs that catalyze the hydrolysis of terminal residues of α -L-rhamnose from a large number of natural compounds (Henrissat 1991). L-Rhamnose is widely distributed in nature, especially used by plants, fungi and bacteria for the conjugation to secondary

metabolites and the construction of complex polysaccharides and glycoproteins, such as gellan gum, rhamnogalacturonan and arabinogalactan-proteins. In bacteria, L-rhamnose appears to be included in membrane rhamnolipids and bacterial α -RHAs are involved in the construction and metabolism of these molecules (Mutter *et al.* 1994). In biotechnological applications α -RHAs are especially used for their ability to hydrolyze rhamnose from natural flavonoids. These molecules have gained increasing recognition in latest years for their health-related qualities, such as their potential antioxidant, antitumor and anti-inflammatory properties (Panche *et al.* 2016). Natural flavonoids are polyphenolic compounds generally characterized by a three-ring structure, which consists of two phenyl rings (A and B) and a heterocyclic ring (C). These molecules are naturally produced in plants in glycosylated forms, showing the presence of either a rutinoside (6- α -L-rhamnosyl- β -D-glucoside) or a neohesperidoside (2- α -L-rhamnosyl- β -D-glucoside) disaccharidic unit bound in different positions (Figure 6B). In humans, endogenous β -glycosidases and α -L-arabinosidases in the small intestine are responsible for removing the glucose (or possibly arabinose or xylose) moiety from flavonoids to allow for their effective absorption. These enzymes, however, are not able to cleave terminal rhamnose units, thereby limiting the bioavailability of rhamnosylated flavonoids that are converted to more bioactive forms by the colon microflora (Bokkenheuser *et al.* 1987). Therefore, enzymatic rhamnose removal from potentially bioactive flavonoids may be the key for improving their intestinal absorption and thus their beneficial properties for human health (Hollman *et al.* 1999). Due to their ability to hydrolyse rhamnose from natural flavonoids, α -RHAs are used in several biotechnological applications. Some examples include the hydrolysis of naringin to improve beverage quality by debittering grapefruit and citrus juices (González-Barrio *et al.* 2004), and the removal of hesperidin crystals from orange-derived preparations. Other applications of α -RHAs are gaining popularity in the oenological industry, where these enzymes are used to hydrolyse terpenyl glycosides to enhance aroma in wine. Despite their biotechnological utility, few attempts have been made so far to engineer bacterial α -RHAs, to unravel the molecular details underlying their catalytic mechanism, to modify their substrate specificity or to optimize their catalytic efficiency towards different substrates. A major obstacle is the limited number of α -RHAs crystal structures that are currently available.

In this regard, a single α -RHA activity, from the microorganism *Novosphingobium* sp. PP1Y, was recombinantly expressed in *E. coli* BL21(DE3) cells with a C-terminal His-tag, purified and a biochemical characterization of the enzyme was obtained. The α -RHA, from now on defined as RHA-P, was characterized as a periplasmic inverting monomeric glycosidase of ca. 120 kDa belonging to the GH106 family. The enzyme resulted to be appealing from a biotechnological point of view for the bioconversion and de-rhamnosylation of natural flavonoids,

displaying high specificity and catalytic efficiency towards flavonoidic compounds, compared to other described bacterial rhamnosidases. A biochemical characterization using the synthetic substrate pNPR (para-nitrophenyl- α -L-rhamnopyranoside) showed that RHA-P has an optimal activity in the temperature range 35–45°C, between pH 6.0–7.5, and has moderate tolerance to the presence of organic solvents in the reaction mixture (Figure 6A) (De Lise, Mensitieri *et al.* 2016). A substrate specificity study followed and initially confirmed that RHA-P is a pure α -L-rhamnosidase, no activity on any other pNP- α - and pNP- β - sugars was detected. Therefore, RHA-P does not act as a naringinase, a class of GHs having both α -L-rhamnosidase and β -D-glucosidase activities, which are generally found in fungi and bacteria. RHA-P activity was then tested on a subset of synthetic rhamnose oligosaccharides and rhamnose-containing polysaccharidic compounds, such as rhamnogalacturonan I and II, and karaya gum. Different incubation times were evaluated, and eventual oligosaccharides hydrolysis was screened by TLC. Data highlighted that RHA-P was not able to hydrolyze rhamnose from saccharidic compounds in any condition, even though a range of different glycosidic linkages and variable chain length in branched or not-branched polysaccharidic chains, were evaluated. Afterwards, the ability of RHA-P to hydrolyse rhamnose from aromatic compounds in natural flavonoids was tested on naringin, rutin, neohesperidin and quercitrin. In this case, rhamnose hydrolysis was observed in all cases also with short incubation times and in presence of organic solvents. Therefore, the kinetic constants of RHA-P hydrolysis on naringin, rutin, hesperidin and quercitrin were defined by time course incubation and HPAEC-PAD analysis. Kinetic constants highlighted that RHA-P hydrolyzes single rhamnose units, with either α -1,2 or α -1,6 O-glycosidic linkages. The k_{cat}/K_M values obtained were higher for rutin and naringin ($586.28\text{ sec}^{-1}\text{ mM}^{-1}$ and $359.21\text{ sec}^{-1}\text{ mM}^{-1}$ respectively), and lower for hesperidin and quercitrin ($190.00\text{ sec}^{-1}\text{ mM}^{-1}$ and $79.83\text{ sec}^{-1}\text{ mM}^{-1}$ respectively) (Figure 6B). The analysis of these values underlined that RHA-P catalytic efficiency was higher than that of other α -RHAs described in literature (Mensitieri *et al.* 2018). In particular, RHA-P hydrolysis of a α ,1-6 glycosidic linkages seemed to be more efficient when bound in C3 position, whereas α ,1-2 hydrolysis is better performed when the glycosidic moiety is bound to C7 position in flavonoids. Moreover, the presence of a disaccharidic unit seems to improve the catalytic efficiency of the enzyme compared to the rhamnose single unit, present in quercitrin. Altogether, this functional characterization suggests that RHA-P active site has evolved to recognize substrates containing aryl- groups and aromatic moieties, rather than poly- and oligosaccharidic compounds. In support to this observation, a structural characterization of the enzyme followed.

The active site topology and catalytic mechanism were initially investigated by mutagenesis studies. An alanine scanning mutagenesis of putative catalytic

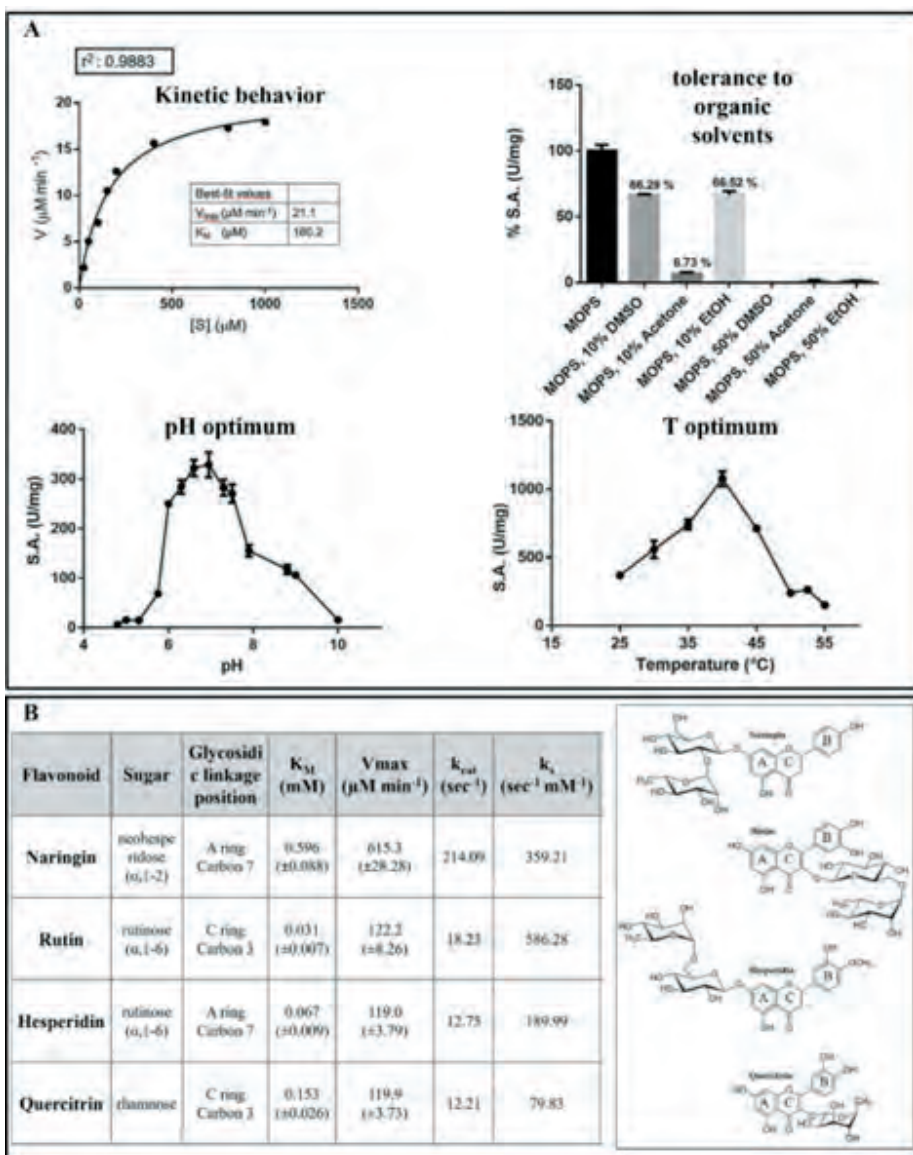


Figure 6 Biochemical characterization of the rhamnosidase RHA-P from *Novosphingobium* sp. PP1Y. **Panel A:** RHA-P kinetic behavior towards pNPR, tolerance to organic solvents, pH and Temperature optimum activity curves. (Adapted from De Lise, Mensitieri *et al.* 2016). **Panel B:** Kinetic constants of RHA-P on natural flavonoids. The chemical structure of the flavonoidic compounds used as substrates are reported. A, B and C flavonoidic rings are indicated. (Adapted from Mensitieri *et al.* 2018).

residues was performed. Five residues of aspartic and glutamic acid highly conserved in the GH106 family were identified: D503, E506, D552, E644, and D763 and an “alanine scanning” strategy was set-up for all 5 residues. This would result in a loss of function of mutants, in which the catalytic residue is replaced with an alanine, through site-directed mutagenesis. RHA-P mutants were purified, and the specific activity of the purified mutants was evaluated. Mutations in residues D503, E506 and E644, led to an almost total inactivation of the enzyme; on the contrary, mutations in positions D552 and D763 allowed maintaining a residual activity of 47.9 % and 15.8% respectively (Figure 7A). Kinetic characterization of D552 and D763 mutants highlighted that in both cases, the decrease in catalytic efficiency was almost exclusively dependent on the k_{cat} value and not on a difference in the apparent affinity of the enzyme for the substrate, thus suggesting that the mutated residues might not be directly involved in the binding or positioning of the substrate in the active site (Figure 7A).

Moreover, the presence of a calcium ion essential for catalysis was hypothesized in RHA-P. It has been reported in different GH families, although with different functions (Zhu *et al.* 2010). To investigate the presence of Ca^{2+} , the enzyme was first incubated in presence of different EDTA concentrations and then the standard pNPR assay was performed. Results showed an almost total inactivation of RHA-P when 2 mM EDTA was used (Figure 7B). The enzymatic activity recovery was then evaluated after adding either CaCl_2 or MgCl_2 , MnCl_2 , or ZnCl_2 at concentrations ranging from 3 to 50 mM. An almost complete recovery of enzymatic activity was achieved after incubating the EDTA-treated enzyme with Ca^{2+} ions (Figure 7B). Overall, data supported the evidence of the presence of Ca^{2+} ion essential for catalysis in RHA-P. These experimental evidences were finally unravelled by the solving of RHA-P crystal structure. The full structural characterization of the protein was obtained in collaboration with Dr. Matthew H. Sazinsky of the Pomona College (USA) (Terrya *et al.* 2019). Among the members of the GH106 family, a single 3D-structure was reported before the one of RHA-P, the BT0986 rhamnosidase from *Bacteroides thetaiotaomicron*. It shows an $(\beta/\alpha)_8$ barrel and catalyzes the hydrolysis of an α -L-rhamnopyranoside bound to the C2 position of an arabinofuranoside (L-Rhap- α -1,2-L-Araf) (Ndeh *et al.* 2017). RHA-P crystal structure is the second GH106 to be solved (Figure 7C). In comparison to BT0986, the morphology, electrostatic potentials and amino acid composition of the substrate binding pocket are significantly different, offering insight into the substrate preference of RHA-P for glycosylated aryl compounds such as hesperidin, naringin, rutin, and quercitrin, over polysaccharides, which are preferred by BT0986. Two disordered loops near the RHA-P active site and

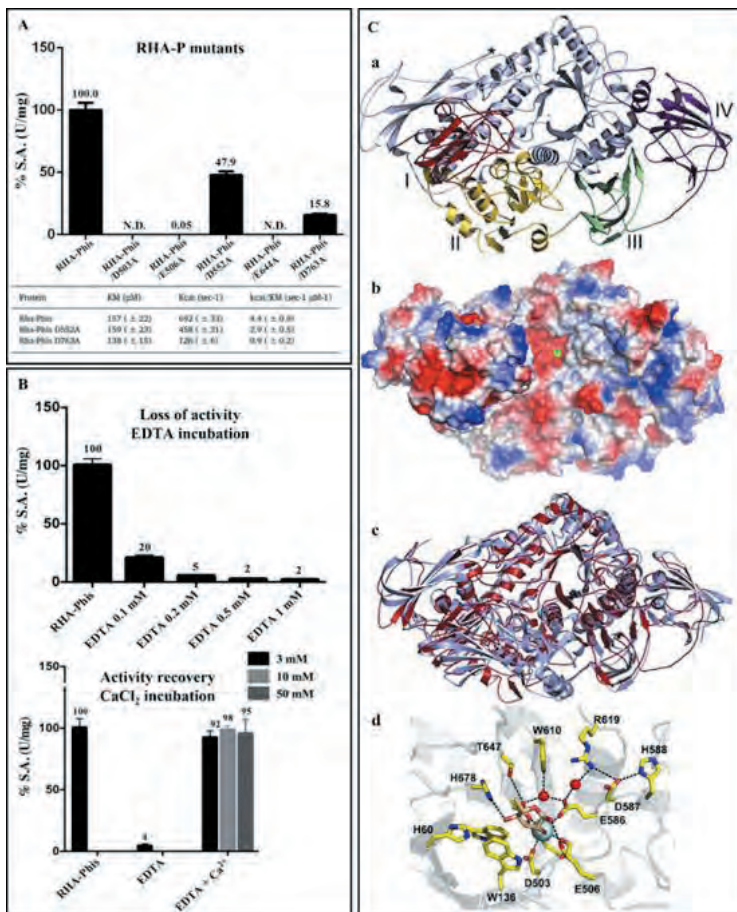


Figure 7 Structural insights of RHA-P. **Panel A:** pNPR activity of RHA-P mutants were compared to the wild type enzyme. Residual specific activity of RHA-P mutants is reported as percentage of residual activity, expressed as U/mg, compared to the control. RHA-P/D552A and RHA-P/D763A mutants kinetic constants on pNPR are reported in the Table, compared to the control (Adapted from Mensitieri *et al.* 2018). **Panel B:** RHA-P loss of specific activity in presence of EDTA increasing concentrations is shown (upper graph). The activity recovery of EDTA-treated RHA-P after incubation with different Ca^{2+} concentration is reported in the lower graph (Adapted from Mensitieri *et al.* 2018). **Panel C:** Global structure, electrostatic surfaces and active site of RHA-P. **a** = Structure of RHA-P depicting the $(\beta/\alpha)_8$ barrel (gray), domain I (red), domain II (yellow), domain III (green), and domain IV (purple). Asterisks (*) denote the relative position of missing loop residues. **b** = Electrostatic surface map of RHA-P. The green sphere denotes the position of the active site calcium ion. **c** = Superposition of RHA-P (red) and the α -L-rhamnosidase BT0986 homolog (gray) from *Bacteroides thetaiotomicron*. **d** = Stereoview of RHA-P with Ca^{2+} and rhamnose modeled into the active site (Adapted from Terry *et al.* 2019).

unique in this protein probably contribute to the differences in substrate preference. However, RHA-P overall catalytic mechanism is probably highly similar to the one of BT0986 (Figure 7C). E506 and E644 were confirmed as the catalytic residues. Here, a water molecule, activated by E644, likely engages in nucleophilic attack on the rhamnose glycosidic bond. Also, as expected, the two proteins share the presence of a calcium ion and residues crucial for its binding at the catalytic site. The calcium ion coordinate to rhamnose O2' and O3' atoms and, along with E506, orients the substrate toward the glycosidic bond. Finally, the implement of RHA-P enzyme for the bioconversion and de-rhamnosylation of natural flavonoids was evaluated using naringin as substrate and whole cell expressing RHA-P as bioreactors. After the recombinant expression of RHA-P in *E. coli* BL21(DE3) strain, cells were suspended in minimal media containing 2 mM naringin, and the hydrolysis of naringin was observed over time by analyzing culture supernatants by HPLC (Figure 8). Time course results highlighted a gradual decrease of naringin and the concomitant appearance of the derhamnosylated product (prunin). 3 OD₆₀₀/mL of recombinant cells expressing RHA-P were able to catalyze the complete hydrolysis of 2 mM naringin with concomitant release of prunin in the growth medium after 2 hours incubation (Figure 8). In conclusion, a full biochemical characterization of rhamnosidase RHA-P was performed in this work and the enzyme resulted to be appealing from a biotechnological point of view for the bioconversion and de-rhamnosylation of natural flavonoids. The biotechnological use of either wild-type or mutant rhamnosidases is currently a need for food and beverages industry to improve the organoleptic properties of processed vegetal products. Moreover, we described the possibility of using efficient whole cells biocatalysts for rhamnose hydrolysis of different natural compounds. This is particularly interesting because whole cells biocatalysts have numerous advantages in industrial bioconversion processes, allowing costs and process steps reduction.

4 - BACTERIAL OUTER MEMBRANE VESICLES (OMVS) SURFACE FUNCTIONALIZATION WITH CHIMERIC PROTEINS AS A TOOL FOR DRUG DELIVERY.

One of the emerging trends in therapeutics is the development of efficient strategies to stabilize and deliver drugs to a specific cellular target, thus improving pharmacokinetic and dynamic properties minimizing adverse effects (Li *et al.* 2017). In this context, a kind of nanocarrier naturally produced in Nature, are the OMVs. OMVs are small bacterial proteo-liposomes (ranging from 20 to 250 nm), which are released from bacteria by membrane bulging. Gram-negative MVs are generated from the outer membrane, which is embedded with LPS and outer-membrane proteins. OMVs lumen comes from the periplasm of which shares the composition, bearing periplasmic proteins, but also toxins and nucleic acids.

OMVs display multiple functions *in vivo*. Examples includes quorum sensing, nutrients

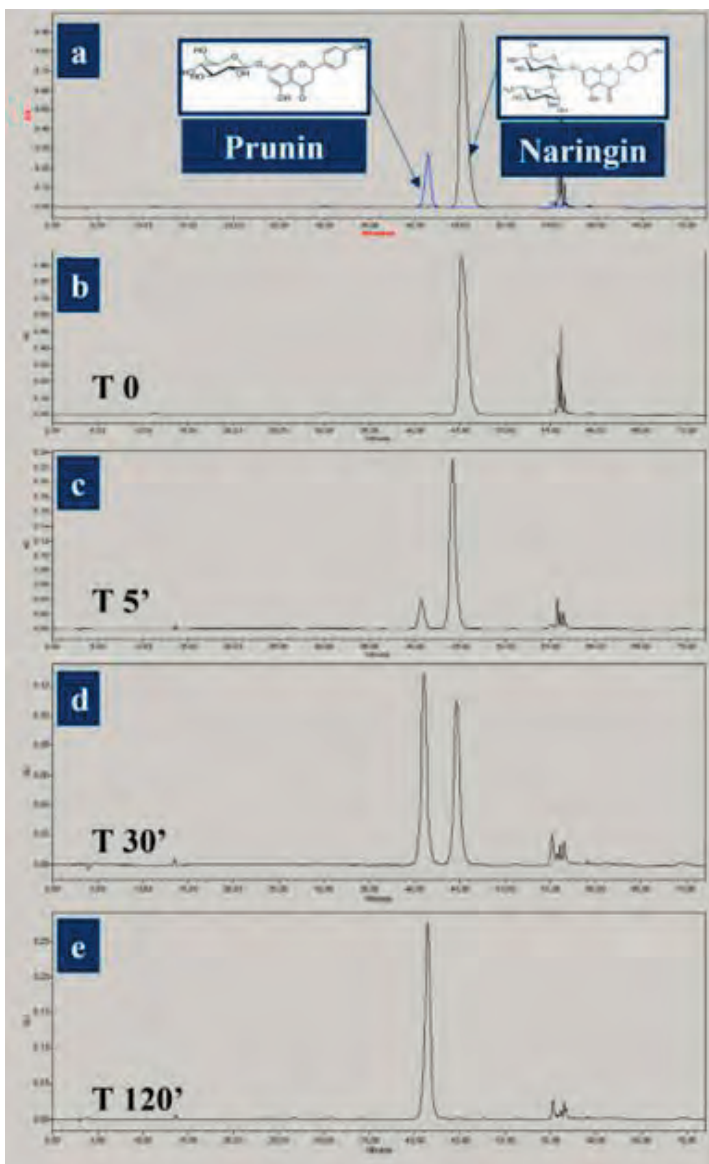


Figure 8 Time-course experiment of whole cells naringin bioconversion using RHA-P. HPLC chromatograms at 330 nm of the growth medium are shown. **a:** 2 mM naringin standard (black line) and 0.5 mM prunin (blue line). **b:** time 0. **c:** time 5 minutes. **d:** time 30 minutes **e:** time 2 hours.

mobilization, toxin secretion and genetic exchanges (Bitto *et al.* 2017). OMVs, as well as or even better than liposomes and polymer particles could be easily engineered and modified in order to tailor a site-specific targeting through their surface modification, antigen exposure or cargo loading, with different recombinant expression technologies. Bacterial OMVs in fact, are being studied for the development of drug delivery systems, vaccines, and different types of immunotherapeutic agents Li M. *et al.* 2020).

In this framework, the recombinant expression approaches currently used in bacteria offer a great advantage for nanocarriers engineering and functionalization with chimeric proteins, to use for immunotherapeutic applications. In this project, the preliminary engineering of bacterial OMVs was set-up. OMVs naturally produced in *E. coli* were initially purified and characterized, in order to focus then on their engineering exploiting the bacterium recombinant protein production machinery. Starting from literature evidence we choose to overexpress in *E. coli* a mutated form of cytolysin A (ClyA) monomer (Murase 2022). In *E. coli* pathogenic strains different ClyA monomers assemble in the outer membrane forming a cytolytic proteic toxin. Even though the secretion pathway of this protein is still unclear, ClyA localizes in the outer membrane and is secreted in OMVs. For these reasons it is one of the most studied proteins to serve as a scaffold for OMV engineering. Several works report the expression of ClyA as a fusion partner for vaccine and tumor antigens building a "plug-and-display" platform (Kim *et al.* 2008). We implemented a truncated isoform of ClyA monomer which prevented cytolysin complex assembly and that was previously described to expose its C-terminus on the outer membrane surface. To this purpose, ClyA sequence with a C-terminal linker and a His-tag was cloned and recombinantly expressed in *E. coli* BL21(DE3) cells. After the recombinant expression, the presence of the recombinant ClyA was evaluated in bacterial cells and OMVs by western blot. An anti His-tag antibody was used to detect the specific presence of the recombinant protein. In OMVs an antibody specific for Outer Membrane Protein A (OMP-A) recognition was also used as a control. In fact, OMP-A is one of the predominant proteins in bacterial OMVs, as we also identified by proteomic analyses. The recombinant expression of the protein was confirmed, and results highlight the presence of the recombinant ClyA in both cell lysates and OMVs. The correct exposure of ClyA C-terminal linker on OMV surface was then verified with Proteinase K partial proteolysis experiments and immunofluorescence assays. Once verified the correct localization and exposure of the ClyA recombinant protein we took a step forward in the engineering process. We choose different fusion partners for ClyA, having a potential in different clinical applications. As an example, a "single chain fragment variable" (scFv) protein of the Anti-CD19 antibody. These antibody fragments are currently used as efficient

and highly specific anti-cancer therapeutic agents (Chavez *et al.* 2019). Alternatively, we also produced ClyA fused to the C-terminus with a small antiviral peptide of 23 residues, named AR-23, derived from frog skin secretions recently identified (Chianese *et al.* 2022). This latter had shown significant antiviral and antibacterial activity in previous studies. The fusion proteins obtained with ClyA, represent two different chimeric proteins with different size and complexity to be localized on OMVs surface and mediate different types of biological activities. We are currently studying the applicability of our system for the decoration of bacterial OMVs to different fusion partners with clinical potential. The correct folding and biological activity of the chimeric proteins bound to OMVs will be evaluated in the next step.

5 –REFERENCES

- Bitto N.J., Liaskos MK. (2017). The Therapeutic Benefit of Bacterial Membrane Vesicles. *Int J Mol Sci.* 18(6): 1287.
- Bokkenheuser V.D., Shackleton C.H., Winter J. (1987). Hydrolysis of dietary flavonoid glycosides by strains of intestinal Bacteroides from humans. *Biochem J.* 248 (3), 953–956.
- Boraston A.B., Bolam D.N., Gilbert H.J., Davies G.J. (2004). Carbohydrate-binding modules: fine-tuning polysaccharide recognition. *Biochem J.* 382(Pt 3):769-81.
- Brown L., Wolf J.M., Prados-Rosales R., Casadevall A. (2015). Through the wall: extracellular vesicles in Gram-positive bacteria, mycobacteria and fungi. *Nat Rev Microbiol.* 13 (10), 620–630.
- Bühler B., Schmid A. (2004). Process implementation aspects for biocatalytic hydrocarbon oxyfunctionalization. *J Biotechnol.* 113, 183–210.
- Chavez J.C., Bachmeier C., Kharfan-Dabaja M.A. (2019). CAR T-cell therapy for B-cell lymphomas: clinical trial results of available products. *Ther Adv Hematol.* 10:2040620719841581.
- Chianese A., Zannella C., Monti A., De Filippis A., Doti N., Franci G., Galdiero M. (2022). The Broad-Spectrum Antiviral Potential of the Amphibian Peptide AR-23. *Int J Mol Sci.* 23(2):883.
- Cirino P.C., Arnold F.H. (2002). Protein engineering of oxygenases for biocatalysis. *Curr Opin Chem Biol.* 6, 130–135.
- Cobucci-Ponzano B., Moracci M. (2012). Glycosynthases as tools for the production of glycan analogs of natural products. *Nat Prod Rep.* 29 (6), 697-709.
- Codera V., Gilbert H.J., Fajes M., Planas A. (2015). Carbohydrate-binding module assisting glycosynthase-catalysed polymerizations. *Biochem J.* 470(1) :15-22.
- D'Argenio V., Notomista E., Petrillo M., Cantiello P., Cafaro V., Izzo V., Naso B., Cozzuto L., Durante L., Troncone L., Paolella G., Salvatore F., Di Donato A. (2014). Complete sequencing of *Novosphingobium* sp. PP1Y reveals a biotechnologically meaningful metabolic pattern. *BMC Genomics.* 15(1) 384.
- De Lise F., Mensitieri F., Tarallo V., Ventimiglia N., Vinciguerra R., Tramice A., Marchetti R., Pizzo E., Notomista E., Cafaro V., Molinaro A., Birolo L., Di Donato A., Izzo V. (2016). RHA-P: isolation, expression and characterization of a bacterial α -L-

- rhamnosidase from *Novosphingobium* sp. PP1Y. *J. Mol. Catal. B: Enzym.* 134, 136–147.
- Drora A., Fishman A. (2012). Engineering Non-Heme Mono- and Dioxygenases for Biocatalysis. *Comput Struct Biotechnol J.* 2 (3) e201209011.
- Flint H.J., Scott K.P., Duncan S.H., Louis P., Forano E. (2012). Microbial degradation of complex carbohydrates in the gut. *Gut Microbes.* 3 (4), 289–306.
- Gilbert H.J. (2003). How carbohydrate binding modules overcome ligand complexity. *Structure* 11(6):609-10.
- Gonsioroski, A., Mourikis, V.E., Flaws, J.A. (2020). Endocrine disruptors in water and their effects on the reproductive system. *Int J Mol Sci.* 21(6), 1929.
- González-Barrio R., Trindade L.M., Manzanares P., de Graaff L.H., Tomás-Barberán F.A., Espín J.C. (2004). Production of bioavailable flavonoid glucosides in fruit juices and green tea by use of fungal alpha-L-rhamnosidases. *J. Agric. Food Chem.* 52 (20), 6136-6142.
- Harayama S., Rekik M. (1989). Bacterial aromatic ring-cleavage enzymes are classified into two different gene families. *J Biol Chem.* 264 (7), 15328-15333.
- Henrissat B. (1991). A classification of glycosyl hydrolases based on amino-acid sequence similarities. *Biochem. J.* 280, 309–316.
- Hollman P.C., Bijlsma M.N., van Gameren Y., Cnossen E.P., de Vries J.H., Katan M.B. (1999). The sugar moiety is a major determinant of the absorption of dietary flavonoid glycosides in man. *Free Radic. Res.* 31 (6), 569-573.
- Hui L.W.G., Jiao X., Sun Y., Sun S., Feng Z., Zhou W., Zhu H. (2016). The preparation and characterization of a novel sphingan WL from marine *Sphingomonas* sp. *Sci. Rep.* 6, 37899.
- Kim, J.Y.; Doody, A.M.; Chen, D.J.; Cremona, G.H.; Shuler, M.L.; Putnam, D.; De Lisa, M.P. (2008). Engineered bacterial outer membrane vesicles with enhanced functionality. *J. Mol. Biol.* 380, 51–66.
- Li M., Zhao X., Zhang X., Wu D., Leng S. (2018). Biodegradation of 17 β -estradiol by bacterial co-culture isolated from manure. *Sci. Rep.* 8, 3787.
- Li M., Zhou H., Yang C., Wu Y., Zhou X., Liu H., Wang Y. (2020). Bacterial outer membrane vesicles as a platform for biomedical applications: An update. *J Control Release* 323:253-268.
- Li Z., Tan S., Li S., Shen Q., Wang K. (2017). Cancer drug delivery in the nano era: An overview and perspectives (Review). *Oncol Rep.* 38(2):611-624.
- McCarter J.D., Withers S.G. (1994). Mechanisms of enzymatic glycoside hydrolysis. *Curr Opin Struct Biol.* 4(6), 885-92.
- Mensitieri F., De Lise F., Strazzulli A., Moracci M., Notomista E., Cafaro V., Bedini E., Sazinsky M.H., Trifuggi M., Di Donato A., Izzo V. (2018). Structural and functional insights into RHA-P, a bacterial GH106 α -L-rhamnosidase from *Novosphingobium* sp. PP1Y. *Arch. Biochem. Biophys.* 15, 648:1-11.
- Mikusová K., Slayden R.A., Besra G.S., Brennan P.J. (1995). Biogenesis of the mycobacterial cell-wall and the site of action of ethambutol. *Antimicrob Agents Chemother.* 39, 2484–2489.
- Murase K. (2020). Cytolysin A (ClyA): A Bacterial Virulence Factor with Potential Applications in Nanopore Technology, Vaccine Development, and Tumor Therapy. *Toxins.* 14(2):78.
- Mutter M., Beldman G., Schols H.A., Voragen A.G.J. (1994). Rhamnogalacturonan α -l-

- rhamnopyranohydrolase. A novel enzyme specific for the terminal nonreducing rhamnosyl unit in rhamnogalacturonan regions of pectin. *Plant Physiol.* 106 (1), 241–250.
- Ndeh D., Rogowski A., Cartmell A., Luis A.S., Baslé A., Gray J., Venditto I., Briggs J., Zhang X., Labourel X., Terrapon N., Buffetto F., Nepogodiev S., Xiao Y., Field R.A., Zhu Y., O'Neill M.A., Urbanowicz B.R., York W.S., Davies G.J., Abbott D.W., Ralet M.C., Martens E.C., Henrissat B., Gilbert H.J. (2017). Complex pectin metabolism by gut bacteria reveals novel catalytic functions. *Nature.* 544 (7648), 65-70.
- Notomista E., Pennacchio F., Cafaro V., Smaldone G., Izzo V., Troncone L., Varcamonti M., Di Donato A. (2011). The Marine Isolate *Novosphingobium* sp. PP1Y Shows Specific Adaptation to Use the Aromatic Fraction of Fuels as the Sole Carbon and Energy Source. *Microb. Ecol.* 61(3): 582-94.
- Panche A.N., Diwan A.D., Chandra S.R. (2016). Flavonoids: an overview. *J Nutr Sci.* 5 e 47.
- Reynolds P. E. (2007). Ernest Frederick Gale. 15 July 1914 -- 7 March 2005". *Biographical Memoirs of Fellows of the Royal Society.* 53:143-161.
- Terrya B., Haa J., DeLise F., Mensitieri F., Izzo V., Sazinsky M.H. (2019). The crystal structure and insight into the substrate specificity of the α -L rhamnosidase RHA-P from *Novosphingobium* sp. PP1Y. *Arch. Biochem. Biophys.* 679, 108189.
- Timmis K.N., Pieper D.H. (1999). Bacteria designed for bioremediation. *Trends Biotechnol.* 17, 200-204.
- Torres Pazmiño D.E., Winkler M., Glieder A., Fraaije M.W. (2010). Monooxygenases as biocatalysts: classification, mechanistic aspects and biotechnological applications. *J Biotechnol.* 146, 9–24.
- Vaillancourt F.H., Bolin J.T., Eltis L.D. (2006). The ins and outs of ring-cleaving dioxygenases. *Crit Rev Biochem Mol Biol.* 41, 241–267.
- Zhu Y., Suits M.D.L., Thompson A.J., Chavan S., Dinev Z., Dumon C., Smith N., Moremen K.W., Xiang Y., Siriwardena A., Williams S.J., Gilbert H.J. (2010). Mechanistic insights into a Ca^{2+} -dependent family of α -mannosidases in a human gut symbiont. *Nat Chem Biol.* 6 (2), 125-132.
- Zuber B., Chami M., Houssin C., Dubochet J., Griffiths G., Daffe' M. (2008). Direct visualization of the outer membrane of mycobacteria and corynebacteria in their native state. *J Bact.* 190, 5672–5680.

Epigenetica e complessità biologica. Correlazioni con lo sviluppo e l'evoluzione?

Nota del socio Giuseppe Geraci¹
(Adunanza del 18 novembre 2022)

Keywords: Epigenetics, complexity, evolution, development

Abstract - Arguments will be presented to support the paradigm that epigenetics concerns a level of gene controls becoming necessary for the evolution of multicellular organisms endowed of complex structures. In these cases, the fundamental genetic mechanisms that control expression of individual genes are required to be operative only at specific and strictly regulated steps in the process of the generation of the particular multicellular structure. To this aim, the concept of genome will be defined in terms of its molecular composition, nucleic acids and proteins, and the structures able to generate the particular living organism. Evidence will be presented that cytosine methylation of CpG dinucleotides was a discovery of the Italian scientist Eduardo Scarano. It will be shown that epigenetic mechanisms are dependent also on the sequence and structures of the genomic DNAs that, independently of their compositions, are different and characteristic of each species. Animal development requires also that the cellular environment, nuclear and cytoplasmic, has all components necessary to understand and express the information at the moment available in the genomic DNA that otherwise would be useless.

Riassunto – Si discuteranno le argomentazioni a sostegno del paradigma che l’epigenetica riguarda il livello di controllo dell’espressione genica divenuto necessario per l’evoluzione di organismi multicellulari dotati di strutture complesse. In questi casi è necessario che i meccanismi fondamentali per il controllo dell’espressione di singoli geni (genetica) siano operativi solo in particolari passi strettamente regolati del processo di generazione di una struttura multicellulare. A questo scopo il concetto di genoma verrà definito in termini della sua composizione in molecole, acidi nucleici e proteine, e loro strutture, capaci di generare un particolare organismo vivente. Si presenterà l’evidenza che la

¹ Università di Napoli Federico II e Accademia di Scienze Fisiche e Matematiche della Società Nazionale di Scienze, Lettere e Arti in Napoli, via Mezzocannone 8, 80134 Napoli.

metilazione esclusiva delle citosine dei dinucleotidi CpG è stata una scoperta dello scienziato italiano Eduardo Scarano. Si mostrerà che i meccanismi epigenetici dipendono anche dalla sequenza e dalla struttura dei DNA genomici, che sono diversi e caratteristici per ogni specie. Lo sviluppo animale, per aver luogo, richiede anche che l'ambiente cellulare, sia nucleare sia citoplasmatico, abbia tutti i componenti necessari per comprendere ed esprimere le informazioni al momento disponibili nel DNA genomico, perché altrimenti il tutto sarebbe senza utilità.

1 - INTRODUZIONE

Prima di affrontare la definizione di epigenetica e delle sue correlazioni con sviluppo ed evoluzione è opportuno definire in cosa effettivamente consiste il genoma di una struttura vitale e, cioè, dotata delle caratteristiche minime di esistere e di riprodursi ognuna nel proprio ambiente. Di queste vi è uno spettro continuo di complessità crescenti i cui genomi sono correlativamente più complessi.

Le forme più primitive, non da tutti considerate viventi, sono semplicemente delle sequenze di DNA o di RNA che esistono e si replicano solo in ambienti particolari dove si trovano i materiali e i meccanismi che permettono la loro esistenza. Le forme più semplici sono viroidi, corte sequenze di RNA, capaci di esistere in cellule prevalentemente vegetali. Ad un livello più elevato ci sono i plasmidi con genoma a DNA, capaci di esistere nelle cellule batteriche a cui possono conferire caratteristiche vantaggiose in particolari situazioni ambientali mediante il prodotto dei loro geni, come ad esempio la resistenza all'azione di antibiotici. Questi oggetti sono semplici molecole senza una struttura che li caratterizza.

Forme vitali più complesse, perché dotate di geni di varia struttura, sono i virus, il cui genoma consiste di sequenze di DNA o di RNA doppio o singolo filamento, codificato in una o più molecole di strutture diverse tra loro. Anche questi sono capaci di esistere solo negli ambienti cellulari in cui si sono formati ma sono dotati di grande tendenza ad adattarsi a cellule diverse da quelle di origine. I virus hanno una propria morfologia con aspetti molto diversi.

Ad un livello vitale superiore ci sono i batteri, capaci di vita autonoma praticamente in tutti gli ambienti della Terra. Essi sono la prima forma di vita di cui si trovano tracce in materiali risalenti a quasi quattro miliardi di anni fa. Il loro genoma è molto più complesso perché comprende geni per la produzione di tutte le molecole necessarie alla loro esistenza autonoma, a partire da materiali semplici presenti nell'ambiente terrestre in cui sono adattati. La loro struttura fisica è monocellulare, con forme varianti da sferoidi a bastoncelli più o meno regolari. Nel loro genoma si trovano codificate tutte le attività enzimatiche con i relativi controlli per generare le vie metaboliche necessarie alla vita e sono in grado di esistere anche in condizioni assolutamente impossibili per organismi più evoluti. Il loro genoma consiste quasi esclusivamente di sequenze di DNA codificant,

senza ridondanze, per la massima efficienza ed economia di duplicazione. È da notare che ancora oggi, dopo miliardi di anni e con cicli duplicativi che possono durare anche pochi minuti, le loro forme fisiche sono rimaste praticamente invariate. Il loro genoma consiste solo di sequenze di DNA, con associate alcune proteine che hanno la sola funzione di compattazione di quella molecola. Anche la presenza di un piccolo DNA plasmidico, utile al batterio per la sua sopravvivenza in momenti particolari, viene tollerato nella popolazione solo per il tempo in cui serve. La sua presenza costituisce un appesantimento genetico che non giova alla facilità di duplicazione per cui, in assenza di un componente selettivo contrastato del plasmide, esso scompare nella popolazione batterica. La capacità dei batteri di esistere in ambienti terrestri estremi è documentata dal loro ritrovamento anche a profondità notevoli nelle perforazioni per la ricerca del petrolio e dal loro ritrovamento perfino in cristalli di salgemma, in cui presumibilmente erano rimasti intrappolati milioni di anni prima, quando i cristalli si erano formati, e capaci ancora oggi di riprodursi. L'essenzialità del messaggio genetico ha però impedito una loro evoluzione in forme e strutture più complesse. Infatti, le aggiunte di materiale genetico, come sopra menzionato, costituendo un appesantimento sfavorevole per la duplicazione, vengono ancora oggi eliminate.

Tutte le forme di vita su accennate hanno il genoma, come componente capace di generare una riproduzione fedele della loro struttura, costituito solo da una o più molecole di acido nucleico, che sia RNA o DNA. La sequenza dei nucleotidi che compone quelle molecole possiede tutte le informazioni necessarie e sufficienti per la loro esistenza nell'ambiente che è loro naturale. In tutti i casi sopra descritti la genetica, intesa come meccanismi locali per la regolazione della espressione dei singoli geni, è sufficiente per la loro duplicazione ed esistenza.

Ad un livello genetico molto più elevato vi sono gli organismi eucarioti formati da strutture particolari, dotati anche di organi e apparati. In questi casi il genoma deve codificare i controlli di espressione differenziata di parte del corredo genico, enormemente più grande, perché deve contenere oltre ai geni di sopravvivenza cellulare, detti "house keeping" o di servizio, altri geni che siano in grado di produrre le funzionalità e le strutture che caratterizzano il particolare organismo, detti geni di lusso. Inoltre, il genoma è separato fisicamente dal citoplasma cellulare da una membrana costituente il nucleo. La sequenza di nucleotidi costituenti il genoma, per quanto complessa possa essere, non può codificare il modo secondo cui i geni di lusso devono esprimersi per generare la varietà di cellule caratteristiche del particolare organismo. L'epigenetica riguarda appunto lo studio dei componenti e dei meccanismi mediante i quali avviene l'attivazione selettiva e sequenziale dei gruppi di geni necessari per generare l'organismo finale. Il genoma, sempre inteso come struttura capace di generare un organismo completo, non è composto in questi casi solo dalla molecola/e del DNA ma anche da proteine che lo strutturano. Qui di seguito si cercherà di illustrare nel modo più semplice possibile questa realtà. Va tenuto fermo il concetto che la genetica,

intesa come meccanismi di controllo locale dell'espressione di geni, è però sempre basilare per effettuare la realizzazione di un organismo complesso a partire da una singola cellula (ontogenesi).

2 – EPIGENETICA

Il termine epigenetica fu coniato negli anni quaranta del secolo scorso da Conrad H. Waddington, direttore dell'Institute of Animal Genetics dell'Università di Edimburgo, per indicare quella parte della genetica che riguarda meccanismi non deducibili direttamente dalla sequenza dei nucleotidi e che sono alla base dello sviluppo degli organismi formati da cellule diverse che producono strutture fisiche diverse con diverse funzioni. Il genoma è unico ma il risultato della sua espressione si concretizza nella produzione di cellule con aspetti e capacità funzionali senza alcuna relazione tra loro, che esplicano le varie esigenze di un organismo animale o vegetale che sia. Questo richiede l'esistenza di controlli capaci di far esprimere in maniera specifica gruppi di geni differenti, selezionati tra migliaia di possibili, quando una cellula si divide per generare cose diverse da quella di origine (Fig. 1). Inoltre, questa selezione deve avvenire in una successione precisa di scelte effettuate esclusivamente quando necessario. È facile capire che la realizzazione di tale meccanismo è molto complessa e complicata. La sequenza nucleotidica deve avere componenti aggiuntivi che operano direttamente a livello del controllo dell'espressione dei geni per il differenziamento cellulare e lo sviluppo. La struttura organizzativa del genoma mediante proteine dedicate e la modifica chimica del DNA sono alla base di quei meccanismi aggiuntivi. Va comunque specificato che per ottenere la formazione di un organismo è necessaria la presenza, nell'ambiente cellulare del genoma, di componenti proteici che siano in grado di utilizzare i segnali genetici presenti ed operare in conseguenza. Vi sono evidenze del contributo anche di altri effettori, nell'induzione del differenziamento cellulare, che operano con meccanismi diversi di cui si farà cenno.

2.1 - Importanza della struttura del genoma

Le differenze più immediatamente percepibili tra il genoma di un procariota (batterio) e di un eucariota sono la presenza in un eucariota di un nucleo e di una quantità di DNA che può essere facilmente migliaia di volte maggiore di quello di un batterio. In quella enorme quantità di materiale genetico la parte che codifica geni e i loro controlli è assolutamente minoritaria. Usando il genoma umano come esempio, su un totale di circa tre miliardi di coppie di basi solo il cinque per cento contiene sequenze codificanti mentre il resto è composto da sequenze corte e lunghe variamente ripetute di varie composizioni e molte di loro

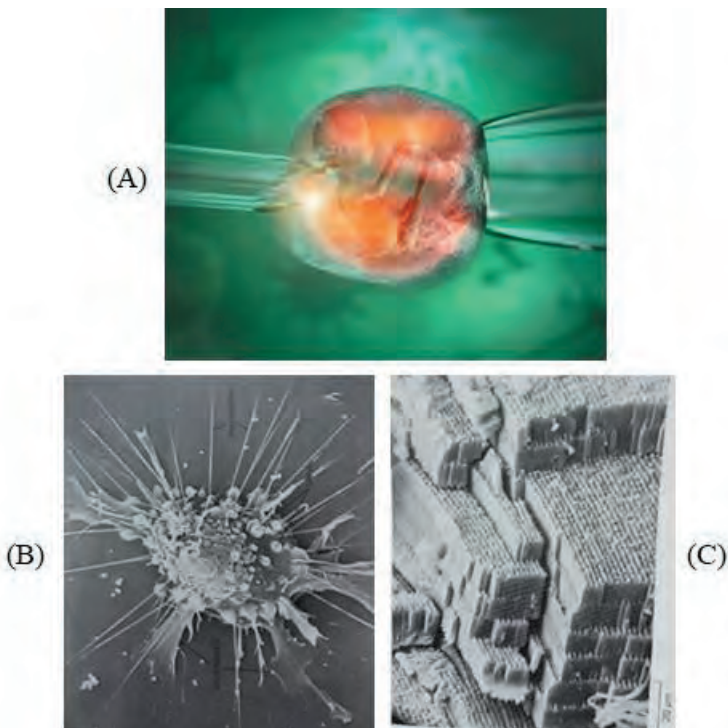


Figura 1 In alto: uovo umano fissato a un sostegno mentre è fecondato per microiniezione. In basso foto al microscopio elettronico. A sinistra un linfocita in coltura con le strutture della sua membrana esterna; a destra cellule esposte per frattura del cristallino dell'occhio, molto simili a tavole affastellate per formare la lente. I meccanismi epigenetici devono generare cellule differenziate con strutture molto differenti a partire da un solo genoma.

chiaramente somiglianti a genomi di virus. Negli eucarioti l'enorme quantità di DNA è compattata da proteine specializzate (istoni), formanti la cromatina, in strutture caratteristiche per numero e forme dette cromosomi, nei quali, localmente, il DNA può essere in strutture alternative a quella canonica detta doppia elica B, con conseguenze sulla possibilità di espressione delle funzioni circostanti. L'insieme dei cromosomi di ogni organismo è detto cariotipo ed è sua caratteristica in modo univoco. Qualunque sua modifica causa danni. Per maggiore chiarezza va specificato che anche se due organismi avessero il DNA genomico con identiche sequenze, i loro cariotipi sarebbero certamente diversi. Un esempio di ciò è dato dall'uomo e dallo scimpanzé che hanno sequenze di DNA identiche al 97% ma i loro cariotipi sono diversi. Queste differenze organizzative, in termini di raggruppamenti dei geni in cromosomi diversi con diverse strutture, è il primo e più importante parametro epigenetico per il controllo dell'espressione

genica. Anche minime variazioni strutturali possono avere conseguenze nefaste sui meccanismi di sviluppo. Un esempio di ciò è dato dalla sindrome di Down, che è causata da una trisomia, anche parziale, del cromosoma umano 21. La strutturazione del DNA genomico con le proteine contribuisce pertanto a determinare la disponibilità all'espressione dei singoli geni. La struttura della cromatina è regolata da varie modifiche chimiche reversibili effettuate sugli istoni che, come conseguenza, cambiano modalità di interazione col DNA cambiando anche la struttura generale.

L'uso della organizzazione dei geni ai fini della loro espressione non è però un meccanismo esclusivo degli eucarioti. Il caso di uno dei più semplici virus batterici illustra bene il concetto. Il virus MS2 ha il genoma consistente in un RNA a singolo filamento, di poco più di tremilacinquecento nucleotidi, che agisce come un messaggio codificante tre geni con identica fase di lettura e un quarto, con diversa fase di lettura, sovrapposto tra il secondo e il terzo gene (Fig. 2). La tripletta di inizio del quarto gene è all'interno del secondo gene che codifica

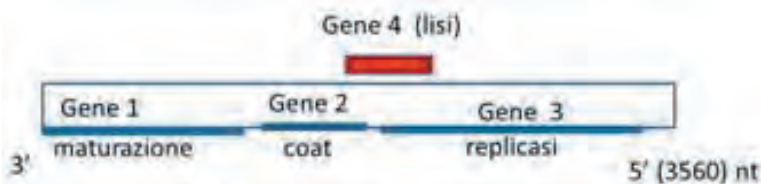


Figura 2 Schema del genoma del virus batterico MS2, consistente in un singolo filamento di RNA positivo (efficace come messaggio) con la posizione dei 4 geni codificati. La posizione del gene 4, della lis, è a cavallo del gene 2, della copertura, e del gene 3 della replicazione, con cornice di lettura +1 rispetto agli altri 3 geni. Il singolo filamento nella realtà è molto strutturato per formazione di regioni in doppia elica con conseguenze sulla regolazione della frequenza di traduzione dei singoli messaggi.

la proteina che forma la capsula del virus e che, quindi, deve essere tradotto circa cento volte per formare una capsula completa. Il quarto gene codifica un enzima che lisa la membrana della cellula batterica e, per questo, si deve esprimere solo dopo che un numero adeguato di virus completi si è formato all'interno di essa. Questo obiettivo è raggiunto rendendo la disponibilità della tripletta di inizio della sintesi proteica della quarta molecola dipendente dallo slittamento della fase di lettura del sistema di sintesi proteica operante sul secondo gene. La probabilità di questo tipo di errore è bassa ma diventa statisticamente sicurezza quando sono state prodotte diverse decine di capsule complete di virus. Quando ciò succede si deve produrre l'enzima che, lisando la membrana del batterio, permette l'uscita dei nuovi virus per la prosecuzione dell'infezione su altre cellule.

Nel genoma di eucarioti vi sono molti altri meccanismi di codifica che generano automaticamente l'espressione alternativa di particolari geni. Ne deriva che il genoma degli eucarioti non è solo DNA ma è formato da cromosomi diversi per numero, forma e organizzazione del DNA mediante proteine istoni. Questo è assolutamente fondamentale per il corretto controllo dell'espressione genica ed è soggetto a modulazione mediante modifiche chimiche degli istoni.

2.2 - Importanza della metilazione per l'ontogenesi e per il differenziamento cellulare

Un altro parametro di fondamentale importanza per i meccanismi epigenetici è quello della modifica chimica mediante metilazione del DNA genomico. Questa modifica fu scoperta negli anni cinquanta del secolo scorso (Chargaff et al., 1952) ma fu lo scienziato italiano Eduardo Scarano (Scarano et. al, 1965; Grippo et al., 1968) che dimostrò che la metilazione riguardava le citosine esclusivamente dei dinucleotidi CpG. La scoperta fu il risultato di una ricerca assolutamente all'avanguardia per i tempi, effettuata con metodi innovativi che identificarono la metilazione sul dinucleotide. Scarano ne previde il ruolo proponendo un meccanismo operativo mediante geni detti concertatori ma, poiché non ci fu prova dell'esistenza di tali geni, la scoperta non fu valorizzata per la sua giusta rilevanza per l'epigenetica. Successivamente risultò da innumerevoli studi che la metilazione delle C dei dinucleotidi CpG è alla base di molteplici meccanismi di grande rilevanza, come sarà chiaro con alcuni esempi riguardanti in particolare la fecondazione e lo sviluppo embrionale, che sono certamente importanti ma non esaustivi del ruolo.

2.3 - Importanza della metilazione per la fecondazione.

I dati riguardano esperimenti fatti sul topo ma sono rilevanti anche per l'uomo. Va ricordato che le cellule somatiche, quelle che compongono il corpo di un organismo, hanno il DNA genomico in doppia copia, una di origine materna e una paterna e sono dette diploidi. Le cellule gametiche, uovo e spermatozoo hanno una sola copia del DNA genomico, materna o paterna, e sono dette aploidi. Il DNA delle cellule gametiche femminili è tipicamente differente da quello maschile per la presenza di diverso stato di metilazione delle citosine di CpG di alcuni geni indispensabili per il positivo sviluppo a partire dall'uovo fecondato (zigote), dove il genoma maschile dello spermatozoo si aggiunge a quello femminile dell'uovo, costituendo la diploidia caratteristica delle cellule somatiche. La metilazione esistente sui geni dei gameti viene detta "imprinting" ed i geni relativi "imprinted" e ciò li rende diversamente espressi, uno sì e l'altro no. Un esempio illustra la loro funzione. Due geni, uno codifica un recettore e l'altro la molecola segnale, sono diversamente "imprinted" nelle cellule gametiche aploidi del maschio e della femmina con il risultato che, perché ci sia funzionalità, è necessaria la presenza di entrambi i cromosomi sia femminile sia maschile, in

quanto ognuno di essi esprime solo una parte del sistema. I tentativi di produrre un topo per stimolazione del solo ovolo (embrione partenogenetico), o per iniezione di un secondo genoma gametico femminile nell'ovolo (embrione ginogenetico) o inattivando il genoma femminile dell'ovolo ed iniettando due genomi gametici maschili (embrione androgenetico) sono falliti. Si avvia lo sviluppo dell'ovolo che possiede tutto quel che occorre per iniziare ma si ferma a stadi precoci e diversi nei tre casi. Una rappresentazione schematica del ciclo dell'imprinting genico è riportata in Fig.3. Ne risulta che la metilazione è essenziale per la produzione di uno zigote funzionale perché assicura che esso

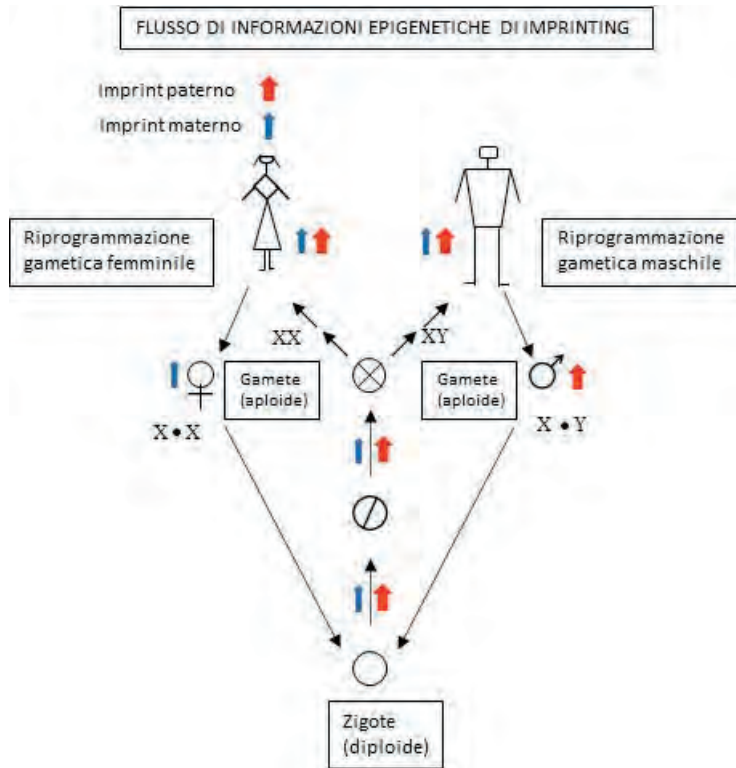


Figura 3 Ciclo dell'imprinting del DNA maschile e femminile nelle cellule somatiche e gametiche. Imprinting femminile con freccia blu, imprinting maschile con freccia rossa. Notare che nello zigote (uovo fecondato) vi sono entrambi i cromosomi femminile e maschile mentre nelle gonadi si riprogrammano di altro sesso per renderli imprinted entrambi o femminili o maschili, nei due casi.

sia prodotto dall'insieme dei cromosomi di una femmina e di un maschio. Va notato che il differenziamento della gonade femminile con il suo corredo di qualche centinaio di ovociti avviene già al terzo mese di sviluppo. Questo organo ha

il compito di alimentare e proteggere gli ovociti per evitare che il loro DNA possa essere esposto a mutazioni perché vi è un solo ovocita alla fecondazione, senza possibilità di selezione, come invece avviene per gli spermatozoi che sono centinaia di milioni di cui uno solo è selezionato. Per questo meccanismo non si devono permettere mutazioni nel DNA dell'uovo anche dopo 40 anni di esistenza. La cellula uovo è speciale per la sua capacità, esclusiva tra le cellule, di avere i componenti necessari per interpretare il corredo genico ed avviare la produzione di un nuovo esemplare della specie.

2.4 - Importanza della metilazione per lo sviluppo (ontogenesi).

Per illustrare l'importanza della metilazione per il corretto sviluppo embrionale si riportano i risultati, interpretabili visivamente, di esperimenti effettuati sullo sviluppo del riccio di mare, che è un'echinoderma considerato alla base della formazione dei vertebrati. Quella scelta fu dovuta alla possibilità di

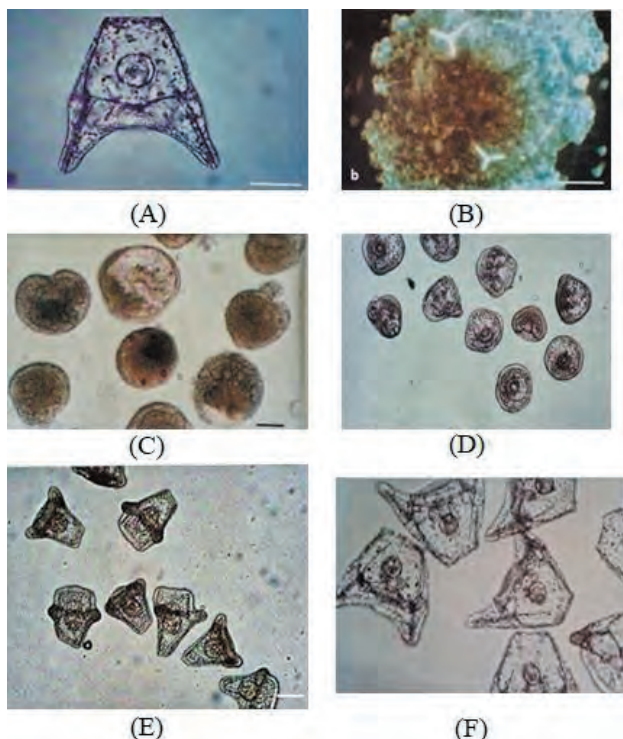


Figura 4 Foto al microscopio ottico di embrioni di riccio di mare a 41 ore di sviluppo normale e dopo esposizione a 50 nM 5AC (blocco della metilazione) in ciascuna delle iniziali 5 divisioni cellulari A, normale; trattati con 5AC tra : B 1 e 2 cellule; C, 2 e 4 cellule; D, 4 e 8 cellule; E, 8 e 16 cellule; F, tra 16 e 32 cellule.

operare su singole divisioni cellulari susseguenti alla fecondazione dell'uovo da parte di uno spermatozoo. Bloccando selettivamente la metilazione del DNA solo durante ognuna delle iniziali divisioni cellulari, successive alla fecondazione ed osservando gli effetti sullo sviluppo dell'embrione, fu possibile definire il ruolo della metilazione nel controllo dell'espressione di alcuni geni e nella formazione delle strutture fisiche che caratterizzano l'embrione più avanzato.

Con l'embrione del riccio di mare l'avvenuta fecondazione è facilmente visibile a causa del sollevamento istantaneo, intorno all'uovo fecondato, di una membrana che impedisce ad altri spermatozoi di entrare dopo l'ingresso del primo. Anche le successive divisioni cellulari sono ben visibili e sincrone nella popolazione di embrioni, permettendo di operare selettivamente durante ognuna di esse.

I risultati, che sono riportati in Fig. 4, mostrano le conseguenze del blocco della metilazione del DNA in ogni singola divisione cellulare.

Si rileva che la metilazione è una attività precoce nello sviluppo embrionario perché avviene ed ha effetto solo nelle prime quattro divisioni cellulari successive alla fecondazione mostrando che in ognuna di esse si programmano diverse strutture dell'embrione a livello di sviluppo di pluteo, che è lo stadio fino al quale è facile mantenere in coltura quell'embrione. Gli effetti di maggior impatto avvengono per blocco della metilazione nelle prime due divisioni cellulari in cui la separazione in due cellule avviene da un polo all'altro dell'uovo producendo cellule assolutamente equivalenti per distribuzione dei materiali presenti. Da notare che dopo la quarta divisione cellulare il blocco della metilazione non ha più alcun effetto sul corretto sviluppo dell'embrione. Quello che doveva stabilirsi è stato stabilito e non dipende più dalla metilazione. È da notare che il blocco della metilazione del DNA non provoca la morte delle cellule ma ha effetti sul loro fenotipo futuro.

La presenza di meccanismi che programmano nelle cellule embrionali quello che sarà il loro differenziamento futuro è dimostrata anche nello sviluppo del moscerino *Drosophila melanogaster* (Fig.5).

In figura è riportato uno schema della larva del moscerino in cui sono evidenziati con falsi colori dei gruppi di cellule embrionali detti dischi immaginali. Da ognuno di essi si forma, negli stadi successivi, una struttura diversa di quell'insetto: zampa, antenna, bilanciere o altra. Se si sposta un gruppetto di quelle cellule immaginali dalla sua posizione ad un'altra diversa, da esso si svilupperà sempre la struttura prevista ma nella nuova posizione. Per esempio, al posto del bilanciere si potrà far generare una zampa. Sono stati prodotti moscerini con tali anomalie. Questo conferma i risultati sullo sviluppo dell'embrione di riccio di mare che mostravano che, quando una cellula embrionale è stata orientata per il suo differenziamento, esso avverrà nelle divisioni cellulari successive quando altri segnali lo stimoleranno.

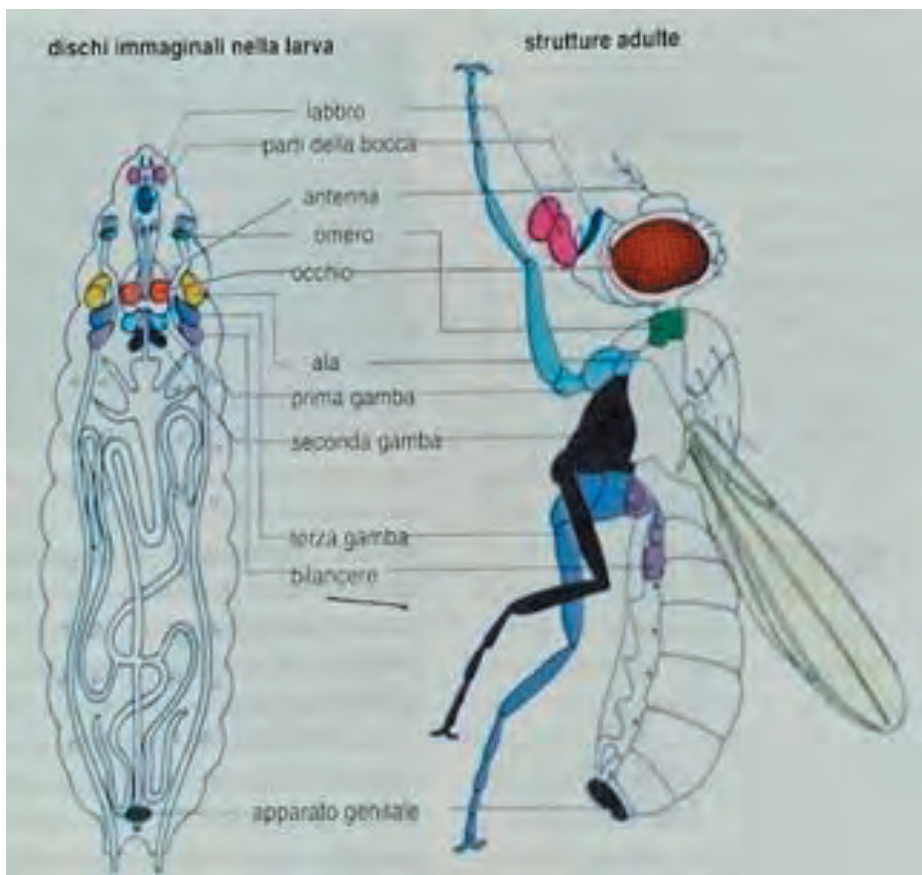


Figura 5 Schema della larva e dell'adulto del moscerino *Drosophila melanogaster*. Sono evidenziati con falsi colori gruppi di cellule della larva, che generano nell'adulto varie parti come indicato. I gruppi di cellule sono dette immaginali e sono di tipo embrionale. Non cambiano il loro prodotto se spostate dal luogo di origine in un altro, dimostrando stabilità della loro espressione.

2.5 - Effetti sul differenziamento dipendenti da azioni diverse.

Il ruolo rilevante della metilazione e demetilazione per il differenziamento cellulare è stato messo in evidenza in esperimenti su cellule di carcinoma del colon CaCO2 (Di Giaimo et al., 2005). Queste cellule quando sono coltivate in sospensione in una fiaschetta sono perenni, nel senso che si duplicano producendo cellule tumorali. Se invece sono coltivate in monostrato, su una superficie nutritiva, quando duplicandosi arrivano in contatto tra loro si differenziano in enterociti. Durante il loro differenziamento si rileva chiaramente l'alternarsi delle attività di metilazione e demetilazione stimolate, però, dal contatto tra cellule. Questo è, ovviamente un altro meccanismo epigenetico.

Una azione post-genetica ben documentata sull'espressione genica, ma ancora in corso di maggiore definizione, è causata da piccole sequenze di RNA dette miRNA e ceRNA. Queste molecole possono bloccare gli effetti dell'espressione di geni inibendo la traduzione dei loro mRNA. Effetti drammatici sullo sviluppo possono avvenire anche non agendo sul DNA se il prodotto di un gene non è immediatamente l'effettore ma avvia una catena di trasmissione di segnali, il cui componente finale esplica la funzione prevista. Molecole che interferiscono con tali meccanismi sono dette teratogene perché causano anomalie. Un esempio di tali effetti si è verificato col caso della talidomide, una molecola assolutamente innocua su individui adulti, con nessuna azione a livello del DNA e con notevole azione tranquillante, per cui venne prescritta a gestanti per eliminare le sensazioni di disagio tipiche dei primi tempi di gravidanza. Negli anni sessanta del secolo scorso quel medicinale fu tolto dalla distribuzione perché aveva prodotto i tragici effetti teratogeni della focomelia, con alterazione di meccanismi di sviluppo di varia natura, tra i quali il più evidente consistente nella interferenza con la formazione degli arti. Quella molecola era un inibitore della sintesi di fattori trascrizionali la cui carenza aveva conseguenze diverse sullo sviluppo. Casi simili non dipendono dalla interferenza con i meccanismi epigenetici, sempre positivi, ma dalla interferenza con attuazione dei loro segnali.

2.6 - Epigenetica, evoluzione e sviluppo

Da quanto sopra esposto risulta evidente che l'epigenetica riguarda una problematica divenuta attuale quando è aumentata la complessità genetica anche solo in termini di quantità di DNA genomico. L'organizzazione strutturale dei batteri, che è la forma di vita più evoluta dal punto di vista della capacità di esistere sulla Terra in condizioni climatiche e ambientali molto problematiche, è descrivibile in termini di meccanismi genetici locali e non richiede meccanismi epigenetici per generare il proprio ciclo vitale. L'epigenetica diviene necessaria per produrre da un unico genoma cellule con strutture e capacità funzionali peculiari e diverse. Tali cellule sono apparse quando il principio inderogabile dell'economia genetica è stato abbandonato (i batteri lo hanno conservato per 4 miliardi di anni), rinunciando all'efficienza adattativa per acquisire la possibilità di generare più ampie caratteristiche funzionali. Questo ha richiesto che l'informazione genetica fosse ridondante. In un grafico che riporta la correlazione tra livello di complessità di un organismo e il numero di coppie di basi del DNA genomico, si osserva una correlazione lineare fino ad un certo punto della complessità strutturale oltre il quale la correlazione si perde. Vero-similmente perché la quantità di DNA non costituisce più il limite alle invenzioni. In questa ottica si distingue tra adattamento e sue conseguenze ed evoluzione. La capacità di adattamento (evoluzione Darwiniana) non richiede che il DNA genomico sia ridondante. La sua azione è continua in continua risposta a condizioni ambientali variabili, che privilegiano le modifiche. La capacità adattativa dei batteri lo dimostra ed ancora di più quelle

dei virus, di cui si ha esperienza diretta. Viceversa, l'evoluzione rappresenta la comparsa di caratteristiche nuove e aggiuntive a quelle precedenti, non prevedibili e inaspettate che compaiano improvvisamente in nuovi organismi con caratteristiche innovative. Per questo motivo l'evoluzione è per sua natura non continua ma episodica nel tempo e per questo detta punteggiata (Grassè, 1978). Per ottenere ciò è necessario che il DNA genomico sia ridondante in modo che le sequenze aggiuntive non siano pregiudizievoli per l'esistenza e costituiscano un compartimento in cui poter accumulare e sperimentare novità senza pregiudizio per la vita. L'epigenetica rappresenta i meccanismi genetici elaboratisi nel tempo che hanno permesso alle novità, formatesi anche loro nel tempo, di trasferirsi dal compartimento del DNA ridondante a quello del DNA operativo.

3 – BIBLIOGRAFIA

- Chargaff, E., Lipshitz, R. and Green, C. (1952), J. Biol. Chem: **195**, 155
Scarano E., Iaccarino M., Grippo P. and Winkelmans D. (1965), J. Mol. Biol. **14**, 603
Grippo P., Iaccarino M., Parisi E and Scarano E. (1968), J. Mol. Biol., **36**, 195
Branno M., Aniello F., Lancieri M., Fucci L. and Geraci G., (1993), J. Submicrosc. Cytol. Path. **25**, 19-27
Di Giaimo R., et al., (2005), Gene **351**, 73-81
Grassè Pierre-P. L'evoluzione del vivente, (1978), pag.54 e seguenti. Adelphi Ed. Milano

PARTE B
Scienze Matematiche

Approximate Computation of the Solutions of Systems of Linear Equations

Nota di Gianfranco Cimmino¹

Presentata dal socio Carlo Sbordone
(Adunanza del 18 febbraio 2022)

Prof. Gianfranco Cimmino can be considered, among other things, one of the founders of the Istituto per le Applicazioni del Calcolo, to which he lent his continuing and productive assistance during the embryonal stages of the Institute itself, in Naples, in the laboratory annexed to that university's Calculus chair, from 1928-VI to 1932-X. Towards the end of that period Prof. Cimmino devised a numerical method for the approximate solution of systems of linear equations that he reminded me of in these days, following the recent publication by Dr. Cesari (cfr. "Ricerca Scientifica", Serie II, Vol. I, n. 11-12, and "Rassegna delle Poste, dei Telegrafi e dei Telefoni", issue 4, 1937) which provides a systematic treatment of the above mentioned computing methods which, however, does not consider the one by Cimmino, a method which, in my opinion, is most worthy of consideration in the applications because of its generality, its efficiency and, finally, because of its guaranteed convergence which can make the method practicable in many cases. Therefore, I consider it useful to publish in this journal Prof. Cimmino's note on the above mentioned method, note that he has accepted to write upon my insistent invitation.

MAURO PICONE

1 - SETTING UP THE APPROXIMATIONS

Let the system of linear equations

$$(1) \quad \sum_{k=1}^n a_{hk} x_k = b_h, \quad (h = 1, 2, \dots, n),$$

¹English translation by Michele Benzi of G. Cimmino, *Calcolo approssimato delle soluzioni dei sistemi di equazioni lineari*, La Ricerca Scientifica, Serie II (9), 1938, pp. 326–333. Michele Benzi: Classe di Scienze, Scuola Normale Superiore, Piazza dei Cavalieri 7, 56126 Pisa, Italy. Email: michele.benzi@sns.it

be given. We think of (1) as the equations of n hyperplanes in S_n . In order to determine a point $O \equiv \xi_k$ common to them, we establish the following successive approximations. Taken, as first approximation, an arbitrary point $P_0 \equiv x_k^{(0)}$ in S_n , let us consider its symmetrical with respect to the hyperplane (1), for $h = 1, 2, \dots, n$.

$$(2) \quad x_k^{(0)} - 2a_{hk} \frac{\sum_{i=1}^n a_{hi}x_i^{(0)} - b_h}{\sum_{i=1}^n a_{hi}^2}, \quad (h = 1, 2, \dots, n).$$

Next, let us fix n arbitrary positive quantities m_1, m_2, \dots, m_n and let us take, as second approximation $P_1 \equiv x_k^{(1)}$, the center of mass of the system formed by the n masses m_k placed respectively at the n points (2)

$$(3) \quad x_k^{(1)} = x_k^{(0)} - \frac{2}{\sum_{h=1}^n m_h} \sum_{h=1}^n m_h a_{hk} \frac{\sum_{i=1}^n a_{hi}x_i^{(0)} - b_h}{\sum_{i=1}^n a_{hi}^2}, \quad (k = 1, 2, \dots, n),$$

In general, let us consider the successive approximations

$$(4) \quad x_k^{(v)} = x_k^{(v-1)} - \frac{2}{\sum_{h=1}^n m_h} \sum_{h=1}^n m_h a_{hk} \frac{\sum_{i=1}^n a_{hi}x_i^{(v-1)} - b_h}{\sum_{i=1}^n a_{hi}^2}, \quad (k = 1, 2, \dots, n),$$

which are suggested by the simple observation that, if the hyperplanes (1) have a point $O \equiv \xi_k$ in common, the point P_0 and the n symmetrical ones (2) will all lie on the same hypersphere with center in O , so that the point P_1 given by (3) must fall inside this hypersphere, that is, it must be at a distance from the desired point O less than the starting point P_0 , and likewise the point P_v given by (4) will be closer and closer to O .

2 - THE CONSISTENT CASE

If system (1) is consistent and the rank of the matrix $\|a_{hk}\|$ is greater than one, the $x_k^{(v)}$ converge, for $v \rightarrow \infty$, towards a solution of the system.

Let us note first of all that the condition that the matrix $\|a_{hk}\|$ have rank greater than one is evidently necessary, for if all the hyperplanes (1) coincide with a single one, our successive approximations will alternately yield the starting point P_0 and its symmetrical with respect to that hyperplane.

Let now $O \equiv \xi_k$ be a point, solution of the system (1). Then (4) can be written as

$$(5) \quad x_k^{(v)} - \xi_k = x_k^{(v-1)} - \xi_k - \frac{2}{\sum_{h=1}^n m_h} \sum_{h=1}^n m_h a_{hk} \frac{\sum_{i=1}^n a_{hi} (x_i^{(v-1)} - \xi_i)}{\sum_{i=1}^n a_{hi}^2}.$$

Squaring and summing over k from 1 to n , then letting

$$(6) \quad \chi_k = \frac{\sum_{i=1}^n a_{ki} (x_i^{(v-1)} - \xi_i)}{\sqrt{\sum_{i=1}^n a_{ki}^2}}, \quad \theta_{hl} = \frac{\sum_{i=1}^n a_{hi} a_{li}}{\sqrt{\sum_{i=1}^n a_{hi}^2} \sqrt{\sum_{l=1}^n a_{li}^2}},$$

we obtain

$$(7) \quad \begin{aligned} \overline{OP}_v^2 &= \sum_{k=1}^n (x_k^{(v)} - \xi_k)^2 = \sum_{k=1}^n (x_k^{(v-1)} - \xi_k)^2 - \\ &\quad - \frac{4}{\sum_{h=1}^n m_h} \sum_{k=1}^n (x_k^{(v-1)} - \xi_k) \sum_{h=1}^n m_h a_{hk} \frac{\sum_{i=1}^n a_{hi} (x_i^{(v-1)} - \xi_i)}{\sum_{i=1}^n a_{hi}^2} + \\ &\quad + \frac{4}{\left(\sum_{h=1}^n m_h\right)^2} \sum_{k=1}^n \sum_{h=1}^n m_h a_{hk} \frac{\sum_{i=1}^n a_{hi} (x_i^{(v-1)} - \xi_i)}{\sum_{i=1}^n a_{hi}^2} \\ &\quad - \sum_{\ell=1}^n m_\ell a_{\ell k} \frac{\sum_{i=1}^n a_{li} (x_i^{(v-1)} - \xi_i)}{\sum_{i=1}^n a_{li}^2} = \\ &= \overline{OP}_{v-1}^2 - \frac{2}{\left(\sum_{h=1}^n m_h\right)^2} \sum_{h=1}^n \sum_{\ell=1}^n m_h m_\ell (\chi_h^2 + \chi_\ell^2 - 2 \theta_{h\ell} \chi_h \chi_\ell), \end{aligned}$$

whence, since the m_k are positive by assumption and $|\theta_{h\ell}| \leq 1$ by virtue of a well known inequality, one deduces that

$$(8) \quad \overline{OP}_v^2 \leq \overline{OP}_{v-1}^2,$$

as indeed expected, in view of the earlier geometrical considerations.

Let us now find out when in (8) the equal sign may occur. First of all, since clearly

$$(9) \quad \chi_h^2 + \chi_\ell^2 - 2 \theta_{h\ell} \chi_h \chi_\ell \geq (|\chi_h| - |\chi_\ell|)^2$$

it will be necessary that $|\chi_k|$ be independent of k . Denoting its value by c , from (7) we have that

$$(10) \quad \overline{OP}_v^2 \leq \overline{OP}_{v-1}^2 - \frac{4c^2}{\left(\sum_{h=1}^n m_h\right)^2} \sum_{h=1}^n \sum_{\ell=1}^n (1 - |\theta_{h\ell}|) m_h m_\ell.$$

But $|\theta_{h\ell}|$ can be = 1 only if the $a_{h1}, a_{h2}, \dots, a_{hn}$ are proportional to the $a_{\ell 1}, a_{\ell 2}, \dots, a_{\ell n}$ and this cannot happen for every pair of indices h, ℓ since the matrix $\|a_{hk}\|$ was assumed to have rank > 1 . Therefore, in order for the $=$ sign to obtain in (8), it is necessary that all the χ_k be zero, that is, the $x_i^{(v-1)}$, like the ξ_i , must satisfy the system (1), and consequently, due to (4), the $x_i^{(v)}$ must coincide with the $x_i^{(v-1)}$.

Therefore, excluding the case where, after a finite number of approximations, a solution to the system has been found (in which case all the subsequent approximations coincide with such solution), expression (8) holds, with the $<$ sign, for all values of v .

In view of this, since all the points P_v fall inside the sphere of center O and radius \overline{OP}_0 , this set of all such points certainly admits an accumulation point $P \equiv x_k$. If we denote by P_{v_s-1} ($s = 1, 2, \dots$) a subsequence of the sequence P_v that converges to the point $P \equiv x_k$, the points P_{v_s} ($s = 1, 2, \dots$) will also converge, owing to (5), and precisely towards the point $P^* \equiv x_k^*$ defined by

$$(11) \quad x_k^* - \xi_k = x_k - \xi_k - \frac{2}{\sum_{h=1}^n m_h} \sum_{h=1}^n m_h a_{hk} \frac{\sum_{i=1}^n a_{hi} (x_i - \xi_i)}{\sum_{i=1}^n a_{hi}^2},$$

Arguing about (11) as we did earlier about (5) we see that, if x_k were not a solution of the system (1), it would be $\overline{OP}^* < \overline{OP}$ and therefore, as soon as r and s are large enough, it would also be $\overline{OP}_{v_r} < \overline{OP}_{v_s-1}$, since $P_{v_r} \rightarrow P^*$, $P_{v_s-1} \rightarrow P$. But this is impossible, since when $r = s - 1$ we have $v_r = v_{s-1} \leq v_s - 1$, and thus $\overline{OP}_{v_r} \geq \overline{OP}_{v_s-1}$, due to (8).

Therefore $P \equiv x_k$ is necessarily a solution of system (1). And therefore, given what we proved, the distance \overline{PP}_v will be decreasing as v increases; and since we know that there is a subsequence of that of the points P_v which has P as its limit, we conclude that P is also the unique limit of the sequence of points P_v .

3 - THE INCONSISTENT CASE

The successive approximations (4) converge even when the system is not consistent, provided that the rank of $\|a_{hk}\|$ be > 1 .

This follows from the observation that for the argument of the previous section to hold it is not necessary that the point $O \equiv \xi_k$ be a solution of the system (1),

rather, it suffices that

$$(12) \quad \sum_{h=1}^n m_h a_{hk} \frac{\sum_{i=1}^n a_{hi} \xi_i - b_h}{\sum_{i=1}^n a_{hi}^2} = 0, \quad (k = 1, 2, \dots, n);$$

presently we will show that this system always admits a solution, even when the (1) are inconsistent.

Let us therefore suppose that the determinant $A = |a_{hk}|$ be equal to zero and that the minor A_p formed by the first p rows and p columns be nonzero. Then there exist numbers λ_{ij} ($i = 1, 2, \dots, n-p$; $j = 1, 2, \dots, p$), such that

$$(13) \quad a_{hk} = \sum_{j=1}^p \lambda_{k-p,j} a_{hj}, \quad (h = 1, 2, \dots, n; k = p+1, p+2, \dots, n),$$

and moreover, the last $n-p$ of the equations (12) are a consequence of the first p .

Let us therefore consider (12) only for $k = 1, 2, \dots, p$ and substitute in place of the a_{hk} with $k > p$ the summation (13). Introducing further the unknowns σ_h defined by

$$(14) \quad \sigma_h = x_h + \sum_{i=1}^{n-p} \lambda_{ih} x_{p+i}, \quad (h = 1, 2, \dots, p),$$

the system (12) becomes

$$(15) \quad \sum_{h=1}^n m_h a_{hk} \frac{\sum_{j=1}^n a_{hj} \sigma_j - b_h}{\sum_{i=1}^n a_{hi}^2} = 0, \quad (k = 1, 2, \dots, p).$$

This, regarded as a system of p equations in the p unknowns σ_j , is certainly solvable, because the determinant formed with the coefficients is

$$\prod_{h=1}^n \frac{m_h}{\sum_{i=1}^n a_{hi}^2} \begin{vmatrix} a_{11} & \dots & a_{n1} \\ \dots & \dots & \dots \\ a_{1p} & \dots & a_{np} \end{vmatrix}^2,$$

and thus positive, being, by hypothesis, $A_p \neq 0$.

Having obtained the σ_j from (15), let us try to determine p quantities t_1, t_2, \dots, t_p in such a way that the x_h defined by

$$(16) \quad x_h = x_h^{(0)} + \sum_{k=1}^p a_{kh} t_k, \quad (h = 1, 2, \dots, n),$$

substituted for the ξ_h in (12), satisfy (12). In order for this to happen, being the σ_h solutions of (15), it suffices that (14) holds true. Now (14), by (16) and (13),

becomes

$$(17) \quad \begin{aligned} \sigma_h &= x_h^{(0)} + \sum_{k=1}^p a_{kh} t_k + \sum_{i=1}^{n-p} \lambda_{ih} \sum_{k=1}^p a_{k,p+i} t_k + \sum_{i=1}^{n-p} \lambda_{ih} x_{p+i}^{(0)} = \\ &= x_h^{(0)} + \sum_{k=1}^p a_{kh} t_k + \sum_{i=1}^{n-p} \lambda_{ih} \sum_{k=1}^p \sum_{j=1}^p \lambda_{ij} a_{kj} t_k + \sum_{i=1}^{n-p} \lambda_{ih} x_{p+i}^{(0)}, \\ &\quad (h = 1, 2, \dots, p), \end{aligned}$$

and this is a system of p equations in the p unknowns t_k , with determinant

$$\begin{aligned} |a_{kh} + \sum_{i=1}^{n-p} \sum_{j=1}^p \lambda_{ih} \lambda_{ij} a_{kj}| &= |a_{kj}| \cdot |\delta_{jh} + \sum_{i=1}^{n-p} \lambda_{ij} \lambda_{ih}|, \\ \left(h, k, j = 1, 2, \dots, p; \quad \delta_{jh} \begin{cases} = 0 & \text{if } j \neq h \\ = 1, & \text{if } j = h \end{cases} \right), \end{aligned}$$

which is certainly different from zero.

4 - ERROR BOUND

Let us now suppose that the determinant $A = |a_{hk}|$ be nonzero, and show how one can easily obtain an upper bound on the error committed at the v -th approximation relative to the initial error.

Let us consider again (7), observing that since we have now a unique solution to the system (1), the expression

$$(18) \quad \frac{2}{\left(\sum_{h=1}^n m_h\right)^2} \sum_{h=1}^n \sum_{\ell=1}^n m_h m_\ell (\chi_h^2 + \chi_\ell^2 - 2 \theta_{h\ell} \chi_h \chi_\ell),$$

can vanish only provided that all the differences $x_k^{(v-1)} - \xi_k$ are zero. Therefore (18) is a positive definite quadratic form in the $x_k^{(v-1)} - \xi_k$. Denoting by ρ its smallest characteristic root, we will then have, because of (17),

$$(19) \quad \overline{OP}_v^2 \leq (1 - \rho) \overline{OP}_{v-1}^2 \leq (1 - \rho)^v \overline{OP}_0^2.$$

In the same manner one finds that

$$(20) \quad \overline{P_v P_{v-1}}^2 \leq (1 - \rho) \overline{P_{v-1} P_{v-2}}^2,$$

whence, more directly than in §2, but under the restrictive assumption $|A| \neq 0$, the convergence of the sequence of points P_v follows.

5 - EXTENSION TO INTEGRAL EQUATIONS

The formal extension of the method of successive approximations of section 1 to the case of an integral equation of the first kind is immediate. Given the equation

$$(21) \quad \int_a^b A(x, y) \varphi(y) dy = f(x),$$

starting from a function $\varphi_0(x)$, arbitrarily chosen as first approximation, and denoting by $m(x)$ a weight function everywhere positive, we let

$$(22) \quad \begin{aligned} \varphi_v(x) &= \varphi_{v-1}(x) - \\ &- \frac{2}{\int_a^b m(s) ds} \int_a^b m(s) A(s, x) \frac{\int_a^b A(s, t) \varphi_{v-1}(t) dt - f(s)}{\int_a^b A^2(s, t) dt} ds. \end{aligned}$$

Assuming the existence of a solution $g(x)$ of (21) and letting, in analogy to (6),

$$\chi(s) = \frac{\int_a^b A(s, t) [\varphi_{v-1}(t) - g(t)] dt}{\sqrt{\int_a^b A^2(s, t) dt}},$$

$$\theta(r, s) = \frac{\int_a^b A(r, x) A(s, x) dx}{\sqrt{\int_a^b A^2(r, t) dt} \sqrt{\int_a^b A^2(s, t) dt}},$$

one finds

$$\begin{aligned} \int_a^b [\varphi_v(x) - g(x)]^2 dx &= \int_a^b [\varphi_{v-1}(x) - g(x)]^2 dx - \\ &- \frac{2}{\left(\int_a^b m(s) ds\right)^2} \int_a^b \int_a^b m(r) m(s) [\chi^2(r) + \chi^2(s) - 2\theta(r, s)\chi(r)\chi(s)] dr ds, \end{aligned}$$

where, if $A(x, y)$ is not the product of a function of x only times a function of y only, the double integral can vanish only provided that $\chi(s)$ is identically zero, and if, more particularly, the kernel $A(x, y)$ is closed, it can vanish only if $\varphi_{v-1}(t) - g(t) \equiv 0$.

It follows, under the latter assumption, that the symmetric kernel

$$\begin{aligned} &\frac{2}{\left(\int_a^b m(t) dt\right)^2} \int_a^b \int_a^b m(r) m(s) \left[\frac{A(r, x) A(r, y)}{\int_a^b A^2(r, t) dt} + \right. \\ &\left. + \frac{A(s, x) A(s, y)}{\int_a^b A^2(s, t) dt} - 2\theta(r, s) \frac{A(r, x) A(s, y)}{\sqrt{\int_a^b A^2(r, t) dt} \sqrt{\int_a^b A^2(s, t) dt}} \right] dr ds \end{aligned}$$

is positive definite and, denoted by ρ its smallest eigenvalue, one has (analogously to (20))

$$\int_a^b [\varphi_v(x) - \varphi_{v-1}(x)]^2 dx \leq (1 - \rho) \int_a^b [\varphi_{v-1}(x) - \varphi_{v-2}(x)]^2 dx,$$

from which it follows in every case the convergence in mean of the $\varphi_v(x)$, and moreover (analogously to (19))

$$\int_a^b [\varphi_v(x) - g(x)]^2 dx \leq (1 - \rho)^v \int_a^b [\varphi_0(x) - g(x)]^2 dx.$$

from which one obtains, assuming the existence of the solution $g(x)$, that the $\varphi_v(x)$ will indeed converge in mean to it,

TRANSLATOR's NOTE

In translating Cimmino's note I have strived to remain as close as possible to the original text, down to the formatting of the equations. Apart from correcting a few obvious typos, I have only departed (slightly) from the original in the numbering of the formulas.

Cimmino's notation is essentially the one still in use today. One exception is the use of the symbol S_n instead of \mathbb{R}^n . The modern reader may find the last displayed formula after equation (15) puzzling. The symbol

$$\left\| \begin{array}{ccc} a_{11}, & \dots, & a_{n1} \\ \dots & \dots & \dots \\ a_{1p}, & \dots, & a_{np} \end{array} \right\|^2,$$

stands for the determinant of the $p \times p$ matrix BB^T , where

$$B = \begin{bmatrix} a_{11}, & \dots, & a_{n1} \\ \dots & \dots & \dots \\ a_{1p}, & \dots, & a_{np} \end{bmatrix}.$$

Finally, I note that Cimmino uses the term *radice caratteristica* for the quantity ρ in section 4, and *autovalore* for the analogous quantity in section 5. I have kept the distinction and used the terms *characteristic root* and *eigenvalue*, respectively, in my translation.

Michele Benzi, Pisa, 24 gennaio 2022.

Gianfranco Cimmino's Contributions to Numerical Mathematics

Nota di Michele Benzi¹

Presentata dal socio Carlo Sbordone
(Adunanza del 18 febbraio 2022)

Keywords: Numerical analysis, Cimmino's method

Abstract – Gianfranco Cimmino (1908-1989) authored several papers in the field of numerical analysis, and particularly in the area of matrix computations. His most important contribution in this field is the iterative method for solving linear algebraic systems that bears his name, published in 1938. This paper reviews Cimmino's main contributions to numerical mathematics, together with subsequent developments inspired by his work. Some background information on Italian mathematics and on Mauro Picone's *Istituto Nazionale per le Applicazioni del Calcolo*, where Cimmino's early numerical work took place, is provided. The lasting importance of Cimmino's work for solving a wide variety of problems in different areas of Science, Engineering and Medicine is demonstrated by analyzing his citations in the technical and scientific literature.

Riassunto – Gianfranco Cimmino (1908-1989) fu autore di diversi lavori nel campo dell'analisi numerica, in particolare relativi a problemi di calcolo matriciale. Il suo maggiore contributo in questo settore è il metodo iterativo per la risoluzione di sistemi lineari algebrici che porta il suo nome, pubblicato nel 1938. Il presente lavoro passa in rassegna i principali contributi di Cimmino alla matematica numerica, insieme ad alcuni degli sviluppi successivi ispirati dal suo lavoro. L'articolo fornisce informazioni sul contesto matematico italiano dell'epoca e sull'*Istituto Nazionale per le Applicazioni del Calcolo* diretto da Mauro Picone, dove vissero la luce i primi contributi di Cimmino all'analisi numerica. La perdurante influenza del lavoro di Cimmino sulla soluzione di un'ampia gamma di problemi in diversi settori scientifici e tecnici e in campo medico è illustrata da un'analisi delle sue citazioni nella letteratura scientifica.

¹Classe di Scienze, Scuola Normale Superiore, Piazza dei Cavalieri 7, 56126 Pisa, Italy. Email: michele.benzi@sns.it

1 - INTRODUCTION

Gianfranco Cimmino was a distinguished Italian mathematician who made notable contributions to the theory of partial differential equations and to other branches of mathematical analysis. Side-by-side with his main research area, Cimmino cultivated other mathematical interests, including numerical analysis. Under the influence of his teacher, Mauro Picone (1885-1977), Cimmino developed an early interest in numerical questions, some of which he will repeatedly revisit in the course of his long career. Outstanding among his contributions is an elegant iterative method for the solution of linear algebraic systems. This method was published in 1938 and is widely known as "Cimmino's method." As we shall see, this algorithm has withstood the test of time and is still widely used, albeit in modified form, in a wide variety of scientific and technical applications.

This paper surveys Cimmino's contributions to numerical mathematics and describes some of the circumstances that led him to work in this area. In order to do so, it is necessary to take a quick look at certain aspects of numerical analysis in the early decades of the 20th century. In particular, Italy's rather exceptional role in this arena, due to Mauro Picone's *Istituto Nazionale per le Applicazioni del Calcolo* (INAC), will be highlighted.

The paper is organized as follows. Section 2 contains a brief overview of Cimmino's career and scientific production. Section 3 is devoted to Mauro Picone and the INAC. Section 4 addresses the status of pre-WWII numerical analysis and discusses some early work in numerical linear algebra, with particular attention to work done at the INAC in the Thirties. Cimmino's method of 1938 is the subject of section 5, while later developments by Cimmino himself and by other researchers are discussed in section 6. The lasting influence of Cimmino's work in scientific computing is assessed in section 7, using in part citation data. Some general reflections on Cimmino's numerical work are given in section 8, which concludes the paper.

2 - A BRIEF OVERVIEW OF CIMMINO'S CAREER

Gianfranco Cimmino was born in Naples on March 12, 1908. His father, Francesco, was a renowned Orientalist and Sanskrit scholar. His mother belonged to an aristocratic family from Novara (in the North of Italy), the Gibellini Tornielli Boniperti. Cimmino died in Bologna on May 30, 1989.

After receiving his *Laurea* degree in Mathematics at the University of Naples under Mauro Picone in 1927 (at age 19), Cimmino became Picone's assistant in Analytic Geometry in 1928. *Libero docente* in 1931, he was in charge of the courses of Higher Analysis and Analytic Geometry until 1938, when he won the chair of Mathematical Analysis at the University of Cagliari, in Sardinia. At the end of 1939 he moved permanently to the University of Bologna to occupy the chair of Mathematical Analysis. In the course of his long career, Cimmino was awarded a number of prestigious awards and distinctions (Pini, 1991). In

addition, he was called to occupy leadership positions both at the University of Bologna (where he served as Dean of the Science Faculty for several years) and in the Italian mathematical community (INdAM and UMI).

Cimmino's scientific production, covering a period of nearly 60 years, consists of seven books (mostly lecture notes for his courses), fifty-six papers, and several additional minor works, including obituaries and writings devoted to the popularization of certain aspects of mathematics. The latter include the text of a talk on *Dante and Mathematics*, which shows Cimmino's broad cultural interests. Cimmino's scientific papers are written in Italian, German, French and English. Furthermore, Cimmino authored hundreds of reviews for the *Zentralblatt für Mathematik*, most of them in German.

Cimmino's first paper, 24 pages long, appeared in 1928; his last paper is a note of 4 pages for the proceedings of the *Accademia dei Lincei*, published posthumously in 1990. None of Cimmino's publications are in collaboration with others. With the exception of two "dry spells" (in 1943-1947, obviously due to the War and its immediate aftermath, and again in 1976-1981 due to the consequences of a serious car accident), Cimmino's scientific output appears to have been remarkably steady, even during his term as Dean of the Faculty of Science. The most fruitful years in Cimmino's career are those from 1937 to 1939, with nine papers, including some truly remarkable ones. Furthermore, there are eight publications from 1982 until his death.

A majority of Cimmino's papers concern the theory of linear partial differential equations, in which he obtained important results. Other topics treated by Cimmino include:

- Two-point boundary value problems for ordinary differential equations;
- Infinite systems of linear differential and integral (Fredholm) equations in infinitely many unknowns;
- The calculus of variations;
- Differential geometry;
- Conformal and quasi-conformal mappings;
- Topological vector spaces;
- The theory of (ultra-)distributions;
- Numerical analysis, especially matrix computations.

Cimmino's publications in numerical analysis amount to 5-6 short papers, which will be discussed below. Some of Cimmino's most remarkable papers date to the period 1937-1938 and concern the theory of partial differential equations of elliptic type. In particular, Cimmino was the first mathematician to study the *Dirichlet problem with generalized boundary conditions* (Cimmino, 1937, 1940). In this problem one considers Laplace's equation $\Delta u = 0$ (or Poisson's, $\Delta u = f$) on a bounded domain $\Omega \subset \mathbb{R}^n$ with sufficiently smooth boundary Γ , subject to the condition that the trace of u on Γ is a prescribed function $g \in L^2(\Gamma)$; see, e.g., (Miranda, 1970, Chapter IV). Cimmino will revisit this topic several times in the

subsequent decades, achieving various generalizations and improvements of his original results from this period. Incidentally, this problem was found many years later to be of central importance in optimal control theory; see (Lions and Magenes, 1972, page vi). For detailed information on Cimmino's work in analysis and partial differential equations (PDEs), we refer the reader to (Pini, 1991).

3 - MAURO PICONE AND THE INAC

Gianfranco Cimmino was one of Picone's first students, together with Giuseppe Scorza Dragoni (1908-1996) and Carlo Miranda (1912-1982). The star of this group was Renato Caccioppoli (1905-1959) who, while not formally a student of Picone's (having received his degree under Ernesto Pascal in 1925), may well be considered a member of his school (Sbordone, 2004). All four members of this remarkable group were bound by a strong sense of camaraderie and friendship (Scorza Dragoni, 1991). Picone's Neapolitan period goes from 1925 until 1932, when he transferred to the University of Rome. For several years (precisely, since his military service in WWI as an artillery officer, during which he became deeply involved with questions in ballistics), Picone nurtured the dream of creating a research institute devoted to numerical analysis and its applications. The dream became reality in 1927, thanks to a grant (amounting to 50,000 Liras) from the *Banco di Napoli*, made possible by the intervention of the economist Luigi Amoroso, a friend of Picone's and a fellow alumn of the Scuola Normale Superiore in Pisa. The *Istituto di Calcolo*, initially attached to the chair of Mathematical Analysis at the University of Naples, grew into the *Istituto Nazionale per le Applicazioni del Calcolo* after its move to Rome in 1932. The INAC is considered by many historians to have been the first research institute specifically devoted to numerical analysis, in the modern sense of the phrase; see, e.g., (Brezinski and Wuytack, 2001; Di Sieno et al., 1998; Fichera, 1978; Hestenes and Todd, 1991). For a detailed history of INAC in the first 40 years of its existence, see (Nastasi, 2006).

Picone was, among other things, an excellent talent scout, and was very good at identifying and attracting promising students. Once he had become convinced that a budding mathematician had the necessary attributes, he did everything in his power to encourage and promote the young researcher's work. And his power was considerable: Picone was highly influential and politically well-connected. Especially in the later years of the Fascist regime, he and Francesco Severi (the famous algebraic geometer) were practically in control of much of Italy's mathematical scene. Over the years the INAC became the first workplace for an impressive assembly of mathematicians, including several who were to become among the leading exponents of Italian mathematics. Among these we mention R. Caccioppoli, G. Cimmino, G. Scorza Dragoni, C. Miranda, T. Viola, L. Cesari, S. Faedo, G. Mammana, D. Caligo, L. Sobrero, R. Einaudi, G. Krall, C. Tolotti, G. Grioli, M. Salvadori, F. Conforto, C. Minelli, G. Doetsch, W. Gröbner, and

others. In addition to this group of researchers, the Institute employed a total of eleven *computers* and *draftsmen*. These were highly skilled men and women, many with university degrees, who carried out all the necessary numerical calculations using the computing equipment available at the time, including various electro-mechanical and graphical devices.²

What kind of mathematical work was the INAC actually concerned with? Besides fundamental research in mathematical analysis, differential and integral equations, functional analysis and numerical analysis, the INAC staff was also engaged in a wide variety of applied research projects. These took the form of consulting agreements and research contracts with government agencies (both Italian and foreign), public utility companies, branches of the military, and a number of private companies ranging from major shipyards to small engineering firms. In addition, there were frequent collaborations with university researchers in various scientific and technical fields. One such collaboration with Enrico Fermi resulted in a detailed study by Miranda (1934) of the Fermi-Thomas equation of atomic physics. See (Amerio, 1987) for a description of the manifold activities carried out at the INAC during the 1930s.

Among the topics treated by INAC researchers we find, in addition to “pure” mathematics, problems in classical mechanics (including celestial mechanics), fluid dynamics, structural analysis, elasticity theory (especially the study of beams), atomic physics, electromagnetism, aeronautics, hydraulics, astronomy, and so forth. One of the strong points of INAC researchers was their penchant for developing and applying sophisticated techniques of mathematical analysis to solve problems stemming from concrete and urgent applications. Among the preferred tools we find: variational methods, including variants of the Rayleigh-Ritz method (a precursor of the modern finite element techniques); fixed point theorems in function spaces; the reformulation of boundary value problems in terms of systems of integral equations; and techniques from asymptotic analysis. Although most of the papers produced by INAC researchers were of a rather theoretical nature, the motivation often came from practical questions that had been submitted to INAC by one or another of its many “customers.”³

Much of the work done at INAC embodied Picone’s philosophy, according to which the mathematical analysis of a problem should not be confined to the study of the existence, uniqueness, and regularity of the solution, but should also supply tools for the (approximate) numerical solution of the problem together with rigorous bounds, in the appropriate norm, of the error incurred. Not surprisingly, Cimmino’s early works (including his first published paper (Cimmino, 1928))

²It is worth mentioning that in the aftermath of World War II, the research group working at the INAC included mathematicians of the caliber of Gaetano Fichera and Ennio De Giorgi.

³Because of the strong theoretical flavor of the papers coming out of it, not all applied mathematicians were favorably disposed towards the INAC. See (Segal, 2003) for some of the opinions circulating among contemporary German mathematicians, especially pages 91, 102–103, and 318.

are informed by this way of thinking. Even later in his career Cimmino always showed a strong preference for constructive proofs, whenever possible. Even in his important paper (Cimmino, 1937) on the generalized Dirichlet problem, Cimmino observes that the method he used to prove the existence of a solution suggests a numerical procedure to compute an approximate solution (see (Cimmino, 1937, footnote 3), or (Cimmino, 2002, page 258)). This philosophy is of course not unique to Picone's school: suffices to mention the celebrated 1928 paper by Courant, Friedrichs and Lewy on the partial difference equations of mathematical physics (Courant et al., 1928).

Within the realm of numerical analysis proper, the problems studied at the INAC included the numerical treatment of initial and boundary value problems for ordinary and partial differential equations, optimization problems, integral and integro-differential equations, the approximation and interpolation of functions, least-squares problems, computational harmonic analysis, the determination of the eigenvalues and eigenvectors of matrices, the numerical solution of linear and nonlinear systems of equations, and so forth. For a more thorough discussion of Picone's Institute and of Italian mathematics in general in the period between the two world wars, we refer the reader to (Benzi and Toscano, 2014; Di Sieno et al., 1998; Fichera, 2002; Guerraggio, 1987; Nastasi, 2006).

4 - NUMERICAL ANALYSIS IN THE THIRTIES

The presence of an institute devoted to numerical analysis in a major mathematical research center like the University of Rome was entirely due to Picone's tenacity and farsightedness. The successes of INAC notwithstanding, it would be a mistake to conclude that numerical analysis had gained by the 1930s the status of a mature mathematical discipline, recognized as important by the wider mathematical establishment and well grounded at the institutional level. Suffices to say that the leading exponent of Italian "pure" mathematics of that time, Francesco Severi, was quite against the notion of an institute devoted to what was unglamorously described as the "ancillary roles" of mathematics. It is also worth mentioning that Picone, who already in the early Thirties had introduced a course on *Numerical and graphical computations* (*Calcoli numerici e grafici*) for students of Statistics and Actuarial Sciences at the University of Rome, failed in his attempts to have the course included among the electives for the degree in Mathematics.

Both at the national and international level, numerical analysis was considered a minor field, a Cinderella among the mathematical sciences. One result of the very modest standing of numerics among mathematicians is that many of the most important advances that took place in this field during the second half of the 19th century and the first half of the 20th were due to scientists and engineers, in particular physicists, astronomers and geodesists. At the beginning of the 1930s there existed only a handful of treatises devoted to numerical analysis. At the

international level we mention those by Whittaker and Robinson (Whittaker and Robinson, 1924) and by Scarborough (Scarborough, 1930). At the national level there were the tract by Cassina (Cassina, 1928), mostly devoted to elementary questions, and the one by Cassinis (Cassinis, 1928). See also (Cassina, 1949) for a complete bibliography up to the 1940s (especially page 16). This situation was due, at least in part, to the increasing specialization among scientists beginning with the first half of the 1800s. Until then most mathematicians were also keenly interested in physics and astronomy, and there are many numerical methods associated with the names of Newton, Lagrange, Euler, Laplace, Gauss, Jacobi, Cauchy, Fourier, and so forth. The picture began to change only after World War II, with the advent of high-speed electronic computers. Numerical analysis also benefitted greatly from the fact that several prestigious mathematicians (especially John von Neumann, but also Alan Turing, Stanislaw Ulam, Eduard Stiefel and others) devoted a great deal of attention to this discipline, at first because of war needs but then with increasing enthusiasm and conviction (Goldstine, 1972; Hestenes and Todd, 1991).

One of the basic problems in scientific computation consists in the solution of systems of linear algebraic equations. Almost all problems of computational mathematics boil down, in the end, to the solution of such systems, often of very large dimensions. A classical example is the numerical solution of boundary value problems for the equations of mathematical physics, such as Poisson's equation or the Stokes system. Upon discretization by—say—finite difference or finite element methods, these problems are reduced to linear algebraic systems of the form $\mathbf{Ax} = \mathbf{b}$ where A is a large, sparse matrix and \mathbf{b} a given right-hand side vector. Over time, a large number of techniques have been developed for solving linear systems. Such methods are traditionally grouped in two main categories: *direct* methods, which (barring rounding errors) are guaranteed to return the exact solution $\mathbf{x}_* = A^{-1}\mathbf{b}$ in a finite number of steps, and *iterative* methods, which produce a sequence of successive approximations $\mathbf{x}^{(k)}$ which, under appropriate conditions, converge to \mathbf{x}_* as $k \rightarrow \infty$. Direct methods include Gaussian elimination, Cholesky factorization, and various orthogonalization schemes. These algorithms are the preferred method of solution for linear systems of small or moderate size. Iterative methods are better suited to solve large-scale linear systems. They form a much larger class, and many new such methods are still being proposed. Among the “classical” iterations we mention those of Jacobi (Jacobi, 1845), Seidel (Seidel, 1874) and Richardson (Richardson, 1910). See (Bodewig, 1956; Householder, 1964; Saad, 2020; Saad and van der Vorst, 2000; Varga, 1962) for historical notes on classical iterative methods.

In 1929, Richard von Mises and Hilda Pollaczek-Geiringer published an important study (von Mises and Pollaczek-Geiringer, 1929) that provided the foundation for the development of a general theory of iterative methods for linear

systems. A few INAC researchers, including Picone and Lamberto Cesari (1910–1990), who after World War II went on to a brilliant career in the United States, knew this paper well and made good use of it. In 1937 *La Ricerca Scientifica*, the journal of the *Consiglio Nazionale delle Ricerche*, published a paper (Cesari, 1937b) by Cesari on iterative methods (an extended abstract of the paper was also published in (Cesari, 1937a)). As customary, the paper was preceded by a brief introduction by Picone, which is worth reporting:

The present work by Dr. Lamberto Cesari, collaborator of the Chair of the *Istituto per le Applicazioni del Calcolo*, makes a most remarkable contribution to the problem of solving systems of linear algebraic equations. With the aid brought by the present paper, the methods for the numerical solution of linear algebraic systems receive a rather advanced treatment in which, one can well expect, the Institute will always find what it needs in order to carry out, with a sufficient degree of approximation, the difficult final numerical evaluations that are required by the challenging scientific and technical problems it faces.⁴

Cesari's paper is truly remarkable. In it, the fundamental concept of *preconditioning* of a linear system is explicitly introduced, apparently for the first time (Cesari uses the word *trasformazione*). In addition, Cesari presents a general formalism, due in part to Picone, which allows him to give a unified convergence theory for the classical methods of Jacobi, Seidel, and von Mises (the latter being a stationary Richardson iteration). Subsequently, Cesari goes on to introduce a polynomial preconditioner $p(A)$ with the goal of reducing the spectral condition number of the linear system $\mathbf{Ax} = \mathbf{b}$. The preconditioner is used to accelerate the rate of convergence of von Mises' method. The theory is illustrated by numerical experiments on a system of normal equations in three unknowns.

Cesari's paper, although not well known today, did not go unnoticed; see the references to it in (Bodewig, 1956; Faddeev and Faddeeva, 1960; Householder, 1964; Wachpress, 1966) as well as (Saad and van der Vorst, 2000). This paper is also important for the effect it had on Cimmino. The following year (1938) *La Ricerca Scientifica* published a short (8 pages) paper (Cimmino, 1938) by Cimmino titled “Calcolo approssimato per le soluzioni dei sistemi lineari” (“Approximate computation of the solutions of systems of linear equations”). Again, the article is preceded by an introductory note by Picone:

⁴The Italian original reads: “Il presente lavoro del dott. Lamberto Cesari, coadiutore della Direzione dell'Istituto per le Applicazioni del Calcolo, apporta un notevolissimo contributo al problema della risoluzione numerica dei sistemi di equazioni lineari algebriche. Con gli apporti recati dal presente lavoro, i metodi di risoluzione numerica dei sistemi di equazioni lineari algebriche, ricevono una sistemazione assai progredita, nella quale, come è ben lecito presumere, l'Istituto potrà sempre trovare quanto occorre per le difficili definitive valutazioni numeriche, con un sufficiente grado di approssimazione, relative agli ardui problemi che gli sono assegnati dalla Scienza e dalla Tecnica.”

Prof. Gianfranco Cimmino can be considered, among other things, one of the founders of the Istituto per le Applicazioni del Calcolo, to which he lent his continuing and productive assistance during the embryonal stages of the Institute itself, in Naples, in the laboratory annexed to that university's Calculus chair, from 1928-VI to 1932-X. Towards the end of that period prof. Cimmino devised a numerical method for the approximate solution of systems of linear equations that he reminded me of in these days, following the recent publication by Dr. Cesari (...), which provides a systematic treatment of the above mentioned computing methods which, however, does not consider the one by Cimmino, a method which, in my opinion, is most worthy of consideration in the applications because of its generality, its efficiency and, finally, because of its guaranteed convergence which can make the method practicable in many cases. Therefore, I consider it useful to publish in this journal Prof. Cimmino's note on the above mentioned method, note that he has accepted to write upon my insistent invitation.⁵

Thus we learn that Cimmino's method dates back at least to 1932 and, moreover, that Cimmino may have never bothered to publish it had it not been for Picone's insistence. It is likely that at that time Cimmino was busy with his research on the generalized Dirichlet problem (Cimmino, 1937, 1940) and reluctant to take time off to write on a topic which was widely regarded as one of lesser importance. Picone's insistence bears witness, once again, to his farsightedness. The content of Cimmino's paper (Cimmino, 1938) is examined next.

5 - CIMMINO'S METHOD

In (Cimmino, 1938), Cimmino considers a system of linear algebraic equations $\mathbf{Ax} = \mathbf{b}$ where A is a real $n \times n$ matrix, initially assumed to be nonsingular, and $\mathbf{b} \in \mathbb{R}^n$. If $\mathbf{a}_i^T = [a_{i1}, a_{i2}, \dots, a_{in}]$ denotes the i th row of A , the solution $\mathbf{x}_* = A^{-1}\mathbf{b}$

⁵«Il prof. Gianfranco Cimmino è da considerarsi, anche, uno dei fautori dell'Istituto per le Applicazioni del Calcolo al quale prestò una assidua e proficua opera di assistenza durante il periodo embrionale dell'Istituto stesso, trascorso a Napoli, nel gabinetto annesso a quella Cattedra di Calcolo infinitesimale, dal 1928-VI al 1932-X. Verso la fine di tale periodo il prof. Cimmino escogitò un metodo numerico di approssimazione delle soluzioni dei sistemi di equazioni lineari che egli mi ha richiamato alla memoria in questi giorni in seguito alla pubblicazione del dott. Cesari, recentemente apparsa (...), nella quale è data una sistemazione dei sopradetti metodi di calcolo che, però, non contempla quello sopradetto del Cimmino, metodo che, secondo il mio avviso, è degnissimo di essere tenuto presente nelle applicazioni e per la sua generalità e per la sua rapidità di calcolo numerico delle successive approssimazioni, ed, infine, per la sua assicurata convergenza che, in molti casi, può dare al metodo il necessario carattere di praticità. Ritengo, perciò, utile pubblicare in questa Rivista la nota del prof. Cimmino relativa al suo sopradetto metodo. nota che egli ha accordinoso a redigere per mio insistente invito.»

is the unique intersection point of the n hyperplanes described by

$$(1) \quad \langle \mathbf{a}_i, \mathbf{x} \rangle = b_i, \quad i = 1, 2, \dots, n.$$

Given an initial approximation $\mathbf{x}^{(0)} \in \mathbb{R}^n$, Cimmino takes, for each $i = 1, 2, \dots, n$, the reflection (mirror image) $\mathbf{x}_i^{(0)}$ of $\mathbf{x}^{(0)}$ with respect to the hyperplane (1):

$$(2) \quad \mathbf{x}_i^{(0)} = \mathbf{x}^{(0)} + 2 \frac{b_i - \langle \mathbf{a}_i, \mathbf{x}^{(0)} \rangle}{\|\mathbf{a}_i\|^2} \mathbf{a}_i$$

(here $\|\cdot\|$ denotes the Euclidean norm.) Given n arbitrarily chosen positive quantities m_1, \dots, m_n , Cimmino constructs the next iterate $\mathbf{x}^{(1)}$ as the center of gravity of the system formed by placing the n masses m_i at the points $\mathbf{x}_i^{(0)}$ given by (2), for $i = 1, 2, \dots, n$. Cimmino notes that the initial point $\mathbf{x}^{(0)}$ and its reflections with respect to the n hyperplanes (1) all lie on a hypersphere the center of which is precisely the point common to the n hyperplanes, namely, the solution of the linear system. Because the center of gravity of the system of masses $\{m_i\}_{i=1}^n$ must necessarily fall inside this hypersphere, it follows that the new iterate $\mathbf{x}^{(1)}$ is a better approximation to the solution than $\mathbf{x}^{(0)}$:

$$\|\mathbf{x}^{(1)} - \mathbf{x}_*\| < \|\mathbf{x}^{(0)} - \mathbf{x}_*\|.$$

At this point the procedure is repeated starting from the new approximation $\mathbf{x}^{(1)}$, and so forth. The sequence $\{\mathbf{x}^{(k)}\}$ converges to $\mathbf{x}_* = A^{-1}\mathbf{b}$ as $k \rightarrow \infty$, as shown by Cimmino.

In matrix form, Cimmino's method can be written as follows:

$$\mathbf{x}^{(k+1)} = \mathbf{x}^{(k)} + \frac{2}{\mu} A^T D^T D (\mathbf{b} - A \mathbf{x}^{(k)})$$

($k = 0, 1, \dots$), where we have set

$$(3) \quad D = \begin{bmatrix} \frac{\sqrt{m_1}}{\|\mathbf{a}_1\|} & & & \\ & \frac{\sqrt{m_2}}{\|\mathbf{a}_2\|} & & \\ & & \ddots & \\ & & & \frac{\sqrt{m_n}}{\|\mathbf{a}_n\|} \end{bmatrix}$$

and $\mu = \sum_{i=1}^n m_i$. In particular, taking $m_i = \|\mathbf{a}_i\|^2$ we obtain

$$\mathbf{x}^{(k+1)} = \mathbf{x}^{(k)} + \frac{2}{\mu} A^T (\mathbf{b} - A \mathbf{x}^{(k)}),$$

which is nothing but a special case of von Mises' method (stationary Richardson iteration) applied to the system of normal equations $A^T A \mathbf{x} = A^T \mathbf{b}$. Moreover, if the rows of A are normalized so that $m_i = \|\mathbf{a}_i\| = 1$ for $i = 1, 2, \dots, n$ then $\mu = n$ and Cimmino's method coincides with the under-relaxed Jacobi iteration for a

special choice of the damping parameter (one that automatically guarantees convergence). Other choices of D besides the one in (3) are possible. In particular D need not be diagonal, and other methods can be obtained with different choices of D . However, this possibility is not noted by Cimmino, who does not appear to be aware of the relationship between his method and existing ones. It is noteworthy that the paper contains no bibliographic references.

Cimmino shows that the iterates converge to a solution of $\mathbf{Ax} = \mathbf{b}$ even in the case of a singular (but consistent) system, provided that $\text{rank}(A) \geq 2$. He then notes that the sequence $\{\mathbf{x}^{(k)}\}$ converges even when the linear system is inconsistent, always provided that $\text{rank}(A) \geq 2$. Revisiting this topic many years later, Cimmino writes in (Cimmino, 1967):

The latter observation, however, is just a curiosity, being obviously devoided of any practical usefulness.⁶

Ironically, it is precisely this property that makes Cimmino's method useful in a variety of applications. We will return on this topic in the section 7 below.

In the singular case, Cimmino obtains a bound on the relative error in the Euclidean norm, showing the linear rate of convergence of his method. Cimmino concludes his note showing how, in principle, the method can be extended in a straightforward manner to the approximate solution of infinite-dimensional problems, in particular to Fredholm integral equations of the first kind. It is worth mentioning that Cimmino's note was reviewed for the *Zentralblatt* by Franz Rellich.

Cimmino's method is striking because of its simplicity and elegance. Unlike so many other algorithms for solving linear equations, it is based on a geometrical-mechanical construction rather than on algebraic manipulations. At the time it was conceived, the greatest attraction of the method was probably the fact that the method is always convergent: no restriction is imposed on the system matrix A except the extremely mild one of having rank at least 2.

It must be mentioned that an iterative method with some similarities (and many common features) to Cimmino's had been published in 1937 by the Polish mathematician Stefan Kaczmarz, a close collaborator of Hugo Steinhaus;⁷ see (Kaczmarz, 1937). In this method, the current approximation $\mathbf{x}^{(k)}$ is orthogonally projected (instead of reflected) onto the hyperplanes (1), not simultaneously but instead sequentially. The projection onto the n th hyperplane is taken as the new approximation $\mathbf{x}^{(k+1)}$, and the process is repeated. It is easy to see (using the triangle inequality) that the sequence $\{\mathbf{x}^{(k)}\}$ constructed in this manner converges to the solution of $\mathbf{Ax} = \mathbf{b}$ as $k \rightarrow \infty$.

⁶“Quest'ultima osservazione ha tuttavia il valore di una semplice curiosità, riuscendo essa evidentemente priva di utilità pratica.”

⁷Tragically, Kaczmarz was killed in 1939 when the German troops invaded Poland.

The methods of Cimmino and Kaczmarz are closely related. Cimmino's algorithm has been found to be better suited for parallel computers, whereas Kaczmarz's method tends to converge somewhat faster. It is of course possible to combine the two ideas to obtain hybrids. For instance, the original reflections in Cimmino's method are often replaced by (simultaneous) orthogonal projections onto the hyperplanes, but this is only a minor modification. Another feature the two methods have in common is that they have both been rediscovered several times over the years. More on this later.

6 - LATER DEVELOPMENTS

For a long time (several decades) Cimmino's method, in spite of its virtues, did not see much use. This is probably due to the fact that linear systems of moderate size were more efficiently solved by Gaussian elimination, while large linear systems arising from the discretization of PDEs were solved faster using specialized iterative methods that could exploit the properties and structure of the matrix (Dax, 1990). It was also soon realized that except for special cases (e.g., when A is nearly orthogonal), the convergence of the method tends to be very slow. After the advent of electronic computers, in the Fifties and Sixties, Cimmino's method was referenced in several surveys and monographs on matrix computations (Bodewig, 1956; Faddeev and Faddeeva, 1960; Forsythe, 1953; Gastinel, 1966; Householder, 1964) but some authors explicitly advised against its use; see, e.g., Caprioli's passionate but somewhat misguided defense of Cimmino's method from Bodewig's criticism in (Caprioli, 1953). Beginning in the early Eighties, however, an ever increasing number of researchers has turned to Cimmino's method. Currently there exist a number of variants and extensions of the algorithm, to the point that in the literature it has become customary to talk of *Cimmino-type methods*. This phrase stands for a large class of algorithms which are based on the idea of projecting a current approximation $\mathbf{x}^{(k)}$ simultaneously on the manifolds defined by a system of (possibly nonlinear) equations or inequalities, and take a weighted average of these projections as the new iterate $\mathbf{x}^{(k+1)}$.

The following is a list of noteworthy developments, together with a few representative references:

- Chebychev, Lanczos and conjugate gradient acceleration of the classical Cimmino method (Arioli et al., 1992, 1995; Benzi et al., 1995; Saad, 2003; Tommasini Montanari, 1984; van der Vorst, 2003);
- Block variants for parallel computers (Aharoni and Censor, 1989; Arioli et al., 1989; Benzi et al., 1995; Bramley and Sameh, 1992; Sukru Torun et al., 2018; Zilli, 1993);
- Extensions to systems of linear inequalities (Censor, 1982; Censor and Zenios, 1997; de Pierro and Iusem, 1985);

- Extensions to nonlinear systems (Censor and Elfving, 1981; Iusem and de Pierro, 1986);
- Extensions to operator equations in infinite-dimensional Hilbert and Banach spaces (Butnariu and Censor, 1994; Butnariu and Markowitz, 2002; Cimmino, 1972; Kammerer and Nashed, 1971; Nashed, 1981);
- Non-deterministic (Monte Carlo) versions of Cimmino's method (Cimmino, 1967, 1972);
- Numerous applications, especially in the medical field (medical imaging, radiation therapy plans) (Bertero and Boccacci, 1998; Censor et al., 1988; Censor and Zenios, 1997; Nashed, 1981; Wu et al., 2004; Xiao et al., 2003).

A theoretical advance with important practical consequences has been the realization that Cimmino's method enjoys the *regularization* property when applied to problems that are ill-posed (in the sense of Hadamard), including all operator equations of the form

$$A\mathbf{u} = \mathbf{f},$$

where A is a compact linear operator on an infinite-dimensional Banach space X . Here the continuous problem is ill-posed because A^{-1} , if defined, is unbounded. In practice, such equations are reduced to finite-dimensional problems by discretization: when the original (continuous) problem is ill-posed, the discrete problem is severely ill-conditioned. This means that the singular values of A decay very rapidly to zero and thus A^{-1} , if it exists, has a huge norm. Therefore, the solution will be generally very sensitive to perturbations in the data.

Simply put, the regularization property means that after a certain number k of iterations Cimmino's method returns a sufficiently good approximation $\mathbf{u}^{(k)}$, and subsequent iterations not only do not improve the quality of the computed solution, but actually result in worse and worse approximations. This is because the iterates become completely dominated by the errors, inevitably present in the data, which are “amplified” by the operator A^{-1} which, in turn, is being approximated better and better as the iteration progresses. More precisely, consider the linear problem with a perturbed right-hand side

$$A\mathbf{u} = \mathbf{f} + \mathbf{e},$$

where \mathbf{e} represents some kind of “noise” (which could be due to measurement error, to discretization error, etc.). The exact solution of the perturbed problem, assuming (for simplicity) that A is invertible and that both \mathbf{f} and \mathbf{e} are in the range of A , is $\hat{\mathbf{u}} = A^{-1}\mathbf{f} + A^{-1}\mathbf{e}$, and since A^{-1} is huge this may have nothing to do with the “true” solution $\mathbf{x}_* = A^{-1}\mathbf{f}$, no matter how small \mathbf{e} is in norm. The iterates computed with Cimmino's method tend to reconstruct first the “good” part of the solution (the *signal*), and only later the unwanted part (the *noise*). Hence, Cimmino's method initially “filters out” the noise, which gets reconstructed only later. The same property is enjoyed by other iterative methods as well, including

Kaczmarz's and the conjugate gradient method (applied to $A^*A\mathbf{u} = A^*\mathbf{f}$, where A^* is the adjoint of A); see (Bakushinskii, 1967; Hansen, 1998; van der Sluis and van der Vorst, 1990).

It is clear that in this context, the fact that convergence is very slow is not necessarily a drawback, and in fact it may be advantageous. The main difficulty with iterative regularization methods is to decide when to stop the iteration process. Several empirical rules have been devised to this end, but no universally agreed criterion exists. It is clear that if a method converges slowly, with the approximations not differing very much from one step to the next, running a few iterations more than strictly necessary is not going to significantly ruin an approximate solution.

It is well-known that a very important class of ill-posed problem is represented by the Fredholm integral equations of the first kind:

$$\int_{\Omega} K(s, t) u(t) dt = f(s), \quad s \in \Omega$$

with suitable assumptions on the domain Ω , on the kernel K , and on the data f . Equations of this type frequently occur, e.g., in image processing—a fundamental problem in medicine, astronomy, microscopy, etc. It is interesting that in his original 1938 paper, Cimmino discussed the extension of his method *precisely to this class of functional equations*. Cimmino himself returned to this topic during the Sixties and again in his last publications. Of special interest is his extension in a probabilistic sense of his method. The gist of his reasoning is the following. In order to improve the quality of an initial guess, it is possible to proceed in one of two ways. The first consists in taking additional iterations: as we know, the method will eventually converge to the exact solution of the linear system. The alternative is to apply one step of the iteration but to an equivalent enlarged system $\hat{A}\mathbf{x} = \hat{\mathbf{b}}$ obtained from the original system $A\mathbf{x} = \mathbf{b}$ by adding a number of equations which are linear combinations of the original ones. Consider for instance the case of a $n \times n$ system with a nonsingular matrix A . It is possible to add to the hyperplanes (1) an arbitrary number of additional hyperplanes passing through the same point \mathbf{x}_* . The new linear system has the coefficient matrix $\hat{A} \in \mathbb{R}^{m \times n}$ with $m > n$. Cimmino shows that taking one step of Cimmino's method on this enlarged system gives a better approximation to \mathbf{x}_* than taking one iteration on the original system. Furthermore the larger m , the better the approximation, and indeed in the limit as $m \rightarrow \infty$ we obtain the exact solution in one step. The question then is how to choose the linear combinations of equations to be added to the system. Choosing the coefficients of the linear combination at random effectively leads to a Monte Carlo-type method for solving linear systems; see (Cimmino, 1967, 1972).

In (Cimmino, 1986) Cimmino went on to consider the situation where instead of a finite number m of masses, a continuous mass distribution is given on the

hypersphere whose center is the solution point \mathbf{x}_* . When the distribution is uniform, the center of gravity of the system is precisely the solution point \mathbf{x}_* , and one step of Cimmino's extended method yields explicit formulas for the solution components in terms of ratios of (hyper-)spherical integrals:

$$(4) \quad \mathbf{x}_* = n \frac{\int_{\omega} \|A^T \mathbf{x}\|^{-n-2} \langle \mathbf{x}, \mathbf{b} \rangle A^T \mathbf{x} d\omega}{\int_{\omega} \|A^T \mathbf{x}\|^{-n} d\omega}$$

where $\omega = \{\mathbf{x} \in \mathbb{R}^n \mid \|\mathbf{x}\| = 1\}$. Such integrals, for n large, can be evaluated by Monte Carlo methods. The expressions (4) offer an alternative to the usual Cramer's formulas. See also (Cimmino, 1987, 1989). It is interesting to note that in (Cimmino, 1986) Cimmino wrote:

I didn't try to check whether formulas (4) are already known, as it seems rather likely.

Indeed, the expression of the solutions of a linear algebraic system in terms of $(n - 1)$ -dimensional (spherical) integrals had already been given by Jacobi in (Jacobi, 1834).

7 - CIMMINO'S LEGACY

To measure the impact of Cimmino's work we can turn to citation data bases such as MathSciNet or Web of Science (managed by the American Mathematical Society and by the Institute for Scientific Information, respectively). Concerning the years up to 1980 we have been able to find just eight journal articles citing Cimmino's 1938 paper (Cimmino, 1938), four of which from the Seventies. After 1980, the interest in Cimmino's method increases sharply.

According to the online citation index Google Scholar, as of January 2022, Cimmino's papers have been cited 659 times; of these, the vast majority (473 citations) are to (Cimmino, 1938). Cimmino's second most cited article is (Cimmino, 1937), with 57 citations. This raw data provides only a rough estimate of the impact of Cimmino's paper (Cimmino, 1938). Especially in recent decades, many authors discuss Cimmino's method based on second-hand accounts and do not cite the original 1938 publication, as is often the case for papers not written in English or published in somewhat obscure venues.

Cimmino's method has been described, or at least mentioned, in a number of monographs, some of which have been highly influential. The list includes books on matrix computations, linear algebra, optimization, functional analysis, numerical analysis, inverse problems, imaging, and economics. Here we mention (Abaffy and Spedicato, 1989; Bertero and Boccacci, 1998; Björck, 2015; Bodewig, 1956; Brezinski, 1997; Byrne, 2007, 2014; Cegielski, 2013; Censor and Zenios, 1997; Cherubino and Passaquinidici, 1965; Escalante and Raydan, 2011; Faddeev and Faddeeva, 1960; Galantai, 2004; Gastinel, 1966; Gilbert and Gilbert, 2004; Hackbusch, 2010; Herman, 2000; Householder, 1964; Meyer, 2000; Pini

and Negrini, 1994; Razoumikhine, 1975; Saad, 2003; van der Vorst, 2003; Zaslavski, 2015); see also (Censor and Cegielski, 2015).

In many of these books, the Cimmino and Kaczmarz methods are often discussed one after the other. Incidentally, the history of Kaczmarz's method is very similar to that of Cimmino's. Both methods have been generalized and extended in similar directions, and both methods have been rediscovered a number of times, especially by researchers in applied areas. A notable example is the field of computerized tomography, where the method of Kaczmarz was rediscovered around 1970 under the name of *ART* (for Algebraic Reconstruction Technique); see (Gordon et al., 1970). A class of algorithms closely related to Cimmino's, known as *SIRT* (for Simultaneous Reconstruction Techniques), was introduced around the same time in (Gilbert, 1972); see also (van der Sluis and van der Vorst, 1990). Closely related to Cimmino's methods are the iterative processes known as *Landweber's method* (Landweber, 1951) and *Bialy's method*, see (Bialy, 1959). A similar method is the one proposed by Fridman (Fridman, 1956); see Grace Wahba's discussion of the "Richardson-Landweber-Fridman-Picard-Cimmino method(s)" in (Wahba, 1987). Several other authors have proposed variants of these methods, usually unaware of previous work.

The resurgence of interest in old algorithms like Cimmino's and Kaczmarz's is primarily due to two technological advances:

- The widespread diffusion, around 1970, of tomography (CAT scans) in radiology;
- The appearance, about a decade later, of parallel computers.

Concerning the first aspect, the methods of Kaczmarz and Cimmino were found to be especially well-suited because of their regularizing properties (image reconstruction from projections is an ill-posed problem) and because of their extremely low storage demand. The latter feature is especially evident for Kaczmarz's method, which only requires one row of the coefficient matrix (and the corresponding entry in the right-hand side vector) to perform one iteration: in other words, Kaczmarz's iteration is a *row-action method*, see (Censor, 1981). However, Cimmino's method can also be implemented in this way. As for parallel computing, we have already commented on the fact that Cimmino's method is ideally suited for parallel implementation, and such implementations have indeed proved to be efficient; see, e.g., (Benzi et al., 1995). Parallel implementation of Kaczmarz's method seems to be less straightforward, but blocks versions of it can be efficiently parallelized; see for instance (D'Apuzzo and Lapegna, 1995; Kamath and Sameh, 1988). Another attractive feature of Cimmino's method (not shared by Kaczmarz's method in its original form) is the fact that the method is always convergent even in the case of a rank-deficient and inconsistent linear system. When the system is inconsistent, the iterates generated by Cimmino's method converge to a weighted least-squares solution; if, moreover, $m_i = \|\mathbf{a}_i\|^2$, Cimmino's method produces a solution to the least-squares

problem, $\|Ax - b\| = \min$. Moreover, choosing $x^{(0)} = \mathbf{0}$ results in the minimum norm solution of the least-squares problem; see (Dax, 1990, pages 628–629). The latter property is of great importance in radiation therapy planning, where minimum norm solutions correspond to feasible treatment plans of minimum intensity.

Over the years, Cimmino’s method (in one or another of its modern “reincarnations”) has found application primarily in the following areas:

- Convex mathematical programming, especially convex feasibility problems (the problem of determining whether a family of convex sets has non-empty intersection, and if so to find a common point (Aharoni and Censor, 1989; Altschuler et al., 2005; Bauschke and Borwein, 1996; Combettes, 1993));
- Fast adaptation of radiation therapy planning (Censor et al., 1988; Wu et al., 2004; Xiao et al., 2003);
- Solution of inverse problems in astronomy, medical physics and geophysics (Hansen and Saxild-Hansen, 2012);
- Image reconstruction from projections (Herman, 2000);
- Adaptive filtering in signal processing (Soni et al., 2004);
- Solution of large linear systems arising from the discretization of Fredholm integral equations of the first kind (Kammerer and Nashed, 1971; Wahba, 1987).

In particular, fast adaptation of radiation therapy plans and image reconstruction in computerized tomography appear to be the most important areas of applications of Cimmino’s method. We notice that virtually all the above mentioned problems are ill-posed. Moreover, these problems are often nonlinear and are expressed in terms of inequalities rather than equalities.

Nowadays, both Cimmino’s method and Kaczmarz’s are rarely used for solving systems of linear equations—the type of problem they were originally conceived for. This is mostly because far more efficient methods exist nowadays for solving large linear systems. This can be best understood by observing that Cimmino’s method is equivalent to a damped Jacobi iteration applied to the normal equations $A^T Ax = A^T b$. Likewise, Kaczmarz’s method is equivalent to the classical Gauss-Seidel method applied to the system $AA^T y = b$, with $A^T y = x$. The normal equations interpretation has led to the suggestion that block versions of the Cimmino and Kaczmarz algorithms may be used as preconditioners for the conjugate gradient method. Such preconditioned solvers have been developed and applied to the solution of large sparse systems arising from the discretization of partial differential equations and other problems (Arioli et al., 1995; Benzi et al., 1995; Bramley and Sameh, 1992; Saad, 2003). However, while very robust, this approach has been found to be generally inferior to preconditioned Krylov methods applied directly to $Ax = b$. We mention that Cimmino-type and

Kaczmarz-type iterations are also used as smoothers for multigrid methods applied to nonsymmetric and indefinite systems, see (Hackbusch, 2010).

The popularity enjoyed by Cimmino's method in various scientific and technical areas can be gained by noting that articles on the use of Cimmino's method have appeared in journals like *Physics in Medicine and Biology*, *Medical Physics*, *Inverse Problems*, *International Journal of Radiation Oncology, Biology and Physics*, *IEEE Transactions on Medical Imaging*, *IEEE Transactions on Image Processing*, *IEEE Transactions on Signal Processing*, *Annals of Opérations Research*, and so forth. In addition to these, dozens of articles on Cimmino's methods and its extensions have appeared in journals devoted to scientific computing, numerical analysis, parallel computing, optimization, functional analysis, convex analysis, linear algebra, etc.

8 - EPILOGUE

The total number of Gianfranco Cimmino's published papers in the field of numerical analysis is small, not exceeding 30 printed pages. Yet, this work (primarily the 1938 paper (Cimmino, 1938)) has had a remarkable, if belated, impact and has proven to be of lasting importance for many areas of applied scientific computing.

While Cimmino did not live to see how extensive the influence of his numerical work would be, he did know that algorithms based on his 1938 paper were being developed and applied in the medical field. Indeed, one of his last reviews for the *Zentralblatt für Mathematik*, appeared in 1988, concerned a paper on the use of Cimmino's method in radiation therapy planning (Censor et al., 1988). He must have been pleased to learn that his elegant, youthful intuition had been found to be useful in the medical field.

The story of Cimmino's method is interesting for several reasons. It shows that good mathematical ideas may take many years to become fully appreciated and to be brought to fruition. Major technological changes may completely transform the perception of an algorithm, from useless curiosity to brilliant invention. If an idea is indeed good, it is almost certain that it will eventually come to the forefront (perhaps through re-discovery), no matter how obscure the original publication or how long the period of oblivion. Of course Cimmino's method is not unique in this respect, and one could give numerous other examples of this phenomenon.

It is also interesting to observe that Cimmino's impact on his main research area, the theory of partial differential equations, while nonnegligible, has not been as great and as lasting as his work in numerical mathematics. The reasons for this are complex, but may be due at least in part to the state of relative isolation in which Cimmino (as well as other members of the Neapolitan mathematical school) conducted his research, publishing his most important papers in Italian and in journals of rather limited circulation. Moreover the techniques (and even the notation) he used were somewhat different from those adopted by many of the

leading mathematicians of the time. On the other hand Cimmino (like Cesari), through his association with Picone's Institute, was well-positioned to make pioneering contributions to the numerical field, which was at the time in a rather primitive stage. It should be noted that Cimmino's later papers on solving linear systems, written at a time when numerical linear algebra was maturing as an independent discipline, have had virtually no impact on the field.

It is clear from reading Cimmino's papers that he regarded his work on solving linear systems almost as a hobby, something he did as an amateur rather than as a professional mathematician. And indeed some of his statements, including ones made at a time when iterative methods for linear systems were already being vigorously developed (in Europe, USA and USSR), strike us as rather naïve. It is also clear from the lack of references in his papers that Cimmino did not follow the numerical analysis literature, in spite of his long-lasting interest in numerical questions. And the lack of numerical experiments suggests that Cimmino was not knowledgeable about (or even interested in) computers. This shows that valuable contributions to a specific discipline may well come from outsiders. However, this is probably unlikely to happen for those fields that have already reached a considerable level of maturity and/or which require a great deal of specialization.

Acknowledgments. This paper is based on the text of a talk first given at the *Seminario di Analisi Matematica* at the University of Bologna on May 7, 2004. The talk was part of a series of lectures devoted to the memory of Gianfranco Cimmino. My sincere thanks to the late Prof. Bruno Pini and to Prof. Ermanno Lanconelli, coordinators of the *Seminario*, for their kind invitation and financial support. Thanks also to Professor Sandro Graffi for useful information on Cimmino and his work. Finally, I would like to thank Prof. Carlo Sbordone for suggesting the publication of an updated version of the original paper (Benzi, 2005), together with my English translation of Cimmino's paper (Cimmino, 1938), and Prof. Ermanno Lanconelli for his kind permission to rework the article and submit it to the Società Nazionale di Scienze, Lettere e Arti in Napoli.

9 - REFERENCES

- J. Abaffy and E. Spedicato, *ABS Projection Methods*, Halstead Press, Chichester, UK, 1989.
- R. Aharoni and Y. Censor, *Block-iterative projection methods for parallel computation of solutions to convex feasibility problems*, Linear Algebra and its Applications, 120 (1989), pp. 165–175.
- M. D. Altschuler, T. C. Zhu, J. Li and S. M. Hahn, *Optimized interstitial PDT prostate treatment planning with the Cimmino feasibility algorithm*, Medical Physics, 32 (2005), pp. 3524–3536.
- L. Amerio, *Mauro Picone e l'Istituto per le Applicazioni del Calcolo*, in Gueraggio (1987), pp. 15–23.

- M. Arioli, I. S. Duff, J. Noailles, and D. Ruiz, *Comparison between block Cimmino and block SSOR algorithms for solving linear systems in a parallel environment*, Proceedings of the conference “Supercomputing Tools for Science and Engineering,” Pisa 1989, Franco Angeli, pp. 47–54.
- M. Arioli, I. S. Duff, J. Noailles, and D. Ruiz, *A block projection method for sparse matrices*, SIAM Journal on Scientific Computing, 13 (1992), pp. 47–70.
- M. Arioli, I. S. Duff, D. Ruiz and M. Sadkane, *Block Lanczos techniques for accelerating the block Cimmino method*, SIAM Journal on Scientific Computing, 16 (1995), pp. 1478–1511.
- A. B. Bakushinskii, *A general method of constructing regularizing algorithms for a linear ill-posed equation in Hilbert space*, USSR Computational Mathematics and Mathematical Physics, 7 (1967), pp. 279–287.
- H. H. Bauschke and J. M. Borwein, *On projection algorithms for solving convex feasibility problems*, SIAM Review, 38 (1996), pp. 367–426.
- M. Benzi, *Gianfranco Cimmino’s contributions to numerical mathematics*, in *Atti del Seminario di Analisi Matematica*, Dipartimento di Matematica dell’Università di Bologna. Volume Speciale: Ciclo di Conferenze in Ricordo di Gianfranco Cimmino, Marzo-Maggio 2004, Tecnoprint, Bologna (2005), pp. 87–109.
- M. Benzi, F. Sgallari and G. Spaletta, *A parallel block projection method of the Cimmino type for finite Markov chains*, in *Computations with Markov Chains*, W. J. Stewart, Editor, Kluwer Academic Publishers, 1995, pp. 65–80.
- M. Benzi and E. Toscano, *Mauro Picone, Sandro Faedo, and the numerical solution of partial differential equations in Italy (1928–1953)*, Numerical Algorithms, 86 (2014), pp. 105–145.
- M. Bertero and P. Boccacci, *Introduction to Inverse Problems in Imaging*, Institute of Physics Publishing, Bristol and Philadelphia, 1998.
- H. Bialy, *Iterative Behandlung linearer Funktionalgleichungen*, Archive for Rational Mechanics and Analysis, 4 (1959), pp. 166–176.
- Å. Björck, *Numerical Methods in Matrix Computations*, Springer, 2015.
- E. Bodewig, *Matrix Calculus*, North-Holland, Amsterdam, 1956.
- R. Bramley and A. Sameh, *Row projection methods for large nonsymmetric linear systems*, SIAM Journal on Scientific Computing, 13 (1992), pp. 168–193.
- C. Brezinski, *Projection Methods for Systems of Equations*, Studies in Computational Mathematics 7, North-Holland, Amsterdam, 1997.
- C. Brezinski and L. Wuytack, *Numerical analysis in the twentieth century*, in *Numerical Analysis: Historical Developments in the 20th Century*, C. Brezinski e L. Wuytack, Editors, North–Holland, Amsterdam, 2001, pp. 1–40.
- D. Butnariu and Y. Censor, *Strong convergence of almost simultaneous block iterative projection methods in Hilbert spaces*, Journal of Computational and Applied Mathematics, 53 (1994), pp. 33–42.

- D. Butnariu and I. Markowitz, *A relaxed Cimmino type method for computing almost common fixed points of totally nonexpansive families of operators*, Proceedings of the International Conference on Nonlinear Operators, Differential Equations and Applications, Seminar on Fixed Point Theory Cluj-Napoca 3 (2002), pp. 149–156.
- C. L. Byrne, *Applied Iterative Methods*, A. K. Peters/CRC Press, New York, 2007.
- C. L. Byrne, *Iterative Optimization in Inverse Problems*, CRC Press, Boca Raton/London/New York, 2014.
- L. Caprioli, *Sulla risoluzione dei sistemi lineari col metodo di Cimmino*, Bollettino dell’Unione Matematica Italiana, III, 7(3), 1953, pp. 260–265.
- U. Cassina, *Calcolo Numerico: Con Numerosi Esempi e Note Storiche Originali*, Zanichelli, Bologna, 1928.
- U. Cassina, *Approssimazioni Numeriche*, in *Enciclopedia delle Matematiche Elementari e Complementi*, Vol. III, Part 2^a, Luigi Berzolari, Editor, Hoepli, Milano, 1949, pp. 1–192.
- G. Cassinis, *Calcoli Numerici, Grafici e Meccanici*, Mariotti-Pacini, Pisa, 1928.
- A. Cegielski, *Iterative Methods for Fixed Point Problems in Hilbert Spaces*, Springer, 2013.
- Y. Censor, *Row-action methods for huge and sparse systems and their applications*, SIAM Review, 23 (1981), pp. 444–466.
- Y. Censor, M. D. Altschuler, W. D. Powell, *On the use of Cimmino’s simultaneous projection method for computing a solution of the inverse problem in radiation therapy treatment planning*, Inverse Problems, 4 (1988), pp. 607–623.
- Y. Censor and A. Cegielski, *Projection methods: an annotated bibliography of books and reviews*, Optimization, 64 (2015), pp. 2343–2358.
- Y. Censor and T. Elfving, *A nonlinear Cimmino algorithm*, Technical Report MIPG 60, Medical Image Processing Group, Department of Radiology, University of Pennsylvania, Philadelphia, PA, USA, August 1981.
- Y. Censor and T. Elfving, *New methods for linear inequalities*, Linear Algebra and its Applications, 42 (1982), pp. 199–211.
- Y. Censor and S. Zenios, *Parallel Optimization. Theory, Algorithms, and Applications*, Oxford University Press, New York and Oxford, 1997.
- L. Cesari, *Sulla risoluzione dei sistemi di equazioni lineari per approssimazioni successive*, Rendiconti della Classe di Scienze Fisiche, Matematiche e Naturali dell’Accademia Nazionale dei Lincei, VI, 25 (1937), pp. 422–428.
- L. Cesari, *Sulla risoluzione dei sistemi di equazioni lineari per approssimazioni successive*, La Ricerca Scientifica, II, 8 (1937), pp. 512–522.
- S. Cherubino and M. Passaquindici, *Economia Matematica*, vol. I, Edizioni Cremonese, Roma, 1965.
- G. Cimmino, *Nuovo metodo d’approssimazione per le soluzioni dei valori al contorno relativi all’equazione del calore*, Giornale di Matematiche (Battaglini),

- III, 19 (1928), pp. 75–98.
- G. Cimmino, *Nuovo tipo di condizioni al contorno e nuovo metodo di trattazione per il problema generalizzato di Dirichlet*, Rendiconti del Circolo Matematico di Palermo, 61 (1937–1938), pp. 177–221. Reprinted in Cimmino (2002), pp. 257–300.
- G. Cimmino, *Calcolo approssimato per le soluzioni dei sistemi di equazioni lineari*, La Ricerca Scientifica, II, 9 (1938), pp. 326–333.
- G. Cimmino, *Sul problema generalizzato di Dirichlet per l'equazione di Poisson*, Rendiconti del Seminario Matematico dell' Università di Padova, 11 (1940), pp. 28–89. Reprinted in Cimmino (2002), pp. 301–362.
- G. Cimmino, *Un metodo Monte Carlo per la risoluzione numerica dei sistemi di equazioni lineari*, Rendiconti dell'Accademia delle Scienze dell'Istituto di Bologna, XII, 2 (1967), pp. 39–44. Reprinted in Cimmino (2002), pp. 505–511.
- G. Cimmino, *Su uno speciale tipo di metodi probabilistici in analisi numerica*, Symposia Mathematica, Istituto Nazionale di Alta Matematica, X, Academic Press, London and New York, 1972, pp. 247–254. Reprinted in Cimmino (2002), pp. 545–552.
- G. Cimmino, *An unusual way of solving linear systems*, Rendiconti della Classe di Scienze Fisiche, Matematiche e Naturali dell'Accademia Nazionale dei Lincei, VIII, 80 (1986), pp. 6–7. Reprinted in Cimmino (2002), pp. 633–634.
- G. Cimmino, *La regola di Cramer svincolata dalla nozione di determinante*, Rendiconti dell'Accademia delle Scienze dell'Istituto di Bologna, XIII, 10 (1986/1987), pp. 115–122. Reprinted in Cimmino (2002), pp. 635–642.
- G. Cimmino, *On some identities involving spherical means*, Rendiconti della Classe di Scienze Fisiche, Matematiche e Naturali dell'Accademia Nazionale dei Lincei, VIII, 83 (1989), pp. 69–73. Reprinted in Cimmino (2002), pp. 649–652.
- G. Cimmino, *Opere Scelte*, C. Sbordone and G. Trombetti, Editors, Accademia di Scienze Fisiche e Matematiche della Società Nazionale di Scienze Lettere e Arti in Napoli, Giannini, Napoli, 2002.
- P. Combettes, *The foundations of set-theoretic estimation*, Proceedings of the IEEE, 81 (1993), pp. 182–208.
- R. Courant, K. Friedrichs, and H. Lewy, *Über die partiellen Differenzengleichungen der mathematischen Physik*, Mathematische Annalen, 100 (1928), pp. 32–74.
- M. D'Apuzzo and M. Lapegna, *A parallel row projection solver for large sparse linear systems*, Proceedings of the Euromicro Workshop on Parallel and Distributed Processing, IEEE Computer Society, Los Alamitos, CA, 1995, pp. 432–441.
- A. Dax, *The convergence of linear stationary iterative processes for solving singular unstructured systems of linear equations*, SIAM Review, 32 (1990),

pp. 611–635.

- A. de Pierro and A. N. Iusem, *A simultaneous projection method for linear inequalities*, Linear Algebra and its Applications, 64 (1985), pp. 243–253.
- S. Di Sieno, A. Guerraggio and P. Nastasi (Eds.), *La Matematica Italiana Dopo l'Unità. Gli Anni tra le Due Guerre Mondiali*, Marcos y Marcos, Milano, 1998.
- R. Escalante and M. Raydan, *Alternating Projection Methods*, SIAM, Philadelphia, 2011.
- D. K. Faddeev and V. N. Faddeeva, *Computational Methods of Linear Algebra*, W. H. Freeman and Co., San Francisco and London, 1963. English translation of Russian original published by Nauka, Moscow, 1960.
- G. Fichera, *Mauro Picone*, Rendiconti dell'Accademia delle Scienze dell'Istituto di Bologna, XIII, 5 (1978), pp. 245–261. Reprinted in Fichera (2002), pp. 85–101.
- G. Fichera, *Opere Storiche, Biografiche, Divulgative*, L. Carbone, P. E. Ricci, C. Sbordone and D. Trigiante, Editors, Accademia di Scienze Fisiche e Matematiche della Società Nazionale di Scienze Lettere e Arti in Napoli, Giannini, Napoli, 2002.
- G. E. Forsythe, *Tentative classification of methods and bibliography on solving systems of linear equations*, Journal of Research of the National Bureau of Standards, Applied Mathematics Series, 29 (1953), pp. 1–28.
- V. M. Fridman, *Method of successive approximations for a Fredholm integral equation of the first kind*, Uspehi Matematicheskikh Nauk, 11 (1956), pp. 233–234.
- A. Galantai, *Projectors and Projection Methods*, Kluwer Academic Publishers, Boston/Dordrecht/London, 2004.
- N. Gastinel, *Linear Numerical Analysis*, Academic Press, New York, 1970. English translation of original French edition published by Hermann, Paris, 1966.
- J. Gilbert and L. Gilbert, *Linear Algebra and Matrix Theory*, Second Edition, Thomson, 2004.
- P. F. C. Gilbert, *Iterative methods for three-dimensional reconstruction from projections*, Journal of Theoretical Biology, 36 (1972), pp. 105–117.
- R. Gordon, R. Bender and G. T. Herman, *Algebraic reconstruction techniques (ART) for three-dimensional electron microscopy and x-ray photography*, Journal of Theoretical Biology, 29 (1970), pp. 471–481.
- H. H. Goldstine, *The Computer from Pascal to von Neumann*, Princeton University Press, 1972.
- A. Guerraggio (Ed.), *La Matematica Italiana tra le Due Guerre Mondiali. Atti del Convegno, Milano e Gargnano del Garda, 8–11 Ottobre 1986*, Pitagora, Bologna, 1987.
- W. Hackbusch, *Iterative Solution of Large Sparse Systems of Equations. Second Edition*, Springer-Verlag, Berlin, 2010.

- P.-C. Hansen, *Rank-Deficient and Discrete Ill-Posed Problems: Numerical Aspects of Linear Inversion*, Society for Industrial and Applied Mathematics, Philadelphia, PA, 1998.
- P. C. Hansen and M. Saxild-Hansen, *AIR Tools — A Matlab package for algebraic iterative reconstruction methods*, Journal of Computational and Applied Mathematics, 236 (2012), pp. 2167–2178.
- G. T. Herman, *Fundamentals of Computerized Tomography: Image Reconstruction from Projections*, Springer-Verlag Ltd., London, 2000.
- M. R. Hestenes and J. Todd, *Mathematicians Learning to Use Computers. The Institute for Numerical Analysis, UCLA 1947-1954*, National Institute of Standard and Technology and The Mathematical Association of America, Washington, DC, 1991.
- A. S. Householder, *The Theory of Matrices in Numerical Analysis*, Blaisdell & Co., New York, 1964. Reprinted by Dover Publishing Inc., New York, 1975.
- A. N. Iusem and A. R. de Pierro, *Convergence results for an accelerated nonlinear Cimmino algorithm*, Numerische Mathematik, 49 (1986), pp. 367–378.
- C. G. J. Jacobi, *Über eine neue Auflösungsart der bei der Methode der kleinsten Quadrate vorkommenden linearen Gleichungen*, Astronomische Nachrichten, 22 (1845), 297–306. Reprinted in *Gesammelte Werke*, vol. III, pp. 469–478.
- C. G. J. Jacobi, *Dato systemate n equationum linearium inter n incognitas, valores incognitarum per integralia definita (n – 1)-tuplicia exhibentur*, Crelle Journal, 14 (1834), pp. 51–55. Reprinted in *Gesammelte Werke*, vol. VI, pp. 79–85.
- S. Kaczmarz, *Angenäherte Auflösung von Systemen linearer Gleichungen*, Bulletin International de l'Académie Polonaise des Sciences et Lettres, A, 35 (1937), pp. 355–357. English translation in *International Journal of Control*, 57 (1993), pp. 1269–1271.
- C. Kamath and A. Sameh, *A projection method for solving nonsymmetric linear systems on multiprocessors*, Parallel Computing, 9 (1988/89), pp. 291–312.
- W. J. Kammerer and Z. M. Nashed, *A generalization of a matrix iterative method of G. Cimmino to best approximate solution to linear integral equations of the first kind*, Rendiconti della Classe di Scienze Fisiche, Matematiche e Naturali dell'Accademia Nazionale dei Lincei, VIII, 51 (1971), pp. 20–25.
- L. Landweber, *An iteration formula for Fredholm integral equations of the first kind*, American Journal of Mathematics, 73 (1951), pp. 615–624.
- J.-L. Lions and E. Magenes, *Non-Homogeneous Boundary Value Problems and Applications*, Vol. I, Springer-Verlag, Berlin, 1972. English translation of original French edition published by Dunod, Paris, 1968.
- C. D. Meyer, *Matrix Analysis and Applied Linear Algebra*, SIAM, Philadelphia, 2000.

- C. Miranda, *Partial Differential Equations of Elliptic Type*, Second Revised Edition, Springer-Verlag, Berlin, 1970.
- M. Z. Nashed, *Continuous and semicontinuous analogues of iterative methods of Cimmino and Kaczmarz with applications to the inverse Radon transform*, Proceedings of the Oberwolfach Conference on Mathematical Aspects of Computerized Tomography, Lecture Notes in Medical Informatics, 8 (1981), pp. 160–178.
- P. Nastasi, *I primi quarant'anni di vita dell'Istituto per le Applicazioni del Calcolo "Mauro Picone,"* Bollettino dell'Unione Matematica Italiana, Sez. A, Fascicolo Monografico, Dicembre 2006.
- B. Pini, *Gianfranco Cimmino*, Bollettino dell'Unione Matematica Italiana, A(7), 5 (1991), pp. 117–123. Reprinted in Cimmino (2002), pp. 653–659.
- B. Pini e P. Negrini, *Lezioni su Metodi di Approssimazione. Il Metodo delle Differenze Finite per Problemi Lineari*, Capitolo 1, Pitagora Editrice, Bologna, 1994.
- B. Razoumikhine, *Modèles Physiques et Méthodes de la Théorie de l'Équilibre en Programmation et en Économie*, Éditions MIR, Moscou, 1978. French translation of original Russian edition published by Nauka, Moscow, 1975.
- L. F. Richardson, *The approximate arithmetical solution by finite differences of physical problems involving differential equations with an application to the stresses in a masonry dam*, Philosophical Transactions of the Royal Society of London, A, 210 (1910), pp. 307–357.
- Y. Saad, *Iterative Methods for Sparse Linear Systems*, Second Edition, SIAM, Philadelphia, 2003.
- Y. Saad, *Iterative methods for linear systems of equations: A brief historical journey*, in S. C. BRENNER, I. SHPARLINSKI, C.-W. SHU AND D. B. SZYLD (EDS.), *75 Years of Mathematics of Computation*, American Mathematical Society, Contemporary Mathematics Vol. 754, Providence, RI, 2020, pp. 197–215.
- Y. Saad and H. A. van der Vorst, *Iterative solution of linear systems in the 20th century*, Journal of Computational and Applied Mathematics, 123 (2000), pp. 1–33.
- C. Sbordone, *Renato Caccioppoli, nel centenario della nascita*, Bollettino dell'Unione Matematica Italiana, A(8), 7 (2004), pp. 193–214.
- J. B. Scarborough, *Numerical Mathematical Analysis*, The Johns Hopkins University Press, Baltimore, 1930.
- G. Scorza Dragoni, *Gianfranco Cimmino*, Rendiconti dell'Accademia dei Licei (Supplemento), 9, 2 (1991), pp. 59–68. Reprinted in Cimmino (2002), pp. 661–668.
- S. L. Segal, *Mathematicians under the Nazis*, Princeton University Press, Princeton, New Jersey, 2003.
- L. Seidel, *Über ein Verfahren, die Gleichungen, auf welche die Methode*

- der kleinsten Quadrate führt, sowie lineäre Gleichungen überhaupt, durch successive Annäherung aufzulösen*, Abhandlungen mathemat.-physikalische Klasse, Bayerische Akademie Wissenschaften, 11 (1874), pp. 81–108.
- R. Soni, K. Gallivan, and K. Jenkins, *Low-complexity data reusing methods in adaptive filtering*, IEEE Transactions in Signal Processing, 52 (2004), pp. 394–405.
- F. Sukru Torun, M. Manguoglu, and C. Aykanat, *A novel partitioning method for accelerating the block Cimmino algorithm*, SIAM Journal on Scientific Computing, 40 (2018), pp. C827–C850.
- T. Tommasini Montanari, *Chebyshev acceleration of the method of Cimmino*, Calcolo, 21 (1984), pp. 61–74.
- A. van der Sluis and H. A. van der Vorst, *SIRT and CG-type methods for the iterative solution of sparse linear least squares problems*, Linear Algebra and its Applications, 130 (1990), pp. 257–302.
- H. A. van der Vorst, *Iterative Krylov Methods for Large Linear Systems*, Cambridge University Press, Cambridge, UK, 2003.
- R. S. Varga, *Matrix Iterative Analysis*, Prentice-Hall, Englewood Cliffs, New Jersey, 1962.
- R. von Mises and H. Pollaczek-Geiringer, *Praktische Verfahren der Gleichungsauflösung*, Zeitschrift für Angewandte Mathematik und Mechanik, 9 (1929), pp. 58–77; 152–164.
- E. L. Wachspress, *Iterative Solution of Elliptic Systems and Applications to the Neutron Diffusion Equations of Reactor Physics*, Prentice-Hall, Englewood Cliffs, New Jersey, 1966.
- G. Wahba, *Three topics in ill-posed problems*, Proceedings of the Conference on Inverse and Ill-Posed Problems, (Sankt Wolfgang, 1986), Notes and Reports in the Mathematical Sciences and Engineering, 4, Academic Press, Boston, MA, 1987, pp. 37–51.
- E. T. Whittaker and G. Robinson, *The Calculus of Observations. A Treatise on Numerical Mathematics*, Blackie & Son, London, 1924.
- C. Wu, R. Jeraj, W. Lu, and T. R. Mackie, *Fast treatment plan modification with an over-relaxed Cimmino algorithm*, Medical Physics, 31 (2004), pp. 191–200.
- Y. Xiao, D. Michalski, J. M. Galvin, and Y. Censor, *The least-intensity feasible solution for aperture-based inverse planning in radiation therapy*, Annals of Operations Research, 119 (2003), pp. 183–203.
- A. J. Zaslavski, *Approximate Solutions of Common Fixed-Point Problems*, Springer, 2015.
- G. Zilli, *Parallel implementation of a row-projection method for solving sparse linear systems*, Supercomputer, 53-X-1 (1993), pp. 33–43.

PARTE C

Vita dell'Accademia

(Nota redatta dal Segretario Marco Napolitano)

Attività dell’Accademia di Scienze Fisiche e Matematiche nell’anno accademico 2022

Nell’anno 2022, le tornate accademiche si sono tenute regolarmente, rispettando l’usuale numero di otto tornate annue. L’attenuarsi dell’emergenza sanitaria, dovuta alla pandemia da covid-19, e la conseguente quasi completa cancellazione delle restrizioni sanitarie hanno permesso di tenere in presenza tutte le tornate, pur lasciando a chi lo volesse la possibilità di partecipare da remoto per mezzo della piattaforma telematica TEAMS. Questa possibilità di partecipazione in presenza o da remoto si sta, ormai, affermando come prassi usuale. Essa ha l’indubbio vantaggio di consentire a ogni socio di partecipare alle tornate accademiche anche quando esistano motivi che ne rendano difficile o impossibile la partecipazione in presenza. D’altra parte, non si può negare che esista la possibilità che essa induca una certa disincentivazione alla partecipazione in presenza, con il rischio di un impoverimento dei rapporti umani e scientifici diretti tra soci, che hanno sempre caratterizzato una comunità accademica. Probabilmente, sarà opportuno, dopo una sufficiente sperimentazione, fare una riflessione collettiva su questa nuova modalità di interazione tra soci.

Come consuetudine, ogni tornata è consistita in una conversazione, aperta al pubblico, seguita dall’adunanza accademica riservata ai soci. Ha fatto eccezione la tornata di dicembre, nella quale la prevista conversazione è stata cancellata all’ultimo momento per una sopraggiunta indisposizione del relatore. Le conversazioni sono tenute da soci o da studiosi esterni ed hanno lo scopo principale di aggiornare i convenuti su tematiche di attualità in campo scientifico. Esse hanno trattato argomenti diversi, tutti di grande interesse, riguardanti la scienza, la sua divulgazione ed il dibattito corrente sull’uso ecologico e sostenibile delle risorse naturali.

Una parte importante dell’attività culturale dell’Accademia è la presentazione, in sede di adunanza, di comunicazioni scientifiche riservate ai soci o a studiosi che godano della presentazione di un socio. Le comunicazioni sono state in totale sette, compresa quella usuale sui dati meteorologici dell’anno decorso,

preparata dai colleghi dell’Osservatorio di San Marcellino. Il loro elenco, comprensivo di titolo e autori, è riportato nella versione a stampa di questa relazione. Quattro riguardano contributi nell’ambito della Classe di Scienze Naturali e due in quella di Scienze Matematiche. Tutte le comunicazioni sono incluse in questo Rendiconto dell’Accademia per il 2022.

In autunno, nella collana Memorie dell’Accademia di Scienze Fisiche e Matematiche, è stato stampato il volume “*Renato Caccioppoli: Teoria delle funzioni di più variabili complesse*”, a cura del socio Luciano Carbone e di Giampiero Esposito, Luca Dell’Aglio, Giuseppe Tomassini. Si è potuto realizzare quest’opera grazie al ritrovamento, avvenuto nel 2020, di un dattiloscritto contenente le note relative al corso sulle funzioni di più variabili complesse, tenuto da Caccioppoli presso l’Università degli Studi di Napoli nell’anno accademico 1947-48. La vicenda del ritrovamento, il contenuto del dattiloscritto, il quadro culturale di riferimento e le indagini che hanno condotto ad identificare in Guido Stampacchia l’estensore del dattiloscritto sono stati oggetto di una nota pubblicata nel Rendiconto 2021 dell’Accademia¹.

1– COOPTAZIONE DI NUOVI SOCI

Nella prima metà dell’anno sono stati eletti tre nuovi soci corrispondenti nazionali nella Classe di Scienze Naturali e due nella Classe di Scienze Matematiche. Sono, nel primo caso, i Proff. Fabio Ambrosino, Domenico Caputo e Luigi Paduano, tutti professori ordinari dell’Università degli Studi di Napoli “Federico II”, il primo presso il Dipartimento di Fisica “E. Pancini”, il secondo presso il Dipartimento di Ingegneria Chimica, dei Materiali e della Produzione Industriale e il terzo presso il Dipartimento di Scienze Chimiche. Nel secondo caso sono le Prof.sse Anna Mercaldo e Cristina Trombetti, ordinarie presso Dipartimento di Matematica e Applicazioni “Renato Caccioppoli” dell’Università “Federico II”. È stata anche eletta una nuova socia straniera nella Classe di Scienze Naturali. È Anne Imberty, Directeur de recherche au Centre National de la Recherche Scientifique (CNRS) CERMAV- CNRS. Per tutti loro la nomina decorre dal 1° giugno 2022.

2 – SOCI SCOMPARI

Durante l’anno si è, purtroppo, registrata la scomparsa di cinque soci: Salvatore Califano, Achille Panunzi, Carlo Pedone e Vincenzo Vitagliano, soci ordinari nella Classe di Scienze Naturali, e Paolo De Lucia, socio ordinario nella Classe di Scienze Matematiche. Per ognuno di loro c’è stato un breve ma intenso

¹ Luciano Carbone, Giampiero Esposito, Luca Dell’Aglio: *Renato Caccioppoli e il libro mai scritto (ma ritrovato)*. Rend. Acc. Scienze Fisiche e Matematiche, vol. LXXXVIII (2021) pp. 103-117.

e commosso ricordo all'inizio dell'adunanza accademica immediatamente successiva alla scomparsa.

Salvatore Califano, scomparso il 17 gennaio 2022, è stato ricordato dal consocio Lelio Mazzarella nell'adunanza del 21 gennaio e un ricordo scritto è allegato al verbale di tale adunanza.

Paolo De Lucia, scomparso il 18 marzo 2022 è stato ricordato dal Presidente Carlo Sbordone nell'adunanza del 22 aprile e un ricordo, scritto da Sbordone e dal socio emerito Guido Trombetti, è allegato al verbale di tale adunanza

Vincenzo Vitagliano, scomparso il 15 agosto 2022, è stato ricordato nell'adunanza del 16 dicembre 2022 dai consoci Luigi Paduano e Lelio Mazzarella e un ricordo scritto è allegato al verbale di tale adunanza

Carlo Pedonre, scomparso il 14 settembre 2022, è stato ricordato dal consocio Lelio Mazzarella nell'adunanza del 18 novembre e un ricordo scritto è allegato al verbale di tale adunanza.

3 – PREMI ACCADEMICI

Sono stati banditi cinque concorsi per l'attribuzione di altrettanti premi accademici. Tuttavia, i premi effettivamente attribuiti sono stati sei. Infatti, per uno di tali concorsi, intitolato a Guido Stampacchia e diretto a giovani dottori di ricerca in matematica che abbiano conseguito risultati significativi relativi al tema “*Calcolo delle Variazioni*”, i premi assegnati sono stati due invece di uno, accogliendo in via del tutto eccezionali la richiesta della commissione esaminatrice che ha proposto due vincitori ugualmente meritevoli. Essi sono il Dott. Elia Bruè (Institute for Advanced Study, Princeton (USA)) e il Dott. Andrea Merlo (post-doc, Université de Fribourg, Svizzera). Due premi, intitolati a Lisa De Conciliis, uno avente per tema “*Approcci molecolari alla progettazione di nuovi agenti terapeutici*” e l'altro “*Approcci molecolari per l'impiego della biodiversità in medicina o in agricoltura*”, sono stati attribuiti rispettivamente alla Dott.ssa Claudia Riccardi (Centro di ricerca CERM dell'Università degli Studi di Firenze) e alla Dott.ssa Lidia Nicola (Dipartimento di Bioscienze dell'Università degli Studi di Milano). Un premio, intitolato a Mariolina Capano, sul tema “*Determinazione strutturale di biomolecole*” è stato attribuito alla Dott.ssa Giarita Ferraro (ric. Dipartimento di Scienze Chimiche, Università degli Studi di Napoli “Federico II”). Infine, un altro premio, intitolato a Maria Bakunin e relativo a ricerche sul tema “*Materiali nanoporosi per la transizione energetica*”, è stato attribuito al Prof. Antonio Abate (prof. ass. presso il Dipartimento di Ingegneria Chimica, dei Materiali e della Produzione Industriale, Università degli Studi di Napoli ‘Federico II’).

4 – CONVERSAZIONI

21 gennaio

La radiografia muonica. Vulcani, piramidi e sottosuolo: i muoni cosmici ci permettono di svelare i loro segreti

Prof. Giulio Saracino, Università degli Studi di Napoli “Federico II”.

Riassunto - All'inizio del XX secolo i raggi X, da poco scoperti, furono utilizzati per osservare l'interno del corpo umano, aprendo così una nuova frontiera nel campo delle indagini mediche. La radiografia a raggi X è possibile grazie alla capacità che questa radiazione ha di non fermarsi sulla superficie degli oggetti, come avviene invece per la luce, ma di penetrare al loro interno. La penetrazione è però limitata e per questo motivo la radiografia a raggi X può essere applicata in pratica solo a materiali che hanno al massimo alcune decine di centimetri di spessore.

In natura esistono però altre forme di radiazione. Tra queste vi sono i muoni, particelle elementari elettricamente cariche che posseggono una notevole capacità di attraversare la materia. La superficie terrestre è continuamente investita da muoni di elevata energia, prodotti dalla cosiddetta radiazione cosmica primaria quando quest'ultima interagisce con i nuclei dei costituenti dell'atmosfera terrestre. La loro capacità di attraversare anche centinaia di metri di roccia ha permesso di utilizzare i muoni in maniera analoga ai raggi X, sviluppando una tecnica di *radiografia muonica* (a volte chiamata anche *muografia*) capace di fornirci informazioni sulla struttura interna di corpi molto spessi. Ad esempio la *muografia* è stata applicata con successo nella ricerca di vuoti all'interno delle piramidi egizie di Chefrén e Cheope, nello studio dei vulcani e del sottosuolo.

Durante la conversazione saranno introdotti i principi della radiografia muonica. Saranno poi discussi alcuni esempi, tra cui due progetti attivi sul nostro territorio: l'esperimento MURAVES presso il Vesuvio e gli studi di cavità all'interno di Monte Echia a Napoli.

18 febbraio

Rydberg Matter and Telekinetic Effects

Prof. Johann Summhammer. Vienna University of Technology, Institute of Atomic and Subatomic Physics.

Abstract - Telekinetic effects are phenomena in which a person manipulates material objects seemingly without physical contact. Such phenomena are very rare but have been reported throughout the ages and have received scientific investigation since the late 19th century. Despite obvious physical characteristics and

side effects, explanations based on physics, chemistry and biology have remained vague hypotheses, because most scientists denied the phenomena.

In this talk I will elucidate a possible connection between Rydberg Matter and telekinetic effects. Rydberg matter was predicted in the 1980's. It is formed from atoms or molecules in highly excited Rydberg states. Until now, it seems to have been produced only a few times. A vapor of Rydberg atoms can condense into soft solid matter, because delocalization of the excited electrons in the conduction band of the solid state lowers the energy. This condensed Rydberg matter is expected to be a metallic conductor of electricity while remaining largely transparent. The lifetime of this state of matter can reach seconds to minutes. Due to the large size of the atoms, the density of this matter is as low as that of ambient air but can also be much lower. The binding energy is on the order of 0.1 eV, making Rydberg matter unstable in visible light and at temperatures above 500 K or so. It is proposed that the nervous system of humans (and animals of similar physiology) can create Rydberg matter outside the body from the air around it, by emitting cascades of very high frequency electromagnetic radiation from the ends of axons of neuron cells. Such radiation in the frequency range around 1 THz could come from oscillating biomolecules with a dipole moment, e.g., the microtubuli of the cytoskeleton. The frequencies are in the range of rotational energy spacing of the diatomic molecules of air, O₂ and N₂, which absorb this energy and get into high rotational states. Together with catalytic effects at the skin this energy transfer could eventually lead to high electronic excitations of the gas molecules. At Rydberg levels of around n=10 the molecules obtain diameters on the order of the mean distance between molecules in the air, and condensation to Rydberg matter might commence. This essentially invisible Rydberg matter would be a kind of outgrowth from the skin, similar to hair. Since there are about 10³ nerve endings per mm² of skin, the hairs might coalesce to form bulges of various shapes. Due to the high polarizability of Rydberg matter, the shape may be controlled by high frequency electromagnetic fields, possibly the same which cause the excitations.

Although Rydberg matter is relatively elastic, it will allow to move and manipulate an object without touching it by the normal body. If Rydberg matter is indeed metallic, its contact with ordinary metals will lead to an equilibration of Fermi levels and to a rearrangement of the electronic surface states of the contacted metal. Recently, very significant changes of the micro hardness have been shown, if two pieces of ordinary metal are brought in contact, and if one is a conductor of electrons and the other one of holes. A similar effect might occur when Rydberg matter touches a normal metal. If that metal has microcrystalline modification, as most everyday metals do, the large internal surface area will experience a change of its electronic states, which will also change the internal hardness of the metal. Hence, the softening of metal to allow the proverbial "spoon bending" could be a normal physical process. The success of a "spoon bender",

as of any "telekinetically" gifted person, will depend on the specific physical makeup of the neuron cells going to the relevant skin area and on the properties of the axonal signals. Since the effect originates from air which has been turned into Rydberg matter, direct touching of the "spoon" may not even be necessary.

18 marzo

L'organizzazione armoniosa del sistema solare: dai pianeti al sole e il clima

Prof. Nicola Scafetta, Università degli Studi di Napoli "Federico II".

Riassunto - Fin dall'antichità i movimenti dei pianeti del sistema solare hanno attirato l'attenzione degli astronomi e dei filosofi perché i periodi orbitali sembrano essere interconnessi da semplici proporzioni armoniche, risonanze e/o commensurabilità. Ad esempio, 5 rivoluzioni di Giove corrispondono approssimativamente a 2 rivoluzioni di Saturno; le tre lune interne di Giove, Io, Europa e Ganimede, sono bloccate in una risonanza orbitale 4:2:1; e molte altre. Tali proprietà suggeriscono che il sistema solare è stato generato da processi di auto-organizzazione gravitazionale e mutua sincronizzazione tra i suoi elementi. Questa ipotesi è storicamente nota come "la Musica delle Sfere" o "l'Armonia dei Mondi". Inoltre, e più sorprendentemente, le armoniche planetarie del nostro sistema solare risultano anche spettralmente coerenti a diversi cicli dell'attività del Sole. Tutto questo suggerisce che il sistema planetario funzioni come un "maestro di orchestra" a cui tutto si sincronizza. Le frequenze base di questa sinfonia sono costituite dai periodi orbitali e dalle loro inequalità invarianti, cioè tra i battimenti tra i vari cicli sinodali. Qui presento una serie di ricerche recenti finalizzate a rivelare queste affascinanti proprietà del mondo in cui viviamo.

22 aprile

La pandemia vista dal gruppo CovidStat INFN

Prof. Luca Lista, Università degli studi di Napoli "Federico II".

Riassunto - Dalle prime fasi della pandemia di Covid-19, il gruppo CovidStat dell'INFN ha monitorato l'andamento dei contagi utilizzando i dati del Dipartimento della Protezione Civile. Un accordo con l'Istituto Superiore di Sanità consente, più di recente, di accedere a dati più capillari. Gli studi effettuati su questi dati e quelli della mortalità pubblicati dall'ISTAT hanno portato a quattro pubblicazioni su rivista.

20 maggio

Aspetti fisici nella medicina clinica virtuale basata sull'evidenza

Prof. Paolo Russo, Università degli Studi di Napoli "Federico II".

Riassunto - La medicina basata sull'evidenza si avvale di trial clinici. Nel campo della diagnostica del cancro al seno si stanno affermando trials clinici virtuali che riproducono in-silico l'esame mammografico, con risparmio di tempi, costi e di dose di radiazione ai pazienti. Tali studi richiedono una accurata descrizione digitale dell'anatomia dell'organo, attraverso cosiddetti fantocci computazionali, il cui sviluppo si affianca a quello di fantocci dell'intero corpo umano utilizzati nella stima della dose di radiazione negli esami radiografici ed in medicina nucleare. Nella conversazione verranno descritti gli studi presso la Federico II per trials clinici virtuali in mammografia 2D e 3D e tomografia dedicata al seno, e per lo sviluppo di fantocci antropomorfi digitali per la stima personalizzata della dose di raggi X basata su simulazioni Monte Carlo in tomografia computerizzata.

17 giugno

Il bosco e la città: una nuova necessaria alleanza

Dr. Antonio di Gennaro, Editorialista di "La Repubblica" (ed. di Napoli).

Riassunto - Lentamente (ma mica tanto) il bosco sta riprendendosi, in Europa e in Italia. lo spazio perso lungo tutta la seconda metà del '900. L'ultimo Inventario forestale nazionale ha stimato in circa un milione di ettari l'aumento della superficie boscata in Italia nell'ultimo decennio, 40.000 ettari solo in Campania. Il processo di riforestazione spontanea interessa l'Appennino in abbandono ma anche, sorprendentemente, le aree metropolitane. Insomma, sembrerebbe che più che piantare nuovi alberi, la priorità dovrebbe essere quella di prendersi cura di quelli che sono nati senza il nostro intervento. Nella post-modernità dobbiamo imparare a praticare un ossimoro: "curare l'abbandono".

19 novembre

Epigenetica e complessità biologica

Prof. Giuseppe Geraci, emerito di Biologia Molecolare, Università degli Studi di Napoli "Federico II". Socio emerito.

Riassunto - Si accennerà all'origine di questo termine che rappresenta lo studio di meccanismi che generano due passi fondamentali per l'incremento della complessità genetica. Il differenziamento cellulare per cui da uno stesso genoma si producono cellule completamente diverse per struttura e capacità operative e l'ontogenesi per cui da un particolare uovo fecondato, attraverso stadi di sviluppo esattamente definiti e successivi, si produce un particolare organismo. Le attività alla base di questi meccanismi non sono direttamente deducibili dalle sequenze del DNA genomico. Si presenteranno evidenze che esse dipendono inizialmente

dalle strutture del genoma opportunamente modificate da attività enzimatiche. Di queste attività la principale consiste nella metilazione di particolari citosine che sono uno dei quattro componenti del DNA. Questo tipo di modifica, scoperta e definita da Eduardo Scarano negli anni sessanta del secolo scorso in una serie di lavori pionieristici, non fu valorizzata per la sua importanza come poi è risultato dalle attività di ricerca successive, che hanno mostrato il suo ruolo essenziale anche nella produzione di uno zigote (uovo fecondato) funzionale e cioè capace di generare un organismo. Si mostrerà che la plasticità della metilazione è di fondamento a passi del differenziamento cellulare. A differenza di altre attività cellulari, la sia pur minima perturbazione di uno qualsiasi dei meccanismi epigenetici è causa di teratogenesi mostrando quanto delicati e critici essi siano.

APPENDICE

L'Osservatorio Meteorologico di San Marcellino Napoli Centro: i dati dell'anno 2022

Nota di Nicola Scafetta^{1*}, Raffaele Di Cristo², Raffaele Viola¹,
Adriano Mazzarella³

Presentata dal socio Carlo Sbordone
(Adunanza del 20 gennaio, 2023)

Key words: air temperature, atmospheric pressure, rainfall, solar radiation, wind intensity-direction, UV index

Abstract - The analysis of all meteorological parameters of the year 2021 shows that: **(a)** The monthly mean pressure ranges between 1014.0 hPa of August and 1023.3 hPa of March, with an annual mean of 1018.3 hPa, with a daily absolute minimum of 995.4 hPa measured on 22 November at 12:50 and with a daily absolute maximum of 1037.6 hPa measured on 15 March at 10:20; **(b)** The monthly mean air temperature ranges from 10.6°C of January and 28.5°C of July, with an annual mean of 19.0°C, with a daily absolute minimum of 3.8°C measured on 23 March at 13:20 and with a daily absolute maximum of 96.0°C measured on 24 December at 11:00; **(c)** The monthly mean relative humidity ranges from 58.0% of March and 78.9% of December, with an annual mean of 66.5%, with a daily absolute minimum of 19.0% measured on 27 January at 5:50 and with a daily absolute maximum of 96.0% measured on 25 February at 5:30; **(d)** The mean monthly global solar radiation ranges between 174.8 W/m² of December and 483.7 W/m² of July, with an annual mean of 340.5 W/m² and with a daily absolute maximum of 1202.0 W/m² measured on 8 May at 12:20; **(e)** The mean monthly UV Index ranges from

¹ Osservatorio Meteorologico

Dipartimento di Scienze della Terra, dell'Ambiente e delle Risorse
Largo San Marcellino 10 80122 Napoli Università degli Studi di Napoli Federico II

² Docente presso Ministero dell'Istruzione e del Merito

³ In pensione dal 1.11.2018

*Correspondence to nicola.scafetta@unina.it

1.0 of December to 3.7 of May, with an annual average of 2.3 and with an daily absolute maximum of 7.4 measured on 9 July at 13.20; **(f)** The monthly mean wind intensity ranges between 1.4 m/s of October and 2.4 m/s of April, with an annual mean of 2.0 m/s and with most intense daily gust of 23.2 m/s measured on 22 November at 7:30; **(g)** The wind direction shows a mode from the North in February, November, December, from North-East in January, from South in June, from South-West in March, April, May, July, August, September; **(h)** The monthly cumulative rainfall ranges from 7.8 mm of June to 277.0 mm of November, with a cumulative annual value of 889.6 mm and with a daily absolute maximum of 94.0 mm measured on 25 December.

Riassunto - Dall'analisi di tutti i parametri meteo dell'anno 2021 emerge quanto segue:
(a) La pressione atmosferica media mensile oscilla fra 1014.0 hPa di agosto e 1023.3hPa di marzo, con una media annua di 1018.3 hPa, con un minimo assoluto giornaliero di 995.4 hPa registrato il 22 novembre alle ore 12.50 e con un massimo assoluto giornaliero di 1037.6 hPa registrato il 15 marzo alle ore 10.20; **(b)** La temperatura dell'aria media mensile oscilla fra 10.6°C di gennaio e 28.5°C di luglio, con una media annua di 19.0°C, con un minimo assoluto giornaliero di 3.8°C registrato il 25 gennaio alle ore 7:30 e con un massimo assoluto giornaliero di 36.1°C registrato il 27 giugno alle ore 15.20; **(c)** L'umidità relativa media mensile oscilla fra 58.0% di marzo e 78.9% di dicembre, con una media annua di 66.5%, con un minimo assoluto giornaliero del 19.0% registrato il 23 marzo alle ore 13:20 e con un massimo assoluto giornaliero di 96.0% registrato il 24 dicembre alle ore 11:00; **(d)** La radiazione solare globale media mensile oscilla fra 174.8 W/m² di dicembre e 483.7 W/m² di luglio, con una media annua di 340.5 W/m² e con un massimo assoluto giornaliero di 1202.0 W/m² registrato l'8 maggio alle ore 12.20; **(e)** L'indice UV medio mensile oscilla fra 1.0 di dicembre e 3.7 di luglio, con una media annua di 2.3 e con un massimo assoluto giornaliero di 7.4 registrato il 9 luglio alle ore 13.20; **(f)** L'intensità media mensile del vento oscilla tra 1.4 m/s di ottobre e 2.4 m/s di aprile, con una media annua di 2.0 m/s e con la raffica giornaliera più intensa di 23.2 m/s registrata il 22 novembre alle ore 7:30; **(g)** La direzione del vento presenta una moda da Nord a febbraio, novembre e dicembre, da Nord-Est a gennaio, da Sud a giugno, da Sud-Ovest a marzo, aprile, maggio, luglio, agosto e settembre; **(h)** La pioggia cumulata mensile oscilla tra il valore 7.8 mm di giugno e i 277.0 mm di novembre, con un valore annuale cumulato di 889.6 mm e con un massimo assoluto giornaliero di 94.0 mm registrato il 25 settembre.

1 – INTRODUZIONE

I dati meteo sono attualmente rilevati da una centralina automatica sita sulla torretta dell'edificio di San Marcellino (lat. 40°50'50" N; long. 14°15'29" E; quota 50m slm), sede attuale del Dipartimento di Scienze della Terra, dell'Ambiente e delle Risorse a meno di 50 m dall'Accademia di Scienze Fisiche e Matematiche della Società Nazionale di Scienze, Lettere ed Arti in Napoli. La stazione gestisce i seguenti sensori: temperatura dell'aria (°C), pressione

atmosferica (hPa) (normalizzata a livello del mare), umidità relativa (%), velocità del vento (m/s), direzione del vento (°Nord), precipitazione (mm), radiazione solare globale (W/m²), indice UV (scala da 0 a 16).

Per ogni mese i valori estremi giornalieri sono evidenziati in grassetto.

I dati sono acquisiti con cadenza di 10 minuti ed i valori, fatta eccezione per la pioggia che viene registrata come cumulata, sono quelli istantanei.

I dati giornalieri di radiazione globale ed indice UV sono mediati sulla loro effettiva durata.

La direzione del vento è calcolata come moda sia a scala di 10 minuti per i grafici orari che a scala giornaliera per i grafici mensili. È considerata variabile (var.) quando la direzione non è stata registrata su uno stesso quadrante per più di 8 ore.

L'assenza del dato indica sensore fuori uso.

2- MATERIALI E METODI

Il bollettino meteorologico dell'anno 2022 è così organizzato:

- Un breve rapporto meteorologico per ogni mese;
- Una catalogazione delle medie orarie mensili (00 -23 h) e dei relativi grafici per ogni mese;
- Una catalogazione dei valori medi giornalieri e dei relativi grafici, per ogni mese, con l'indicazione dei valori estremi registrati;
- Un riepilogo mensile di tutti i parametri meteo relativo all'anno in corso;
- Un riepilogo mensile delle frequenze di precipitazione, temperature minime e massime distinte per soglia.

È possibile accedere via web alla consultazione dei dati rilevati in tempo reale all'indirizzo: <https://www.meteo.unina.it>.

3- RAPPORTI METEO MENSILI

GENNAIO 2021

Gennaio è stato caratterizzato da una notevole variabilità atmosferica: la prima settimana con temperature di 2-3°C al di sopra della media, la seconda con temperature un grado al di sotto, la terza con 2-3°C al di sopra e finalmente fino a fine mese con temperature 1-2°C al di sotto.

In sintesi, il freddo è stato intermittente e l'Italia intera è stata sottoposta di continuo ad impulsi artici in discesa da latitudini elevate e a rimonte anticicloniche responsabili di nebbie notturne e accumulo di inquinanti. Le medie mensili sono risultate così di 8.1°C per le temperature minime (un grado e mezzo in più della media) e di 13.4°C per le massime (un grado in più). Le temperature sono scese al di sotto dei 4°C il 25 e il 26 e il cono del Vesuvio è stato ricoperto di

neve dall'11 al 14 e dal 24 al 25. La temperatura del mare è passata da 17°C degli inizi di gennaio a 14°C a fine mese.

La pioggia, distribuita in 8 giorni, è stata pari a 31 mm, il 70% in meno di quella che cade normalmente a gennaio. Nella cultura contadina, però, la mancanza di pioggia a gennaio ha un risvolto positivo. Il detto "*Iennaro sicco, mas-saro ricco*" significa che un gennaio secco permette al grano di radicare meglio sottoterra, di evitare il danno delle improvvise gelate e di fare un ottimo raccolto estivo con grande soddisfazione economica del proprietario terriero.

FEBBRAIO 2022

La temperatura dell'aria di febbraio è stata costantemente al di sopra della media con l'eccezione del primo e degli ultimi tre giorni. Il mancato freddo di questo febbraio è imputabile alle ripetute invasioni del Mediterraneo da parte di aree anticicloniche che hanno impedito l'ingresso alle perturbazioni atlantiche e alle correnti fredde settentrionali. Le medie delle temperature minime e massime dell'intero mese sono state, perciò, di 9.2°C per le temperature minime, due gradi in più della media stagionale, e di 15.1°C, per le temperature massime, un grado e mezzo in più.

La quantità di pioggia è stata di 56 mm, il 25% in meno di quella che cade normalmente a febbraio, distribuita su 9 giorni e concentrata nel giorno 26. Il giorno più freddo è stato il 26 febbraio con 5.1°C mentre il vento ha raggiunto picchi di 60 km/h nei giorni 1, 7 e 26. Il cono del Vesuvio è stato ricoperto di neve nei primi due giorni e negli ultimi tre. La temperatura del mare nel golfo ha oscillato intorno ai 14.7°C per l'intero mese. Negli ultimi giorni, una profonda area ciclonica nel Tirreno è riuscita a risucchiare area gelida direttamente dai Balcani che ha determinato un colpo di coda dell'inverno. La neve è caduta copiosa a quote collinari nelle zone interne dell'Irpinia, Sannio, Matese e sul cono del Vesuvio.

MARZO 2022

La prima metà di marzo sarà ricordata per il colpo di coda dell'inverno con valori di temperatura dell'aria di 4/5°C al di sotto della media e con il cono del Vesuvio ininterrottamente coperto di neve. Sarà ricordata come la prima metà di marzo più fredda dal 1872, da quando è stato operativo l'Osservatorio Meteorologico della Federico II a Napoli centro. Nella seconda metà del mese, ad eccezione dei giorni 19, 20 e 21 ancora al di sotto della media, i valori di temperatura sono stati in linea con quelli tipicamente primaverili. L'inatteso scenario termico della prima metà del mese è stato determinato dall'anticiclone delle Azzorre che si è posizionato ad ovest della penisola iberica, ha bloccato la circolazione atmosferica da ovest ed ha così agevolato l'arrivo sull'Italia di un flusso d'aria gelida direttamente dalla Russia. A seguire, e per una intera settimana, una ondulazione anticyclonica di ben 1040 hPa a forma della lettera greca omega (indicativa di una

circolazione atmosferica bloccata) si è impossessata dell'Europa centrale e del Mediterraneo determinando ancora assenza di pioggia, nebbie notturne e temperature diurne più elevate di 10°C rispetto alla notte. Solo negli ultimi 5 giorni, la circolazione atmosferica si è sbloccata con una diminuzione di pressione atmosferica di ben 30 hPa, con l'arrivo di aria umida e mite direttamente dall'atlantico e finalmente con le piogge negli ultimi due giorni del mese. Le medie mensili delle temperature minime sono state di così di 8.4°C per le minime, mezzo grado in meno della media stagionale, e di 15.0°C per le massime, un grado in in meno. La temperatura del mare ha oscillato fra 15°C e 16°C.

La pioggia caduta è stata pari a 33 mm, la metà di quella che cade normalmente a marzo, distribuita in 7 giorni e concentrata nell'ultimo giorno quando la protezione civile ha lanciato l'allerta meteo per la pioggia e la ventilazione.

APRILE 2022

Le temperature massime di aprile sono state sistematicamente al di sotto della media di 3-4°C nel periodo compreso tra l'1 e il 12, e di 1-2°C nel periodo compreso tra il 17 e il 25. Questo a causa di un'area depressionaria centrata sul Mar Ligure che ha agevolato la discesa di aria fredda direttamente dal polo. Dal 13 al 16 e negli ultimi cinque giorni del mese, la risalita di un'area anticlonica tropicale e venti meridionali hanno causato un notevole rialzo termico con la presenza in quota di sabbia sahariana che ha reso lattiginoso il cielo. La media delle temperature minime è stata così di 12.2°C, mezzo grado in più della media stagionale, e quella delle temperature massime è stata di 18.7 °C, mezzo grado in meno.

La pioggia caduta nell'intero mese è stata di 58 mm, il 15% in meno di quanto piove normalmente ad aprile e distribuita in 9 giorni. Il giorno più freddo è stato il 2 con 5.0°C, lontano dai record di temperatura minima del 6 aprile 1894 con 2.5°C e del 10 aprile 1956 con 3.6°C. Il cono del Vesuvio è stato ricoperto di neve dal 2 al 4. La temperatura del mare nel golfo si è portata dai 14°C di inizio mese ai 17°C di fine mese.

MAGGIO 2022

Il meteo di maggio può essere sostanzialmente diviso in due parti. Nella prima parte, fino al giorno 15, la risalita su alte latitudini dell'anticiclone delle Azzorre ha bloccato la circolazione atmosferica da ovest verso est ed ha permesso l'ingresso sul Mediterraneo di masse d'aria fredde settentrionali con una sensibile diminuzione termica. Nella seconda parte, la discesa di latitudine dell'anticiclone delle Azzorre e la contemporanea risalita di un'area anticlonica tropicale con venti meridionali hanno portato in quota sabbia sahariana che ha reso lattiginoso il cielo e determinato un notevole rialzo termico, specie nell'ultima settimana. Le medie delle temperature minime e massime sono state, perciò, pari a 18.3°C e a 24.8°C, più elevate di 3.4°C e di 1.5°C rispetto alle relative medie mensili calcolate su 150 anni. Il giorno più caldo è stato il 27 maggio con 33.3°C ma inferiore

al record assoluto di 34.6°C del 17 maggio 2020. La temperatura del mare nel golfo si è portata dai 17°C di inizio mese ai 22°C di fine mese.

Le precipitazioni sono state di 9 mm, l'80% in meno di quelle che cadono normalmente a maggio. Il 2022 si sta rivelando siccioso: la cumulata dei primi 5 mesi di quest'anno è stata pari a 192 mm contro un andamento normale di 352 mm, a significare che nei primi 5 mesi di quest'anno è caduta il 45% in meno di pioggia. Il conseguente abbassamento delle falde acquifere, se non dovesse essere recuperato nei prossimi mesi, potrebbe dare grossi problemi di approvvigionamento d'acqua.

GIUGNO 2022

La temperatura dell'aria di giugno è stata sempre al di sopra della media del periodo di 2-3°C con l'eccezione dei giorni 7,8,9 e 10. I giorni più caldi sono stati il 26, il 27 e il 28 con una temperatura massima pari a 35.2, 36.2° e 36.1, 6-7°C al di sopra della media del periodo. L'anticiclone delle Azzorre si è posizionato su tutto il Nord Atlantico in modo da bloccare la normale circolazione da Ovest verso Est e agevolare l'ingresso del bollente ed umido anticiclone nordafricano che i meteofili chiamano *il cammello*. Il carico di aria e di polveri si è spostato dal nord Africa sul Mediterraneo ed ha reso lattiginoso il cielo. Tale scenario ha così determinato una media delle temperature massime di 30.4°C, tre gradi in più della media del periodo e una media delle temperature minime di 23.6°C, cinque gradi in più.

Le precipitazioni sono state pari a 8 mm e distribuite nei giorni 9, 10 e 17. La pioggia di questo primo semestre è stata il 50% in meno della cumulata normale stagionale e proprio la mancanza di precipitazioni ha reso i suoli molto secchi. Un suolo secco si riscalda molto di più di un suolo umido e ciò determina, per contatto, un ulteriore riscaldamento dell'atmosfera sovrastante. La temperatura del mare nel golfo è schizzata da 22.0°C di inizio mese a 26.0°C di fine mese. Giova sottolineare che il caldo di questo giugno non è da record ma rientra nella fisiologia delle avvezioni sahariane. L'archivio storico dell'Osservatorio della Federico II, sito a Napoli centro e funzionante ininterrottamente dal 1872, mostra che, sempre a causa dell'anticiclone africano, mesi di giugno sono stati più caldi di questo 2022: il 1945 con 30.7°C e il 1937 con 30.5. Ancora, le temperature massime del 27 e 28 giugno del 1935 e del 27 giugno del 1947 raggiunsero, rispettivamente, valori di 36.4°C, 37.2°C e 40.2°C.

LUGLIO 2022

La temperatura dell'aria di luglio è stata sempre al di sopra della media del periodo di 2-3°C con l'eccezione del giorno 15. I giorni più caldi sono stati il 2, il 3 e il 19 con una temperatura massima pari a 35.3, 35.2° e 34.6, 5-6°C al di sopra della media del periodo. La causa è da ricercarsi nella particolare disposizione che aree cicloniche e anticycloniche hanno assunto sull'Europa centro-

meridionale, denominata "blocco ad omega". Il bollente anticiclone africano è stato bloccato ed alimentato per l'intero mese di luglio da due centri di bassa pressione localizzati nell'oceano Atlantico e sull'Europa sud-orientale causando disagio nella popolazione specie di notte per l'elevato tasso di umidità. La media delle temperature massime è stata così di 32.1°C, due gradi e mezzo in più della media del periodo, quella delle minime di 25.5°C, quattro gradi in più. L'aumento maggiore delle temperature minime nelle aree metropolitane non è anomalo durante il periodo estivo perché fortemente legato al surriscaldamento delle strade bituminose e dei manufatti che di notte impedisce al suolo di raffreddarsi come nelle aree rurali.

La pioggia è stata pari a 14 mm, in linea con la cumulata del mese di luglio e concentrata nell'unico rovescio del giorno 8. La pioggia caduta da gennaio a luglio è stata pari a 214 mm, il 50% in meno della cumulata normale, e questo significa che, fino ad oggi, nell'area dell'intera città di Napoli, pari a 111 km², mancano all'appello circa 21 milioni di metri cubi di acqua piovana. Solamente un forte recupero del deficit pluviometrico potrebbe evitare di ricordare il 2022 come un anno molto siccitoso alla pari del 1946 (490 mm), 1949 (453 mm), 1981 (488 mm), 2002 (473mm) e 2017 (530 mm). La temperatura del mare nel golfo è oscillata tra i 28.5°C dei giorni 7 e 25 e i 23.0°C del giorno 9. È opportuno ricordare che, diversamente da quanto affermato dai mass media, il caldo di questo luglio non è da record. L'archivio storico dell'Osservatorio della Federico II, sito a Napoli centro e funzionante ininterrottamente dal 1872, mostra, infatti, che, sempre a causa dell'anticiclone africano, numerosi mesi di luglio sono stati più caldi di questo 2022: il 1945 (32.4°C), il 1947 (32.7°C), il 1950 (33.2°C) e il 1952 (33.1°C). Ancora, le temperature massime del 5 e 8 luglio del 1881 raggiunsero valori di 39.6°C e 39.9°C, il 20 luglio del 1887 il valore di 39.2°C, il 21 e il 22 luglio del 1939 valori di 38.8°C e 38.0°C.

AGOSTO 2022

Nelle prime due decadi, bollenti ed umidi anticicloni di origine africana in successione hanno invaso il Mediterraneo e determinato valori di temperatura ed umidità al di sopra delle medie stagionali con notevole disagio notturno nella popolazione. Le temperature elevate del suolo hanno spesso portato alla formazione di bolle d'aria calda che nelle zone interne e di pomeriggio si sono trasformate in temporali di calore. Solo nell'ultima decade, la ritirata dell'anticiclone africano su latitudini più basse ha facilitato l'ingresso di masse d'aria fredda settentrionale con pioggia e una netta diminuzione della temperatura. La media delle temperature minime a Napoli centro è stata così di 24.0°C, due gradi e mezzo in più della media, quella delle temperature massime di 31.3°C, un grado in più. I giorni più caldi sono stati l'1 e il 18 agosto, entrambi con una temperatura massima di 35.6°C. La temperatura del mare nel golfo è aumentata progressivamente fino alla prima decade da 24.3°C a 28.8°C per poi ridiscendere e stabilizzarsi sui 26.5°C.

I mass media ritengono che le temperature raggiunte in questo agosto siano da record ma l'archivio della “Federico II” mostra valori di gran lunga più elevati: il 6 agosto del 1885 con 39.2°C, il 19 agosto del 1946 con 39.0°C, il 9 agosto del 1956 con 39.1°C e tanti altri. Anche la media delle temperature massime dell'intero mese non è da record: il 1947 con 32.7°C, il 1952 con 32.5°C, il 1943 e il 1971 con 32.4°C, il 2012 con 32.0°C e tanti altri.

La pioggia è stata pari a 60 mm, più del doppio della cumulata normale, distribuita in nove giorni e concentrata nei forti temporali del mattino del 16 (con un vento di 60 km/h) e del pomeriggio del 23 (con un vento di 45 km/h). La pioggia di agosto ha portato il deficit pluviometrico del 2022 dal 55% al 35%.

SETTEMBRE 2022

Settembre è stato un mese dai due volti così come accaduto nei quattro anni precedenti. Nella prima metà, la temperatura dell'aria è stata di 2-3°C al di sopra della media stagionale, nella seconda metà di 3-4°C al di sotto. A livello mensile, la media delle temperature minime è stata così di 20.5°C, un grado e mezzo in più della media stagionale, mentre quella delle temperature massime è stata di 26.6°C, mezzo grado in meno. Questo perché, nei primi 16 giorni, una persistente area di alta pressione di origine subtropicale si è impadronita del sud Italia ed ha sempre respinto tutte le perturbazioni provenienti dall'Atlantico e dal nord. Solo a partire dal 17 settembre, la situazione barica è cambiata drasticamente: l'anticlone delle Azzorre si è posizionato sull'Atlantico ed ha agevolato l'ingresso di masse d'aria fredda settentrionale con piogge, temperature in discesa e venti intensi. La temperatura del mare nel golfo, vero termometro ambientale, ha raggiunto i 26.5°C nei primi 16 giorni per poi stabilizzarsi sui 23°C. Il giorno più caldo è stato il 5 settembre con 33.3°C.

La pioggia è stata pari a 244 mm (più di tre volte quella che cade di norma a settembre), distribuita su 13 giorni. In particolare, un fronte caldo (dovuto ad uno scontro fra aria calda proveniente da sud-ovest su aria fredda preesistente) ha determinato, per tutto il giorno 25, la caduta a Napoli centro di 94 mm di pioggia, accompagnata da un vento di libeccio di 75 km/h che ha messo a dura prova la navigazione nel golfo. Quest'anno i mass media hanno bombardato continuamente gli italiani sul rischio siccità legato al global warming indotto dall'uomo dimenticando che i conti sulla siccità vanno fatti a fine anno. In Campania, per esempio, la pioggia caduta da gennaio a luglio è stata scarsa con un deficit pluviometrico pari al 55%. Ma già la pioggia di agosto e quella di settembre hanno azzerato completamente il deficit e questo è in accordo al detto contadino che recita: *L'acqua in cielo sta pesata /quella che non fa d'inverno fa d'estate.*

OTTOBRE 2022

La temperatura dell'aria dell'intero mese di ottobre è stata sistematicamente al di sopra della media. La mitezza delle temperature, tipica delle cosiddette

“ottobrate”, è ascrivibile alla presenza di aree di alta pressione di origine subtropicale che in successione si sono impadronite del Mediterraneo. L’assenza di nuvolosità ha determinato temperature alte di giorno e basse di notte, nebbie notturne nelle zone interne e polveri sottili nelle aree metropolitane per lo scarso ricambio d’aria. A livello mensile, la media delle temperature minime è stata così di 17.8°C, due gradi e mezzo in più della media mensile, mentre quella delle temperature massime è stata di 24.3°C, due gradi in più. Il giorno più caldo è stato il 3 ottobre con 27.2°C e la temperatura del mare nel golfo è passata dal valore di 23°C di inizio mese al valore di 22.5°C.

La pioggia caduta è stata di 33 mm, il 70% in meno di quanto piove normalmente ad ottobre e concentrata nell’unico evento del giorno 13. Tale deficit pluviometrico è già capitato negli anni 1913 (28.5 mm), 1954 (21.1 mm), 1967 (0 mm), 1969 (0 mm) e 2014 (0.6 mm). I mass-media hanno evidenziato che la temperatura massima di questo ottobre è stata la più elevata degli ultimi 150 anni ma l’analisi dell’archivio storico dell’Osservatorio Federiciano mostra che questo non risponde al vero perché la media della temperatura massima di questo ottobre 2022 è stata più bassa di altri anni quali il 1942 con 25.2°C, il 1876 e il 1964 con 24.7°C, il 1948 con 24.6°C.

NOVEMBRE 2022

La temperatura dell’aria nelle prime due decadi di novembre è stata di 2-3 gradi al di sopra della media mensile e, nell’ultima decade, in linea o al di sotto di 1 2°C. A livello mensile, le medie delle temperature minima e massima hanno raggiunto, rispettivamente, 13.5°C, due gradi in più della media, e 18.9°C, un grado e mezzo in più. La temperatura del mare è passata da 23°C degli inizi di novembre a 19°C a fine mese. Raffiche di vento di 90 km/h hanno messo a dura prova la stabilità degli alberi e la navigazione nel golfo nei giorni 22 e 26. In particolare, il vento di libeccio del giorno 22 ha generato onde alte circa 4 metri che hanno investito violentemente il lungomare di Napoli e i litorali domizio e silentano.

La quantità di pioggia caduta a Napoli centro è stata pari a 277 mm, due volte quella che cade normalmente a novembre, distribuita in 12 giorni e concentrata nei giorni 4 con 81 mm e 26 con 74 mm. Questo perché la presenza costante dell’anticiclone delle Azzorre a sud-ovest del golfo di Biscaglia e dell’anticiclone Russo-Siberiano sull’Europa orientale ha bloccato la circolazione normale da ovest verso est e creato un corridoio preferenziale lungo il quale masse d’aria atlantica, fresca ed instabile hanno raggiunto a ripetizione la nostra penisola con forti piogge. L’orografia del territorio e il surplus di caldo del mare hanno, poi, agito congiuntamente per conferire alle precipitazioni di novembre ulteriore energia e mettere così a nudo la fragilità di alcune aree quale l’isola d’Ischia. A partire dal primo mattino del giorno 26, infatti, una perturbazione molto intensa e duratura ha scaricato più di 130 mm di pioggia sul monte Epomeo innescando una

frana colossale che ha distrutto e portato a mare manufatti, alberi e auto, con 8 vittime e 4 dispersi. Ischia è un'isola vulcanica e perciò ricoperta da una coltre piroclastica prodotta dalle eruzioni che si sono susseguite nell'arco della sua storia. Eventi franosi distruttivi hanno devastato più volte l'isola per improvvisi slittamenti della coltre piroclastica causati da terremoti, eruzioni e piogge. E' molto probabile che la notevole quantità di pioggia caduta nel giorno 26 sulla sommità del monte Epomeo abbia innescata la movimentazione della coltre piroclastica già sufficientemente saturata dai 100 mm di pioggia caduta dall'inizio di novembre.

DICEMBRE 2022

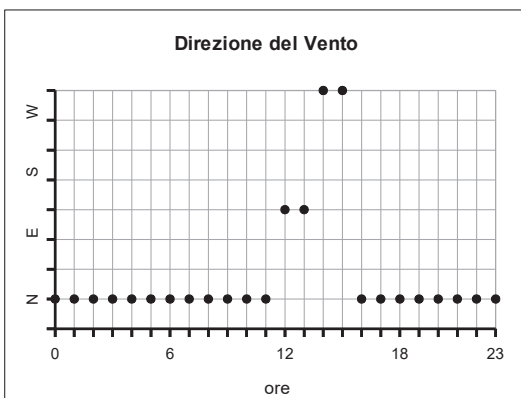
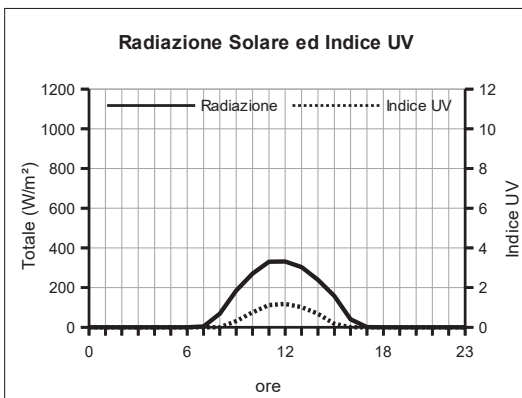
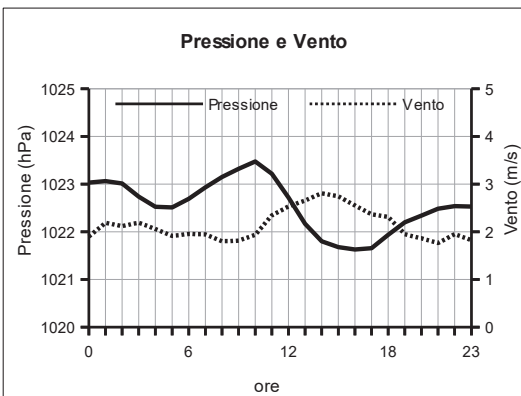
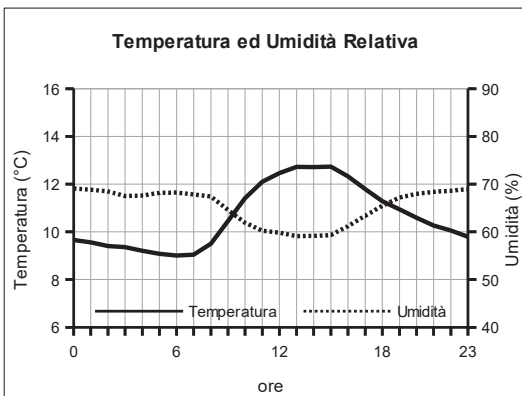
Dicembre ha sorpreso i meteorologi per la presenza, specie nella seconda metà del mese, di un potente e duraturo anticiclone africano che è riuscito a bloccare la normale circolazione atmosferica sul Mediterraneo. Tale scenario barico ha determinato assenza di ventilazione, foschie mattutine ed elevati valori di umidità notturna dell'ordine del 90%, come hanno avuto modo di verificare coloro che non sono riusciti ad asciugare i panni nei tempi soliti. E' curioso osservare che anticloni così poderosi sono in grado di causare un abbassamento del livello del mare (il cosiddetto barometro invertito) e che i napoletani a via Caracciolo hanno verificato attraverso l'insolito affioramento di una striscia scura nella parte inferiore sia della scogliera che del Castel dell'Ovo. La temperatura dell'aria di dicembre 2022 è stata sempre al di sopra della media del periodo con l'eccezione dei giorni 2 e 13 e le medie mensili hanno così raggiunto valori di 12.4°C per le temperature minime (4°C in più della media del periodo) e di 17.3°C per le massime (3.5°C in più). Tali valori sono da record per il mese di dicembre almeno sin dal 1872 cioè da quando sono iniziate le rilevazioni sistematiche presso l'Observatorio Meteorologico della Federico II, a Napoli centro.

La pioggia è stata di 67 mm, il 45% in meno di quella che cade normalmente a dicembre. Il giorno più freddo è stato il 13 con una temperatura minima di 8.8°C mentre quello più caldo è stato proprio il giorno di Natale con 19.2°C. A chiusura d'anno risulta utile riportarne il bilancio termo-pluviometrico. La media delle temperature massime del 2022 è stata di 22.4°C con i mesi di marzo, aprile e settembre un grado al di sotto delle medie stagionali e con i rimanenti mesi di 2-3°C al di sopra. La temperatura massima dell'aria del 2022 non è, però, da record perché minore del valore di 22.6°C dell'anno 1950. La pioggia caduta è stata di 890 mm, 25 mm in più della cumulata storica annuale, concentrata nei mesi di settembre e novembre ma con deficit in gennaio, maggio, ottobre e dicembre.

TABELLE E GRAFICI

GENNAIO 2022
(medie orarie)

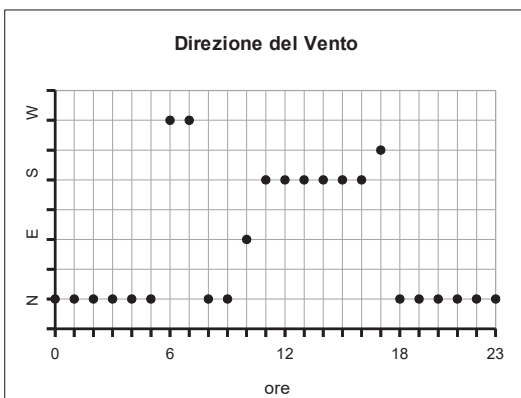
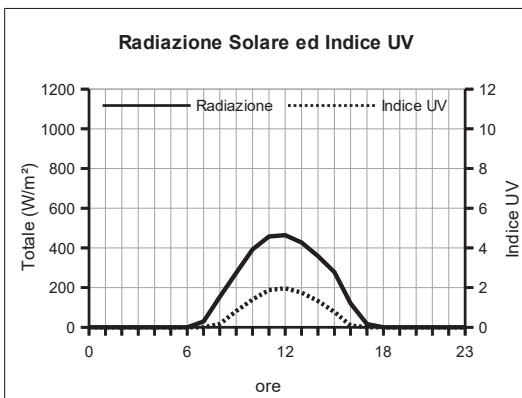
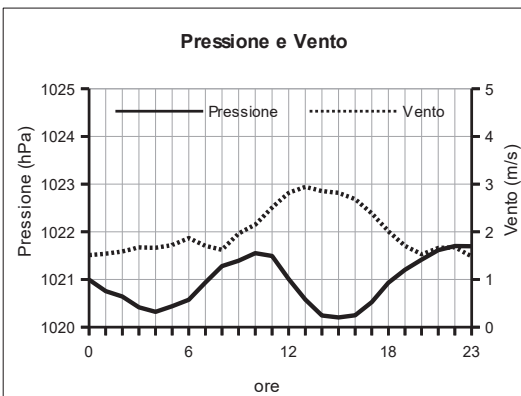
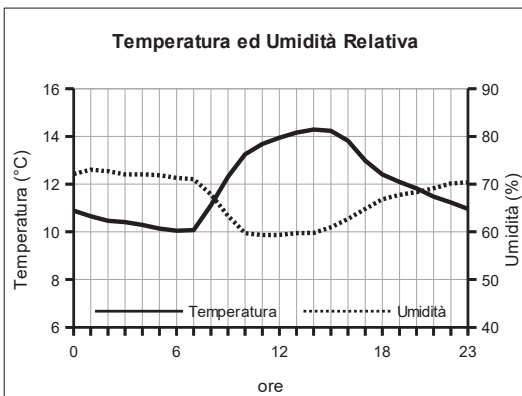
Ore	Temperatura °C	Umidità %	Pressione hPa	Vento velocità m/s	direzione	Radiazione Solare W/m²	Indice UV
0	9.7	69.1	1023.0	1.9	N	0.0	0.0
1	9.6	68.8	1023.1	2.2	N	0.0	0.0
2	9.4	68.5	1023.0	2.1	N	0.0	0.0
3	9.4	67.5	1022.7	2.2	N	0.0	0.0
4	9.2	67.6	1022.5	2.1	N	0.0	0.0
5	9.1	68.2	1022.5	1.9	N	0.0	0.0
6	9.0	68.2	1022.7	2.0	N	0.0	0.0
7	9.0	67.8	1022.9	1.9	N	4.7	0.0
8	9.5	67.4	1023.1	1.8	N	68.5	0.0
9	10.5	64.6	1023.3	1.8	N	184.5	0.3
10	11.4	61.9	1023.5	1.9	N	270.7	0.8
11	12.1	60.3	1023.2	2.3	N	329.9	1.1
12	12.5	59.8	1022.7	2.5	SE	331.4	1.2
13	12.7	59.1	1022.2	2.7	SE	303.4	1.0
14	12.7	59.2	1021.8	2.8	NW	238.4	0.7
15	12.7	59.3	1021.7	2.7	NW	157.0	0.2
16	12.3	61.2	1021.6	2.6	N	39.6	0.0
17	11.8	63.4	1021.7	2.4	N	1.3	0.0
18	11.3	65.5	1021.9	2.3	N	0.0	0.0
19	10.9	67.2	1022.2	1.9	N	0.0	0.0
20	10.6	68.0	1022.3	1.9	N	0.0	0.0
21	10.3	68.4	1022.5	1.8	N	0.0	0.0
22	10.1	68.6	1022.5	2.0	N	0.0	0.0
23	9.8	69.0	1022.5	1.8	N	0.0	0.0



FEBBRAIO 2022

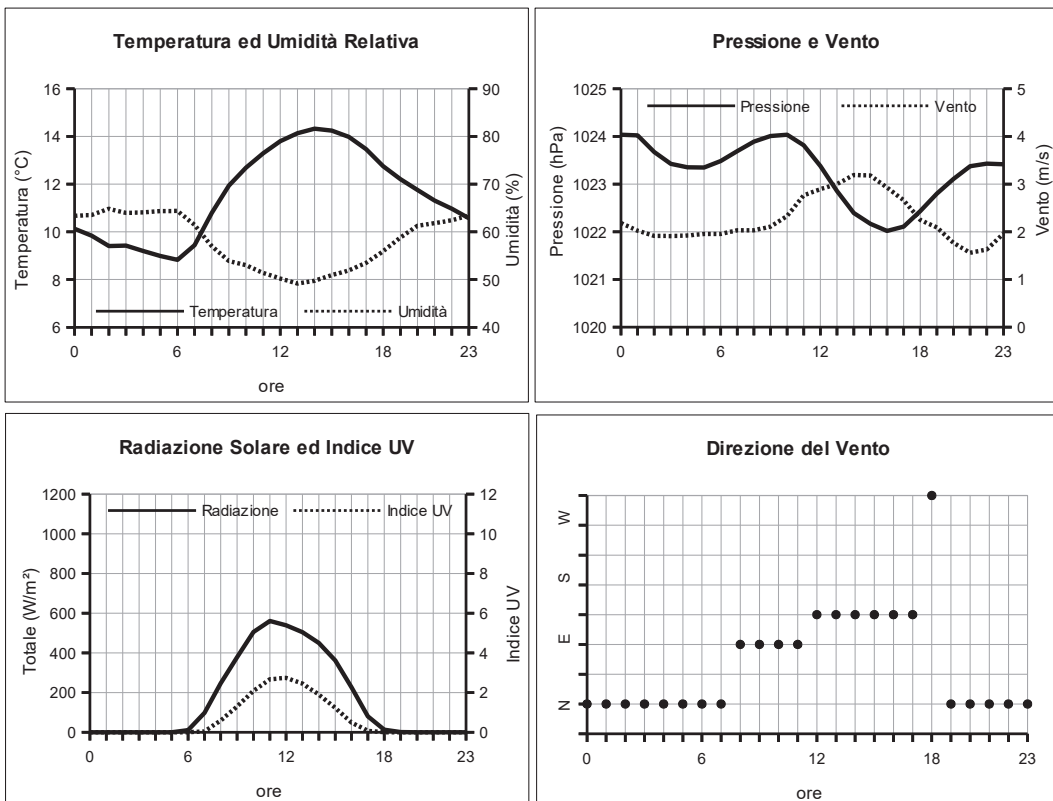
(medie orarie)

Ore	Temperatura °C	Umidità %	Pressione hPa	Vento velocità m/s	direzione	Radiazione Solare W/m²	Indice UV
0	10.9	72.1	1021.0	1.5	N	0.0	0.0
1	10.7	73.0	1020.8	1.5	N	0.0	0.0
2	10.5	72.7	1020.6	1.6	N	0.0	0.0
3	10.4	72.0	1020.4	1.7	N	0.0	0.0
4	10.3	72.1	1020.3	1.7	N	0.0	0.0
5	10.1	71.9	1020.4	1.7	N	0.0	0.0
6	10.0	71.3	1020.6	1.9	W	0.2	0.0
7	10.1	71.0	1020.9	1.7	W	29.3	0.0
8	11.1	67.9	1021.3	1.6	N	153.3	0.2
9	12.3	63.4	1021.4	2.0	N	273.4	0.8
10	13.3	59.7	1021.6	2.2	E	391.9	1.4
11	13.7	59.3	1021.5	2.5	S	456.8	1.9
12	13.9	59.4	1021.0	2.8	S	463.5	2.0
13	14.2	59.7	1020.6	2.9	S	427.1	1.7
14	14.3	59.8	1020.2	2.9	S	358.4	1.3
15	14.2	61.0	1020.2	2.8	S	277.6	0.8
16	13.8	62.7	1020.2	2.7	S	120.1	0.1
17	13.0	64.8	1020.5	2.4	SW	16.0	0.0
18	12.4	66.8	1020.9	2.0	N	0.0	0.0
19	12.1	67.8	1021.2	1.7	N	0.0	0.0
20	11.8	68.3	1021.4	1.5	N	0.0	0.0
21	11.5	69.1	1021.6	1.7	N	0.0	0.0
22	11.2	70.1	1021.7	1.7	N	0.0	0.0
23	11.0	70.4	1021.7	1.5	N	0.0	0.0



MARZO 2022
(medie orarie)

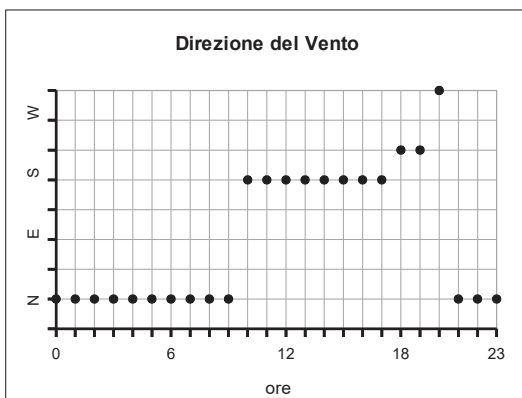
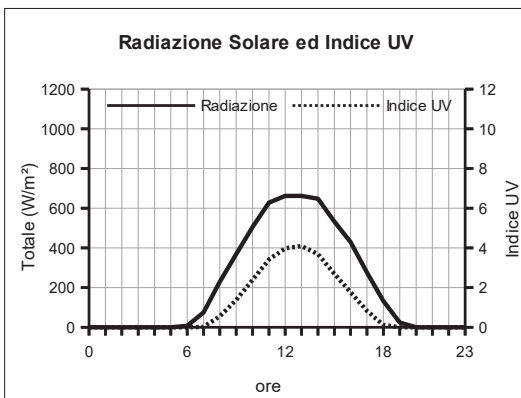
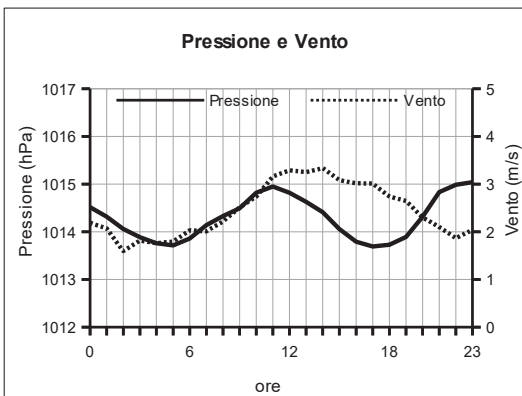
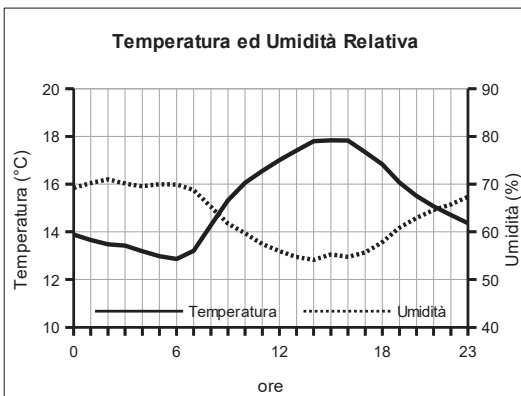
Ore	Temperatura °C	Umidità %	Pressione hPa	Vento velocità m/s	direzione	Radiazione Solare W/m²	Indice UV
0	10.1	63.3	1024.0	2.2	N	0.0	0.0
1	9.8	63.5	1024.0	2.0	N	0.0	0.0
2	9.4	64.8	1023.7	1.9	N	0.0	0.0
3	9.4	64.0	1023.4	1.9	N	0.0	0.0
4	9.2	64.1	1023.4	1.9	N	0.0	0.0
5	9.0	64.3	1023.3	2.0	N	0.0	0.0
6	8.8	64.4	1023.5	2.0	N	10.7	0.0
7	9.4	61.4	1023.7	2.0	N	97.4	0.0
8	10.8	57.0	1023.9	2.0	E	245.9	0.6
9	11.9	53.9	1024.0	2.1	E	377.9	1.3
10	12.7	53.0	1024.0	2.3	E	504.8	2.1
11	13.3	51.4	1023.8	2.8	E	560.2	2.7
12	13.8	50.2	1023.4	2.9	SE	538.7	2.7
13	14.1	49.2	1022.9	3.0	SE	503.5	2.4
14	14.3	49.7	1022.4	3.2	SE	449.6	1.9
15	14.3	50.9	1022.2	3.2	SE	361.8	1.2
16	14.0	51.9	1022.0	2.9	SE	227.5	0.5
17	13.5	53.5	1022.1	2.7	SE	80.2	0.1
18	12.8	56.0	1022.4	2.2	NW	12.5	0.0
19	12.2	58.8	1022.8	2.1	N	0.9	0.0
20	11.8	61.3	1023.1	1.8	N	0.0	0.0
21	11.3	61.8	1023.4	1.6	N	0.0	0.0
22	11.0	62.4	1023.4	1.6	N	0.0	0.0
23	10.6	63.4	1023.4	2.0	N	0.0	0.0



APRILE 2022

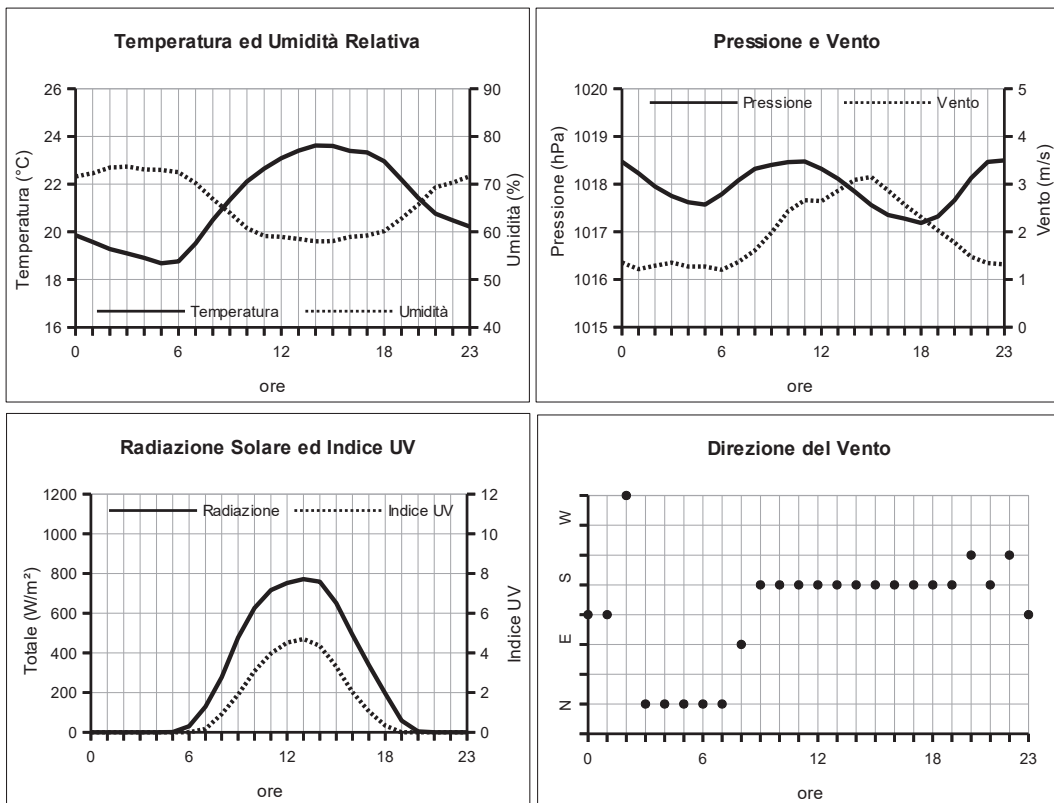
(medie orarie)

Ore	Temperatura °C	Umidità %	Pressione hPa	Vento velocità m/s	direzione	Radiazione Solare W/m²	Indice UV
0	13.9	69.2	1014.5	2.2	N	0.0	0.0
1	13.7	70.3	1014.3	2.1	N	0.0	0.0
2	13.5	71.0	1014.1	1.6	N	0.0	0.0
3	13.4	70.1	1013.9	1.8	N	0.0	0.0
4	13.2	69.6	1013.8	1.8	N	0.0	0.0
5	13.0	70.0	1013.7	1.8	N	0.0	0.0
6	12.9	69.9	1013.9	2.0	N	7.8	0.0
7	13.2	68.8	1014.1	2.0	N	74.7	0.0
8	14.3	65.3	1014.3	2.2	N	228.9	0.6
9	15.3	61.7	1014.5	2.5	N	367.9	1.4
10	16.1	59.7	1014.8	2.7	S	504.4	2.4
11	16.6	57.4	1015.0	3.2	S	628.3	3.4
12	17.0	56.0	1014.8	3.3	S	662.2	4.0
13	17.4	54.7	1014.6	3.3	S	661.7	4.1
14	17.8	54.1	1014.4	3.3	S	647.5	3.7
15	17.8	55.3	1014.1	3.1	S	531.6	2.7
16	17.8	54.8	1013.8	3.0	S	428.6	1.8
17	17.3	55.7	1013.7	3.0	S	275.8	0.8
18	16.8	57.8	1013.7	2.7	SW	132.5	0.1
19	16.1	60.9	1013.9	2.6	SW	23.8	0.0
20	15.5	62.9	1014.3	2.3	NW	0.1	0.0
21	15.1	64.6	1014.8	2.1	N	0.0	0.0
22	14.7	65.8	1015.0	1.9	N	0.0	0.0
23	14.4	67.3	1015.0	2.0	N	0.0	0.0



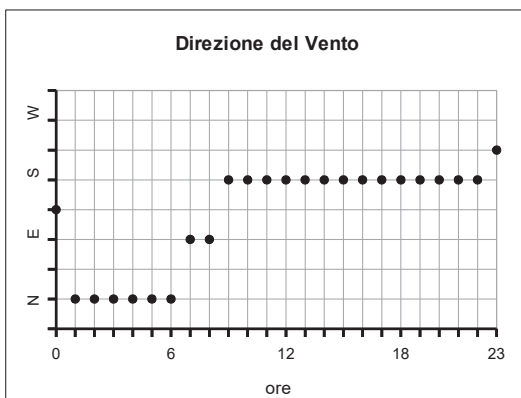
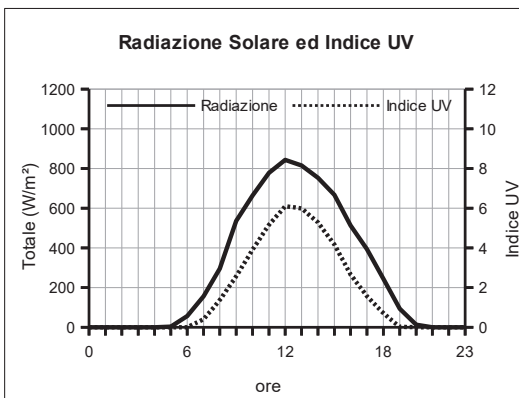
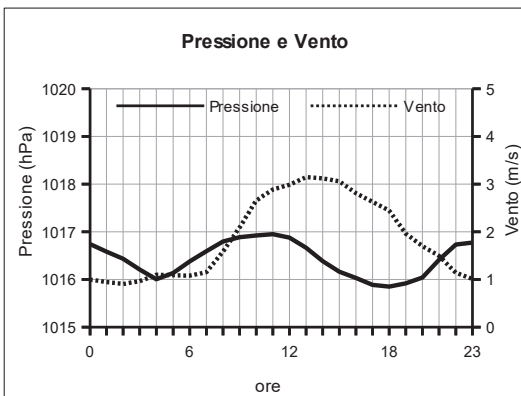
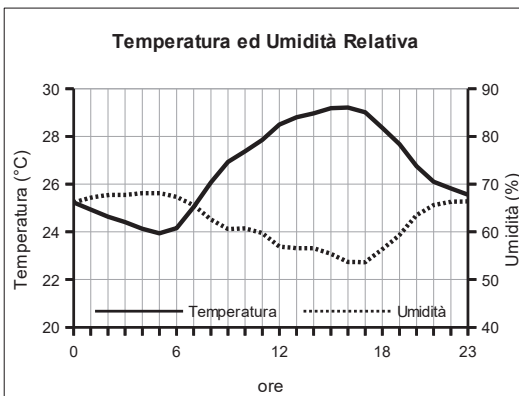
MAGGIO 2022
(medie orarie)

Ore	Temperatura °C	Umidità %	Pressione hPa	Vento velocità m/s	direzione	Radiazione Solare W/m²	Indice UV
0	19.9	71.6	1018.5	1.4	SE	0.0	0.0
1	19.6	72.3	1018.2	1.2	SE	0.0	0.0
2	19.3	73.5	1017.9	1.3	NW	0.0	0.0
3	19.1	73.7	1017.8	1.4	N	0.0	0.0
4	18.9	73.1	1017.6	1.3	N	0.0	0.0
5	18.7	73.0	1017.6	1.3	N	0.7	0.0
6	18.8	72.5	1017.8	1.2	N	30.1	0.0
7	19.5	70.2	1018.1	1.4	N	129.3	0.2
8	20.5	66.9	1018.3	1.6	E	276.7	0.9
9	21.3	64.0	1018.4	2.0	S	476.2	1.9
10	22.1	60.8	1018.5	2.4	S	625.8	3.1
11	22.7	59.1	1018.5	2.7	S	716.2	4.0
12	23.1	58.9	1018.3	2.6	S	752.2	4.5
13	23.4	58.5	1018.1	2.9	S	771.7	4.7
14	23.6	58.0	1017.8	3.1	S	758.0	4.3
15	23.6	58.1	1017.6	3.1	S	650.2	3.3
16	23.4	58.9	1017.3	2.9	S	491.2	2.0
17	23.3	59.2	1017.3	2.6	S	339.2	1.1
18	23.0	60.1	1017.2	2.3	S	195.3	0.3
19	22.2	62.8	1017.3	2.0	S	58.5	0.0
20	21.4	65.8	1017.7	1.8	SW	3.8	0.0
21	20.8	69.3	1018.1	1.5	S	0.0	0.0
22	20.5	70.3	1018.5	1.3	SW	0.0	0.0
23	20.2	71.7	1018.5	1.3	SE	0.0	0.0



GIUGNO 2022
(medie orarie)

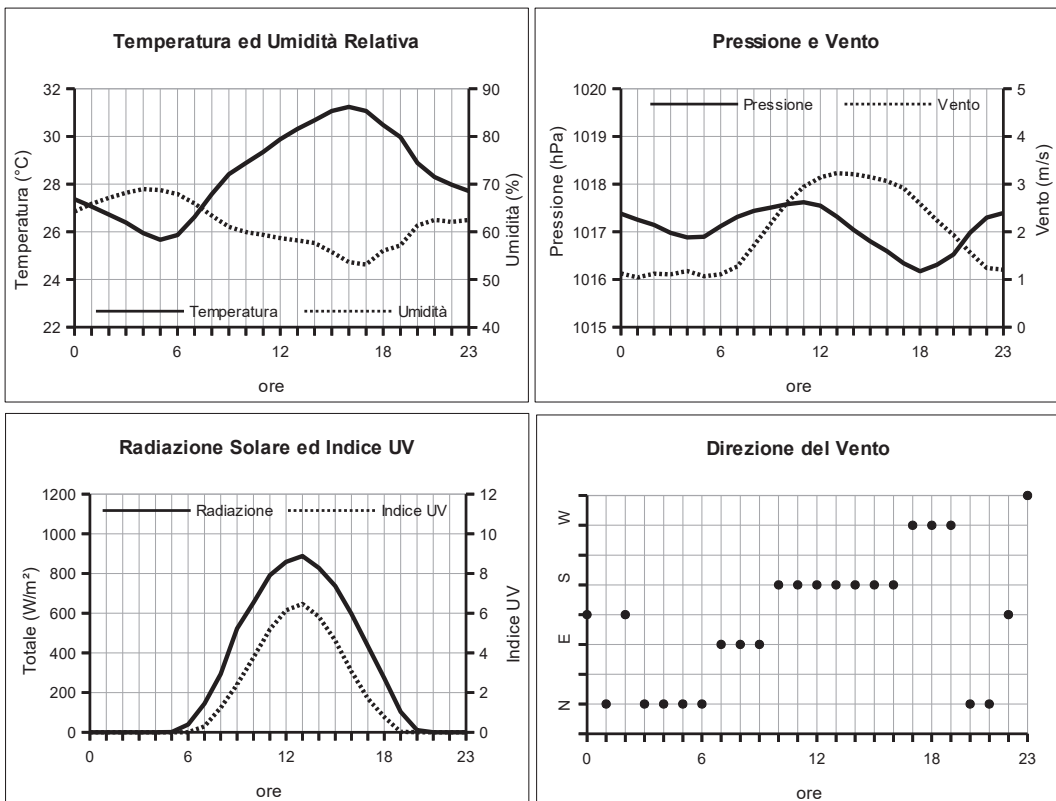
Ore	Temperatura °C	Umidità %	Pressione hPa	Vento velocità m/s	direzione	Radiazione Solare W/m²	Indice UV
0	25.2	66.2	1016.7	1.0	SE	0.0	0.0
1	24.9	67.2	1016.6	0.9	N	0.0	0.0
2	24.6	67.7	1016.4	0.9	N	0.0	0.0
3	24.4	67.8	1016.2	1.0	N	0.0	0.0
4	24.1	68.1	1016.0	1.1	N	0.0	0.0
5	23.9	68.1	1016.1	1.1	N	2.6	0.0
6	24.2	67.3	1016.4	1.1	N	56.7	0.0
7	25.0	65.6	1016.6	1.2	E	155.8	0.4
8	26.1	62.6	1016.8	1.6	E	295.0	1.4
9	26.9	60.6	1016.9	2.1	S	535.9	2.6
10	27.4	60.7	1016.9	2.7	S	663.9	3.9
11	27.9	59.8	1016.9	2.9	S	778.4	5.2
12	28.5	56.9	1016.9	3.0	S	842.7	6.1
13	28.8	56.6	1016.7	3.1	S	815.3	6.0
14	29.0	56.5	1016.4	3.1	S	752.9	5.3
15	29.2	55.4	1016.2	3.1	S	666.8	4.2
16	29.2	53.7	1016.0	2.8	S	512.9	2.7
17	29.0	53.7	1015.9	2.6	S	392.5	1.6
18	28.4	56.3	1015.8	2.4	S	244.2	0.7
19	27.7	59.3	1015.9	2.0	S	93.7	0.0
20	26.8	63.5	1016.0	1.7	S	12.5	0.0
21	26.1	65.6	1016.4	1.5	S	0.0	0.0
22	25.8	66.3	1016.7	1.1	S	0.0	0.0
23	25.6	66.4	1016.8	1.0	SW	0.0	0.0



LUGLIO 2022

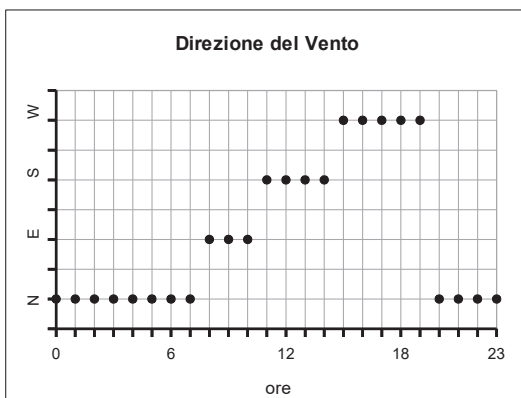
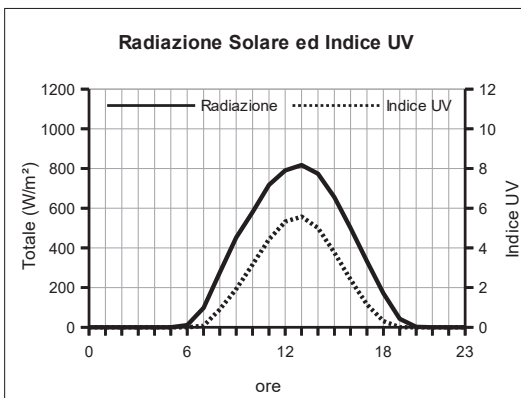
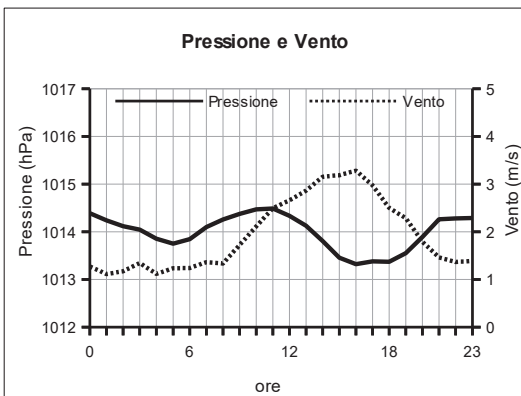
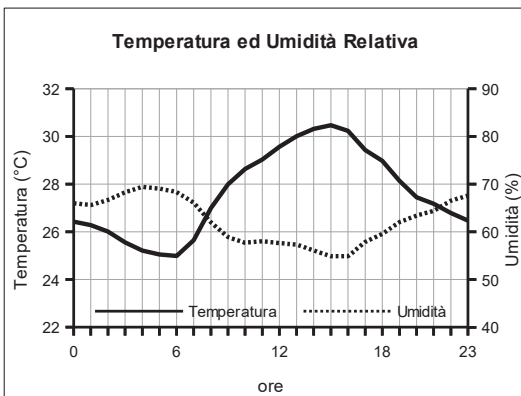
(medie orarie)

Ore	Temperatura °C	Umidità %	Pressione hPa	Vento velocità m/s	direzione	Radiazione Solare W/m²	Indice UV
0	27.4	64.3	1017.4	1.1	SE	0.0	0.0
1	27.1	65.9	1017.3	1.0	N	0.0	0.0
2	26.7	67.1	1017.1	1.1	SE	0.0	0.0
3	26.4	68.2	1017.0	1.1	N	0.0	0.0
4	26.0	69.0	1016.9	1.2	N	0.0	0.0
5	25.7	68.8	1016.9	1.1	N	0.8	0.0
6	25.9	67.9	1017.1	1.1	N	38.9	0.0
7	26.6	66.0	1017.3	1.3	E	144.2	0.3
8	27.6	63.4	1017.4	1.7	E	293.7	1.2
9	28.4	61.1	1017.5	2.2	E	522.0	2.4
10	28.9	60.0	1017.6	2.6	S	652.5	3.8
11	29.3	59.4	1017.6	2.9	S	790.8	5.2
12	29.9	58.7	1017.5	3.1	S	858.4	6.1
13	30.3	58.2	1017.3	3.2	S	888.1	6.5
14	30.7	57.7	1017.0	3.2	S	827.7	5.8
15	31.1	55.8	1016.8	3.2	S	736.7	4.6
16	31.2	53.7	1016.6	3.1	S	596.5	3.1
17	31.1	53.1	1016.3	2.9	W	433.8	1.7
18	30.5	56.0	1016.2	2.6	W	272.6	0.8
19	30.0	57.1	1016.3	2.2	W	102.7	0.0
20	28.9	61.3	1016.5	1.9	N	10.5	0.0
21	28.3	62.5	1017.0	1.6	N	0.0	0.0
22	28.0	62.1	1017.3	1.2	SE	0.0	0.0
23	27.7	62.5	1017.4	1.2	NW	0.0	0.0



AGOSTO 2022
(medie orarie)

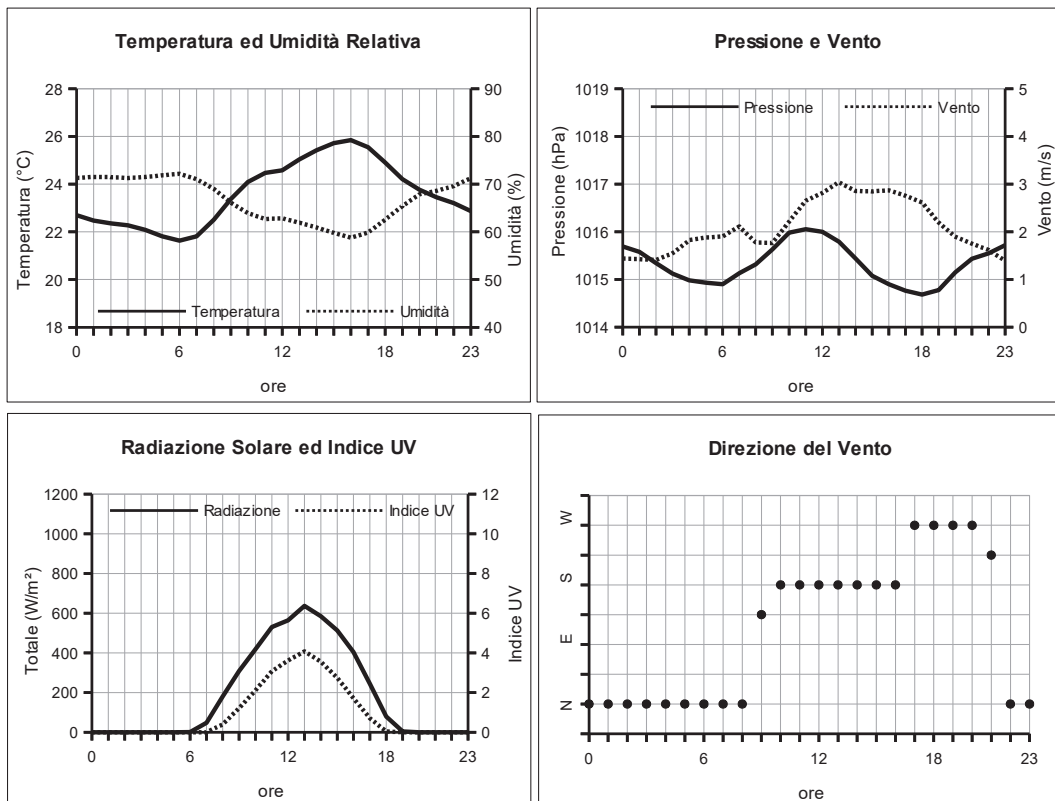
Ore	Temperatura °C	Umidità %	Pressione hPa	Vento velocità m/s	direzione	Radiazione Solare W/m²	Indice UV
0	26.4	66.0	1014.4	1.3	N	0.0	0.0
1	26.3	65.6	1014.2	1.1	N	0.0	0.0
2	26.0	66.7	1014.1	1.2	N	0.0	0.0
3	25.6	68.3	1014.0	1.3	N	0.0	0.0
4	25.2	69.4	1013.9	1.1	N	0.0	0.0
5	25.1	69.1	1013.8	1.2	N	0.0	0.0
6	25.0	68.4	1013.8	1.2	N	11.2	0.0
7	25.6	66.1	1014.1	1.4	N	97.5	0.1
8	27.0	62.0	1014.3	1.3	E	275.7	0.9
9	28.0	58.9	1014.4	1.7	E	451.7	1.9
10	28.6	57.7	1014.5	2.1	E	579.6	3.2
11	29.0	58.0	1014.5	2.5	S	717.2	4.4
12	29.6	57.6	1014.3	2.7	S	789.6	5.3
13	30.0	57.3	1014.1	2.9	S	817.4	5.6
14	30.3	56.1	1013.8	3.2	S	773.1	5.0
15	30.5	54.9	1013.5	3.2	W	655.3	3.8
16	30.2	54.9	1013.3	3.3	W	499.6	2.4
17	29.4	57.9	1013.4	3.0	W	332.1	1.1
18	29.0	59.6	1013.4	2.5	W	171.6	0.3
19	28.1	62.0	1013.6	2.3	W	42.3	0.0
20	27.5	63.4	1013.9	1.8	N	1.6	0.0
21	27.2	64.4	1014.3	1.5	N	0.0	0.0
22	26.8	66.5	1014.3	1.4	N	0.0	0.0
23	26.5	67.6	1014.3	1.4	N	0.0	0.0



SETTEMBRE 2022

(medie orarie)

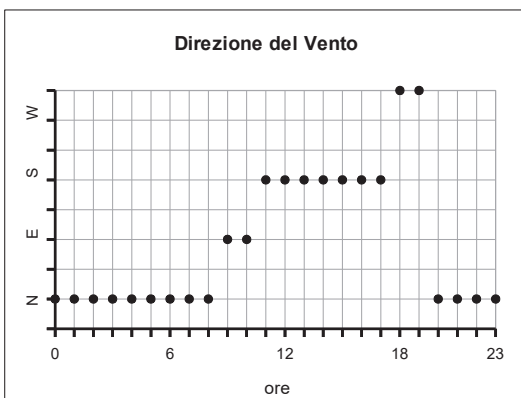
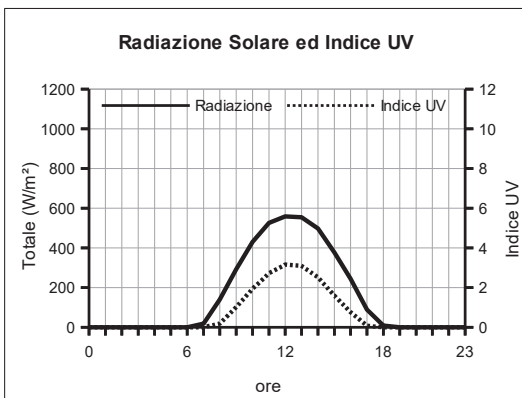
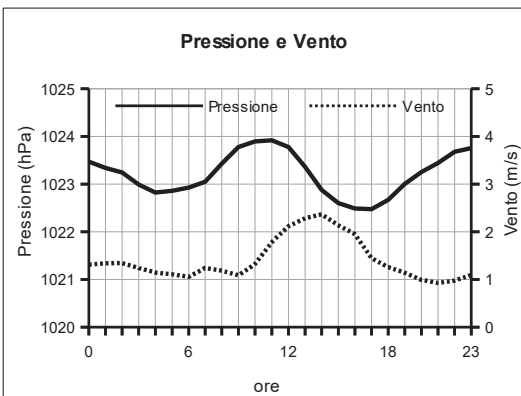
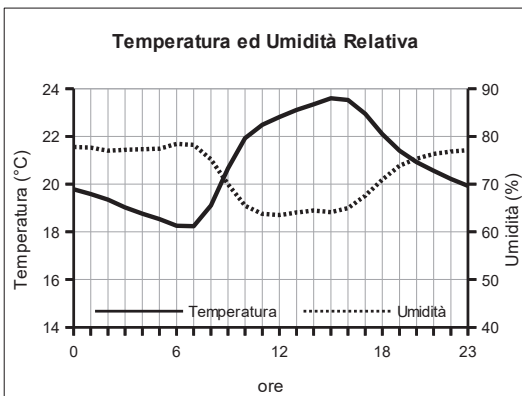
Ore	Temperatura °C	Umidità %	Pressione hPa	Vento velocità m/s	direzione	Radiazione Solare W/m²	Indice UV
0	22.7	71.3	1015.7	1.4	N	0.0	0.0
1	22.5	71.5	1015.6	1.4	N	0.0	0.0
2	22.4	71.5	1015.3	1.4	N	0.0	0.0
3	22.3	71.3	1015.1	1.6	N	0.0	0.0
4	22.1	71.5	1015.0	1.8	N	0.0	0.0
5	21.8	71.9	1014.9	1.9	N	0.0	0.0
6	21.6	72.2	1014.9	1.9	N	1.1	0.0
7	21.8	71.1	1015.1	2.1	N	47.5	0.0
8	22.5	69.0	1015.3	1.8	N	180.5	0.4
9	23.4	66.1	1015.6	1.8	SE	308.7	1.2
10	24.1	63.9	1016.0	2.2	S	418.4	2.1
11	24.5	62.7	1016.1	2.7	S	529.4	3.1
12	24.6	62.8	1016.0	2.8	S	563.2	3.6
13	25.0	61.9	1015.8	3.0	S	636.8	4.1
14	25.4	60.9	1015.4	2.9	S	584.5	3.5
15	25.7	59.8	1015.1	2.8	S	512.7	2.7
16	25.9	58.8	1014.9	2.9	S	404.1	1.7
17	25.6	59.9	1014.8	2.8	W	244.6	0.7
18	24.9	62.6	1014.7	2.6	W	79.2	0.0
19	24.2	65.4	1014.8	2.2	W	4.4	0.0
20	23.8	67.9	1015.1	1.9	W	0.0	0.0
21	23.5	68.6	1015.4	1.8	SW	0.0	0.0
22	23.2	69.6	1015.5	1.6	N	0.0	0.0
23	22.9	71.3	1015.7	1.4	N	0.0	0.0



OTTOBRE 2022

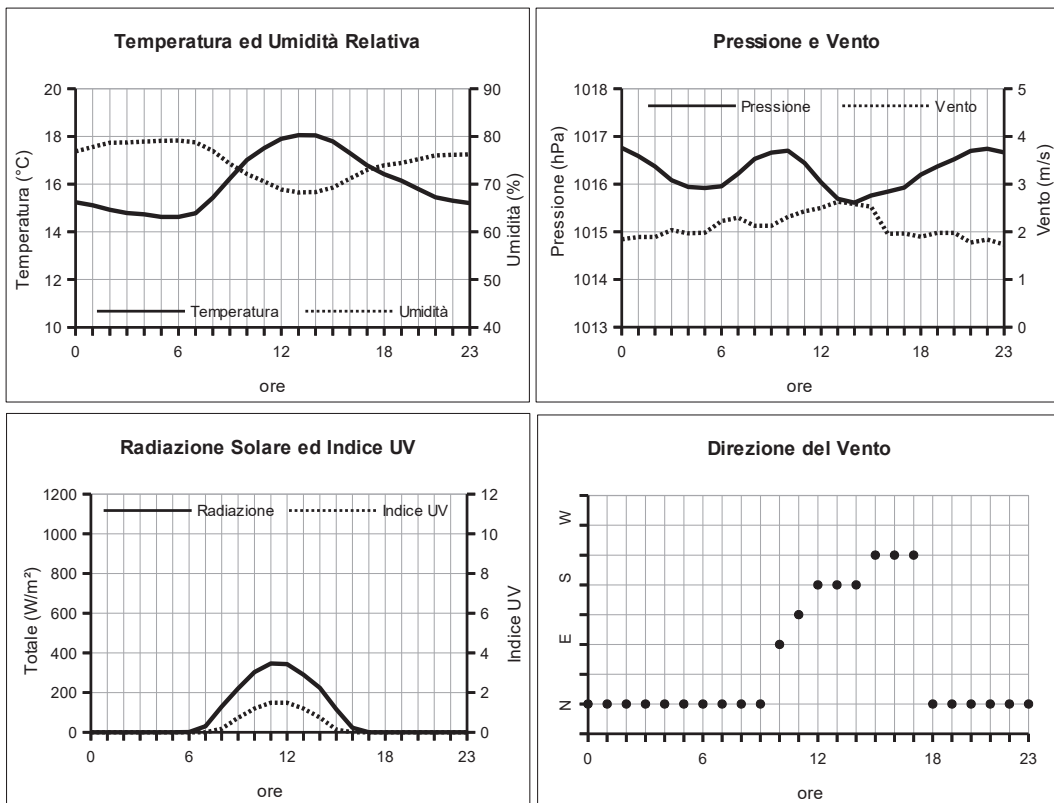
(medie orarie)

Ore	Temperatura °C	Umidità %	Pressione hPa	Vento velocità m/s	direzione	Radiazione Solare W/m²	Indice UV
0	19.8	77.8	1023.5	1.3	N	0.0	0.0
1	19.6	77.7	1023.3	1.3	N	0.0	0.0
2	19.4	77.0	1023.2	1.3	N	0.0	0.0
3	19.0	77.2	1023.0	1.2	N	0.0	0.0
4	18.8	77.3	1022.8	1.1	N	0.0	0.0
5	18.5	77.4	1022.9	1.1	N	0.0	0.0
6	18.3	78.4	1022.9	1.1	N	0.2	0.0
7	18.2	78.2	1023.0	1.2	N	18.5	0.0
8	19.1	75.2	1023.4	1.2	N	140.0	0.2
9	20.7	70.0	1023.8	1.1	E	292.5	1.0
10	21.9	65.5	1023.9	1.3	E	430.6	1.9
11	22.5	63.8	1023.9	1.8	S	525.9	2.7
12	22.8	63.5	1023.8	2.1	S	558.1	3.2
13	23.1	64.1	1023.4	2.3	S	553.7	3.1
14	23.4	64.5	1022.9	2.4	S	497.8	2.5
15	23.6	64.1	1022.6	2.1	S	376.7	1.6
16	23.5	65.0	1022.5	1.9	S	243.8	0.8
17	23.0	67.6	1022.5	1.4	S	89.3	0.1
18	22.1	70.9	1022.7	1.3	NW	8.7	0.0
19	21.4	73.9	1023.0	1.1	NW	0.0	0.0
20	20.9	75.3	1023.3	1.0	N	0.0	0.0
21	20.6	76.3	1023.4	0.9	N	0.0	0.0
22	20.2	76.8	1023.7	1.0	N	0.0	0.0
23	19.9	77.1	1023.8	1.1	N	0.0	0.0



NOVEMBRE 2022
(medie orarie)

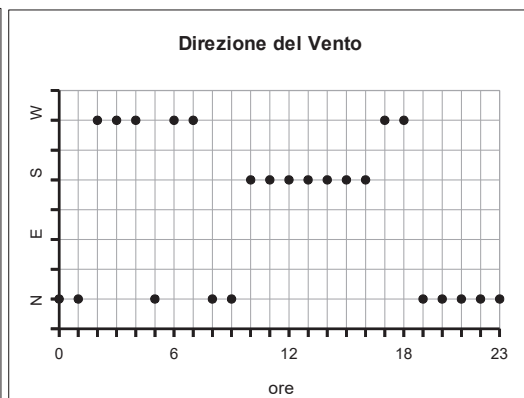
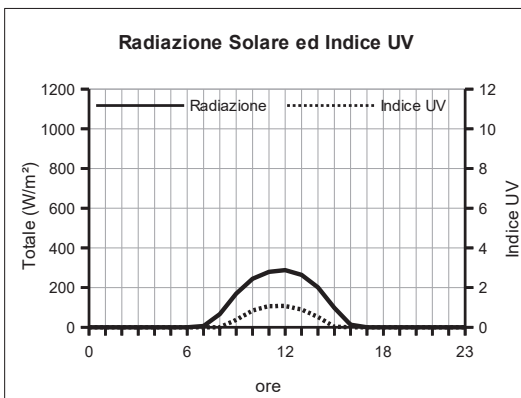
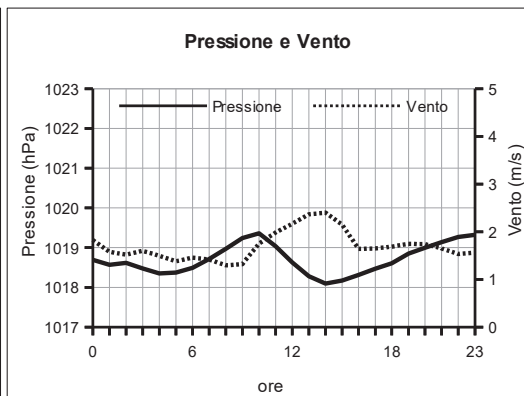
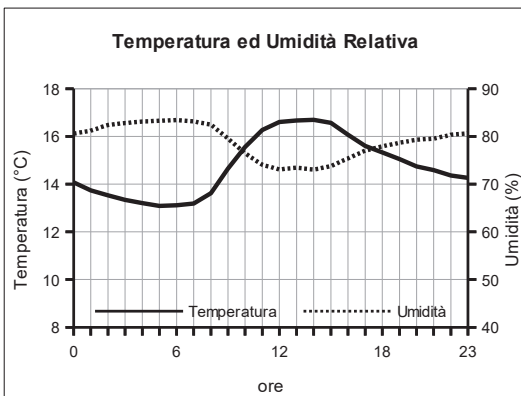
Ore	Temperatura °C	Umidità %	Pressione hPa	Vento velocità m/s	direzione	Radiazione Solare W/m²	Indice UV
0	15.2	76.9	1016.8	1.8	N	0.0	0.0
1	15.1	77.8	1016.6	1.9	N	0.0	0.0
2	14.9	78.7	1016.4	1.9	N	0.0	0.0
3	14.8	78.8	1016.1	2.0	N	0.0	0.0
4	14.7	78.9	1015.9	2.0	N	0.0	0.0
5	14.6	79.1	1015.9	2.0	N	0.0	0.0
6	14.6	79.1	1016.0	2.2	N	0.6	0.0
7	14.8	78.8	1016.2	2.3	N	30.6	0.0
8	15.4	77.0	1016.5	2.1	N	129.3	0.2
9	16.2	74.3	1016.7	2.1	N	220.2	0.7
10	17.0	72.1	1016.7	2.3	E	303.1	1.2
11	17.5	70.6	1016.4	2.4	SE	346.8	1.5
12	17.9	68.9	1016.0	2.5	S	343.6	1.5
13	18.1	68.3	1015.7	2.6	S	289.5	1.2
14	18.0	68.4	1015.6	2.6	S	223.9	0.7
15	17.8	69.3	1015.8	2.5	SW	116.2	0.1
16	17.3	71.2	1015.8	2.0	SW	23.0	0.0
17	16.8	73.0	1015.9	2.0	SW	0.1	0.0
18	16.4	73.9	1016.2	1.9	N	0.0	0.0
19	16.2	74.5	1016.4	2.0	N	0.0	0.0
20	15.8	75.2	1016.5	2.0	N	0.0	0.0
21	15.5	76.0	1016.7	1.8	N	0.0	0.0
22	15.3	76.2	1016.7	1.8	N	0.0	0.0
23	15.2	76.3	1016.7	1.7	N	0.0	0.0



DICEMBRE 2022

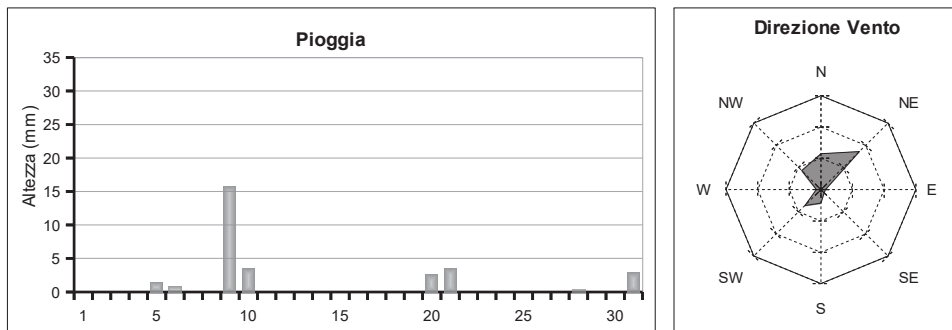
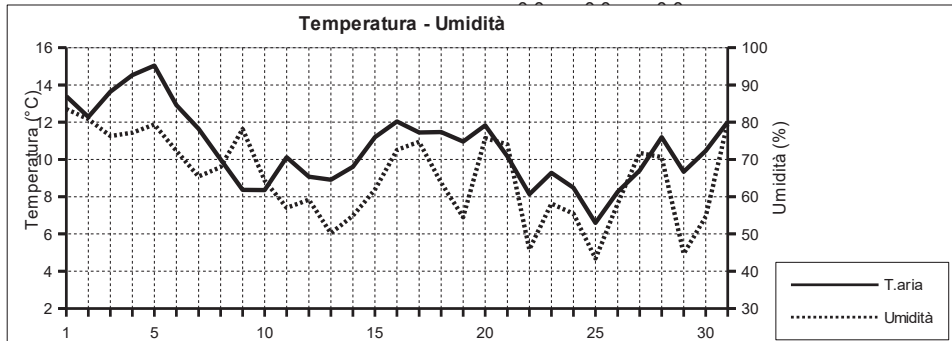
(medie orarie)

Ore	Temperatura °C	Umidità %	Pressione hPa	Vento velocità m/s	direzione	Radiazione Solare W/m²	Indice UV
0	14.1	80.6	1018.7	1.8	N	0.0	0.0
1	13.7	81.2	1018.6	1.6	N	0.0	0.0
2	13.5	82.4	1018.6	1.5	W	0.0	0.0
3	13.3	82.8	1018.5	1.6	W	0.0	0.0
4	13.2	83.1	1018.4	1.5	W	0.0	0.0
5	13.1	83.3	1018.4	1.4	N	0.0	0.0
6	13.1	83.4	1018.5	1.5	W	0.0	0.0
7	13.2	83.1	1018.7	1.4	W	6.7	0.0
8	13.6	82.5	1019.0	1.3	N	66.3	0.0
9	14.7	79.6	1019.2	1.3	N	169.4	0.4
10	15.6	76.5	1019.4	1.7	S	243.7	0.8
11	16.3	74.1	1019.0	2.0	S	279.2	1.1
12	16.6	73.1	1018.6	2.2	S	287.7	1.1
13	16.7	73.5	1018.3	2.4	S	263.3	0.9
14	16.7	73.0	1018.1	2.4	S	201.3	0.5
15	16.6	73.8	1018.2	2.2	S	97.3	0.0
16	16.1	75.4	1018.3	1.6	S	13.1	0.0
17	15.6	77.0	1018.5	1.6	W	0.0	0.0
18	15.3	77.9	1018.6	1.7	W	0.0	0.0
19	15.0	78.7	1018.9	1.7	N	0.0	0.0
20	14.7	79.3	1019.0	1.7	N	0.0	0.0
21	14.6	79.6	1019.1	1.7	N	0.0	0.0
22	14.4	80.3	1019.3	1.5	N	0.0	0.0
23	14.3	80.7	1019.3	1.6	N	0.0	0.0



GENNAIO 2022
(medie giornaliere)

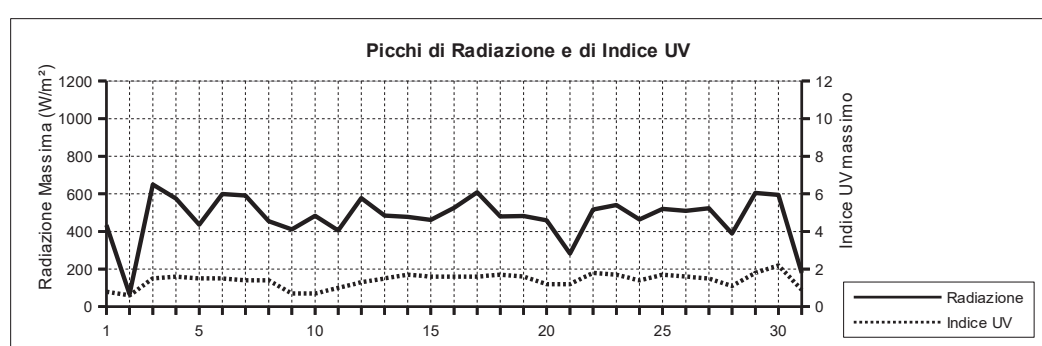
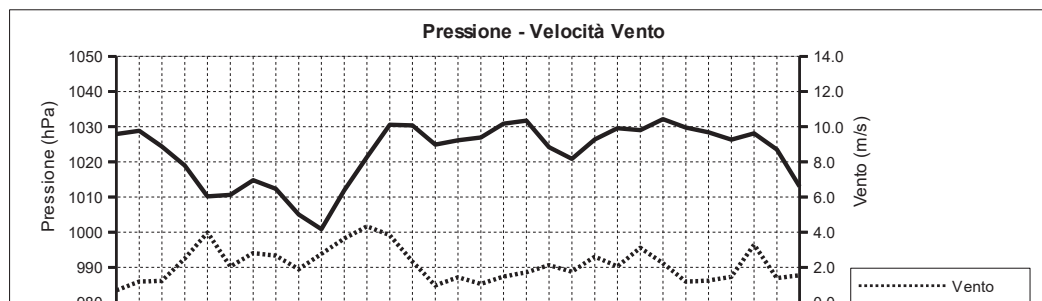
Data	Temperatura °C	Umidità %	Pressione hPa	Vento m/s direzione	Rad. Solare W/m² durata	Pioggia mm	Indice UV medio	Indice UV max (ore)
01/01/22	13.4	83.5	1027.9	0.7 NE	100.2 9:00	0.0	0.8	0.8 (11:10)
02/01/22	12.3	80.8	1028.9	1.2 NE	37.1 8:50	0.0	0.5	0.6 (11:20)
03/01/22	13.6	76.3	1024.3	1.2 SW	109.2 8:40	0.0	1.0	1.5 (11:30)
04/01/22	14.5	77.2	1018.9	2.5 S	153.9 9:10	0.0	1.0	1.6 (11:20)
05/01/22	15.0	79.4	1010.2	4.0 S	257.4 8:50	1.4	1.1	1.5 (11:40)
06/01/22	12.9	72.3	1010.6	2.0 --	154.0 9:20	0.8	1.0	1.5 (12:40)
07/01/22	11.6	65.4	1014.8	2.8 N	222.5 9:20	0.0	1.0	1.4 (12:50)
08/01/22	10.0	67.9	1012.3	2.7 NW	260.4 9:30	0.0	0.9	1.4 (11:30)
09/01/22	8.4	78.1	1005.0	1.9 NE	64.8 9:10	15.8	0.3	0.7 (11:40)
10/01/22	8.4	64.3	1000.9	2.8 N	104.6 9:00	3.6	0.7	0.7 (10:40)
11/01/22	10.1	57.0	1011.9	3.6 NE	144.7 9:30	0.0	0.9	1.0 (12:30)
12/01/22	9.1	59.2	1021.3	4.3 NE	209.1 9:40	0.0	0.9	1.3 (12:20)
13/01/22	8.9	50.2	1030.5	3.8 NE	278.9 9:40	0.0	1.1	1.5 (11:50)
14/01/22	9.6	54.9	1030.4	2.3 NW	277.2 9:40	0.0	1.3	1.7 (12:10)
15/01/22	11.2	61.9	1024.9	1.0 NE	269.8 9:40	0.0	1.3	1.6 (11:50)
16/01/22	12.0	72.6	1026.1	1.4 SW	244.3 9:40	0.0	1.3	1.6 (11:40)
17/01/22	11.4	74.7	1026.9	1.1 NW	187.8 9:50	0.0	1.0	1.6 (12:40)
18/01/22	11.5	63.7	1030.9	1.5 N	273.8 9:50	0.0	1.2	1.7 (12:20)
19/01/22	11.0	54.5	1031.7	1.7 --	279.0 9:50	0.0	1.3	1.6 (12:30)
20/01/22	11.8	75.7	1024.2	2.1 SW	116.7 9:40	2.6	0.8	1.2 (11:30)
21/01/22	10.2	74.0	1020.8	1.7 NE	107.3 9:30	3.6	0.9	1.2 (12:50)
22/01/22	8.1	45.8	1026.4	2.6 NE	298.1 10:00	0.0	1.4	1.8 (11:50)
23/01/22	9.3	58.1	1029.6	2.1 N	278.8 10:00	0.0	1.3	1.7 (11:50)
24/01/22	8.5	55.4	1029.0	3.1 NE	131.6 9:40	0.0	1.0	1.4 (11:30)
25/01/22	6.6	43.4	1032.1	2.2 NE	302.9 10:00	0.0	1.3	1.7 (11:40)
26/01/22	8.3	58.1	1029.7	1.2 N	291.5 10:10	0.0	1.3	1.6 (11:50)
27/01/22	9.4	71.7	1028.4	1.2 N	254.2 10:00	0.0	1.0	1.5 (11:40)
28/01/22	11.2	70.6	1026.3	1.5 NW	142.2 9:30	0.2	0.9	1.1 (13:00)
29/01/22	9.3	44.7	1028.1	3.3 N	300.4 10:00	0.0	1.3	1.8 (12:10)
30/01/22	10.5	54.7	1023.5	1.4 NW	264.6 10:00	0.0	1.4	2.2 (12:20)
31/01/22	12.0	80.0	1013.0	1.5 SW	69.4 9:50	3.0	0.8	0.9 (12:40)



GENNAIO 2022

(estremi giornalieri)

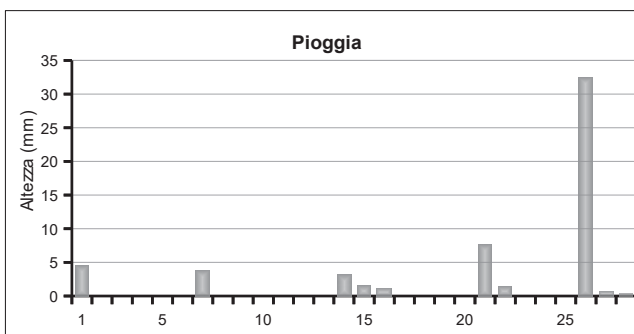
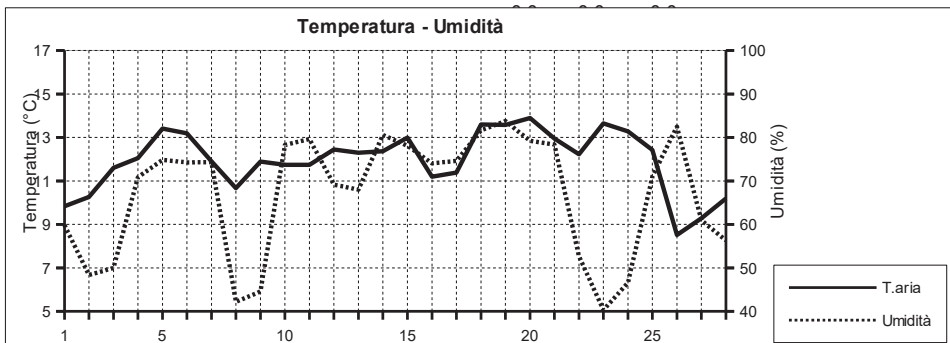
Data	Temperatura (°C)			Umidità (%)			Pressione (hPa)			Vento (m/s)		Radiazione (W/m²)
	min (ore)	max (ore)	min (ore)	max (ore)	min (ore)	max (ore)	min (ore)	max (ore)	max (ore)	max (ore)	max (ore)	
01/01/22	10.6 (1:30)	15.9 (14:20)	72.0 (14:20)	94.0 (2:10)	1026.6 (5:30)	1029.6 (23:30)	3.6 (7:40)	434.0 (14:00)				
02/01/22	11.3 (9:30)	13.4 (00:00)	72.0 (20:50)	85.0 (8:20)	1027.7 (23:40)	1029.9 (9:50)	5.4 (19:50)	67.0 (12:00)				
03/01/22	12.3 (7:20)	15.0 (11:40)	70.0 (2:50)	80.0 (19:30)	1021.9 (23:40)	1027.5 (00:00)	7.6 (13:50)	650.0 (11:40)				
04/01/22	13.4 (8:10)	16.2 (12:50)	70.0 (5:20)	83.0 (21:10)	1015.3 (23:50)	1021.7 (00:00)	8.5 (18:00)	575.0 (12:20)				
05/01/22	13.3 (23:20)	16.7 (13:40)	72.0 (13:00)	87.0 (19:20)	1006.7 (18:50)	1015.4 (00:00)	15.2 (17:30)	436.0 (12:10)				
06/01/22	11.1 (7:50)	14.6 (12:40)	61.0 (11:50)	82.0 (0:40)	1008.3 (00:00)	1014.6 (23:30)	7.2 (1:10)	599.0 (11:20)				
07/01/22	9.8 (23:50)	14.9 (12:50)	53.0 (12:20)	76.0 (1:40)	1013.9 (14:00)	1015.8 (10:00)	8.0 (14:20)	591.0 (12:50)				
08/01/22	7.8 (22:50)	12.9 (14:00)	57.0 (4:50)	75.0 (4:50)	1011.1 (14:50)	1013.7 (00:00)	6.7 (2:10)	454.0 (12:00)				
09/01/22	6.1 (5:10)	11.7 (17:30)	66.0 (11:30)	91.0 (15:40)	998.2 (17:20)	1012.3 (0:10)	12.5 (18:00)	411.0 (9:40)				
10/01/22	5.9 (5:40)	10.0 (21:40)	48.0 (14:30)	86.0 (0:50)	997.3 (4:20)	1006.5 (23:20)	9.4 (18:10)	483.0 (10:40)				
11/01/22	8.4 (23:50)	12.4 (14:00)	50.0 (13:30)	63.0 (21:50)	1006.7 (0:10)	1017.1 (23:00)	12.5 (13:40)	406.0 (13:30)				
12/01/22	7.8 (5:40)	11.0 (15:30)	55.0 (5:00)	63.0 (00:00)	1016.2 (1:00)	1027.4 (23:20)	17.9 (12:10)	578.0 (10:50)				
13/01/22	6.8 (7:00)	11.8 (14:10)	38.0 (15:20)	61.0 (1:20)	1027.5 (00:00)	1033.7 (23:30)	14.3 (12:00)	485.0 (12:10)				
14/01/22	7.1 (6:30)	13.2 (13:40)	32.0 (13:50)	75.0 (23:10)	1027.0 (23:50)	1033.4 (00:00)	7.2 (7:30)	478.0 (12:30)				
15/01/22	6.6 (5:30)	17.7 (14:40)	45.0 (13:30)	75.0 (00:00)	1023.6 (17:10)	1026.9 (00:00)	4.9 (6:20)	462.0 (12:20)				
16/01/22	8.7 (5:30)	15.1 (13:10)	59.0 (1:40)	83.0 (21:50)	1023.5 (1:40)	1027.7 (21:30)	5.8 (12:10)	526.0 (13:00)				
17/01/22	8.9 (23:20)	14.7 (15:40)	58.0 (15:20)	84.0 (1:50)	1025.4 (14:50)	1029.2 (10:20)	5.8 (12:10)	608.0 (11:10)				
18/01/22	7.7 (6:10)	16.9 (15:30)	37.0 (15:20)	84.0 (00:00)	1028.1 (0:20)	1034.0 (22:50)	5.8 (23:40)	480.0 (12:20)				
19/01/22	8.5 (6:30)	13.6 (11:50)	37.0 (11:20)	66.0 (3:00)	1029.3 (23:40)	1033.7 (00:00)	5.8 (15:20)	482.0 (12:20)				
20/01/22	10.3 (21:10)	13.4 (9:20)	65.0 (00:00)	87.0 (20:20)	1020.9 (23:50)	1029.3 (00:00)	10.3 (3:40)	459.0 (9:50)				
21/01/22	7.7 (23:50)	12.4 (15:30)	54.0 (22:50)	88.0 (0:10)	1019.1 (5:10)	1024.5 (23:30)	12.1 (20:00)	283.0 (15:30)				
22/01/22	5.7 (6:20)	11.6 (15:00)	32.0 (13:20)	60.0 (20:00)	1024.6 (0:20)	1029.0 (23:50)	12.5 (1:40)	517.0 (12:20)				
23/01/22	6.6 (6:40)	12.6 (14:00)	38.0 (12:50)	75.0 (21:30)	1028.5 (22:30)	1031.4 (10:40)	8.9 (17:00)	541.0 (12:00)				
24/01/22	5.3 (23:50)	10.7 (15:10)	38.0 (18:30)	75.0 (00:00)	1027.4 (3:40)	1032.3 (23:30)	14.3 (16:10)	464.0 (14:40)				
25/01/22	3.8 (7:30)	10.2 (16:00)	30.0 (15:10)	52.0 (21:10)	1031.3 (17:30)	1033.0 (10:30)	10.3 (1:30)	520.0 (12:00)				
26/01/22	3.9 (6:40)	12.3 (13:30)	45.0 (10:30)	76.0 (23:40)	1027.9 (16:30)	1031.8 (00:00)	4.9 (14:10)	510.0 (12:30)				
27/01/22	6.2 (7:20)	13.0 (15:50)	57.0 (16:30)	80.0 (2:20)	1027.6 (16:00)	1029.5 (10:50)	5.4 (14:20)	524.0 (11:40)				
28/01/22	8.0 (23:30)	13.7 (15:10)	58.0 (15:00)	82.0 (4:30)	1024.0 (17:00)	1028.6 (00:00)	12.1 (22:20)	390.0 (14:50)				
29/01/22	7.1 (4:50)	12.3 (15:20)	20.0 (16:10)	64.0 (4:30)	1025.8 (00:00)	1030.2 (11:10)	13.4 (2:00)	605.0 (11:20)				
30/01/22	5.9 (7:30)	13.8 (12:20)	29.0 (5:20)	78.0 (23:00)	1021.0 (23:50)	1027.6 (00:00)	9.8 (13:20)	594.0 (12:40)				
31/01/22	9.9 (21:30)	13.1 (11:00)	64.0 (11:00)	91.0 (21:20)	1001.5 (23:50)	1021.1 (00:00)	7.6 (14:10)	179.0 (12:50)				



FEBBRAIO 2022

(medie giornaliere)

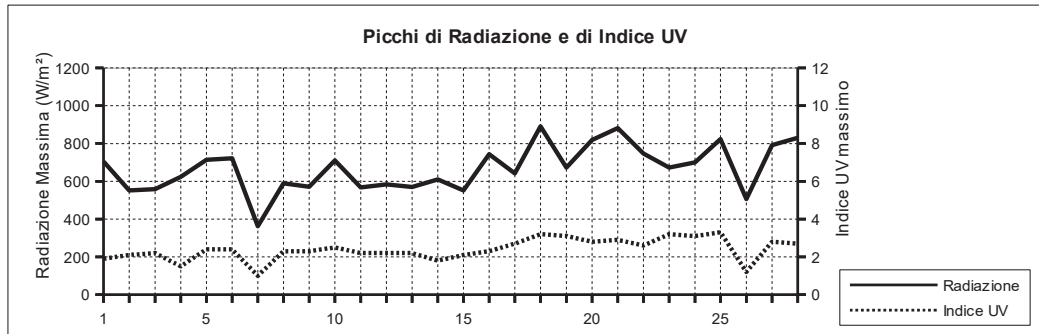
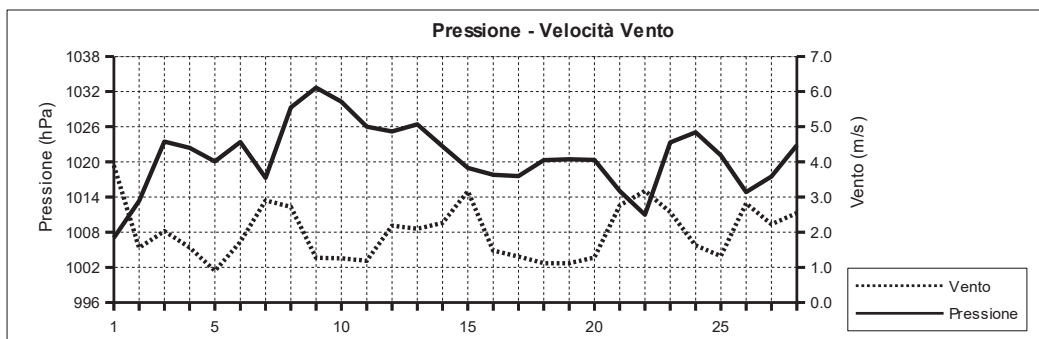
Data	Temperatura °C	Umidità %	Pressione hPa	Vento m/s direzione	Rad. Solare W/m² durata	Pioggia mm	Indice UV medio	Indice UV max (ore)
01/02/22	9.8	59.9	1007.0	3.9 NE	250.7 10:10	4.6	1.1	1.9 (11:50)
02/02/22	10.3	48.3	1013.3	1.6 NW	326.2 10:10	0.0	1.5	2.1 (11:20)
03/02/22	11.6	50.0	1023.5	2.0 N	324.7 10:20	0.0	1.5	2.2 (11:50)
04/02/22	12.1	70.9	1022.4	1.6 SW	147.7 10:10	0.0	0.9	1.5 (10:20)
05/02/22	13.4	74.8	1020.1	0.9 --	181.7 10:10	0.0	1.3	2.4 (11:40)
06/02/22	13.2	74.2	1023.4	1.7 SW	302.0 10:10	0.0	1.5	2.4 (11:50)
07/02/22	11.9	74.3	1017.3	2.9 NW	103.9 9:50	3.8	0.7	1.0 (12:10)
08/02/22	10.7	42.2	1029.3	2.7 N	349.7 10:30	0.0	1.5	2.3 (12:00)
09/02/22	11.9	44.6	1032.7	1.3 NW	342.7 10:30	0.0	1.6	2.3 (11:30)
10/02/22	11.7	78.3	1030.3	1.3 --	302.7 10:30	0.0	1.6	2.5 (12:20)
11/02/22	11.7	79.7	1026.0	1.2 NW	327.9 10:40	0.0	1.5	2.2 (12:00)
12/02/22	12.4	69.1	1025.2	2.2 N	320.1 10:40	0.0	1.5	2.2 (12:10)
13/02/22	12.3	68.0	1026.4	2.1 NW	321.7 10:50	0.0	1.5	2.2 (11:50)
14/02/22	12.4	80.6	1022.7	2.3 S	151.2 10:40	3.2	0.9	1.8 (12:20)
15/02/22	13.0	78.1	1019.0	3.2 SW	139.8 10:20	1.6	1.1	2.1 (13:50)
16/02/22	11.2	74.0	1017.8	1.5 NW	272.0 10:50	1.0	1.3	2.3 (12:10)
17/02/22	11.4	74.6	1017.6	1.3 --	320.8 11:00	0.0	1.7	2.7 (12:30)
18/02/22	13.6	81.6	1020.3	1.1 S	228.5 10:40	0.0	1.6	3.2 (12:40)
19/02/22	13.6	83.8	1020.5	1.1 S	322.4 10:50	0.0	2.0	3.1 (12:20)
20/02/22	13.9	79.2	1020.3	1.3 NW	244.6 11:00	0.0	1.3	2.8 (11:30)
21/02/22	13.0	78.4	1015.0	2.8 SW	103.4 11:00	7.6	0.8	2.9 (12:40)
22/02/22	12.2	52.7	1011.0	3.2 N	384.6 11:00	1.4	1.8	2.6 (11:10)
23/02/22	13.7	40.3	1023.3	2.6 NE	393.1 11:10	0.0	2.1	3.2 (12:00)
24/02/22	13.3	46.6	1025.1	1.6 --	387.9 11:10	0.0	2.0	3.1 (11:50)
25/02/22	12.4	71.0	1021.1	1.3 S	386.4 11:10	0.0	2.0	3.3 (12:20)
26/02/22	8.5	82.5	1014.9	2.8 NE	75.3 10:20	32.4	0.7	1.2 (15:10)
27/02/22	9.3	61.0	1017.5	2.2 NE	344.3 11:10	0.6	1.8	2.8 (12:10)
28/02/22	10.2	56.3	1022.8	2.5 NE	400.4 11:00	0.2	1.8	2.7 (12:00)



FEBBRAIO 2022

(estremi giornalieri)

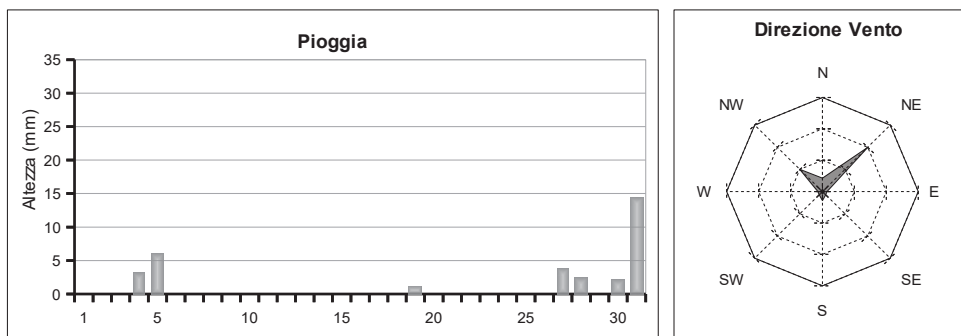
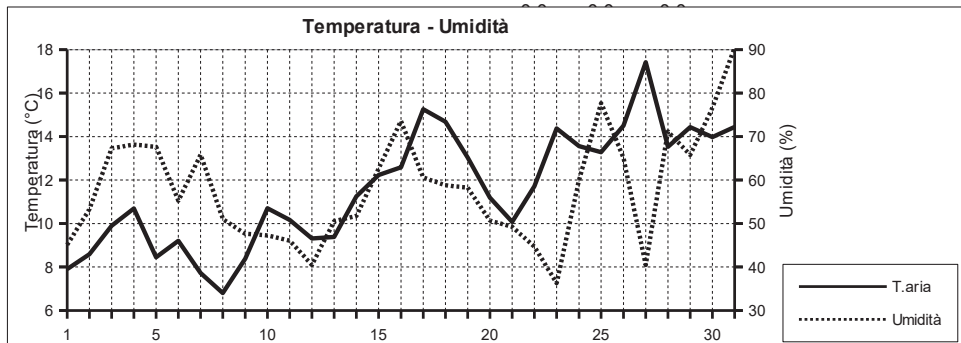
Data	Temperatura (°C)			Umidità (%)			Pressione (hPa)		Vento (m/s)	Radiazione (W/m²)
	min (ore)	max (ore)	min (ore)	max (ore)	min (ore)	max (ore)	min (ore)	max (ore)	max (ore)	
01/02/22	7.9 (2:10)	13.2 (13:40)	41.0 (13:40)	90.0 (1:30)	1000.9 (0:30)	1013.8 (21:40)	15.6 (16:10)	705.0 (12:30)		
02/02/22	5.8 (7:20)	14.7 (15:50)	35.0 (10:30)	63.0 (7:50)	1011.7 (14:40)	1018.3 (23:50)	5.4 (0:20)	552.0 (12:30)		
03/02/22	8.4 (3:30)	16.0 (15:50)	36.0 (14:10)	66.0 (22:10)	1018.5 (0:00)	1025.8 (23:10)	11.2 (9:40)	559.0 (12:10)		
04/02/22	9.1 (6:30)	14.6 (15:40)	59.0 (10:30)	77.0 (19:40)	1019.5 (23:40)	1025.6 (0:10)	8.0 (12:20)	624.0 (10:20)		
05/02/22	11.4 (5:10)	15.6 (13:10)	61.0 (10:50)	81.0 (17:30)	1018.3 (3:50)	1023.3 (23:50)	5.4 (13:20)	714.0 (13:20)		
06/02/22	10.9 (5:00)	16.2 (12:10)	55.0 (12:10)	87.0 (22:30)	1021.4 (23:00)	1025.0 (10:10)	5.8 (14:10)	722.0 (12:00)		
07/02/22	8.5 (23:00)	14.2 (15:50)	43.0 (21:00)	90.0 (12:40)	1012.5 (15:10)	1023.4 (23:30)	17.0 (22:10)	362.0 (15:00)		
08/02/22	7.8 (7:20)	14.1 (15:40)	30.0 (14:30)	57.0 (0:20)	1023.4 (0:10)	1032.8 (21:30)	13.4 (10:10)	589.0 (12:00)		
09/02/22	7.3 (5:40)	17.1 (15:40)	29.0 (11:00)	75.0 (23:40)	1031.4 (23:50)	1034.1 (8:40)	5.4 (15:20)	571.0 (12:40)		
10/02/22	9.2 (6:50)	14.5 (13:30)	71.0 (10:10)	85.0 (23:10)	1028.5 (23:50)	1031.5 (0:20)	8.0 (11:50)	710.0 (12:50)		
11/02/22	9.4 (7:00)	15.2 (15:00)	69.0 (15:30)	89.0 (4:20)	1023.9 (16:00)	1028.5 (0:00)	5.8 (14:00)	568.0 (12:20)		
12/02/22	8.9 (3:10)	16.4 (14:10)	54.0 (10:40)	85.0 (3:20)	1023.6 (5:50)	1027.4 (23:30)	9.4 (18:10)	584.0 (12:40)		
13/02/22	9.7 (7:10)	15.4 (15:00)	53.0 (12:30)	80.0 (20:40)	1025.1 (15:30)	1027.8 (10:10)	6.3 (14:20)	570.0 (12:30)		
14/02/22	10.7 (1:50)	14.7 (14:40)	70.0 (14:50)	88.0 (19:20)	1020.7 (23:50)	1025.2 (0:00)	9.8 (10:20)	610.0 (14:10)		
15/02/22	11.1 (23:00)	14.1 (16:20)	69.0 (16:30)	87.0 (9:50)	1017.9 (9:10)	1020.7 (0:10)	14.3 (9:00)	552.0 (15:20)		
16/02/22	9.1 (4:30)	14.1 (14:00)	53.0 (13:50)	87.0 (4:10)	1016.0 (15:10)	1019.5 (0:50)	7.2 (0:40)	744.0 (11:20)		
17/02/22	8.1 (7:10)	14.6 (14:10)	67.0 (9:50)	83.0 (0:40)	1016.3 (4:00)	1018.7 (23:00)	7.2 (12:50)	642.0 (13:00)		
18/02/22	12.3 (0:30)	15.5 (15:20)	75.0 (10:50)	90.0 (23:40)	1018.2 (3:20)	1021.7 (11:40)	6.7 (14:20)	891.0 (13:30)		
19/02/22	11.2 (6:30)	16.2 (13:50)	71.0 (11:40)	93.0 (7:30)	1019.0 (19:10)	1021.6 (0:00)	6.7 (14:30)	673.0 (13:20)		
20/02/22	11.2 (7:30)	16.7 (15:40)	69.0 (14:10)	88.0 (5:50)	1018.6 (6:00)	1022.0 (20:40)	6.3 (17:30)	819.0 (11:40)		
21/02/22	11.7 (22:50)	14.4 (12:40)	69.0 (21:00)	88.0 (15:40)	1005.0 (23:50)	1021.7 (0:00)	13.9 (19:30)	881.0 (12:40)		
22/02/22	9.1 (6:20)	16.0 (14:20)	23.0 (14:30)	85.0 (3:30)	1004.3 (1:00)	1019.8 (23:50)	13.0 (14:00)	747.0 (11:20)		
23/02/22	8.9 (6:40)	18.7 (15:10)	28.0 (14:10)	57.0 (6:00)	1019.9 (0:00)	1027.0 (22:40)	14.3 (14:20)	673.0 (12:20)		
24/02/22	9.9 (6:50)	16.8 (10:50)	23.0 (10:30)	69.0 (23:30)	1022.2 (23:40)	1027.5 (1:50)	6.7 (15:20)	700.0 (12:40)		
25/02/22	10.2 (6:50)	14.7 (13:20)	64.0 (17:40)	78.0 (23:20)	1019.5 (23:30)	1022.5 (0:10)	7.6 (13:50)	823.0 (12:30)		
26/02/22	5.6 (21:00)	11.6 (1:50)	75.0 (0:30)	91.0 (6:50)	1011.9 (17:00)	1019.5 (0:10)	13.9 (14:10)	506.0 (15:30)		
27/02/22	5.1 (1:40)	13.6 (13:40)	39.0 (12:20)	89.0 (0:10)	1013.5 (0:40)	1021.8 (23:40)	9.4 (17:30)	791.0 (13:30)		
28/02/22	7.7 (5:10)	13.8 (13:00)	36.0 (15:50)	70.0 (0:50)	1021.8 (0:20)	1024.5 (22:00)	10.3 (23:50)	830.0 (13:10)		



MARZO 2022

(medie giornaliere)

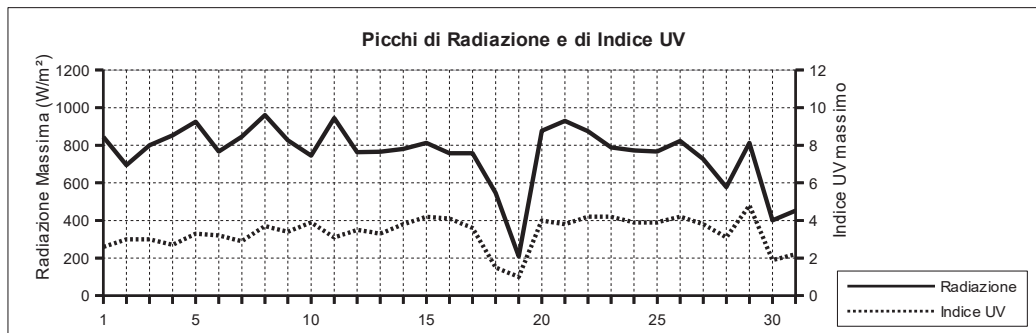
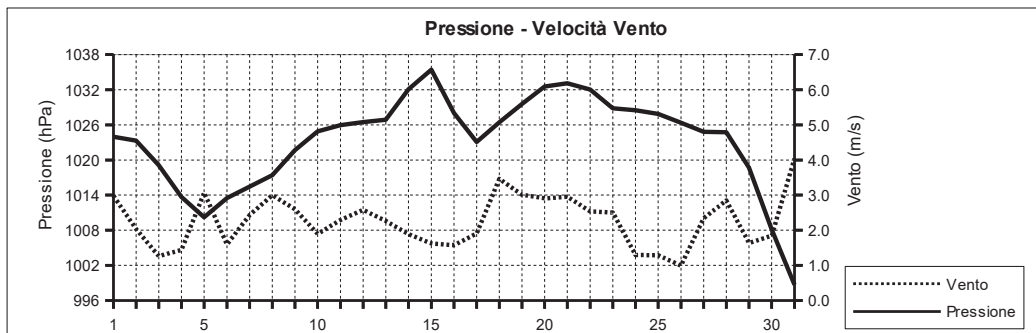
Data	Temperatura °C	Umidità %	Pressione hPa	Vento m/s direzione	Rad. Solare W/m²	durata	Pioggia mm	Indice UV medio	Indice UV max (ore)
01/03/22	7.9	45.1	1024.0	3.0 NE	372.1	11:30	0.0	1.6	2.6 (12:50)
02/03/22	8.6	53.3	1023.3	2.0 NW	396.7	11:30	0.0	2.0	3.0 (12:00)
03/03/22	9.9	67.3	1019.1	1.3 --	311.6	11:20	0.0	1.6	3.0 (11:30)
04/03/22	10.7	68.2	1013.7	1.4 --	326.5	11:30	3.2	1.4	2.7 (11:30)
05/03/22	8.5	67.6	1010.2	3.1 NE	243.1	11:10	6.0	1.5	3.3 (13:10)
06/03/22	9.2	55.3	1013.5	1.6 NW	271.7	11:40	0.0	1.4	3.2 (11:30)
07/03/22	7.7	65.8	1015.4	2.4 NE	301.3	11:40	0.0	1.6	2.9 (11:30)
08/03/22	6.8	51.0	1017.4	3.0 NE	303.2	11:40	0.0	1.8	3.7 (12:20)
09/03/22	8.4	47.6	1021.7	2.6 NW	247.5	11:40	0.0	1.5	3.4 (12:30)
10/03/22	10.7	47.3	1024.9	1.9 NW	436.5	11:40	0.0	2.3	3.9 (12:30)
11/03/22	10.2	46.1	1026.0	2.3 NE	366.6	11:50	0.0	1.8	3.1 (11:50)
12/03/22	9.3	40.5	1026.5	2.6 NE	424.3	11:50	0.0	2.1	3.5 (11:50)
13/03/22	9.4	50.5	1026.9	2.3 --	440.7	12:00	0.0	2.0	3.3 (11:50)
14/03/22	11.2	51.7	1032.1	1.9 NW	437.1	12:00	0.0	2.4	3.8 (11:40)
15/03/22	12.2	62.6	1035.4	1.6 --	419.3	12:10	0.0	2.5	4.2 (12:20)
16/03/22	12.6	73.6	1028.0	1.6 --	414.4	11:50	0.0	2.4	4.1 (12:00)
17/03/22	15.3	60.6	1023.1	1.9 NE	381.2	12:00	0.0	2.1	3.6 (11:50)
18/03/22	14.7	58.8	1026.4	3.5 NE	178.7	11:40	0.0	0.9	1.5 (15:00)
19/03/22	13.0	58.3	1029.6	3.0 NE	104.7	11:30	1.0	1.0	1.0 (9:50)
20/03/22	11.2	50.7	1032.5	2.9 NE	386.1	12:10	0.0	2.3	4.0 (12:30)
21/03/22	10.1	49.3	1033.1	3.0 NE	325.3	12:20	0.0	2.0	3.8 (12:50)
22/03/22	11.7	44.7	1032.0	2.5 NE	436.1	12:20	0.0	2.4	4.2 (12:30)
23/03/22	14.4	36.3	1028.8	2.5 N	453.8	12:20	0.0	2.5	4.2 (12:00)
24/03/22	13.6	59.9	1028.5	1.3 --	441.9	12:30	0.0	2.4	3.9 (12:00)
25/03/22	13.3	77.7	1027.9	1.3 --	435.0	12:30	0.0	2.5	3.9 (11:50)
26/03/22	14.5	65.1	1026.4	1.0 --	338.2	12:20	0.0	2.2	4.2 (12:00)
27/03/22	17.4	40.5	1024.8	2.3 NE	280.5	12:20	3.8	1.7	3.8 (12:00)
28/03/22	13.5	71.2	1024.7	2.8 N	172.4	12:00	2.4	1.5	3.1 (12:30)
29/03/22	14.4	65.8	1018.7	1.6 --	432.9	12:40	0.0	2.8	4.8 (13:00)
30/03/22	14.0	76.6	1008.1	1.8 NW	115.3	12:10	2.2	0.9	1.9 (12:50)
31/03/22	14.4	90.5	998.7	4.0 S	91.6	11:50	14.4	0.7	2.2 (14:40)



MARZO 2022

(estremi giornalieri)

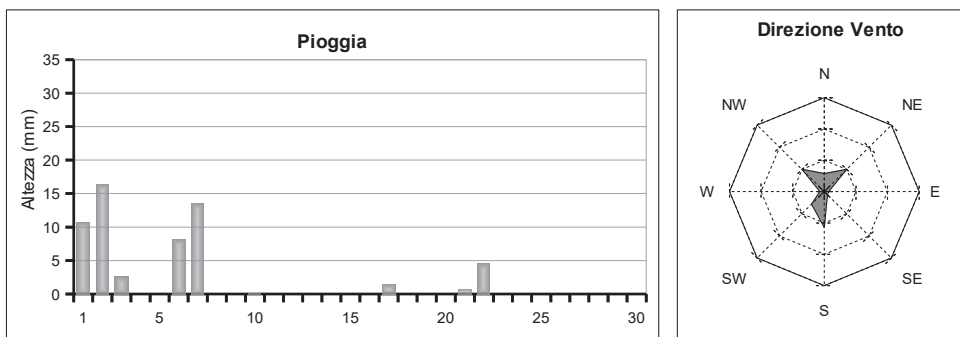
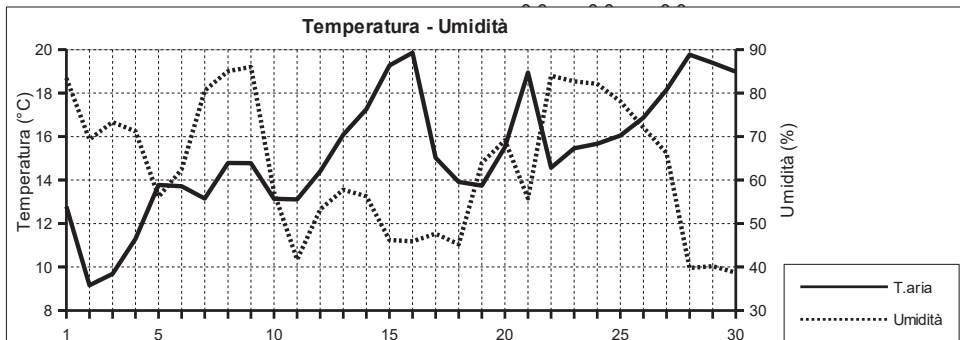
Data	Temperatura (°C)			Umidità (%)			Pressione (hPa)			Vento (m/s)		Radiazione (W/m²)	
	min (ore)	max (ore)	min (ore)	max (ore)	min (ore)	max (ore)	min (ore)	max (ore)	max (ore)	max (ore)	max (ore)		
01/03/22	5.7	(7:00)	10.7	(13:20)	37.0	(16:50)	58.0	(23:00)	1023.0	(15:40)	1025.5	(21:30)	12.5 (12:20) 844.0 (13:10)
02/03/22	5.4	(6:10)	12.4	(14:00)	35.0	(13:50)	70.0	(23:50)	1021.5	(16:40)	1025.1	(0:20)	8.0 (16:20) 694.0 (11:20)
03/03/22	6.8	(6:40)	12.4	(11:50)	61.0	(16:50)	76.0	(6:40)	1015.8	(23:50)	1022.0	(0:00)	6.7 (14:30) 800.0 (11:30)
04/03/22	8.1	(23:40)	13.2	(10:30)	57.0	(10:30)	85.0	(23:50)	1012.3	(15:50)	1015.9	(0:10)	7.2 (14:00) 853.0 (13:50)
05/03/22	6.4	(5:00)	11.3	(14:00)	50.0	(15:20)	89.0	(2:10)	1008.9	(13:50)	1012.4	(0:00)	13.0 (11:30) 925.0 (13:10)
06/03/22	6.4	(6:40)	11.8	(16:00)	42.0	(11:30)	70.0	(23:50)	1011.8	(0:20)	1014.8	(21:20)	5.4 (16:50) 766.0 (10:00)
07/03/22	4.2	(7:00)	10.8	(14:10)	51.0	(17:50)	82.0	(0:30)	1014.4	(4:50)	1017.4	(23:50)	10.3 (0:10) 846.0 (12:30)
08/03/22	5.2	(5:40)	9.2	(12:40)	38.0	(14:20)	61.0	(2:00)	1015.9	(6:20)	1020.2	(23:10)	13.0 (14:50) 960.0 (13:10)
09/03/22	5.8	(0:30)	11.7	(16:00)	38.0	(10:50)	58.0	(20:00)	1020.1	(2:30)	1024.8	(23:50)	8.9 (14:10) 826.0 (12:30)
10/03/22	5.8	(5:50)	14.8	(13:40)	32.0	(11:20)	65.0	(20:00)	1023.4	(15:50)	1026.0	(8:50)	8.5 (14:10) 745.0 (12:30)
11/03/22	7.4	(23:40)	13.7	(14:30)	34.0	(16:10)	60.0	(0:30)	1025.0	(17:10)	1027.2	(10:10)	8.0 (11:20) 944.0 (12:30)
12/03/22	5.6	(6:30)	13.5	(14:30)	30.0	(12:50)	52.0	(23:10)	1024.8	(15:30)	1027.5	(1:10)	8.5 (12:30) 763.0 (11:50)
13/03/22	5.2	(5:20)	13.3	(15:30)	34.0	(9:50)	66.0	(21:20)	1025.8	(4:30)	1029.3	(23:50)	6.7 (4:50) 765.0 (12:10)
14/03/22	6.9	(6:20)	15.1	(13:10)	31.0	(13:10)	66.0	(22:20)	1029.3	(0:10)	1035.7	(23:50)	6.3 (14:00) 780.0 (12:40)
15/03/22	8.3	(6:40)	15.4	(12:30)	45.0	(9:20)	77.0	(22:50)	1032.7	(23:50)	1037.6	(10:20)	7.2 (11:10) 812.0 (13:00)
16/03/22	9.6	(4:30)	15.5	(14:10)	58.0	(9:20)	83.0	(6:10)	1024.9	(17:20)	1032.6	(0:00)	6.3 (12:10) 758.0 (12:00)
17/03/22	10.8	(6:50)	20.7	(13:10)	38.0	(11:10)	82.0	(0:10)	1021.9	(14:10)	1025.0	(0:10)	9.4 (17:10) 758.0 (11:00)
18/03/22	13.2	(5:30)	17.0	(15:20)	50.0	(14:20)	69.0	(23:50)	1024.1	(3:50)	1028.9	(23:20)	13.0 (16:00) 547.0 (15:10)
19/03/22	10.6	(23:10)	14.2	(9:50)	41.0	(10:00)	73.0	(0:40)	1028.7	(15:20)	1031.6	(22:50)	11.6 (9:50) 209.0 (10:00)
20/03/22	8.3	(23:50)	15.1	(12:50)	32.0	(14:40)	67.0	(0:00)	1031.4	(15:00)	1034.0	(21:50)	11.6 (15:20) 877.0 (12:40)
21/03/22	6.7	(6:00)	14.6	(15:50)	34.0	(16:00)	61.0	(2:10)	1031.1	(16:30)	1034.6	(8:20)	12.1 (18:00) 930.0 (12:50)
22/03/22	7.6	(5:10)	16.3	(15:30)	34.0	(14:20)	60.0	(4:00)	1030.1	(16:10)	1033.7	(8:30)	10.7 (14:00) 875.0 (12:40)
23/03/22	9.4	(5:00)	20.4	(15:30)	19.0	(13:20)	59.0	(20:40)	1026.1	(16:10)	1031.0	(0:40)	8.5 (14:40) 789.0 (12:00)
24/03/22	10.1	(6:10)	16.9	(16:40)	37.0	(8:30)	84.0	(21:00)	1027.5	(16:10)	1029.7	(10:20)	7.6 (13:30) 772.0 (12:00)
25/03/22	10.8	(3:30)	16.7	(13:40)	66.0	(13:10)	87.0	(6:00)	1026.6	(16:20)	1029.1	(7:30)	7.6 (14:00) 766.0 (12:10)
26/03/22	10.3	(5:50)	18.4	(14:40)	39.0	(14:00)	84.0	(3:20)	1024.7	(16:30)	1027.3	(9:40)	5.8 (23:40) 823.0 (12:20)
27/03/22	13.2	(23:20)	21.0	(12:00)	19.0	(11:40)	76.0	(23:10)	1023.2	(16:40)	1026.5	(22:50)	12.5 (20:40) 726.0 (12:00)
28/03/22	10.4	(4:20)	15.8	(13:50)	61.0	(18:30)	86.0	(3:20)	1022.3	(23:50)	1027.2	(1:10)	9.4 (2:50) 577.0 (12:30)
29/03/22	11.3	(5:20)	17.9	(15:30)	53.0	(15:30)	77.0	(5:30)	1015.5	(23:50)	1022.5	(0:00)	7.6 (16:00) 812.0 (13:20)
30/03/22	11.7	(10:20)	16.7	(23:40)	67.0	(7:10)	86.0	(11:00)	1001.6	(23:40)	1015.3	(0:00)	13.4 (15:40) 401.0 (11:50)
31/03/22	12.7	(23:50)	17.1	(0:00)	72.0	(0:00)	95.0	(7:20)	997.2	(15:50)	1001.7	(0:00)	16.1 (1:00) 452.0 (17:20)



APRILE 2022

(medie giornaliere)

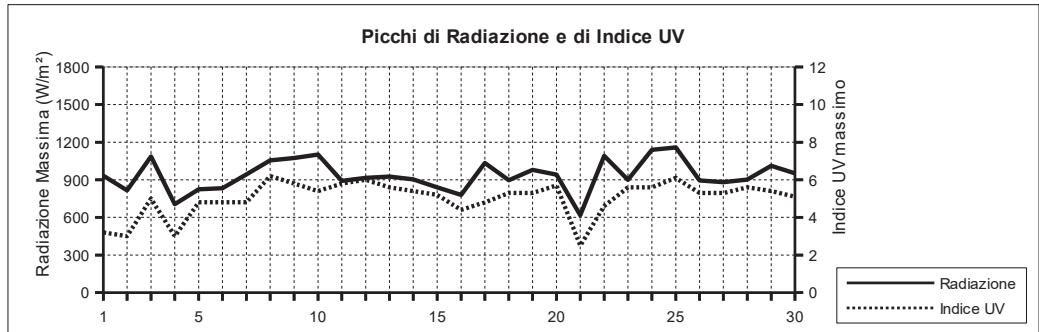
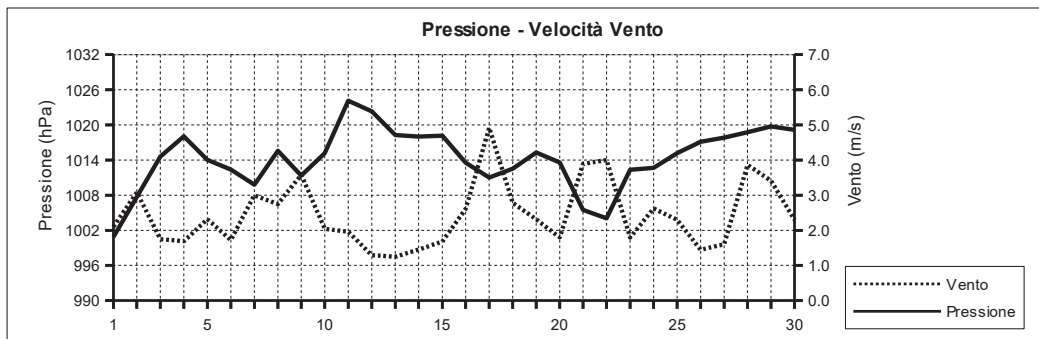
Data	Temperatura	Umidità	Pressione	Vento	Rad. Solare	Pioggia	Indice UV		
	°C	%	hPa	m/s direzione	W/m² durata	mm	medio	max	(ore)
01/04/22	12.8	83.5	1000.9	2.1 SW	240.5 12:40	10.6	1.6	3.2	(14:20)
02/04/22	9.2	69.3	1007.7	3.1 SW	149.1 12:50	16.4	1.0	3.0	(15:00)
03/04/22	9.7	73.3	1014.6	1.7 NW	328.2 12:50	2.6	2.0	5.0	(12:50)
04/04/22	11.3	71.2	1018.0	1.7 N	233.2 12:40	0.0	1.5	3.0	(15:20)
05/04/22	13.8	56.1	1014.0	2.3 NW	472.6 12:50	0.0	2.9	4.8	(12:40)
06/04/22	13.7	62.5	1012.4	1.7 NW	348.9 12:40	8.2	2.5	4.8	(12:30)
07/04/22	13.2	80.6	1009.8	3.0 NW	440.6 12:30	13.4	2.8	4.8	(12:50)
08/04/22	14.8	85.0	1015.6	2.7 S	363.1 13:00	0.0	2.6	6.2	(12:10)
09/04/22	14.8	86.0	1011.3	3.6 S	346.2 12:30	0.0	2.5	5.8	(13:40)
10/04/22	13.1	57.1	1015.2	2.0 NE	323.4 13:10	0.2	2.3	5.4	(13:10)
11/04/22	13.1	41.7	1024.1	2.0 N	500.4 13:20	0.0	3.3	5.8	(13:10)
12/04/22	14.4	53.2	1022.3	1.3 --	488.3 13:20	0.0	3.4	6.0	(12:50)
13/04/22	16.1	57.8	1018.2	1.2 NE	461.5 13:10	0.0	3.1	5.6	(13:00)
14/04/22	17.3	56.3	1018.0	1.5 --	436.5 13:20	0.0	3.0	5.4	(13:00)
15/04/22	19.3	46.2	1018.2	1.7 NW	436.2 13:20	0.0	3.0	5.2	(12:40)
16/04/22	19.9	45.9	1013.6	2.6 NE	330.1 13:30	0.0	2.4	4.4	(11:40)
17/04/22	15.0	47.7	1011.0	4.9 NE	270.4 12:50	1.4	2.1	4.8	(13:40)
18/04/22	13.9	45.2	1012.5	2.8 N	503.9 13:30	0.0	3.0	5.3	(12:50)
19/04/22	13.7	63.9	1015.3	2.3 S	433.9 13:40	0.0	2.8	5.3	(12:30)
20/04/22	15.5	69.2	1013.6	1.8 S	461.6 13:30	0.0	3.2	5.7	(13:10)
21/04/22	18.9	55.8	1005.5	3.9 --	131.4 13:20	0.6	1.0	2.5	(10:10)
22/04/22	14.6	84.0	1004.0	4.0 S	203.3 13:20	4.6	1.4	4.6	(14:40)
23/04/22	15.5	82.7	1012.3	1.8 S	455.8 13:40	0.0	3.0	5.6	(12:40)
24/04/22	15.7	82.1	1012.7	2.6 S	441.0 13:30	0.0	2.7	5.6	(13:10)
25/04/22	16.0	78.1	1015.2	2.3 SW	346.9 13:50	0.0	2.4	6.1	(12:40)
26/04/22	16.9	72.1	1017.1	1.4 --	503.4 14:00	0.0	3.1	5.3	(13:00)
27/04/22	18.2	66.2	1017.8	1.6 --	503.8 14:00	0.0	3.0	5.3	(13:10)
28/04/22	19.8	39.8	1018.7	3.9 NE	507.0 14:00	0.0	3.2	5.6	(13:00)
29/04/22	19.4	40.2	1019.7	3.4 NE	444.4 14:10	0.0	2.8	5.4	(12:20)
30/04/22	19.0	38.7	1019.2	2.3 NW	508.5 14:00	0.0	3.0	5.1	(12:10)



APRILE 2022

(estremi giornalieri)

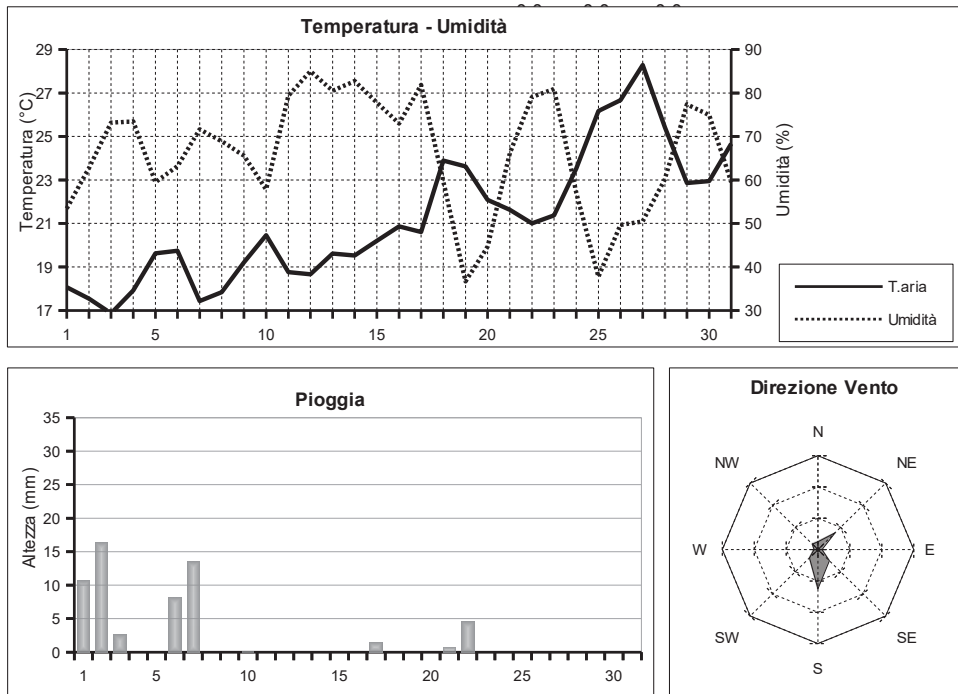
Data	Temperatura (°C)			Umidità (%)			Pressione (hPa)			Vento (m/s)		Radiazione (W/m²)	
	min	(ore)	max	(ore)	min	(ore)	max	(ore)	min	(ore)	max	(ore)	
01/04/22	10.3	(23:50)	15.4	(9:50)	63.0	(14:40)	92.0	(3:00)	999.2	(6:20)	1004.0	(23:40)	10.7 (11:20)
02/04/22	5.1	(22:30)	11.5	(9:10)	49.0	(9:20)	88.0	(0:10)	1003.7	(0:00)	1010.5	(23:30)	13.9 (0:30)
03/04/22	5.3	(00:00)	13.5	(16:10)	52.0	(17:20)	88.0	(7:20)	1009.5	(3:00)	1019.4	(23:40)	7.6 (14:20)
04/04/22	8.7	(4:50)	14.8	(17:40)	51.0	(16:10)	84.0	(6:40)	1015.0	(23:50)	1020.2	(11:20)	6.7 (19:50)
05/04/22	9.6	(6:50)	17.7	(15:50)	39.0	(12:40)	71.0	(4:50)	1012.7	(17:50)	1015.3	(23:40)	6.7 (15:50)
06/04/22	10.3	(23:20)	17.8	(13:40)	32.0	(12:40)	91.0	(23:30)	1008.3	(23:50)	1015.4	(0:20)	8.5 (17:50)
07/04/22	10.3	(00:00)	16.3	(15:10)	54.0	(14:10)	94.0	(3:00)	1005.6	(4:50)	1015.2	(23:40)	13.9 (14:50)
08/04/22	13.4	(6:40)	16.9	(14:00)	78.0	(1:10)	92.0	(23:30)	1014.6	(23:40)	1017.0	(10:40)	9.8 (1:20)
09/04/22	13.4	(23:50)	16.3	(14:10)	61.0	(23:10)	92.0	(0:00)	1009.7	(19:20)	1014.6	(0:00)	11.2 (15:00)
10/04/22	9.8	(9:50)	16.2	(13:50)	36.0	(16:40)	80.0	(6:30)	1009.5	(2:50)	1022.7	(23:50)	11.6 (9:30)
11/04/22	9.4	(6:30)	16.8	(16:00)	29.0	(11:20)	62.0	(23:30)	1022.7	(0:00)	1025.9	(11:20)	8.5 (15:00)
12/04/22	10.1	(6:00)	18.3	(14:30)	30.0	(13:30)	69.0	(21:50)	1020.0	(19:30)	1024.0	(0:00)	6.3 (16:00)
13/04/22	11.9	(6:50)	21.9	(14:40)	40.0	(14:30)	84.0	(23:30)	1016.2	(16:10)	1020.4	(0:00)	6.3 (17:00)
14/04/22	13.7	(2:50)	21.2	(13:30)	37.0	(9:50)	88.0	(2:10)	1016.9	(16:50)	1019.8	(21:20)	6.3 (17:00)
15/04/22	14.9	(4:30)	24.2	(16:30)	30.0	(12:50)	70.0	(3:00)	1016.3	(17:10)	1019.7	(0:00)	7.2 (15:40)
16/04/22	16.9	(4:00)	23.9	(13:50)	26.0	(11:50)	61.0	(1:00)	1011.2	(18:30)	1016.7	(0:00)	13.0 (22:20)
17/04/22	12.4	(23:40)	18.4	(0:20)	40.0	(0:10)	66.0	(7:10)	1009.7	(17:00)	1012.8	(0:00)	16.5 (12:20)
18/04/22	11.1	(7:00)	18.0	(15:10)	29.0	(12:30)	62.0	(22:40)	1011.1	(5:30)	1015.3	(23:20)	9.8 (0:40)
19/04/22	10.7	(5:10)	16.1	(13:50)	48.0	(8:30)	73.0	(15:20)	1014.3	(19:20)	1016.1	(11:10)	9.8 (14:20)
20/04/22	12.7	(6:50)	18.6	(14:20)	58.0	(13:50)	79.0	(3:40)	1010.3	(19:40)	1015.5	(0:40)	7.6 (1:20)
21/04/22	16.2	(6:00)	22.7	(12:10)	36.0	(12:20)	76.0	(0:00)	1000.5	(18:30)	1012.2	(0:10)	21.5 (20:40)
22/04/22	13.1	(15:40)	16.6	(0:00)	73.0	(8:40)	91.0	(13:30)	1000.7	(0:40)	1009.2	(23:40)	15.6 (7:50)
23/04/22	13.3	(3:50)	17.9	(15:20)	74.0	(16:10)	91.0	(4:10)	1009.4	(0:00)	1014.3	(13:20)	8.5 (15:30)
24/04/22	13.1	(6:30)	17.8	(16:00)	75.0	(10:00)	88.0	(20:00)	1010.6	(9:20)	1013.8	(22:50)	12.1 (11:10)
25/04/22	14.4	(6:00)	18.6	(16:40)	62.0	(16:50)	91.0	(3:00)	1012.7	(5:10)	1017.4	(23:20)	8.9 (14:20)
26/04/22	12.9	(5:10)	21.3	(17:40)	49.0	(17:30)	89.0	(7:00)	1016.3	(17:50)	1017.9	(22:30)	8.9 (14:10)
27/04/22	14.0	(5:50)	23.2	(15:40)	40.0	(16:50)	85.0	(5:20)	1017.1	(2:40)	1018.8	(11:30)	6.7 (12:40)
28/04/22	16.8	(6:10)	23.8	(14:50)	30.0	(10:40)	55.0	(3:20)	1017.7	(17:20)	1020.2	(22:20)	11.6 (11:00)
29/04/22	15.5	(6:20)	23.6	(14:50)	30.0	(14:30)	50.0	(5:40)	1018.2	(16:40)	1021.1	(23:40)	11.2 (11:20)
30/04/22	15.5	(4:30)	22.8	(16:20)	31.0	(17:00)	53.0	(23:50)	1017.5	(17:50)	1021.2	(0:40)	8.0 (14:10)



MAGGIO 2022

(media giornaliera)

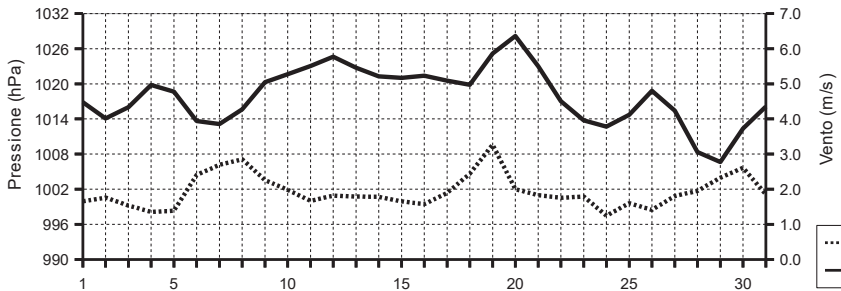
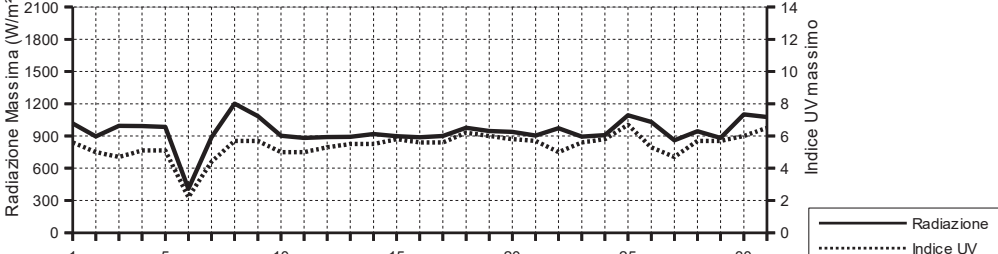
Data	Temperatura °C	Umidità %	Pressione hPa	Vento m/s	direzione	Rad. Solare W/m²	durata	Pioggia mm	Indice UV
								medio	max (ore)
01/05/22	18.1	53.4	1016.9	1.7	--	497.3	14:00	0.0	3.0 5.6 (13:30)
02/05/22	17.5	62.7	1014.1	1.8	--	461.3	14:00	0.0	2.9 5.0 (13:00)
03/05/22	16.9	73.2	1016.0	1.5	--	419.2	14:10	0.4	2.6 4.7 (12:00)
04/05/22	17.9	73.5	1019.8	1.4	SE	461.0	14:10	0.0	2.7 5.1 (13:20)
05/05/22	19.6	59.5	1018.7	1.4	NE	299.7	13:50	0.0	2.0 5.1 (13:10)
06/05/22	19.7	63.2	1013.7	2.4	--	160.9	13:00	3.4	1.1 2.2 (14:50)
07/05/22	17.4	71.6	1013.1	2.7	NE	176.6	13:50	3.4	1.3 4.4 (14:30)
08/05/22	17.8	68.9	1015.6	2.9	NE	328.8	14:10	1.4	2.6 5.7 (13:20)
09/05/22	19.2	65.6	1020.3	2.3	N	410.8	14:00	0.0	2.9 5.7 (12:40)
10/05/22	20.5	57.8	1021.6	2.0	NW	429.3	14:10	0.4	3.2 5.0 (12:50)
11/05/22	18.8	79.3	1023.0	1.7	SE	490.7	14:30	0.0	3.0 5.0 (13:20)
12/05/22	18.7	85.0	1024.6	1.8	S	490.4	14:30	0.0	3.1 5.3 (12:50)
13/05/22	19.6	80.5	1022.8	1.8	S	495.7	14:30	0.0	3.2 5.5 (12:50)
14/05/22	19.5	82.7	1021.3	1.8	S	493.2	14:30	0.0	3.1 5.5 (12:20)
15/05/22	20.2	77.8	1021.0	1.7	S	495.2	14:40	0.0	3.2 5.8 (13:20)
16/05/22	20.9	73.0	1021.4	1.6	SE	493.8	14:40	0.0	3.2 5.6 (13:10)
17/05/22	20.6	81.8	1020.5	1.9	S	493.1	14:40	0.0	3.2 5.6 (13:00)
18/05/22	23.9	59.7	1019.8	2.4	NE	498.3	14:40	0.0	3.5 6.2 (13:10)
19/05/22	23.6	36.7	1025.2	3.3	NE	529.2	14:40	0.0	3.4 6.0 (12:50)
20/05/22	22.1	44.7	1028.2	2.0	--	523.6	14:40	0.0	3.3 5.8 (12:40)
21/05/22	21.6	66.1	1023.0	1.8	SW	491.0	14:50	0.0	3.2 5.7 (12:50)
22/05/22	21.0	79.1	1017.1	1.8	S	336.9	14:30	0.0	2.3 5.0 (14:50)
23/05/22	21.4	80.9	1013.8	1.8	S	474.6	14:30	0.0	3.2 5.6 (12:50)
24/05/22	23.5	57.1	1012.7	1.2	--	505.1	14:40	0.0	3.3 5.8 (12:40)
25/05/22	26.2	37.7	1014.7	1.6	--	426.6	14:50	0.0	2.9 6.7 (12:40)
26/05/22	26.7	49.7	1018.8	1.4	--	422.3	14:50	0.0	2.8 5.3 (13:10)
27/05/22	28.3	50.5	1015.4	1.8	--	238.2	14:30	0.0	2.0 4.7 (11:30)
28/05/22	25.4	60.2	1008.3	2.0	SW	487.4	14:30	0.0	3.2 5.7 (12:40)
29/05/22	22.9	77.4	1006.6	2.3	S	466.8	15:00	0.0	3.3 5.7 (12:40)
30/05/22	22.9	74.9	1012.4	2.6	S	482.7	15:00	0.0	3.3 6.0 (12:10)
31/05/22	24.7	59.5	1016.1	1.9	--	440.1	15:00	0.0	3.1 6.5 (13:10)



MAGGIO 2022

(estremi giornalieri)

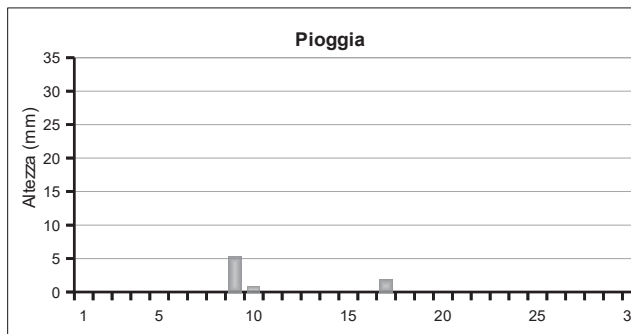
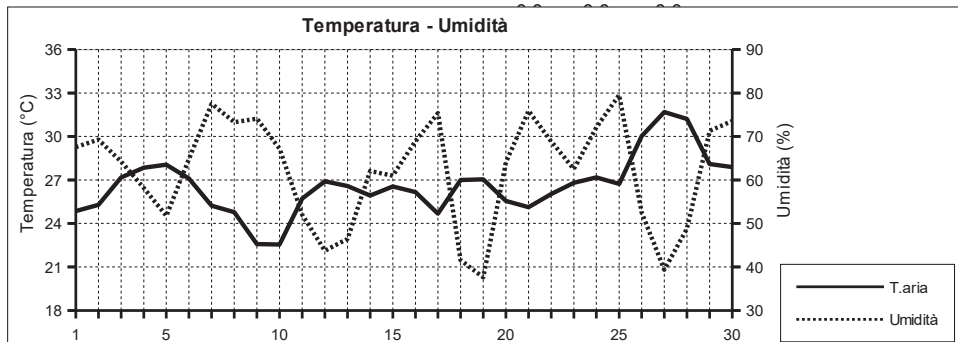
Data	Temperatura (°C)			Umidità (%)			Pressione (hPa)			Vento (m/s)		Radiazione (W/m²)
	min (ore)	max (ore)	min (ore)	max (ore)	min (ore)	max (ore)	min (ore)	max (ore)	max (ore)	max (ore)	max (ore)	
01/05/22	14.6 (5:50)	22.2 (15:40)	31.0 (17:20)	73.0 (9:40)	1014.7 (18:00)	1018.6 (0:40)	8.0 (11:50)	1016.0 (14:00)				
02/05/22	14.9 (6:20)	21.6 (15:20)	46.0 (15:20)	78.0 (3:50)	1012.9 (14:40)	1015.5 (0:00)	8.5 (16:30)	896.0 (14:50)				
03/05/22	14.1 (6:00)	19.8 (18:40)	56.0 (18:40)	80.0 (6:10)	1014.5 (4:30)	1018.6 (23:30)	8.5 (14:40)	995.0 (11:50)				
04/05/22	14.6 (6:30)	21.6 (15:10)	51.0 (16:00)	85.0 (5:10)	1018.4 (2:00)	1021.2 (21:50)	7.2 (14:20)	993.0 (13:20)				
05/05/22	15.6 (6:40)	25.2 (17:30)	37.0 (13:20)	81.0 (1:50)	1015.4 (18:10)	1021.0 (0:00)	6.7 (17:50)	984.0 (13:10)				
06/05/22	17.4 (21:00)	22.6 (9:00)	45.0 (8:40)	80.0 (21:20)	1012.2 (18:40)	1016.6 (0:10)	13.0 (8:40)	408.0 (14:50)				
07/05/22	16.2 (13:00)	19.7 (11:30)	58.0 (11:30)	83.0 (1:00)	1012.2 (15:30)	1014.8 (23:30)	12.1 (15:40)	888.0 (11:00)				
08/05/22	16.0 (5:30)	22.2 (13:30)	50.0 (13:50)	83.0 (21:20)	1013.8 (4:50)	1018.8 (23:50)	10.3 (4:00)	1202.0 (12:20)				
09/05/22	16.5 (3:10)	23.5 (16:00)	51.0 (16:00)	76.0 (0:00)	1018.6 (1:40)	1022.6 (23:10)	7.6 (20:40)	1086.0 (11:10)				
10/05/22	16.2 (6:20)	25.4 (14:40)	40.0 (10:10)	75.0 (23:50)	1020.3 (15:30)	1023.0 (22:30)	8.9 (15:20)	902.0 (13:40)				
11/05/22	16.4 (5:50)	21.0 (14:30)	62.0 (10:30)	91.0 (23:40)	1021.4 (2:50)	1024.6 (23:40)	8.9 (14:00)	882.0 (13:20)				
12/05/22	17.0 (2:10)	20.7 (13:30)	74.0 (15:40)	93.0 (3:00)	1023.5 (19:30)	1025.6 (11:20)	8.5 (13:00)	889.0 (13:00)				
13/05/22	17.5 (6:50)	21.9 (15:10)	62.0 (20:20)	93.0 (0:00)	1021.0 (18:30)	1024.4 (0:10)	7.6 (14:30)	891.0 (12:50)				
14/05/22	17.8 (5:40)	21.7 (17:20)	72.0 (15:00)	91.0 (4:30)	1020.2 (18:40)	1022.1 (0:00)	8.5 (14:50)	918.0 (13:50)				
15/05/22	17.8 (5:00)	24.0 (17:30)	60.0 (19:00)	91.0 (1:20)	1019.9 (18:20)	1021.7 (11:20)	7.2 (13:40)	898.0 (13:10)				
16/05/22	17.6 (5:10)	25.1 (15:40)	56.0 (18:20)	82.0 (21:20)	1020.4 (15:30)	1022.4 (11:30)	8.0 (15:50)	888.0 (13:10)				
17/05/22	18.7 (5:30)	23.0 (15:10)	72.0 (0:00)	89.0 (22:50)	1018.9 (16:50)	1021.9 (0:00)	8.0 (14:30)	900.0 (14:00)				
18/05/22	19.2 (5:10)	29.3 (13:20)	33.0 (13:50)	91.0 (1:20)	1018.6 (3:20)	1023.2 (23:50)	12.1 (13:50)	976.0 (12:00)				
19/05/22	19.9 (5:40)	27.7 (17:50)	20.0 (19:10)	57.0 (6:00)	1022.8 (3:20)	1027.9 (23:50)	13.4 (10:40)	947.0 (12:50)				
20/05/22	18.2 (5:00)	25.6 (17:30)	30.0 (9:10)	60.0 (15:30)	1026.3 (23:50)	1029.8 (9:20)	7.6 (13:50)	937.0 (12:50)				
21/05/22	19.1 (5:40)	24.4 (11:30)	42.0 (10:50)	80.0 (22:40)	1020.1 (23:40)	1026.3 (0:00)	8.9 (14:30)	904.0 (13:40)				
22/05/22	18.8 (5:30)	24.1 (17:00)	68.0 (17:00)	87.0 (4:20)	1015.1 (17:20)	1019.9 (0:00)	6.7 (16:10)	972.0 (15:10)				
23/05/22	19.6 (4:20)	24.0 (15:40)	67.0 (13:10)	91.0 (5:20)	1012.3 (18:00)	1015.6 (0:00)	7.2 (16:20)	893.0 (13:30)				
24/05/22	18.8 (4:50)	27.9 (13:30)	26.0 (18:00)	92.0 (1:40)	1012.0 (18:10)	1013.5 (8:30)	7.6 (15:00)	909.0 (12:50)				
25/05/22	21.8 (2:20)	31.6 (17:30)	22.0 (12:10)	70.0 (22:00)	1012.3 (5:00)	1018.5 (23:50)	6.7 (17:40)	1092.0 (12:30)				
26/05/22	22.7 (5:00)	31.7 (18:20)	32.0 (12:20)	64.0 (1:40)	1017.2 (5:10)	1020.1 (12:40)	6.7 (13:50)	1030.0 (13:10)				
27/05/22	24.8 (23:40)	33.2 (12:50)	39.0 (11:30)	64.0 (23:30)	1011.8 (20:20)	1018.9 (0:00)	8.5 (7:30)	860.0 (11:30)				
28/05/22	21.9 (23:40)	28.4 (14:10)	35.0 (14:00)	80.0 (23:20)	1006.0 (18:40)	1012.3 (0:50)	8.9 (17:10)	944.0 (12:40)				
29/05/22	20.8 (3:50)	25.3 (11:30)	63.0 (11:30)	85.0 (3:40)	1004.8 (2:30)	1009.5 (23:30)	9.4 (22:40)	882.0 (13:10)				
30/05/22	20.7 (5:10)	24.8 (13:50)	63.0 (23:20)	83.0 (0:40)	1009.5 (0:00)	1016.1 (23:10)	10.7 (16:30)	1100.0 (12:10)				
31/05/22	21.5 (5:40)	28.3 (12:10)	36.0 (10:40)	82.0 (23:50)	1015.2 (6:10)	1017.0 (22:40)	8.5 (13:30)	1076.0 (13:10)				

Pressione - Velocità Vento

Picchi di Radiazione e di Indice UV


GIUGNO 2022

(media giornaliera)

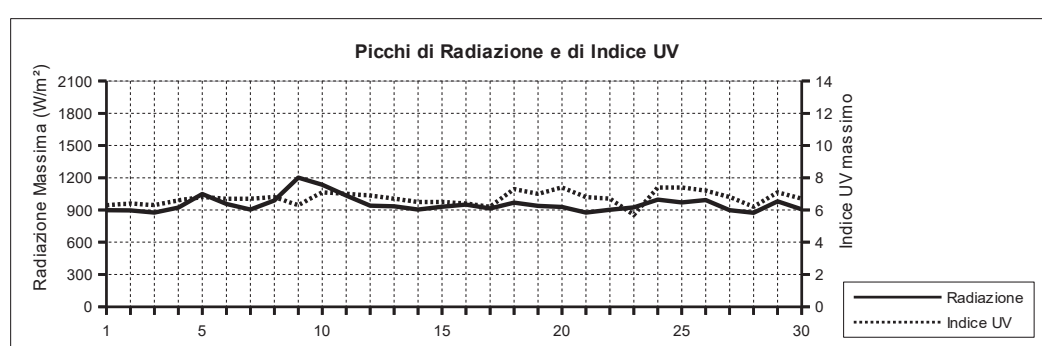
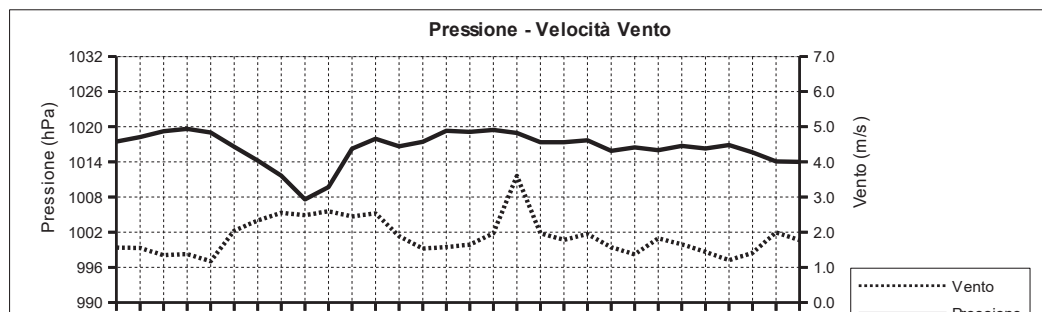
Data	Temperatura °C	Umidità %	Pressione hPa	Vento m/s direzione	Rad. Solare W/m² durata	Pioggia mm	Indice UV		
							medio	max	(ore)
01/06/22	24.9	67.5	1017.5	1.6 --	497.8 15:00	0.0	3.6	6.3	(12:50)
02/06/22	25.3	69.3	1018.3	1.6 SE	489.8 15:00	0.0	3.5	6.4	(12:50)
03/06/22	27.2	64.3	1019.3	1.3 SE	471.5 15:00	0.0	3.5	6.3	(13:10)
04/06/22	27.9	58.2	1019.7	1.4 SE	451.1 15:00	0.0	3.5	6.6	(13:10)
05/06/22	28.1	51.7	1019.0	1.2 SE	436.2 14:50	0.0	3.3	6.8	(12:50)
06/06/22	27.1	64.9	1016.6	2.0 S	452.0 15:00	0.0	3.4	6.7	(12:40)
07/06/22	25.2	77.5	1014.2	2.3 S	496.8 15:00	0.0	3.8	6.7	(12:50)
08/06/22	24.8	73.3	1011.7	2.6 SW	464.2 15:00	0.0	3.7	6.8	(12:40)
09/06/22	22.6	74.1	1007.6	2.5 SW	269.9 14:50	5.2	2.2	6.3	(12:30)
10/06/22	22.5	67.2	1009.7	2.6 NE	432.6 14:40	0.8	3.2	7.1	(13:00)
11/06/22	25.7	52.0	1016.3	2.4 N	427.4 15:00	0.0	3.3	7.0	(13:00)
12/06/22	26.9	43.7	1017.9	2.5 N	502.8 15:20	0.0	3.9	6.9	(12:50)
13/06/22	26.6	46.4	1016.7	1.9 --	510.8 15:20	0.0	3.8	6.7	(12:30)
14/06/22	25.9	62.1	1017.4	1.5 --	455.9 15:00	0.0	3.6	6.5	(12:50)
15/06/22	26.6	61.0	1019.3	1.6 --	456.5 15:00	0.0	3.7	6.5	(13:00)
16/06/22	26.2	68.9	1019.1	1.6 S	469.8 15:10	0.0	3.5	6.4	(13:30)
17/06/22	24.7	75.4	1019.5	2.0 --	277.7 14:50	1.8	2.9	6.2	(12:50)
18/06/22	27.0	41.5	1019.0	3.6 NE	522.7 15:10	0.0	4.0	7.3	(13:10)
19/06/22	27.0	37.6	1017.4	2.0 --	517.6 15:10	0.0	3.9	7.0	(13:10)
20/06/22	25.5	64.0	1017.4	1.8 S	503.8 15:10	0.0	3.8	7.4	(13:00)
21/06/22	25.1	75.9	1017.7	1.9 S	479.6 15:10	0.0	3.7	6.8	(13:10)
22/06/22	26.0	68.9	1015.9	1.6 S	448.8 15:20	0.0	3.5	6.7	(13:20)
23/06/22	26.8	62.5	1016.5	1.4 S	307.8 15:00	0.0	2.4	5.7	(15:10)
24/06/22	27.2	72.1	1016.0	1.8 S	411.0 15:10	0.0	3.6	7.4	(13:30)
25/06/22	26.7	79.5	1016.7	1.7 S	381.6 15:00	0.0	3.0	7.4	(12:40)
26/06/22	30.0	52.5	1016.3	1.4 --	490.9 15:10	0.0	3.9	7.2	(12:40)
27/06/22	31.7	39.3	1016.9	1.2 --	495.5 15:00	0.0	3.8	6.8	(12:40)
28/06/22	31.2	48.8	1015.6	1.4 SE	452.0 15:10	0.0	3.5	6.2	(12:40)
29/06/22	28.1	71.3	1014.1	2.0 S	512.8 15:10	0.0	4.0	7.1	(13:00)
30/06/22	27.9	73.6	1014.0	1.8 SE	490.4 15:10	0.0	3.7	6.7	(13:00)



GIUGNO 2022

(estremi giornalieri)

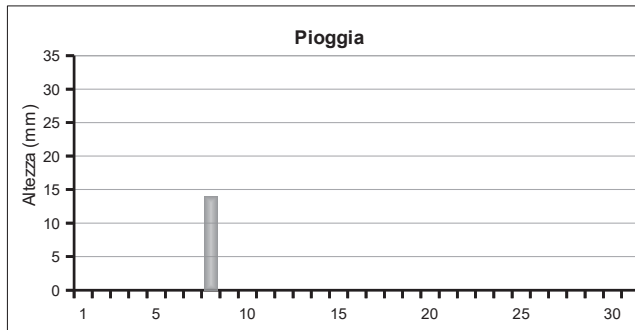
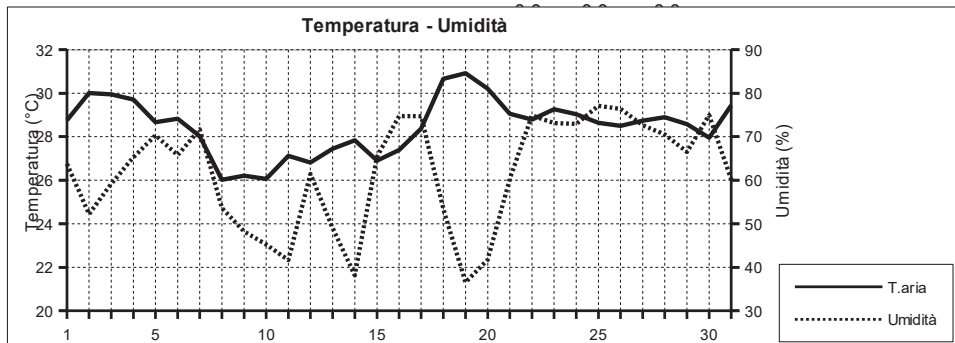
Data	Temperatura (°C)			Umidità (%)			Pressione (hPa)			Vento (m/s)		Radiazione (W/m²)	
	min (ore)	max (ore)	min (ore)	max (ore)	min (ore)	max (ore)	min (ore)	max (ore)	max (ore)	max (ore)	max (ore)	max (ore)	max (ore)
01/06/22	21.3 (5:10)	29.1 (15:10)	45.0 (18:50)	87.0 (1:30)	1016.8 (3:10)	1018.5 (23:00)	7.2 (17:30)	898.0 (13:00)					
02/06/22	22.0 (5:20)	30.3 (14:50)	53.0 (12:50)	82.0 (18:40)	1017.1 (18:00)	1019.5 (9:50)	6.3 (15:30)	896.0 (12:50)					
03/06/22	23.9 (1:50)	31.2 (14:30)	49.0 (17:50)	83.0 (1:30)	1018.4 (3:40)	1020.0 (11:00)	6.7 (14:50)	875.0 (13:10)					
04/06/22	25.7 (5:20)	33.3 (17:20)	32.0 (17:20)	76.0 (22:00)	1018.2 (4:10)	1020.7 (9:20)	7.6 (14:40)	921.0 (13:10)					
05/06/22	24.5 (5:50)	33.1 (18:00)	27.0 (17:20)	70.0 (20:40)	1016.9 (23:50)	1020.3 (10:00)	6.3 (14:40)	1049.0 (14:20)					
06/06/22	24.7 (23:50)	29.4 (16:40)	41.0 (1:50)	86.0 (23:40)	1015.3 (20:10)	1017.7 (3:10)	7.6 (14:40)	956.0 (14:10)					
07/06/22	23.7 (23:50)	27.2 (14:20)	71.0 (14:20)	85.0 (0:00)	1012.4 (18:20)	1016.1 (0:00)	8.9 (14:30)	904.0 (13:00)					
08/06/22	23.4 (4:40)	27.1 (12:30)	65.0 (14:30)	80.0 (0:10)	1010.4 (17:40)	1013.2 (0:00)	8.9 (12:10)	988.0 (12:50)					
09/06/22	19.8 (23:20)	25.0 (12:30)	65.0 (16:20)	82.0 (22:00)	1005.1 (15:30)	1011.2 (0:00)	12.5 (14:00)	1201.0 (12:30)					
10/06/22	18.2 (7:00)	26.6 (14:50)	51.0 (16:00)	86.0 (6:50)	1006.4 (5:00)	1014.5 (23:30)	10.7 (15:40)	1136.0 (15:10)					
11/06/22	21.6 (4:40)	30.1 (14:00)	39.0 (13:30)	64.0 (4:40)	1014.4 (0:00)	1018.9 (22:30)	9.8 (15:20)	1034.0 (14:30)					
12/06/22	22.8 (5:40)	31.4 (15:10)	32.0 (15:30)	54.0 (4:50)	1016.7 (16:20)	1019.0 (1:00)	9.4 (12:30)	939.0 (13:20)					
13/06/22	23.4 (4:10)	30.6 (15:00)	34.0 (12:50)	79.0 (22:10)	1014.9 (17:50)	1018.2 (0:10)	7.2 (13:30)	935.0 (13:20)					
14/06/22	22.7 (5:40)	30.8 (16:00)	41.0 (16:20)	78.0 (5:20)	1016.6 (1:20)	1018.6 (23:00)	7.6 (15:30)	905.0 (13:10)					
15/06/22	23.7 (5:30)	29.7 (16:40)	47.0 (17:50)	71.0 (18:50)	1018.2 (19:20)	1020.0 (10:10)	7.2 (13:50)	930.0 (13:10)					
16/06/22	23.9 (6:00)	29.3 (18:30)	48.0 (19:30)	85.0 (23:50)	1018.4 (18:30)	1019.9 (22:40)	7.6 (14:50)	951.0 (14:10)					
17/06/22	22.6 (18:20)	27.4 (15:10)	54.0 (15:40)	86.0 (0:00)	1018.3 (15:00)	1021.2 (18:20)	9.4 (18:20)	914.0 (12:50)					
18/06/22	23.2 (5:50)	31.3 (15:10)	22.0 (16:20)	67.0 (0:50)	1018.0 (18:00)	1020.4 (8:30)	13.0 (18:00)	969.0 (13:10)					
19/06/22	23.3 (4:20)	30.7 (15:50)	28.0 (13:50)	66.0 (23:30)	1015.9 (18:00)	1018.4 (1:00)	7.6 (0:00)	937.0 (13:20)					
20/06/22	23.0 (5:50)	28.6 (16:20)	52.0 (1:40)	76.0 (10:40)	1016.4 (3:50)	1018.1 (14:20)	8.5 (14:00)	928.0 (12:50)					
21/06/22	22.8 (5:50)	27.7 (15:40)	65.0 (15:50)	84.0 (4:00)	1016.8 (18:30)	1018.8 (9:30)	8.9 (14:30)	875.0 (13:20)					
22/06/22	23.2 (5:10)	30.2 (17:50)	32.0 (18:40)	84.0 (1:30)	1014.9 (18:00)	1017.3 (0:00)	8.5 (12:40)	902.0 (13:50)					
23/06/22	23.6 (6:20)	30.4 (16:20)	43.0 (10:30)	82.0 (2:00)	1015.1 (2:20)	1018.2 (13:20)	6.3 (13:30)	925.0 (11:00)					
24/06/22	24.8 (5:30)	30.9 (16:50)	47.0 (9:50)	89.0 (22:10)	1014.8 (5:20)	1017.1 (1:10)	7.6 (13:20)	997.0 (13:30)					
25/06/22	24.4 (6:40)	29.2 (17:40)	64.0 (18:20)	93.0 (4:20)	1015.7 (19:20)	1018.1 (12:20)	7.2 (11:50)	970.0 (13:00)					
26/06/22	25.2 (4:20)	35.1 (15:30)	29.0 (15:20)	73.0 (0:30)	1015.4 (18:50)	1016.9 (12:30)	6.3 (15:40)	993.0 (12:40)					
27/06/22	27.1 (5:00)	36.1 (15:20)	24.0 (15:20)	53.0 (3:10)	1016.1 (17:50)	1018.0 (12:10)	6.7 (16:30)	898.0 (13:10)					
28/06/22	27.6 (5:40)	36.1 (14:50)	29.0 (19:00)	76.0 (20:40)	1013.7 (20:10)	1017.0 (0:10)	6.7 (18:40)	874.0 (13:10)					
29/06/22	25.8 (23:50)	31.0 (16:50)	45.0 (16:30)	82.0 (4:30)	1012.8 (18:30)	1015.8 (0:30)	8.5 (14:20)	981.0 (11:50)					
30/06/22	25.1 (4:10)	32.1 (18:00)	52.0 (19:20)	83.0 (0:20)	1013.1 (18:30)	1015.2 (11:40)	7.6 (11:20)	907.0 (13:10)					



LUGLIO 2022

(medie giornaliere)

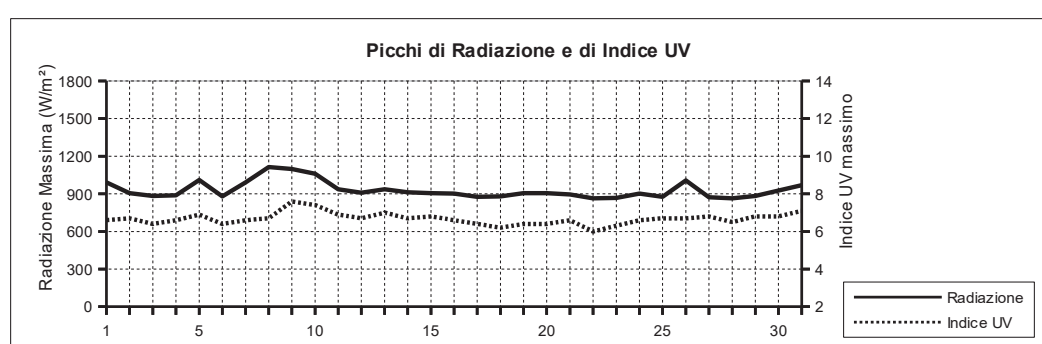
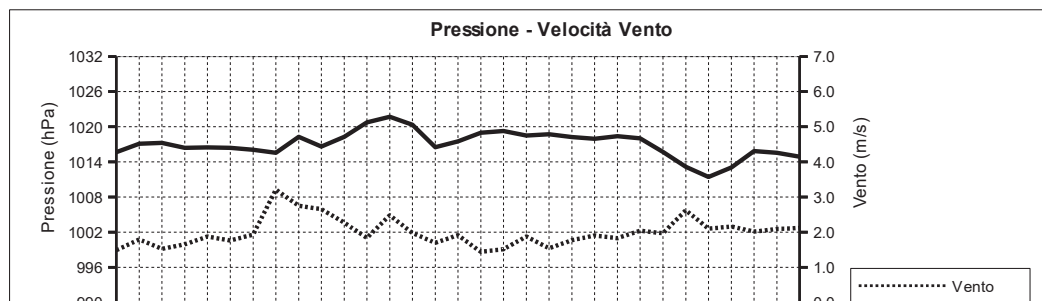
Data	Temperatura °C	Umidità %	Pressione hPa	Vento m/s	direzione	Rad. Solare W/m²	durata	Pioggia mm	Indice UV
								medio	max (ore)
01/07/22	28.8	63.8	1015.7	1.5	SE	439.0	15:10	0.0	3.4 6.6 (12:50)
02/07/22	30.0	52.2	1017.1	1.8	--	503.6	15:00	0.0	3.9 6.7 (13:20)
03/07/22	29.9	59.2	1017.2	1.5	SE	477.7	15:10	0.0	3.5 6.4 (13:00)
04/07/22	29.7	65.3	1016.4	1.7	--	476.6	15:10	0.0	3.6 6.6 (13:20)
05/07/22	28.7	70.3	1016.5	1.9	S	483.7	15:10	0.0	3.7 6.9 (13:10)
06/07/22	28.8	65.8	1016.4	1.8	SE	482.6	15:10	0.0	3.5 6.4 (13:30)
07/07/22	28.0	71.7	1016.1	1.9	--	428.8	15:10	0.0	3.2 6.6 (13:20)
08/07/22	26.0	53.6	1015.6	3.2	NE	477.0	14:50	14.0	3.4 6.7 (13:00)
09/07/22	26.2	48.2	1018.3	2.8	NE	450.2	14:50	0.0	3.6 7.6 (13:20)
10/07/22	26.1	45.2	1016.6	2.7	NE	527.6	15:10	0.0	4.0 7.4 (13:20)
11/07/22	27.1	41.6	1018.3	2.3	NW	513.9	15:00	0.0	3.9 6.9 (13:10)
12/07/22	26.8	61.5	1020.7	1.8	SE	502.4	15:00	0.0	3.7 6.7 (13:30)
13/07/22	27.5	49.0	1021.7	2.5	NE	502.3	15:00	0.0	3.8 7.0 (13:20)
14/07/22	27.8	38.2	1020.4	2.0	NW	515.3	14:50	0.0	3.8 6.7 (13:10)
15/07/22	26.9	65.4	1016.5	1.7	SE	505.4	14:50	0.0	3.8 6.8 (12:50)
16/07/22	27.4	74.8	1017.5	1.9	SE	510.3	14:50	0.0	3.7 6.6 (13:10)
17/07/22	28.4	74.7	1019.0	1.4	SE	486.5	14:50	0.0	3.6 6.4 (13:10)
18/07/22	30.7	53.4	1019.3	1.5	--	448.7	14:50	0.0	3.6 6.2 (12:50)
19/07/22	30.9	36.5	1018.5	1.9	--	495.0	14:50	0.0	3.6 6.4 (12:50)
20/07/22	30.2	41.8	1018.7	1.5	--	498.7	14:50	0.0	3.6 6.4 (12:40)
21/07/22	29.1	60.3	1018.2	1.8	--	496.4	14:40	0.0	3.7 6.6 (13:00)
22/07/22	28.8	74.9	1017.9	1.9	S	481.5	14:20	0.0	3.4 6.0 (13:10)
23/07/22	29.3	73.1	1018.4	1.8	S	470.8	14:40	0.0	3.6 6.3 (13:00)
24/07/22	29.0	72.9	1018.0	2.0	SW	489.5	14:40	0.0	3.7 6.6 (13:00)
25/07/22	28.6	77.1	1015.7	2.0	S	490.8	14:40	0.0	3.8 6.7 (13:20)
26/07/22	28.5	76.4	1013.2	2.6	S	470.3	14:30	0.0	3.6 6.7 (12:50)
27/07/22	28.7	72.7	1011.4	2.1	SW	489.5	14:30	0.0	3.9 6.8 (13:10)
28/07/22	28.9	70.5	1013.1	2.2	NW	483.2	14:30	0.0	3.6 6.5 (13:10)
29/07/22	28.6	66.5	1015.9	2.0	--	495.7	14:30	0.0	3.9 6.8 (13:00)
30/07/22	28.0	75.0	1015.6	2.1	SW	419.9	14:30	0.0	3.6 6.8 (13:20)
31/07/22	29.4	60.1	1014.9	2.1	NE	481.0	14:20	0.0	3.8 7.1 (12:30)



LUGLIO 2022

(estremi giornalieri)

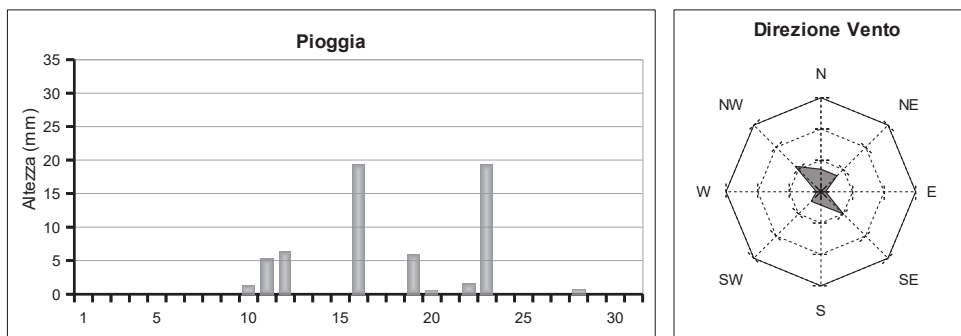
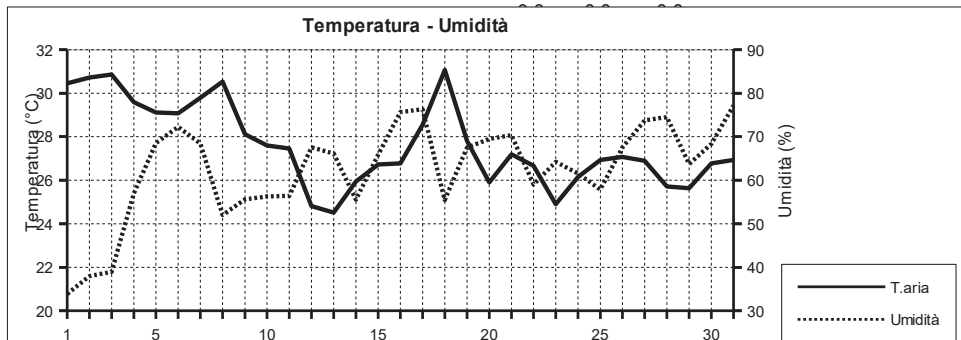
Data	Temperatura (°C)				Umidità (%)				Pressione (hPa)		Vento (m/s)	Radiazione (W/m²)
	min (ore)	max (ore)	min (ore)	max (ore)	min (ore)	max (ore)	min (ore)	max (ore)	min (ore)	max (ore)	max (ore)	max (ore)
01/07/22	25.7 (5:40)	32.2 (11:50)	40.0 (10:50)	76.0 (00:00)	1014.4 (1:20)	1017.1 (22:20)	9.4 (15:50)	991.0 (12:50)				
02/07/22	25.4 (5:40)	35.3 (18:00)	25.0 (17:40)	71.0 (6:20)	1016.2 (1:00)	1017.7 (8:40)	8.0 (13:50)	905.0 (13:20)				
03/07/22	27.1 (5:00)	34.9 (17:10)	35.0 (17:30)	76.0 (21:10)	1016.1 (17:50)	1018.1 (11:40)	8.0 (15:20)	884.0 (13:00)				
04/07/22	27.2 (6:00)	32.2 (16:10)	51.0 (20:50)	75.0 (2:20)	1014.7 (19:10)	1017.4 (7:00)	8.0 (15:30)	888.0 (13:20)				
05/07/22	26.8 (4:40)	31.4 (18:50)	39.0 (18:50)	82.0 (7:00)	1015.6 (3:30)	1017.5 (12:50)	8.5 (11:50)	1011.0 (12:50)				
06/07/22	26.1 (5:10)	33.2 (17:30)	39.0 (17:30)	74.0 (20:20)	1015.6 (16:30)	1017.1 (10:50)	8.0 (14:40)	879.0 (13:00)				
07/07/22	26.2 (4:50)	29.9 (12:50)	63.0 (19:40)	77.0 (3:40)	1014.4 (18:30)	1017.6 (10:10)	8.5 (10:10)	991.0 (11:50)				
08/07/22	18.6 (5:10)	30.3 (15:10)	34.0 (15:10)	86.0 (4:30)	1013.2 (5:40)	1018.7 (23:00)	17.9 (4:10)	1114.0 (13:40)				
09/07/22	23.1 (5:40)	30.2 (15:30)	35.0 (15:30)	58.0 (6:10)	1016.9 (18:20)	1019.0 (8:20)	10.3 (10:40)	1099.0 (12:40)				
10/07/22	23.1 (5:40)	29.8 (14:50)	30.0 (14:50)	63.0 (23:20)	1015.2 (17:00)	1018.6 (0:10)	8.9 (14:20)	1060.0 (13:30)				
11/07/22	23.0 (6:00)	31.2 (15:20)	33.0 (10:10)	61.0 (23:40)	1017.3 (3:20)	1020.3 (23:40)	8.5 (15:10)	937.0 (14:40)				
12/07/22	24.3 (4:10)	30.4 (15:10)	38.0 (15:50)	76.0 (23:10)	1019.9 (3:40)	1021.9 (11:50)	7.6 (12:30)	909.0 (13:10)				
13/07/22	23.7 (4:40)	31.7 (15:50)	31.0 (13:50)	78.0 (0:10)	1020.5 (18:10)	1022.6 (11:40)	10.3 (15:10)	937.0 (13:30)				
14/07/22	23.9 (5:20)	31.4 (17:10)	25.0 (10:30)	59.0 (23:40)	1017.9 (19:20)	1022.6 (0:00)	8.0 (14:00)	912.0 (13:10)				
15/07/22	24.6 (5:50)	29.2 (18:10)	42.0 (8:00)	87.0 (23:30)	1015.6 (19:10)	1018.0 (0:00)	8.5 (13:40)	905.0 (13:00)				
16/07/22	24.5 (6:30)	32.2 (18:50)	49.0 (22:20)	89.0 (2:10)	1016.9 (0:00)	1018.4 (23:30)	7.2 (12:10)	902.0 (13:10)				
17/07/22	25.2 (3:10)	34.2 (16:40)	56.0 (16:30)	90.0 (2:30)	1018.5 (0:00)	1019.9 (23:30)	6.7 (14:10)	877.0 (13:10)				
18/07/22	26.6 (5:40)	34.2 (13:10)	36.0 (12:30)	74.0 (0:00)	1018.5 (18:40)	1019.9 (11:30)	6.7 (16:00)	879.0 (14:40)				
19/07/22	27.8 (5:50)	34.6 (14:50)	22.0 (10:30)	55.0 (19:10)	1017.4 (18:10)	1019.4 (7:50)	7.6 (19:30)	905.0 (13:00)				
20/07/22	27.4 (22:30)	34.1 (18:10)	23.0 (12:10)	80.0 (21:50)	1017.9 (17:40)	1019.8 (0:50)	6.7 (12:20)	905.0 (13:20)				
21/07/22	25.9 (5:40)	33.1 (16:20)	41.0 (18:00)	74.0 (10:30)	1017.0 (18:30)	1019.0 (8:20)	8.0 (11:30)	895.0 (13:10)				
22/07/22	26.5 (6:40)	31.8 (19:40)	63.0 (0:00)	84.0 (4:30)	1017.3 (19:20)	1018.7 (10:40)	7.2 (12:30)	865.0 (13:20)				
23/07/22	26.7 (5:30)	32.9 (16:40)	46.0 (17:00)	90.0 (5:00)	1017.4 (17:50)	1019.2 (10:50)	7.6 (12:40)	867.0 (13:30)				
24/07/22	26.8 (4:30)	32.3 (16:30)	52.0 (16:40)	87.0 (4:00)	1016.4 (18:50)	1018.9 (10:50)	8.0 (11:40)	902.0 (13:00)				
25/07/22	26.6 (6:00)	30.9 (13:50)	65.0 (18:10)	86.0 (4:50)	1013.7 (20:00)	1017.6 (0:00)	7.6 (11:30)	877.0 (13:20)				
26/07/22	26.7 (5:40)	31.1 (17:40)	61.0 (21:50)	86.0 (0:50)	1011.7 (18:40)	1014.6 (2:00)	8.9 (13:10)	1007.0 (12:30)				
27/07/22	26.6 (5:40)	32.2 (17:20)	48.0 (17:30)	81.0 (3:40)	1009.9 (16:50)	1012.7 (0:00)	7.6 (12:10)	872.0 (13:10)				
28/07/22	26.3 (6:20)	32.3 (15:10)	53.0 (18:00)	81.0 (2:40)	1011.2 (0:40)	1015.7 (23:00)	8.0 (16:50)	865.0 (13:10)				
29/07/22	26.0 (6:00)	32.1 (15:20)	48.0 (15:10)	79.0 (5:40)	1015.0 (17:40)	1016.8 (10:50)	8.0 (12:30)	884.0 (13:20)				
30/07/22	25.8 (5:20)	30.3 (14:30)	70.0 (13:20)	79.0 (4:50)	1014.4 (19:40)	1016.6 (0:00)	8.9 (13:40)	926.0 (12:30)				
31/07/22	26.1 (6:30)	33.3 (14:00)	29.0 (23:10)	80.0 (3:10)	1013.3 (18:20)	1016.2 (0:00)	8.9 (14:40)	969.0 (12:20)				



AGOSTO 2022

(medie giornaliere)

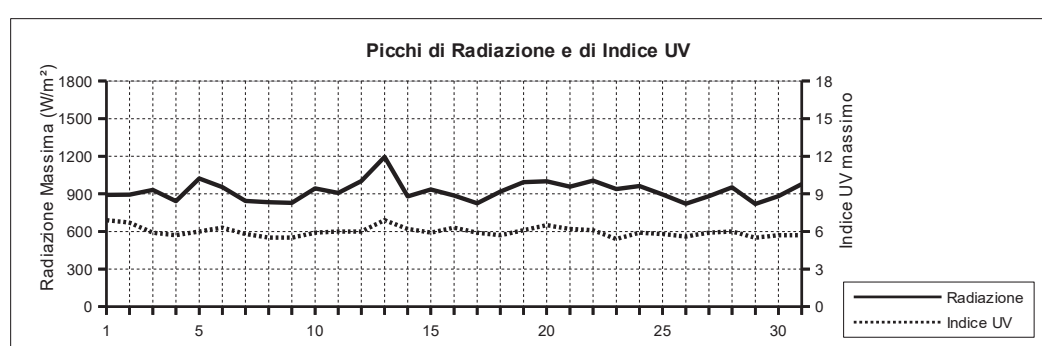
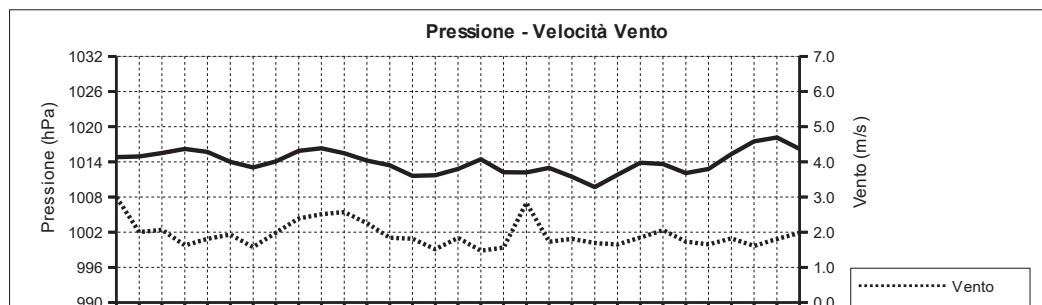
Data	Temperatura °C	Umidità %	Pressione hPa	Vento m/s direzione	Rad. Solare W/m² durata	Pioggia mm	Indice UV medio	Indice UV max (ore)
01/08/22	30.5	33.9	1014.8	3.0 N	502.4 14:30	0.0	3.9	6.9 (13:10)
02/08/22	30.7	38.0	1014.9	2.0 NW	484.5 14:20	0.0	3.6	6.7 (13:00)
03/08/22	30.9	39.0	1015.5	2.1 --	482.9 14:20	0.0	3.4	5.9 (13:10)
04/08/22	29.6	57.0	1016.2	1.6 SE	482.0 14:10	0.0	3.3	5.7 (12:50)
05/08/22	29.1	68.5	1015.7	1.8 SW	437.4 14:10	0.0	3.6	6.0 (13:10)
06/08/22	29.1	72.3	1014.0	1.9 SE	438.6 14:10	0.0	3.3	6.3 (13:10)
07/08/22	29.8	68.4	1013.1	1.6 SE	461.1 14:10	0.0	3.3	5.8 (12:30)
08/08/22	30.5	52.0	1014.1	2.0 N	464.2 14:20	0.0	3.2	5.5 (12:50)
09/08/22	28.1	55.6	1015.9	2.4 N	412.3 14:00	0.0	3.6	5.5 (12:30)
10/08/22	27.6	56.3	1016.3	2.5 N	449.7 14:00	1.2	3.3	5.9 (13:40)
11/08/22	27.5	56.4	1015.5	2.6 --	474.9 14:20	5.2	3.2	6.0 (12:40)
12/08/22	24.8	67.6	1014.2	2.3 --	401.1 13:30	6.4	3.2	6.0 (13:10)
13/08/22	24.5	66.1	1013.4	1.8 --	387.2 14:00	0.0	2.8	6.9 (13:10)
14/08/22	25.9	55.5	1011.6	1.8 NW	502.0 13:50	0.0	3.4	6.2 (13:20)
15/08/22	26.7	65.9	1011.7	1.5 --	460.7 13:50	0.0	3.4	5.9 (13:00)
16/08/22	26.8	75.7	1012.8	1.8 S	432.0 13:50	19.4	3.4	6.3 (13:10)
17/08/22	28.6	76.3	1014.4	1.5 SE	456.7 13:50	0.0	3.4	5.9 (12:40)
18/08/22	31.1	55.5	1012.2	1.6 S	423.1 13:20	0.0	2.8	5.7 (13:30)
19/08/22	27.8	67.5	1012.2	2.8 NW	391.7 13:00	5.8	3.0	6.1 (12:50)
20/08/22	25.9	69.5	1013.0	1.7 NW	464.7 13:50	0.4	3.3	6.5 (12:50)
21/08/22	27.2	70.4	1011.5	1.8 SE	473.8 13:40	0.0	3.4	6.2 (12:50)
22/08/22	26.7	59.0	1009.7	1.7 NE	463.7 13:50	1.6	3.5	6.1 (13:00)
23/08/22	24.9	64.2	1011.8	1.7 NE	264.8 13:30	19.4	2.0	5.4 (12:00)
24/08/22	26.1	61.6	1013.9	1.8 NW	496.4 13:30	0.0	3.4	5.9 (12:40)
25/08/22	26.9	57.9	1013.6	2.1 NW	468.9 13:30	0.0	3.4	5.8 (12:50)
26/08/22	27.1	67.6	1012.1	1.7 --	472.2 13:40	0.0	3.3	5.6 (12:50)
27/08/22	26.9	73.8	1012.8	1.7 SE	475.5 13:20	0.0	3.4	5.9 (12:40)
28/08/22	25.7	74.5	1015.3	1.8 NE	417.9 13:30	0.6	3.1	6.0 (13:30)
29/08/22	25.6	63.7	1017.5	1.6 NE	466.2 13:30	0.0	3.2	5.5 (13:10)
30/08/22	26.8	68.4	1018.2	1.8 NW	466.4 13:30	0.0	3.2	5.7 (13:10)
31/08/22	26.9	77.2	1016.2	2.0 SW	468.9 13:00	0.0	3.3	5.7 (12:20)



AGOSTO 2022

(estremi giornalieri)

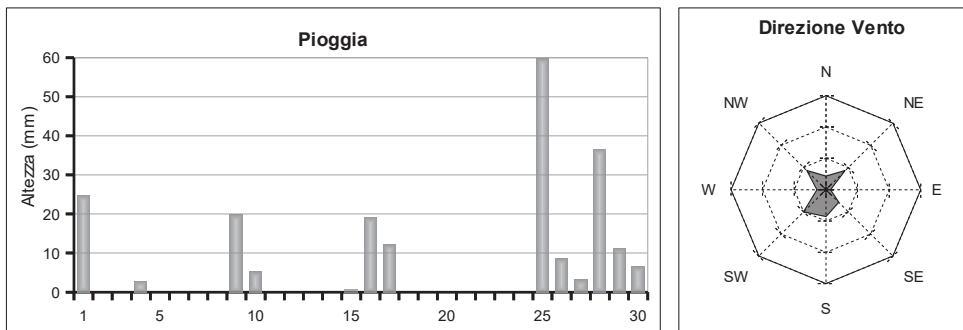
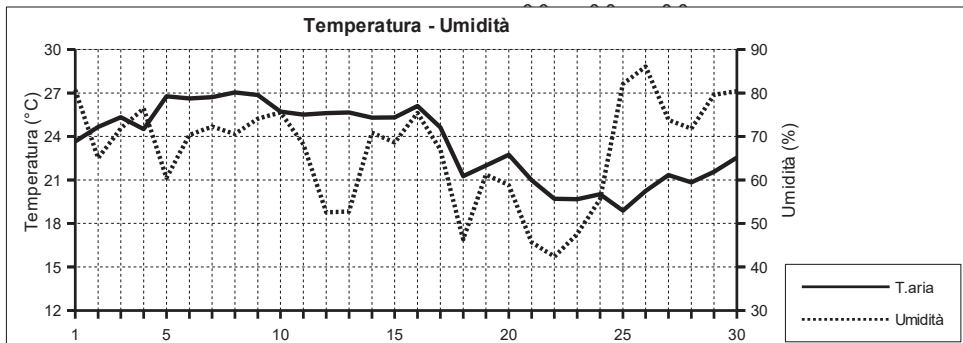
Data	Temperatura (°C)			Umidità (%)			Pressione (hPa)			Vento (m/s)		Radiazione (W/m²)				
	min (ore)	max (ore)	min (ore)	max (ore)	min (ore)	max (ore)	min (ore)	max (ore)	max (ore)	max (ore)	max (ore)					
01/08/22	27.1	(6:00)	35.3	(15:30)	25.0	(15:30)	48.0	(21:40)	1013.2	(17:20)	1015.8	(8:50)	11.2	(12:00)	891.0	(13:10)
02/08/22	26.7	(6:10)	35.0	(13:20)	28.0	(13:00)	52.0	(22:10)	1013.6	(16:10)	1015.7	(22:10)	8.5	(17:00)	893.0	(13:00)
03/08/22	27.8	(6:20)	34.3	(16:00)	31.0	(15:20)	55.0	(23:50)	1014.5	(16:50)	1016.5	(10:40)	7.6	(14:40)	932.0	(13:50)
04/08/22	26.6	(6:00)	33.1	(17:00)	43.0	(18:10)	72.0	(22:30)	1015.1	(17:20)	1017.1	(11:10)	8.5	(16:30)	842.0	(13:20)
05/08/22	26.6	(6:30)	33.1	(14:50)	41.0	(15:00)	87.0	(6:50)	1014.5	(19:50)	1016.7	(11:30)	9.4	(13:30)	1023.0	(14:30)
06/08/22	26.7	(5:40)	32.3	(14:30)	51.0	(17:50)	87.0	(5:40)	1012.7	(18:30)	1015.1	(00:00)	8.5	(13:20)	954.0	(14:50)
07/08/22	26.7	(5:10)	34.8	(15:50)	48.0	(16:30)	81.0	(4:40)	1011.4	(16:00)	1014.0	(0:10)	8.0	(17:10)	844.0	(12:50)
08/08/22	27.6	(5:20)	34.3	(16:20)	42.0	(22:00)	64.0	(0:00)	1012.7	(16:10)	1016.0	(21:50)	8.9	(18:00)	833.0	(12:50)
09/08/22	23.8	(17:50)	32.1	(15:30)	46.0	(14:00)	74.0	(17:50)	1014.6	(15:30)	1017.2	(18:30)	12.5	(17:10)	828.0	(13:00)
10/08/22	23.3	(20:30)	32.9	(15:20)	42.0	(13:50)	76.0	(20:00)	1014.8	(16:20)	1017.5	(19:40)	9.8	(18:40)	944.0	(14:00)
11/08/22	22.6	(22:50)	31.7	(16:20)	44.0	(13:50)	77.0	(23:10)	1013.7	(17:00)	1016.6	(0:40)	11.6	(21:20)	907.0	(12:40)
12/08/22	20.1	(19:40)	29.2	(16:00)	54.0	(9:10)	84.0	(19:30)	1013.1	(17:40)	1015.7	(19:40)	10.7	(17:20)	1002.0	(14:30)
13/08/22	20.6	(5:50)	27.8	(15:00)	55.0	(21:30)	74.0	(4:30)	1011.9	(18:00)	1014.9	(0:00)	7.6	(15:30)	1194.0	(13:10)
14/08/22	22.3	(3:50)	29.4	(18:30)	46.0	(10:40)	65.0	(3:50)	1010.3	(18:40)	1013.4	(0:00)	7.2	(15:20)	879.0	(13:20)
15/08/22	24.2	(6:20)	29.1	(16:30)	56.0	(9:00)	73.0	(19:40)	1010.6	(19:50)	1012.9	(14:10)	8.0	(13:10)	935.0	(14:20)
16/08/22	19.1	(3:20)	30.7	(15:10)	59.0	(11:50)	92.0	(4:10)	1010.6	(6:30)	1014.7	(3:10)	17.0	(3:20)	886.0	(12:20)
17/08/22	26.0	(5:30)	30.9	(16:30)	60.0	(22:20)	89.0	(0:40)	1013.0	(20:50)	1015.5	(12:00)	6.7	(12:00)	824.0	(13:20)
18/08/22	26.3	(7:00)	35.5	(14:30)	33.0	(17:10)	79.0	(3:40)	1010.0	(23:40)	1014.2	(1:30)	8.9	(16:00)	918.0	(13:30)
19/08/22	21.9	(23:30)	31.3	(0:20)	51.0	(0:10)	85.0	(4:30)	1009.5	(3:20)	1014.0	(21:50)	10.7	(22:50)	993.0	(13:00)
20/08/22	22.3	(0:00)	28.9	(15:50)	55.0	(13:50)	84.0	(4:00)	1012.3	(4:10)	1013.8	(0:10)	8.5	(13:20)	1000.0	(12:50)
21/08/22	24.4	(6:30)	30.7	(15:30)	51.0	(16:20)	79.0	(6:00)	1009.8	(18:10)	1013.4	(0:00)	8.9	(16:30)	958.0	(13:00)
22/08/22	23.3	(17:10)	29.8	(14:10)	42.0	(9:50)	73.0	(0:00)	1008.5	(15:50)	1010.6	(22:20)	12.1	(16:30)	1005.0	(13:50)
23/08/22	20.5	(15:30)	28.9	(10:00)	44.0	(10:10)	79.0	(15:30)	1010.0	(3:40)	1014.5	(21:20)	12.5	(15:20)	939.0	(12:00)
24/08/22	22.4	(6:00)	30.1	(17:00)	48.0	(13:40)	77.0	(0:00)	1013.0	(15:50)	1015.4	(23:50)	6.7	(14:50)	962.0	(12:40)
25/08/22	23.8	(6:30)	30.7	(15:30)	47.0	(11:10)	68.0	(23:10)	1012.0	(18:20)	1015.4	(0:00)	7.2	(14:20)	895.0	(13:40)
26/08/22	24.0	(5:20)	29.7	(15:10)	59.0	(10:00)	81.0	(4:30)	1010.8	(17:10)	1013.4	(0:00)	7.6	(15:10)	821.0	(12:50)
27/08/22	24.4	(5:40)	29.2	(17:00)	64.0	(16:40)	82.0	(3:20)	1011.7	(4:20)	1014.7	(23:30)	8.5	(15:00)	882.0	(12:30)
28/08/22	22.6	(23:50)	28.7	(14:10)	58.0	(16:10)	83.0	(5:50)	1014.1	(4:50)	1016.6	(17:20)	10.7	(17:00)	953.0	(14:10)
29/08/22	21.4	(6:00)	29.9	(15:10)	48.0	(17:20)	76.0	(6:00)	1016.6	(15:00)	1018.4	(2:40)	8.9	(17:30)	819.0	(13:20)
30/08/22	22.9	(4:40)	30.3	(15:10)	59.0	(15:10)	81.0	(23:20)	1016.7	(17:10)	1019.4	(11:00)	8.5	(15:40)	882.0	(13:20)
31/08/22	25.4	(6:10)	29.2	(14:50)	65.0	(18:10)	84.0	(1:40)	1014.9	(23:10)	1017.5	(0:00)	8.9	(13:20)	977.0	(12:30)



SETTEMBRE 2022

(medie giornaliere)

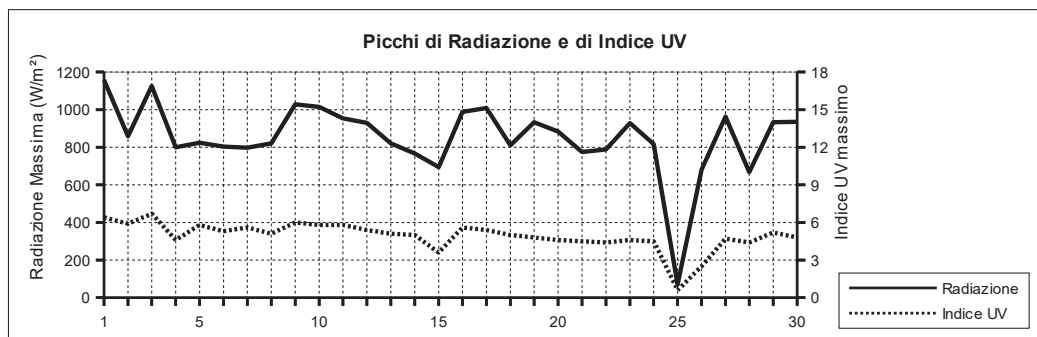
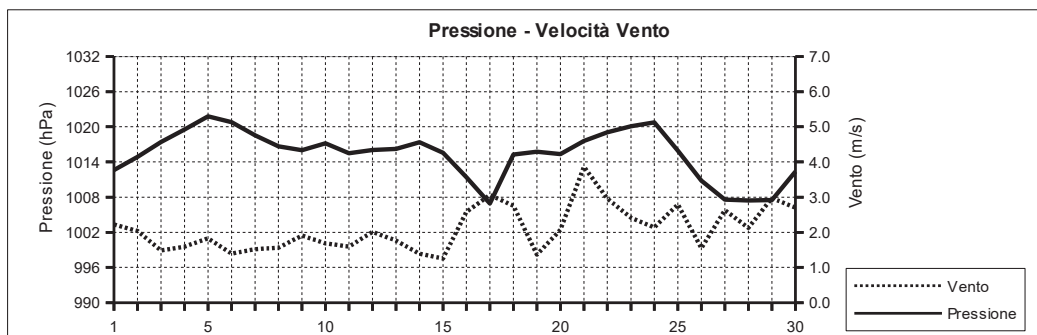
Data	Temperatura aria (°C)	Umidità %	Pressione hPa	Vento		Rad. Solare W/m²	Pioggia mm	Indice UV		
				m/s	direzione			medio	max (ore)	
01/09/22	23.7	80.7	1012.6	2.2	NW	242.4	13:00	24.6	2.5	6.4 (13:50)
02/09/22	24.7	65.0	1014.9	2.0	NW	484.6	13:10	0.0	3.4	5.9 (13:10)
03/09/22	25.3	71.9	1017.4	1.5	--	435.5	13:10	0.0	3.2	6.7 (13:30)
04/09/22	24.5	76.4	1019.5	1.6	N	178.5	12:30	2.8	1.4	4.6 (14:50)
05/09/22	26.8	60.5	1021.8	1.8	NW	478.2	13:00	0.0	3.4	5.8 (13:20)
06/09/22	26.6	70.4	1020.8	1.4	--	445.8	13:00	0.0	3.1	5.3 (13:00)
07/09/22	26.7	72.3	1018.5	1.5	S	446.8	12:40	0.0	3.3	5.6 (13:00)
08/09/22	27.0	70.6	1016.7	1.6	S	388.2	12:50	0.0	2.9	5.1 (13:00)
09/09/22	26.9	74.1	1016.0	1.9	SW	418.1	12:30	19.8	3.4	6.0 (13:10)
10/09/22	25.7	75.5	1017.2	1.7	SW	335.7	12:50	5.2	3.0	5.8 (12:50)
11/09/22	25.5	68.2	1015.5	1.6	SW	414.7	12:50	0.0	2.8	5.8 (13:10)
12/09/22	25.6	52.6	1016.0	2.0	N	471.1	12:50	0.0	3.1	5.4 (13:40)
13/09/22	25.7	52.8	1016.2	1.8	NW	468.6	12:40	0.0	3.0	5.1 (13:10)
14/09/22	25.3	70.9	1017.4	1.4	S	430.7	12:40	0.0	2.9	5.0 (12:30)
15/09/22	25.3	68.6	1015.6	1.3	NE	238.7	12:30	0.4	1.6	3.6 (14:40)
16/09/22	26.1	75.4	1011.4	2.6	S	274.0	11:20	19.2	2.1	5.6 (13:10)
17/09/22	24.6	67.0	1006.9	3.1	W	388.2	12:30	12.2	2.7	5.4 (12:40)
18/09/22	21.3	46.3	1015.3	2.8	NE	468.3	12:30	0.0	3.0	5.0 (12:40)
19/09/22	22.0	61.2	1015.7	1.4	--	403.6	12:20	0.0	2.6	4.8 (12:50)
20/09/22	22.7	58.8	1015.3	2.1	NW	443.9	12:20	0.0	2.5	4.6 (13:00)
21/09/22	21.0	45.7	1017.6	3.9	NE	440.6	12:10	0.0	2.7	4.5 (13:00)
22/09/22	19.7	42.4	1019.0	3.0	NE	448.9	12:20	0.0	2.6	4.4 (12:30)
23/09/22	19.7	47.6	1020.1	2.4	NE	419.2	12:20	0.0	2.5	4.6 (13:20)
24/09/22	20.0	55.6	1020.7	2.1	SE	423.0	12:10	0.0	2.6	4.5 (13:20)
25/09/22	18.9	82.1	1015.9	2.8	SE	17.4	11:30	94.0	0.5	0.6 (14:20)
26/09/22	20.2	86.1	1010.8	1.5	SE	124.1	11:30	8.6	1.1	2.5 (15:50)
27/09/22	21.3	73.8	1007.6	2.6	SW	350.6	11:50	3.2	2.2	4.7 (13:20)
28/09/22	20.8	71.8	1007.4	2.1	SW	221.7	11:50	36.6	1.8	4.4 (12:00)
29/09/22	21.6	79.6	1007.5	3.0	SW	285.5	11:40	11.0	1.9	5.2 (13:10)
30/09/22	22.5	80.4	1012.4	2.7	S	238.1	11:50	6.6	2.1	4.8 (13:10)



SETTEMBRE 2022

(estremi giornalieri)

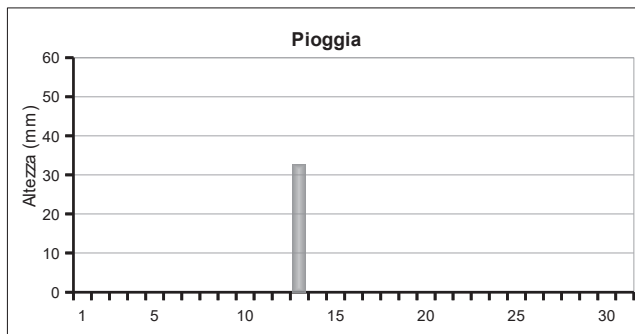
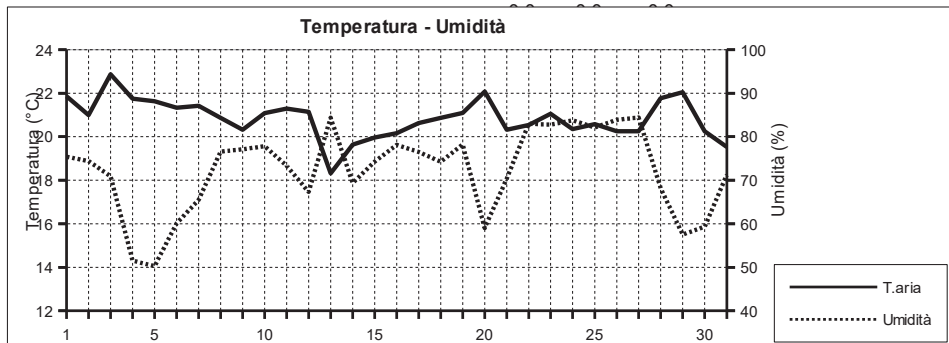
Data	Temperatura (°C)			Umidità (%)			Pressione (hPa)			Vento (m/s)		Radiazione (W/m²)
	min (ore)	max (ore)	min (ore)	max (ore)	min (ore)	max (ore)	min (ore)	max (ore)	max (ore)	max (ore)	max (ore)	
01/09/22	21.3 (6:40)	26.6 (16:20)	68.0 (18:40)	91.0 (5:00)	1011.2 (16:00)	1015.0 (00:00)	16.5 (4:40)	1158.0 (13:50)				
02/09/22	20.9 (6:20)	28.1 (15:50)	52.0 (10:50)	76.0 (0:10)	1013.5 (5:50)	1016.7 (23:20)	7.2 (14:00)	858.0 (14:10)				
03/09/22	22.5 (4:50)	27.8 (14:30)	63.0 (10:50)	80.0 (20:30)	1016.0 (2:00)	1018.5 (23:50)	7.2 (15:10)	1125.0 (13:30)				
04/09/22	22.7 (8:00)	27.2 (17:00)	62.0 (16:00)	86.0 (14:40)	1017.8 (2:00)	1021.6 (23:10)	9.8 (14:40)	800.0 (14:50)				
05/09/22	22.5 (6:20)	33.2 (16:40)	31.0 (16:30)	77.0 (3:20)	1020.6 (16:20)	1023.5 (11:30)	6.7 (18:20)	824.0 (13:30)				
06/09/22	23.7 (6:00)	29.9 (16:00)	61.0 (16:00)	80.0 (23:40)	1019.3 (19:00)	1022.3 (10:00)	8.5 (16:10)	803.0 (12:10)				
07/09/22	23.8 (7:20)	29.8 (17:10)	48.0 (16:40)	85.0 (23:10)	1017.1 (19:00)	1019.5 (0:50)	6.7 (15:40)	798.0 (12:30)				
08/09/22	24.4 (6:50)	29.6 (13:10)	48.0 (11:10)	85.0 (0:00)	1015.2 (16:40)	1018.1 (0:30)	6.7 (13:30)	821.0 (14:20)				
09/09/22	20.8 (8:40)	29.7 (16:50)	47.0 (17:00)	91.0 (9:00)	1014.3 (6:10)	1017.4 (23:40)	15.2 (8:00)	1028.0 (13:30)				
10/09/22	24.4 (9:00)	27.8 (17:00)	60.0 (16:50)	86.0 (8:50)	1016.2 (19:20)	1018.4 (10:30)	8.5 (13:40)	1014.0 (14:30)				
11/09/22	23.3 (5:50)	27.9 (15:00)	61.0 (15:10)	75.0 (6:20)	1014.0 (18:20)	1017.0 (0:50)	8.5 (13:10)	954.0 (12:50)				
12/09/22	22.3 (6:40)	29.2 (14:20)	38.0 (11:20)	73.0 (0:00)	1015.1 (18:00)	1017.2 (10:50)	6.7 (15:40)	930.0 (13:50)				
13/09/22	22.0 (4:40)	29.4 (15:40)	38.0 (10:00)	70.0 (23:10)	1015.5 (18:10)	1017.2 (23:50)	8.0 (13:30)	821.0 (13:30)				
14/09/22	22.7 (5:50)	27.9 (15:50)	64.0 (17:00)	79.0 (6:50)	1016.5 (6:10)	1018.5 (12:10)	7.2 (11:50)	766.0 (12:40)				
15/09/22	22.3 (7:00)	28.4 (16:20)	47.0 (16:20)	85.0 (20:40)	1013.0 (18:30)	1018.2 (10:40)	7.6 (11:50)	694.0 (14:50)				
16/09/22	22.3 (7:30)	28.2 (13:40)	61.0 (18:50)	90.0 (8:50)	1008.7 (23:50)	1014.2 (0:00)	19.2 (7:00)	988.0 (13:10)				
17/09/22	20.4 (23:50)	26.7 (12:50)	46.0 (17:30)	88.0 (3:00)	1005.6 (15:10)	1010.0 (23:40)	12.5 (3:40)	1009.0 (12:40)				
18/09/22	17.7 (6:50)	25.7 (15:30)	27.0 (14:30)	64.0 (0:00)	1010.1 (0:00)	1017.2 (21:10)	11.2 (2:30)	810.0 (12:50)				
19/09/22	18.4 (6:50)	24.7 (14:50)	51.0 (14:50)	74.0 (7:00)	1014.6 (19:10)	1017.0 (0:10)	7.2 (14:10)	933.0 (12:00)				
20/09/22	19.3 (6:40)	26.6 (14:50)	48.0 (11:40)	67.0 (3:10)	1014.2 (16:40)	1016.3 (23:40)	6.7 (14:00)	884.0 (12:20)				
21/09/22	18.3 (23:10)	24.9 (14:00)	33.0 (14:20)	58.0 (3:20)	1016.1 (4:00)	1020.2 (23:20)	11.2 (16:50)	775.0 (12:50)				
22/09/22	16.8 (6:00)	23.4 (16:00)	30.0 (16:50)	53.0 (6:50)	1017.4 (16:40)	1020.1 (0:00)	9.8 (0:40)	788.0 (14:10)				
23/09/22	16.2 (7:10)	23.3 (14:40)	35.0 (14:20)	57.0 (23:00)	1019.1 (4:10)	1021.4 (22:50)	11.2 (11:30)	928.0 (14:00)				
24/09/22	16.0 (5:40)	23.0 (13:40)	42.0 (14:00)	68.0 (5:20)	1019.2 (18:40)	1022.3 (11:10)	8.5 (15:00)	817.0 (13:30)				
25/09/22	17.1 (11:50)	23.1 (8:30)	57.0 (0:00)	94.0 (10:30)	1013.0 (8:20)	1019.2 (0:00)	20.1 (7:00)	70.0 (17:30)				
26/09/22	18.0 (0:30)	21.4 (3:20)	78.0 (18:10)	93.0 (0:50)	1008.5 (16:00)	1014.0 (0:00)	10.7 (1:50)	680.0 (15:50)				
27/09/22	19.1 (2:50)	23.5 (13:40)	59.0 (13:40)	93.0 (4:00)	1006.8 (22:20)	1009.2 (0:00)	13.4 (13:40)	963.0 (12:10)				
28/09/22	18.7 (22:30)	22.3 (12:40)	61.0 (10:00)	89.0 (22:40)	1006.7 (17:00)	1008.0 (10:50)	14.3 (20:50)	668.0 (9:50)				
29/09/22	19.4 (21:10)	23.1 (14:00)	69.0 (9:40)	89.0 (21:40)	1006.6 (4:00)	1008.5 (23:50)	16.1 (16:00)	933.0 (14:50)				
30/09/22	17.4 (12:40)	24.7 (16:00)	66.0 (15:20)	91.0 (12:50)	1008.7 (0:00)	1015.8 (23:50)	13.4 (11:30)	935.0 (13:10)				



OTTOBRE 2022

(medie giornaliere)

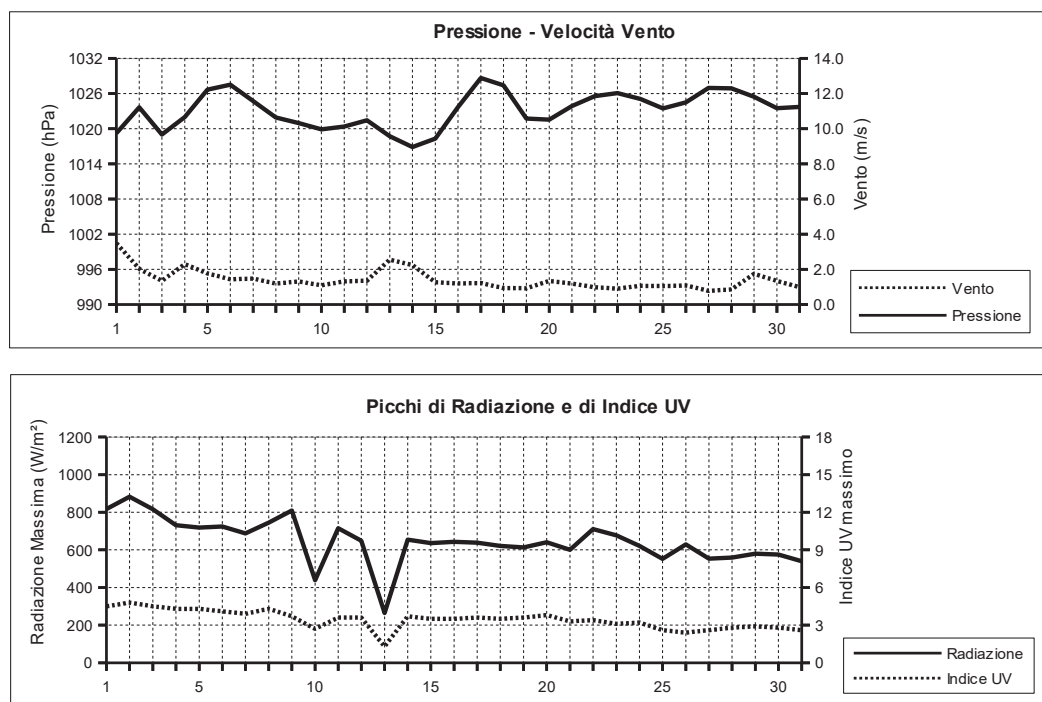
Data	Temperatura	Umidità	Pressione	Vento	Rad. Solare	Pioggia	Indice UV		
	°C	%	hPa	m/s direzione	W/m² durata	mm	medio	max	(ore)
01/10/22	21.9	75.4	1019.2	3.5 NW	314.4 11:40	0.0	2.2	4.5	(12:10)
02/10/22	21.0	74.4	1023.7	2.0 SW	344.8 11:50	0.0	2.6	4.8	(12:50)
03/10/22	22.9	70.9	1019.0	1.3 SE	388.1 11:50	0.0	2.5	4.5	(12:30)
04/10/22	21.8	51.5	1022.0	2.3 N	428.6 11:50	0.0	2.6	4.3	(12:40)
05/10/22	21.6	50.3	1026.7	1.8 NE	417.8 11:40	0.0	2.6	4.3	(12:30)
06/10/22	21.3	60.1	1027.5	1.4 NE	395.1 11:50	0.0	2.5	4.1	(12:50)
07/10/22	21.4	65.5	1024.7	1.5 --	314.4 11:40	0.0	2.2	3.9	(12:30)
08/10/22	20.9	76.6	1021.9	1.2 --	398.0 11:30	0.0	2.5	4.3	(13:10)
09/10/22	20.3	77.1	1021.0	1.3 --	293.3 11:20	0.0	2.2	3.7	(11:20)
10/10/22	21.1	77.8	1019.9	1.1 NE	227.6 11:20	0.0	1.5	2.7	(12:30)
11/10/22	21.3	73.3	1020.4	1.3 NE	368.8 11:30	0.0	2.2	3.6	(12:10)
12/10/22	21.1	67.3	1021.5	1.4 --	351.0 11:10	0.0	2.3	3.6	(12:20)
13/10/22	18.3	84.4	1018.7	2.6 N	65.9 9:50	32.6	0.9	1.3	(10:20)
14/10/22	19.6	69.4	1016.9	2.2 NW	378.1 11:20	0.0	2.3	3.7	(12:40)
15/10/22	20.0	74.3	1018.3	1.3 N	379.1 11:10	0.0	2.2	3.5	(12:20)
16/10/22	20.2	78.1	1023.7	1.2 NE	362.7 11:20	0.0	2.2	3.5	(12:20)
17/10/22	20.6	76.5	1028.7	1.2 --	366.5 11:10	0.0	2.3	3.6	(12:10)
18/10/22	20.9	74.2	1027.4	0.9 NE	358.2 11:10	0.0	2.2	3.5	(12:10)
19/10/22	21.1	78.2	1021.7	0.9 NE	342.0 11:10	0.0	2.1	3.6	(13:00)
20/10/22	22.1	59.0	1021.5	1.3 N	368.1 11:10	0.0	2.3	3.8	(12:50)
21/10/22	20.3	70.3	1023.9	1.2 --	300.6 11:10	0.0	2.1	3.3	(12:40)
22/10/22	20.5	83.0	1025.6	1.0 --	295.4 10:50	0.0	2.0	3.4	(12:20)
23/10/22	21.1	82.8	1026.1	0.9 NE	299.2 10:50	0.0	1.8	3.1	(13:00)
24/10/22	20.3	83.8	1025.1	1.1 --	345.9 10:50	0.0	2.0	3.2	(13:00)
25/10/22	20.6	82.1	1023.5	1.0 --	308.6 10:50	0.0	1.7	2.6	(13:10)
26/10/22	20.2	83.9	1024.5	1.1 NE	300.6 10:40	0.0	1.6	2.4	(12:20)
27/10/22	20.3	84.4	1026.9	0.8 NE	304.8 10:30	0.0	1.7	2.6	(12:40)
28/10/22	21.8	68.1	1026.9	0.9 NE	322.7 10:40	0.0	1.9	2.8	(12:00)
29/10/22	22.0	57.5	1025.5	1.7 N	337.6 10:40	0.0	2.0	2.9	(12:20)
30/10/22	20.3	59.3	1023.5	1.3 NE	336.2 10:40	0.0	1.9	2.8	(11:20)
31/10/22	19.5	71.2	1023.7	1.0 NE	316.4 10:30	0.0	1.8	2.6	(11:40)



OTTOBRE 2022

(estremi giornalieri)

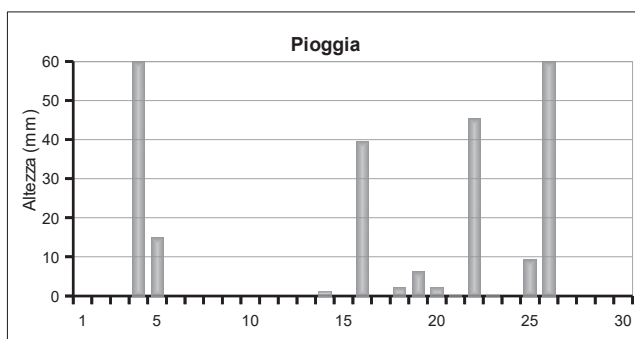
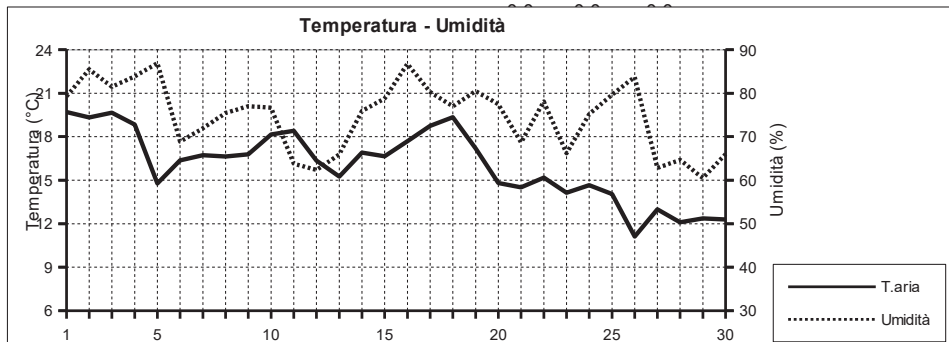
Data	Temperatura (°C)			Umidità (%)			Pressione (hPa)			Vento (m/s)		Radiazione (W/m²)
	min (ore)	max (ore)	min (ore)	max (ore)	min (ore)	max (ore)	min (ore)	max (ore)	max (ore)	max (ore)	max (ore)	
01/10/22	19.7 (22:40)	23.6 (10:00)	58.0 (16:20)	91.0 (6:30)	1015.7 (00:00)	1022.7 (23:50)	11.6 (16:40)	817.0 (14:40)				
02/10/22	18.0 (6:10)	23.2 (14:50)	66.0 (2:10)	82.0 (20:30)	1021.3 (23:50)	1025.5 (10:40)	7.6 (14:40)	882.0 (14:40)				
03/10/22	19.8 (7:10)	26.9 (14:50)	53.0 (16:40)	86.0 (7:00)	1017.6 (15:20)	1021.3 (0:10)	7.6 (2:50)	816.0 (11:30)				
04/10/22	18.3 (6:40)	25.7 (16:20)	36.0 (15:00)	68.0 (5:00)	1019.9 (00:00)	1025.7 (23:30)	8.5 (13:00)	731.0 (12:50)				
05/10/22	17.7 (7:30)	26.4 (16:10)	36.0 (12:00)	73.0 (23:20)	1025.7 (00:00)	1028.3 (22:40)	7.6 (13:10)	719.0 (12:40)				
06/10/22	17.6 (6:30)	24.8 (11:50)	38.0 (13:00)	76.0 (0:40)	1026.5 (17:00)	1028.3 (00:00)	6.3 (13:50)	724.0 (13:20)				
07/10/22	18.9 (6:00)	23.7 (15:30)	54.0 (11:20)	76.0 (22:10)	1022.7 (17:50)	1027.6 (00:00)	5.4 (12:50)	687.0 (11:50)				
08/10/22	18.4 (7:00)	23.3 (13:30)	64.0 (15:50)	86.0 (5:50)	1020.9 (17:10)	1023.2 (00:00)	6.7 (16:30)	745.0 (13:10)				
09/10/22	17.9 (6:20)	23.1 (11:30)	63.0 (11:30)	85.0 (6:30)	1019.7 (17:20)	1022.1 (9:30)	5.8 (12:00)	809.0 (11:10)				
10/10/22	19.3 (4:50)	24.1 (16:50)	67.0 (17:30)	84.0 (3:50)	1018.9 (16:20)	1020.8 (00:00)	4.9 (13:20)	438.0 (12:30)				
11/10/22	18.0 (7:30)	26.0 (13:40)	52.0 (13:40)	87.0 (4:40)	1019.3 (4:30)	1021.7 (23:00)	6.7 (15:20)	715.0 (13:20)				
12/10/22	18.2 (6:20)	23.9 (13:20)	53.0 (14:00)	75.0 (1:10)	1020.5 (18:30)	1022.4 (10:10)	5.4 (13:50)	649.0 (13:00)				
13/10/22	16.8 (15:50)	21.1 (00:00)	72.0 (0:30)	93.0 (16:30)	1016.3 (20:50)	1021.6 (00:00)	10.3 (19:40)	264.0 (10:20)				
14/10/22	16.7 (6:30)	23.4 (14:00)	50.0 (13:30)	82.0 (22:40)	1015.7 (16:00)	1017.8 (22:10)	9.4 (1:40)	654.0 (12:40)				
15/10/22	16.7 (7:10)	23.5 (14:50)	61.0 (11:40)	85.0 (23:50)	1016.6 (4:10)	1021.5 (23:40)	6.3 (13:50)	636.0 (12:20)				
16/10/22	16.7 (7:40)	24.7 (16:10)	64.0 (10:50)	88.0 (3:50)	1021.6 (00:00)	1026.8 (23:10)	5.8 (14:10)	643.0 (13:10)				
17/10/22	16.9 (6:50)	24.6 (15:40)	54.0 (12:10)	87.0 (0:30)	1026.7 (0:10)	1030.3 (22:00)	5.4 (14:50)	638.0 (12:30)				
18/10/22	17.3 (6:30)	25.4 (16:30)	57.0 (11:10)	87.0 (1:10)	1024.6 (23:50)	1029.9 (00:00)	6.3 (13:50)	621.0 (12:20)				
19/10/22	17.9 (7:30)	25.4 (16:30)	66.0 (14:00)	87.0 (4:40)	1019.8 (16:50)	1024.6 (00:00)	4.5 (12:40)	613.0 (13:00)				
20/10/22	17.9 (7:00)	26.4 (13:40)	34.0 (16:10)	78.0 (0:00)	1020.6 (3:50)	1023.2 (23:30)	5.4 (15:30)	640.0 (12:30)				
21/10/22	17.3 (6:50)	23.1 (13:00)	54.0 (10:40)	84.0 (21:50)	1022.8 (3:50)	1025.4 (23:40)	6.7 (14:00)	601.0 (13:20)				
22/10/22	18.3 (7:40)	23.1 (14:40)	75.0 (12:20)	88.0 (21:50)	1024.5 (5:00)	1026.9 (12:10)	5.8 (15:30)	710.0 (12:30)				
23/10/22	18.6 (6:00)	24.2 (14:30)	74.0 (14:00)	90.0 (5:00)	1025.0 (17:50)	1027.4 (11:30)	4.9 (14:30)	677.0 (13:10)				
24/10/22	17.2 (7:40)	23.8 (14:30)	65.0 (13:20)	92.0 (6:30)	1023.9 (16:40)	1026.2 (10:50)	4.9 (13:40)	621.0 (13:00)				
25/10/22	18.4 (6:10)	23.4 (15:30)	73.0 (10:30)	90.0 (2:20)	1022.2 (17:50)	1024.7 (0:40)	4.9 (14:50)	552.0 (13:20)				
26/10/22	18.2 (5:50)	24.1 (16:10)	72.0 (16:10)	91.0 (7:00)	1023.2 (4:30)	1026.4 (22:20)	4.5 (11:50)	629.0 (11:50)				
27/10/22	17.2 (5:30)	23.4 (13:20)	66.0 (13:30)	92.0 (5:50)	1026.2 (1:20)	1028.0 (11:20)	4.5 (14:10)	554.0 (12:50)				
28/10/22	17.7 (7:20)	26.4 (15:10)	51.0 (15:20)	82.0 (0:00)	1025.8 (15:30)	1027.8 (10:20)	4.0 (13:10)	559.0 (12:40)				
29/10/22	18.9 (7:50)	27.1 (15:50)	40.0 (16:00)	76.0 (20:10)	1023.9 (16:20)	1027.1 (0:00)	6.7 (6:10)	580.0 (13:00)				
30/10/22	16.4 (6:20)	24.1 (15:30)	45.0 (12:10)	78.0 (22:00)	1022.1 (17:00)	1024.8 (0:10)	5.4 (13:40)	575.0 (11:40)				
31/10/22	16.1 (6:40)	22.8 (13:50)	56.0 (9:50)	78.0 (0:00)	1022.9 (15:00)	1024.7 (9:20)	5.4 (14:10)	540.0 (11:50)				



NOVEMBRE 2022

(medie giornaliere)

Data	Temperatura	Umidità	Pressione	Vento	Rad. Solare	Pioggia	Indice UV		
	°C	%	hPa	m/s direzione	W/m² durata	mm	medio	max (ore)	
01/11/22	19.7	79.3	1025.0	1.1 NE	308.3 10:30	0.0	1.7	2.6	(11:30)
02/11/22	19.3	85.5	1025.1	1.1 NE	262.2 10:30	0.0	1.6	2.3	(11:00)
03/11/22	19.7	81.5	1022.3	1.8 SE	235.2 10:20	0.0	1.4	2.4	(12:00)
04/11/22	18.8	83.9	1011.3	4.0 SE	109.2 8:20	81.4	1.1	2.1	(11:40)
05/11/22	14.8	86.9	1006.1	1.2 N	128.4 10:00	15.0	1.1	2.2	(12:20)
06/11/22	16.4	68.9	1013.8	1.4 N	316.7 10:30	0.0	1.7	2.6	(11:50)
07/11/22	16.7	71.9	1021.2	1.2 NW	310.0 10:30	0.0	1.6	2.5	(11:10)
08/11/22	16.6	75.5	1023.1	1.1 NW	311.8 10:20	0.0	1.5	2.3	(11:00)
09/11/22	16.8	77.0	1023.0	1.1 NW	308.5 10:10	0.0	1.7	2.7	(11:40)
10/11/22	18.1	76.7	1024.8	1.3 NW	202.6 10:10	0.0	1.2	2.4	(11:40)
11/11/22	18.4	63.8	1029.9	2.6 NE	298.3 10:10	0.0	1.5	2.2	(11:20)
12/11/22	16.4	62.4	1026.9	2.1 N	104.9 9:30	0.0	0.9	1.2	(9:40)
13/11/22	15.2	65.9	1022.8	2.0 N	188.0 10:00	0.0	1.1	2.0	(12:40)
14/11/22	16.9	75.9	1021.4	2.5 SW	138.4 10:00	1.0	0.9	2.1	(12:50)
15/11/22	16.7	78.8	1020.1	1.4 --	250.0 9:50	0.0	1.3	2.2	(12:00)
16/11/22	17.7	86.8	1008.9	1.9 SW	67.3 9:50	39.6	0.7	1.3	(13:20)
17/11/22	18.7	80.3	1006.8	1.6 SW	251.4 10:00	0.0	1.4	2.6	(11:40)
18/11/22	19.3	77.0	1006.0	3.3 SW	243.4 9:50	2.2	1.4	2.6	(12:00)
19/11/22	17.2	80.5	1007.3	2.6 SW	61.8 9:00	6.2	0.6	1.2	(11:30)
20/11/22	14.8	77.5	1008.2	1.5 NW	104.4 9:30	2.0	0.9	1.0	(11:40)
21/11/22	14.5	68.7	1012.3	1.7 --	288.5 9:50	0.2	1.4	1.9	(11:30)
22/11/22	15.2	78.1	999.6	6.1 SW	60.7 9:00	45.4	0.6	0.8	(12:20)
23/11/22	14.1	66.2	1005.6	1.5 NW	286.7 9:40	0.2	1.4	1.9	(11:20)
24/11/22	14.7	75.2	1014.8	1.1 NW	263.3 9:50	0.0	1.4	1.9	(11:40)
25/11/22	14.0	79.6	1020.6	1.5 N	151.5 9:20	9.4	1.1	1.9	(11:40)
26/11/22	11.1	83.7	1016.9	4.3 N	11.2 8:40	74.4	0.5	0.6	(12:10)
27/11/22	13.0	62.8	1021.7	3.7 NE	266.7 9:30	0.0	1.4	1.8	(11:50)
28/11/22	12.1	64.7	1018.4	1.6 NW	266.2 9:30	0.0	1.4	1.9	(11:10)
29/11/22	12.4	60.5	1012.7	2.4 N	215.8 9:30	0.0	1.1	1.7	(11:40)
30/11/22	12.3	66.0	1011.4	2.7 NE	99.0 9:40	0.0	1.0	0.8	(10:40)

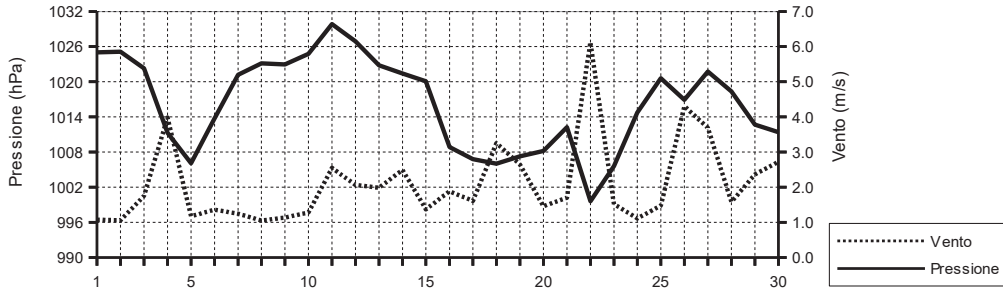


NOVEMBRE 2022

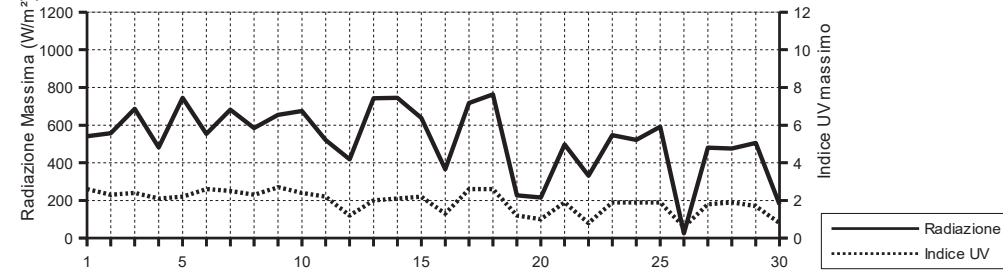
(estremi giornalieri)

Data	Temperatura (°C)			Umidità (%)			Pressione (hPa)			Vento (m/s)		Radiazione (W/m²)
	min (ore)	max (ore)		min (ore)	max (ore)		min (ore)	max (ore)		max (ore)	max (ore)	
01/11/22	16.3 (6:00)	22.8 (14:00)		67.0 (9:40)	88.0 (22:10)		1024.0 (3:20)	1025.9 (22:20)		5.8 (13:00)	541.0 (11:40)	
02/11/22	16.7 (5:50)	22.1 (11:20)		75.0 (11:20)	92.0 (6:50)		1024.0 (15:20)	1026.7 (8:50)		4.9 (12:40)	557.0 (11:20)	
03/11/22	17.6 (4:30)	21.9 (13:10)		73.0 (12:50)	89.0 (3:50)		1018.2 (23:50)	1024.6 (0:00)		6.7 (13:40)	687.0 (11:50)	
04/11/22	14.4 (23:30)	22.8 (11:40)		75.0 (5:40)	94.0 (22:00)		1006.2 (23:40)	1018.1 (0:00)		17.9 (9:00)	482.0 (11:40)	
05/11/22	12.8 (22:50)	16.5 (13:00)		79.0 (14:40)	94.0 (0:00)		1004.1 (6:00)	1009.3 (22:50)		6.3 (15:40)	745.0 (12:40)	
06/11/22	13.1 (2:30)	20.3 (14:20)		53.0 (13:00)	88.0 (2:40)		1008.7 (1:10)	1018.9 (23:30)		8.5 (7:00)	554.0 (11:00)	
07/11/22	13.7 (6:50)	20.4 (12:00)		62.0 (11:00)	81.0 (21:10)		1018.9 (0:00)	1023.4 (22:00)		4.9 (12:40)	682.0 (11:40)	
08/11/22	13.6 (6:30)	20.4 (14:20)		64.0 (14:10)	83.0 (2:20)		1022.3 (15:10)	1024.0 (9:30)		4.9 (14:40)	585.0 (11:50)	
09/11/22	13.7 (7:20)	20.1 (15:00)		67.0 (15:00)	83.0 (1:30)		1022.2 (14:20)	1023.9 (10:00)		4.9 (13:20)	654.0 (13:00)	
10/11/22	15.7 (1:00)	21.2 (13:10)		63.0 (22:40)	84.0 (4:30)		1022.2 (3:00)	1028.8 (23:50)		6.7 (18:20)	675.0 (11:40)	
11/11/22	16.1 (5:10)	22.1 (13:50)		52.0 (12:30)	76.0 (6:40)		1028.6 (3:20)	1031.1 (10:30)		9.4 (14:30)	520.0 (12:00)	
12/11/22	14.3 (23:50)	18.1 (15:30)		54.0 (9:40)	69.0 (4:00)		1024.0 (23:50)	1030.5 (0:00)		10.7 (10:00)	418.0 (9:40)	
13/11/22	13.2 (6:50)	18.6 (14:00)		53.0 (14:00)	72.0 (19:50)		1021.5 (6:30)	1023.9 (21:10)		7.2 (3:00)	742.0 (12:40)	
14/11/22	14.4 (5:30)	19.2 (14:40)		69.0 (0:00)	84.0 (22:30)		1020.4 (6:10)	1023.0 (0:00)		10.3 (13:20)	745.0 (12:50)	
15/11/22	13.9 (6:40)	18.9 (14:50)		70.0 (14:00)	88.0 (4:00)		1016.0 (23:50)	1022.4 (1:20)		6.3 (11:50)	638.0 (12:10)	
16/11/22	14.9 (9:20)	19.7 (23:40)		77.0 (0:50)	93.0 (10:10)		1004.7 (23:10)	1015.8 (0:00)		11.6 (8:10)	366.0 (14:20)	
17/11/22	16.4 (6:20)	20.8 (12:20)		67.0 (13:30)	91.0 (4:30)		1004.9 (0:00)	1008.1 (18:30)		8.0 (21:30)	717.0 (11:40)	
18/11/22	17.5 (23:00)	22.1 (12:20)		63.0 (20:10)	89.0 (8:20)		1004.1 (13:00)	1009.1 (23:30)		14.3 (14:30)	763.0 (11:00)	
19/11/22	14.6 (7:40)	19.4 (14:50)		66.0 (0:10)	91.0 (9:30)		1004.8 (14:40)	1009.1 (0:00)		16.5 (19:00)	227.0 (13:50)	
20/11/22	13.0 (23:40)	16.9 (0:00)		71.0 (20:00)	87.0 (8:40)		1006.3 (15:30)	1010.1 (23:20)		8.5 (5:40)	216.0 (13:10)	
21/11/22	10.7 (7:00)	17.3 (13:30)		52.0 (11:10)	82.0 (21:40)		1008.4 (23:50)	1014.3 (11:20)		11.6 (23:50)	497.0 (11:30)	
22/11/22	11.0 (22:40)	19.0 (6:30)		64.0 (14:40)	90.0 (1:00)		995.4 (12:50)	1008.1 (0:00)		23.2 (7:30)	332.0 (14:10)	
23/11/22	11.4 (2:50)	17.3 (15:10)		47.0 (11:30)	82.0 (0:00)		1001.8 (0:20)	1010.6 (23:40)		8.5 (11:10)	547.0 (12:20)	
24/11/22	11.1 (5:50)	18.4 (14:30)		63.0 (11:10)	85.0 (20:40)		1010.7 (0:10)	1019.3 (23:40)		4.9 (6:00)	522.0 (12:00)	
25/11/22	11.6 (5:40)	17.1 (13:40)		71.0 (11:50)	89.0 (19:20)		1018.4 (23:40)	1022.4 (9:00)		6.3 (17:20)	591.0 (11:40)	
26/11/22	9.7 (12:10)	13.2 (0:00)		67.0 (21:10)	92.0 (2:50)		1013.7 (5:20)	1020.5 (23:40)		15.6 (20:10)	26.0 (10:40)	
27/11/22	11.2 (23:30)	15.9 (13:10)		50.0 (14:00)	74.0 (0:10)		1020.0 (0:40)	1022.7 (21:20)		14.3 (11:40)	480.0 (11:40)	
28/11/22	9.7 (6:40)	15.9 (13:50)		49.0 (12:20)	73.0 (6:40)		1015.2 (22:40)	1022.5 (0:00)		4.5 (0:00)	476.0 (11:20)	
29/11/22	10.6 (6:30)	16.1 (12:10)	42.0 (12:10)	68.0 (5:10)	1011.0 (22:20)		1015.2 (0:00)	1014.0 (22:40)		7.2 (20:10)	506.0 (11:50)	
30/11/22	11.3 (0:40)	13.9 (13:50)		60.0 (13:40)	70.0 (2:00)		1009.9 (5:30)	1014.0 (22:40)		9.4 (4:10)	179.0 (13:40)	

Pressione - Velocità Vento



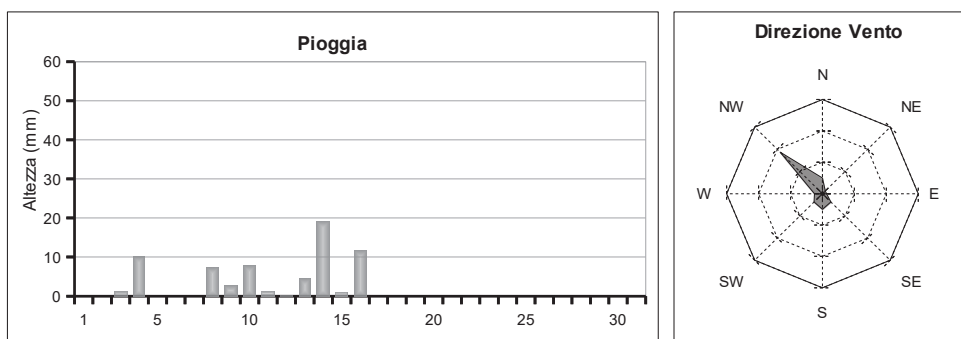
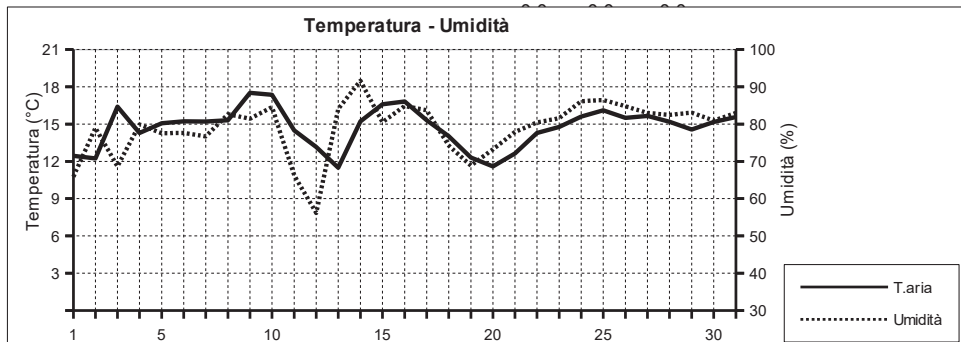
Picchi di Radiazione e di Indice UV



DICEMBRE 2022

(medie giornaliere)

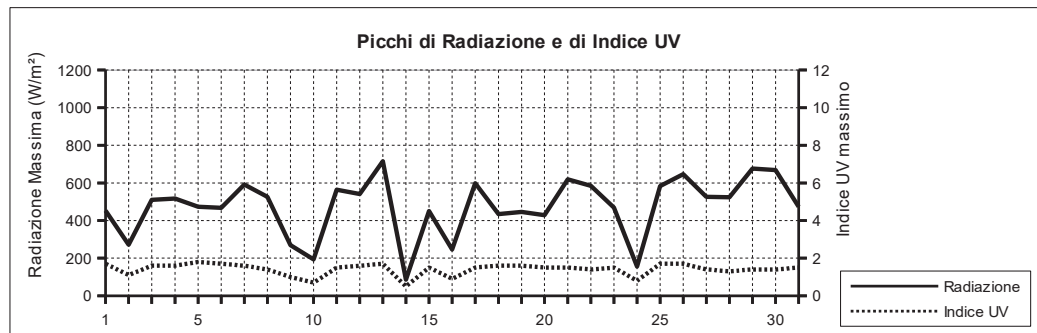
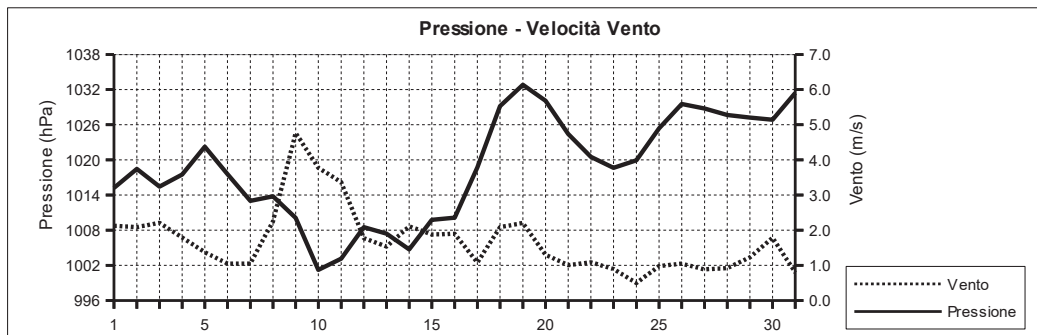
Data	Temperatura °C	Umidità %	Pressione hPa	Vento		Rad. Solare W/m²	Pioggia mm	Indice UV		
				m/s	direzione			medio	max	ora
01/12/22	12.5	65.9	1015.2	2.1	NW	258.6	9:40	0.0	1.3	1.7 (11:30)
02/12/22	12.2	79.0	1018.5	2.1	NW	88.0	9:20	0.0	0.8	1.1 (12:20)
03/12/22	16.4	68.7	1015.5	2.2	SE	154.5	9:10	1.2	1.0	1.6 (10:50)
04/12/22	14.3	79.9	1017.5	1.8	NW	259.6	9:30	10.2	1.3	1.6 (11:20)
05/12/22	15.1	77.5	1022.3	1.4	NW	238.2	9:20	0.0	1.3	1.8 (11:40)
06/12/22	15.2	77.6	1017.6	1.1	NW	234.4	9:20	0.0	1.3	1.7 (12:00)
07/12/22	15.2	76.7	1013.0	1.0	NW	228.6	9:30	0.0	1.3	1.6 (10:50)
08/12/22	15.3	82.6	1013.8	2.3	--	153.2	9:20	7.4	0.9	1.4 (11:00)
09/12/22	17.5	81.5	1010.1	4.8	S	78.9	9:00	2.6	0.8	1.0 (11:20)
10/12/22	17.4	84.5	1001.2	3.8	S	45.6	9:10	8.0	1.0	0.7 (9:50)
11/12/22	14.5	66.3	1003.1	3.4	W	192.1	9:30	1.0	0.9	1.5 (11:30)
12/12/22	13.2	56.2	1008.5	1.8	NW	217.7	9:20	0.2	1.0	1.6 (11:50)
13/12/22	11.5	84.1	1007.4	1.5	N	95.6	8:20	4.6	0.8	1.7 (11:40)
14/12/22	15.2	91.6	1004.7	2.1	SW	24.5	8:10	19.0	0.0	0.5 (13:20)
15/12/22	16.6	80.5	1009.8	1.9	SW	164.7	9:10	0.8	1.0	1.5 (11:50)
16/12/22	16.8	84.9	1010.2	1.9	NW	107.7	9:10	11.6	1.0	0.9 (10:50)
17/12/22	15.3	83.7	1018.7	1.1	NW	188.6	9:20	0.0	0.9	1.5 (11:00)
18/12/22	14.0	74.2	1029.2	2.1	N	253.0	9:20	0.0	1.3	1.6 (11:30)
19/12/22	12.3	68.8	1032.8	2.2	NW	254.6	9:30	0.0	1.3	1.6 (11:30)
20/12/22	11.6	73.2	1030.1	1.3	N	246.0	9:30	0.0	1.1	1.5 (11:30)
21/12/22	12.6	77.9	1024.4	1.0	NW	293.1	9:20	0.0	1.1	1.5 (11:30)
22/12/22	14.3	80.5	1020.5	1.1	SE	111.8	8:40	0.0	0.8	1.4 (11:50)
23/12/22	14.8	81.6	1018.6	0.9	NW	161.4	9:20	0.0	1.0	1.5 (12:10)
24/12/22	15.6	86.1	1019.9	0.5	NW	56.8	9:00	0.0	0.4	0.8 (13:00)
25/12/22	16.1	86.5	1025.4	1.0	--	224.6	9:20	0.0	1.2	1.7 (11:50)
26/12/22	15.5	84.8	1029.5	1.0	--	182.0	9:10	0.0	1.0	1.7 (12:20)
27/12/22	15.7	83.0	1028.8	0.9	--	119.8	9:00	0.0	0.9	1.4 (12:30)
28/12/22	15.2	82.5	1027.7	0.9	NW	183.7	9:20	0.0	0.9	1.3 (12:30)
29/12/22	14.6	83.1	1027.2	1.2	--	234.3	9:20	0.0	0.9	1.4 (12:30)
30/12/22	15.2	81.0	1026.9	1.8	S	175.1	9:10	0.0	0.9	1.4 (11:10)
31/12/22	15.6	83.0	1031.4	0.8	--	192.3	9:30	0.0	0.9	1.5 (12:10)



DICEMBRE 2022

(estremi giornalieri)

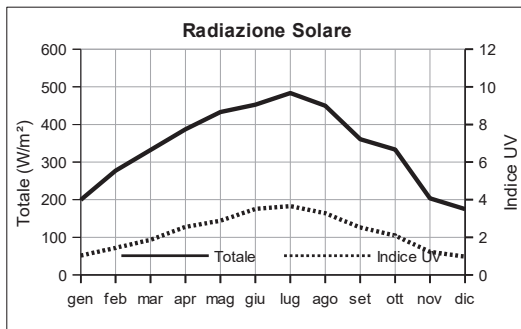
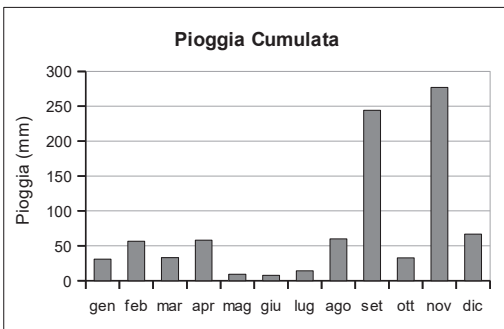
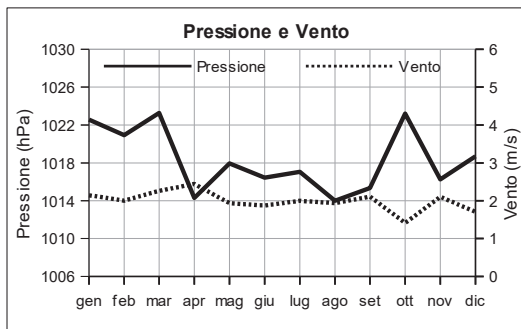
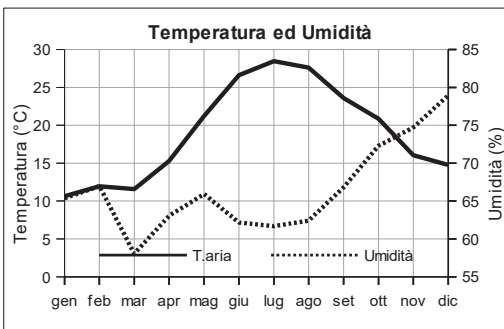
Data	Temperatura (°C)		Umidità (%)		Pressione (hPa)		Vento (m/s) max (ore)	Radiazione (W/m²) max (ore)
	min (ore)	max (ore)	min (ore)	max (ore)	min (ore)	max (ore)		
01/12/22	9.8 (5:30)	17.0 (13:40)	53.0 (12:50)	76.0 (21:40)	1013.4 (4:10)	1018.3 (23:20)	7.2 (8:10)	452.0 (11:50)
02/12/22	11.1 (0:20)	13.4 (12:30)	74.0 (1:50)	85.0 (18:40)	1017.7 (23:10)	1019.3 (10:10)	7.6 (18:20)	272.0 (12:30)
03/12/22	13.4 (5:20)	19.1 (15:20)	58.0 (15:30)	83.0 (5:10)	1012.6 (22:40)	1017.7 (0:00)	11.6 (14:30)	510.0 (10:50)
04/12/22	9.8 (2:00)	18.7 (0:00)	61.0 (0:00)	90.0 (2:10)	1013.1 (0:40)	1021.9 (22:40)	12.5 (0:00)	517.0 (13:20)
05/12/22	12.5 (2:00)	18.2 (11:40)	64.0 (11:10)	85.0 (2:00)	1021.4 (23:50)	1023.9 (10:00)	4.9 (13:20)	473.0 (11:40)
06/12/22	12.8 (4:40)	18.4 (12:00)	65.0 (11:30)	85.0 (1:20)	1014.7 (23:30)	1021.3 (0:00)	4.5 (12:40)	468.0 (11:40)
07/12/22	12.7 (5:30)	19.1 (14:30)	56.0 (14:00)	84.0 (0:00)	1011.8 (14:10)	1014.6 (0:00)	4.5 (15:20)	592.0 (11:00)
08/12/22	12.8 (2:10)	17.2 (13:40)	74.0 (12:20)	91.0 (23:40)	1012.9 (3:40)	1014.9 (9:50)	9.4 (20:00)	526.0 (12:20)
09/12/22	16.2 (0:00)	18.4 (22:30)	72.0 (12:10)	90.0 (0:10)	1007.3 (22:10)	1013.6 (0:00)	14.3 (8:20)	269.0 (9:20)
10/12/22	15.3 (22:40)	18.6 (0:30)	78.0 (4:50)	90.0 (12:40)	997.6 (16:40)	1007.4 (0:00)	13.0 (15:30)	193.0 (9:50)
11/12/22	13.6 (17:00)	15.8 (0:50)	50.0 (19:30)	84.0 (0:10)	998.5 (0:00)	1006.2 (23:30)	12.5 (12:30)	564.0 (12:00)
12/12/22	11.0 (22:20)	15.1 (11:50)	46.0 (11:40)	70.0 (7:40)	1006.0 (3:40)	1011.9 (23:30)	7.6 (13:50)	541.0 (12:20)
13/12/22	8.8 (4:10)	13.7 (12:10)	55.0 (0:00)	92.0 (17:10)	1004.9 (14:10)	1011.8 (0:00)	6.7 (10:30)	715.0 (11:20)
14/12/22	11.4 (0:50)	17.9 (15:10)	86.0 (21:50)	96.0 (11:00)	1001.8 (14:30)	1008.7 (0:00)	12.1 (11:30)	86.0 (13:20)
15/12/22	13.9 (5:40)	19.6 (22:10)	66.0 (19:30)	89.0 (0:00)	1006.6 (0:00)	1013.0 (9:50)	13.4 (22:10)	450.0 (12:00)
16/12/22	14.3 (21:30)	19.3 (0:00)	73.0 (18:40)	89.0 (3:10)	1007.6 (0:00)	1013.1 (23:40)	13.9 (0:30)	246.0 (14:50)
17/12/22	13.4 (5:20)	17.7 (13:40)	69.0 (16:40)	91.0 (8:00)	1013.1 (0:00)	1024.8 (23:40)	5.4 (0:00)	598.0 (11:40)
18/12/22	11.8 (5:10)	17.7 (13:30)	60.0 (14:30)	88.0 (0:30)	1024.7 (0:00)	1033.1 (22:30)	6.7 (19:30)	434.0 (12:10)
19/12/22	10.1 (6:50)	15.7 (13:30)	52.0 (14:10)	78.0 (2:10)	1032.2 (15:50)	1034.2 (9:50)	6.3 (1:40)	446.0 (12:00)
20/12/22	8.7 (5:40)	15.4 (14:30)	62.0 (11:40)	84.0 (22:50)	1027.7 (23:50)	1032.4 (0:00)	4.5 (13:10)	429.0 (11:50)
21/12/22	9.0 (5:00)	15.8 (15:00)	68.0 (14:00)	87.0 (5:00)	1021.7 (23:50)	1027.8 (0:10)	4.9 (13:20)	619.0 (12:40)
22/12/22	12.6 (6:10)	15.5 (11:50)	71.0 (1:00)	89.0 (18:20)	1019.1 (23:50)	1021.7 (0:00)	5.4 (2:40)	585.0 (11:50)
23/12/22	13.2 (6:40)	17.4 (15:30)	64.0 (15:20)	89.0 (4:40)	1017.4 (6:30)	1019.9 (22:30)	5.4 (12:10)	469.0 (12:00)
24/12/22	13.4 (0:20)	16.8 (15:00)	84.0 (1:40)	89.0 (8:30)	1018.4 (4:10)	1022.6 (23:50)	3.1 (13:50)	156.0 (13:00)
25/12/22	14.4 (3:50)	19.2 (14:40)	72.0 (12:20)	91.0 (4:10)	1022.7 (0:00)	1027.9 (23:50)	5.4 (15:00)	584.0 (12:10)
26/12/22	13.5 (2:00)	17.9 (12:40)	77.0 (11:10)	91.0 (2:10)	1028.2 (0:00)	1030.7 (10:10)	4.9 (13:10)	647.0 (12:10)
27/12/22	14.1 (4:00)	17.1 (12:50)	77.0 (10:30)	89.0 (4:10)	1027.6 (14:30)	1029.8 (0:00)	5.4 (15:50)	526.0 (12:30)
28/12/22	13.8 (23:20)	17.8 (14:30)	72.0 (14:30)	88.0 (7:40)	1026.6 (14:20)	1028.8 (0:00)	4.9 (13:30)	524.0 (12:40)
29/12/22	12.6 (6:00)	17.1 (12:50)	75.0 (14:20)	89.0 (1:40)	1026.3 (14:20)	1028.4 (9:10)	5.8 (13:10)	677.0 (12:30)
30/12/22	12.3 (3:40)	17.4 (11:40)	74.0 (11:30)	86.0 (1:30)	1025.7 (5:00)	1029.1 (23:00)	7.6 (17:00)	668.0 (11:40)
31/12/22	c (7:10)	18.5 (13:40)	70.0 (13:20)	91.0 (7:20)	1028.8 (0:10)	1033.9 (23:20)	4.0 (14:00)	473.0 (10:30)



MEDIE MENSILI 2022

Mese	Temperatura °C	Umidità %	Pressione hPa	Vento m/s	direzione	Radiazione Solare W/m²	Indice UV	Pioggia mm
Gennaio	10.6	65.4	1022.6	2.1	NE	199.6	1.0	31.0
Febbraio	11.9	67.0	1020.9	2.0	N	277.0	1.4	56.4
Marzo	11.6	58.0	1023.3	2.3	SW	331.8	1.9	33.0
Aprile	15.3	63.1	1014.3	2.4	SW	387.1	2.6	58.0
Maggio	21.2	65.9	1018.0	1.9	SW	432.9	2.9	9.0
Giugno	26.6	62.2	1016.4	1.9	S	452.6	3.5	7.8
Luglio	28.5	61.7	1017.1	2.0	SW	483.7	3.7	14.0
Agosto	27.6	62.4	1014.0	1.9	SW	449.8	3.3	60.0
Settembre	23.6	66.8	1015.3	2.1	SW	360.8	2.5	244.2
Ottobre	20.8	72.3	1023.2	1.4	--	333.2	2.1	32.6
Novembre	16.1	74.7	1016.3	2.1	N	203.7	1.2	277.0
Dicembre	14.7	78.9	1018.7	1.7	N	174.8	1.0	66.6
Anno	19.0	66.5	1018.3	2.0	SW	340.6	2.3	889.6

Mese	Temperatura (°C) min	Temperatura (°C) max	Umidità (%) min	Umidità (%) max	Pressione (hPa) min	Pressione (hPa) max	Raffiche m/s	Radiazione Massima W/m²	Indice UV
Gennaio	8.1	13.4	51.0	77.5	1019.8	1025.8	9.2	477.1	1.4
Febbraio	9.2	15.1	52.4	81.0	1018.0	1024.0	9.4	668.3	2.4
Marzo	8.4	15.0	43.1	73.0	1021.3	1025.6	9.5	754.7	3.3
Aprile	12.2	18.7	46.1	78.5	1011.9	1016.9	10.2	934.3	5.0
Maggio	18.3	24.8	48.4	81.0	1016.2	1020.1	8.7	940.6	5.4
Giugno	23.6	30.4	44.2	78.1	1015.1	1017.9	8.1	952.9	6.7
Luglio	25.5	32.1	42.6	77.2	1015.8	1018.3	8.5	929.6	6.7
Agosto	24.0	31.3	48.2	76.2	1012.6	1015.4	9.4	923.1	6.0
Settembre	20.5	26.6	51.7	79.6	1013.7	1017.1	10.6	852.5	4.9
Ottobre	17.8	24.3	57.1	83.8	1021.7	1025.0	6.3	646.4	3.4
Novembre	13.5	18.9	62.8	84.0	1013.7	1019.2	9.3	522.3	1.9
Dicembre	12.4	17.3	67.0	87.1	1016.4	1021.4	7.6	474.5	1.4
Anno	16.1	22.3	51.2	79.7	1016.4	1020.5	8.9	756.4	4.1



Riepilogo mensile delle precipitazioni								
Mese	Pioggia Totale mm.	N. Totale giorni con pioggia	N. giorni con pioggia fino ad 1 mm	N. giorni con pioggia da 1.1 a 10 mm	N. giorni con pioggia da 10.1 a 20 mm	N. giorni con pioggia da 20.1, a 40 mm	N. giorni con pioggia da 40.1 a 60 mm	N. giorni con pioggia maggiore di 60 mm
Gennaio	31.0	8	2	5	1	0	0	0
Febbraio	56.4	10	3	6	0	1	0	0
Marzo	33.0	7	1	5	1	0	0	0
Aprile	58.0	9	2	4	3	0	0	0
Maggio	9.0	5	2	3	0	0	0	0
Giugno	7.8	3	1	2	0	0	0	0
Luglio	14.0	1	0	0	1	0	0	0
Agosto	60.0	9	2	5	2	0	0	0
Settembre	244.2	13	1	5	4	2	0	1
Ottobre	32.6	1	0	0	0	1	0	0
Novembre	277.0	12	3	4	1	1	1	2
Dicembre	66.6	11	3	5	3	0	0	0
Totali	889.6	89	20	44	16	5	1	3

Riepilogo mensile delle Tmax					Riepilogo mensile delle Tmin				
Mese	N. giorni con Tmax > 10°C	N. giorni con Tmax > 20°C	N. giorni con Tmax > 30°C	N. giorni con Tmax > 35°C	Mese	N. giorni con Tmin ≤ 15°C	N. giorni con Tmin ≤ 10°C	N. giorni con Tmin ≤ 5°C	N. giorni con Tmin ≤ 0°C
Gennaio	30	0	0	0	Gennaio	31	24	2	0
Febbraio	28	0	0	0	Febbraio	28	19	0	0
Marzo	11	0	0	0	Marzo	31	20	1	0
Aprile	9	10	0	0	Aprile	25	6	0	0
Maggio	31	7	0	0	Maggio	0	0	0	0
Giugno	30	28	0	0	Giugno	0	0	0	0
Luglio	31	31	28	1	Luglio	0	0	0	0
Agosto	22	22	10	1	Agosto	0	0	0	0
Settembre	30	30	1	0	Settembre	0	0	0	0
Ottobre	31	31	0	0	Ottobre	0	0	0	0
Novembre	30	12	0	0	Novembre	23	2	0	0
Dicembre	31	0	0	0	Dicembre	2	0	0	0
Totali	314	171	39	2	Totali	140	71	3	0

ISTRUZIONI E MODELLO

Istruzioni per la realizzazione dei dattiloscritti

Il *Rendiconto* pubblica le comunicazioni fatte dai soci in una delle adunanze ordinarie dell'Accademia. I soci possono presentare anche lavori di altri autori. In questo caso l'accettazione della *Nota* per la pubblicazione è condizionata al parere favorevole di una commissione designata dall'Accademia.

Le Note dovranno essere inviate al segretario per posta elettronica sia in formato doc che pdf. Il file pdf dovrà incorporare tutti i font utilizzati nel documento originario.

La stesura dovrà essere conforme al modello che è riportato di seguito, riprodotto sotto forma di *template* sul sito web dell'Accademia. Non sono ammesse modifiche al modello fornito.

Layout di pagina. Margine superiore: 5,8 - margine inferiore: 4,8 - margine sinistro e margine destro: 4,25.

Spaziatura prima e dopo: 0; interlinea: singola. Sillabazione automatica.

I riferimenti bibliografici sono indicati nel testo tra parentesi (cognome primo autore, anno di pubblicazione). Se gli autori sono due si indicheranno entrambi, se più di due si indicherà il primo autore seguito da "*et al.*". Nella sezione Bibliografia, i riferimenti bibliografici dovranno riportare quanto indicato nei seguenti esempi per periodici e libri:

Cognome A.B., Cognome C.D. [...] e Cognome E.F. (anno) Titolo. Rivista (corsivo). Numero volume (grassetto), numeri pagina iniziale-finale.

Cognome G.H. and Cognome I.L. (anno) Titolo. Casa editrice, città, stato, numeri pagina iniziale-finale.

Le illustrazioni dovranno avere una risoluzione minima di 300 dpi e dimensioni non superiori a mm 125x180 comprensive dell'eventuale didascalia. Le fotografie a mezzi toni e quelle a colori, devono rispondere a criteri di riproducibilità ed essere utilizzate solo se necessarie per la completezza dell'esposizione.

A richiesta, che dovrà essere fatta all'atto della presentazione del dattiloscritto all'Editore, saranno forniti gratuitamente 10 estratti, senza copertina, di ciascuna *Nota*, anche nel caso in cui il numero degli autori dovesse essere superiore a uno. Ulteriori estratti e/o la richiesta di una copertina personalizzata, da presentare contestualmente alla precedente, saranno a carico degli autori. L'Editore inoltrerà agli interessati un preventivo di spesa.

COMPOSIZIONE DEL DATTILOSCRITTO CON WORD

Prima pagina (vedi modello .doc sul sito web dell'Accademia) 7 righi vuoti
Titolo: centrato, Times New Roman (TNR) 13, grassetto. Rigo vuoto.

Autori della nota: centrato, TNR 11. Gli apici numerici per indicare indirizzi e affiliazioni di ciascun autore sono da precisare a fondo pagina. La formula da adottare è: “Nota del socio e di...” oppure “Nota dei soci...” ovvero “Nota di Nome e Cognome (1), Nome e Cognome (2)...”.

Rigo vuoto.

Presentatore: centrato, TNR 10. (“Presentata dal socio...”)

Data adunanza: centrato, in parentesi, TNR 10. La data dell'adunanza va posta direttamente sotto gli autori, ovvero sotto il presentatore, senza lasciare spazi.

Due righi vuoti.

Keywords: in inglese, TNR 10. Rigo vuoto.

Abstract: in inglese, TNR 10. Rigo vuoto.

Riassunto: in italiano, TNR 10. Due righi vuoti.

1 - INTRODUZIONE, TNR 10, grassetto maiuscolo Rigo vuoto.

Testo, TNR 11, giustificato, indentatura paragrafi 6 mm Rigo vuoto.

Altri titoli (tutti numerati in sequenza), TNR 10, grassetto maiuscolo Rigo vuoto.

Altro testo, TNR 11, giustificato, indentatura paragrafi 6 mm Rigo vuoto.

RINGRAZIAMENTI, TNR 10. grassetto maiuscolo Rigo vuoto.

Testo, TNR 10, giustificato, indentatura paragrafi 6 mm Rigo vuoto.

BIBLIOGRAFIA, TNR 10, grassetto maiuscolo

Testo della bibliografia, TNR 10. Primo rigo intero, secondo ed altri: indentatura 6 mm

COMPOSIZIONE DEL DATILOSCRITTO CON LaTeX

1) È possibile richiedere al segretario dell'Accademia una copia dei file di stile *rendicontocls* e *rendiconto.bst* che possono essere utilizzati per formattare il testo secondo il modello richiesto dalla rivista.

Per quanto riguarda i riferimenti bibliografici, si può procedere in due modi:

- a) Se si usa BiB-TeX, è possibile creare un documento *nomefile.bib* nel quale i dati di ogni pubblicazione da inserire compaiono nella forma

```
@article{ref_name,  
    AUTHOR = {Nome1, M. and Nome2, T. and Nome3 I.},  
    TITLE = {TITOLO},  
    JOURNAL = {RIVISTA},  
    VOLUME = {VOLUME},  
    YEAR = {ANNO},  
    NUMBER = {FASCICOLO},  
    PAGES = {47--70}}
```

L'applicazione BiB-TeX genera un file *nomefile.bbl* nel quale i dati della pubblicazione da inserire compaiono nella forma

```
\bibitem[Nome1 et~al.(anno)Nome2, Nome3]{ref_name}  
Nome M., Nome2 T. and Nome3 I. (1992) TITOLO.  
\newblock \emph{RIVISTA}  
\newblock \textbf{13}\penalty0 (fascicolo), \penalty0 47--70.
```

- b) Se non si usa BiB-TeX, è possibile creare direttamente il documento *nomefile.bbl* nella forma descritta sopra, avendo cura di scrivere tra parentesi quadre (dopo il comando \bibitem) la stringa degli autori esattamente come apparirà nel testo, secondo le istruzioni generali previste nei vari casi in cui ci sono 1, 2 o più autori, e, eventualmente, usando una lettera dopo l'anno in modo da evitare ambiguità.

2) Se si preferisce non utilizzare i file di stile, è possibile utilizzare le seguenti istruzioni:

```
\documentclass[a4paper, 14pt, oneside, openright]{article}  
\usepackage{geometry}
```

```

\usepackage[latin1]{inputenc}
\usepackage[italian,english]{babel}
\usepackage{amsmath, amsfonts, amsthm}
\usepackage{paralist, times, indentfirst}
\usepackage[T1]{fontenc}
\usepackage{amsthm}
\usepackage{mathptmx}

\geometry{a4paper}

\setcounter{secnumdepth}{0}

\newtheorem{prop}{Proposition}
\newtheorem{lem}{Lemma}
\newtheorem{thm}{Theorem}
\newtheorem{theorem}{Theorem}
\newtheorem{cor}{Corollary}
\newtheorem{obs}{Observation}
\newtheorem{exa}{Example}
\newtheorem{defn}{Definition}
\theoremstyle{remark}
\newtheorem{rem}{Notation}
\newenvironment{sistema}%
{\left\{ \begin{array}{l}{} \end{array} \right.}%
{\end{array} \right\} %}

\linespread{1.00}

\title{titolo}
\textwidth = 12.4 cm
\textheight = 19.5 cm
\topmargin = 2 cm
\oddsidemargin = 2 cm

\begin{document}

\vspace*{20 mm}

\pagestyle{empty}

\begin{center}
\selectfont \textbf{13}{14}


```

```

{Titolo}\\"}

\bigskip

\fontsize{12}{11}\selectfont

Nota di Autore \footnote{\fontsize{10}{10}\selectfont Dipartimento di ..., Universit\`a di ..., Via ... , cap, Citt\`a, Nazione. e-mail: ...@...}\\"

\vspace{11pt}

{\fontsize{10}{10}\selectfont Presentata dal socio ... \linebreak (Adunanza del ...)}
\end{center}

\vspace{11pt}

\fontsize{10}{10}\selectfont \noindent \emph{Key words:} Qui bisogna mettere le parole chiave\\"

\fontsize{10}{11}\selectfont \noindent
\textbf{Abstract -- }
qui bisogna mettere il riassunto in inglese\\"

\fontsize{10}{11}\selectfont \noindent
\textbf{Riassunto -- }
e qui il riassunto in italiano

\vspace{11pt}

\section{\fontsize{10}{12}\selectfont \bf 1 - INTRODUCTION}
{\fontsize{11}{12}\selectfont

\section{\fontsize{10}{10}\selectfont \bf2- }

\fontsize{11}{12}\selectfont

\section{\fontsize{10}{10}\selectfont \bf3 - REFERENCES}

\noindent Il primo rigo di ciascuna referenza non deve rientrare, gli altri s\'i.

```

```
{\fontsize{10}{11}\selectfont  
\noindent  
\noindent  
\end{document}}
```

SEGUE MODELLO DI TESTO

Titolo della nota

Nota del socio Nomea Cognomea¹ e di Nomeb Cognomeb² (Adunanza del 21 mese 2100)

Keywords: word1, word2, word3, word4.

1 - INTRODUZIONE

Questa è l'introduzione questa è l'introduzione. Qui si introduce un riferimento alla bibliografia (Hnome *et al.*, 2000). L'introduzione continua l'introduzione continua l'introduzione continua l'introduzione continua l'introduzione continua l'introduzione. Qui c'è un richiamo a una figura (Fig. 1).

¹ Accademia di Scienze Fisiche e Matematiche della Società Nazionale di Scienze, Lettere e Arti in Napoli, via Mezzocannone 8, 80134 Napoli.

² Istituzione di appartenenza.

Qui troviamo un altro riferimento alla bibliografia (Tnome *et al.*, 2012). L'introduzione continua l'introduzione continua l'introduzione continua l'introduzione continua l'introduzione.



Figura 1 Questa è la figura 1, per la quale è stata scelta, come esempio, una fotografia a colori. La didascalia continua la didascalia continua la didascalia continua la didascalia continua. Qui finisce.

Ora l'introduzione finisce ora l'introduzione finisce.

2 – PARAGRAFO DUE

Questo è il paragrafo due questo è il paragrafo due questo è il paragrafo due questo è il paragrafo due questo è il paragrafo due questo è il paragrafo due questo è il paragrafo due questo è il paragrafo due questo è il paragrafo due questo è il paragrafo due questo è il paragrafo due.

Questo è ancora il paragrafo due questo è il paragrafo due e qui c'è un richiamo alla bibliografia (Pnome *et al.*, 1992).

Il paragrafo due continua ancora e ora troviamo il richiamo alla figura due (Fig. 2). Questo è ancora il paragrafo due questo è il paragrafo due. Questo è ancora il paragrafo due questo è il paragrafo due questo è il paragrafo due questo è il paragrafo due questo

è il paragrafo due. Questo è ancora il paragrafo due questo è il paragrafo due questo è il paragrafo due.

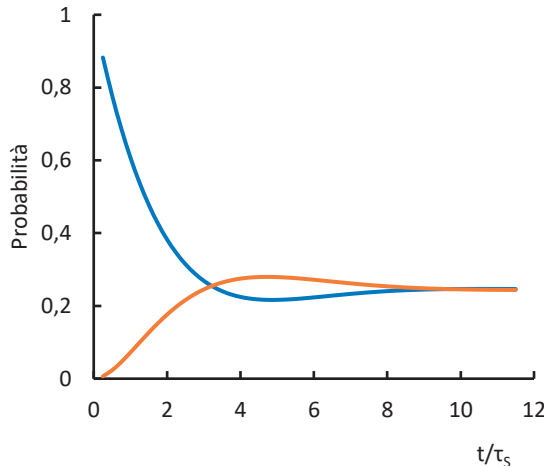


Figura 2 Questa è la figura 2. La didascalia continua la didascalia continua la didascalia continua la didascalia continua. Qui finisce.

Il paragrafo due continua ancora e, qui, abbiamo un ulteriore richiamo alla bibliografia (Anome, 2006).

In questo paragrafo c'è anche un richiamo ad una tabella (Tab. 1)

Tabella 1 Primi zeri delle funzioni sferiche di Bessel di ordine più basso (valori approssimati alla seconda cifra decimale).

Z_{nl}				
l	n=1	n=2	n=3	n=4
0	3,14	6,28	9,42	12,57
1	4,49	7,73	10,90	14,07
2	5,76	9,10	12,32	15,51
3	6,99	10,42	13,70	16,92
4	8,18	11,70	15,04	18,30
5	9,36	12,97	16,35	19,65
6	10,51	14,21	17,65	20,98

ancora continua ancora continua ancora continua ancora continua continua ancora continua ancora continua ancora continua ancora continua ancora.

Il paragrafo due continua ancora e poi finisce e poi finisce.

3 – PARAGRAFO TRE

Questo è il paragrafo tre questo è il paragrafo tre.

4 – CONCLUSIONI

Qui si traggono le conclusioni, conclusioni, conclusioni, conclusioni, conclusioni, conclusioni, conclusioni, conclusioni, conclusioni, conclusioni.

RINGRAZIAMENTI

Qui, prima di passare alla bibliografia, si ringrazia chi si vuole per quanto ha fatto si ringrazia chi si vuole per quanto ha fatto si ringrazia chi si vuole per quanto ha fatto.

BIBLIOGRAFIA

Anome D. J. (2006). Titolo del lavoro titolo del lavoro titolo del lavoro titolo del lavoro titolo del lavoro. *Nome della rivista*. **11**, 306-14.

Hnome M., Nome2 T., Nome3 I., Nome4 H. e Nome5 C.A. (2000). Title of the paper title of the paper. *Name of the journal*. **21**, 327-30.

Pnome W., Nome6 M., Nome7 K., Nome8 H., Nome9 K. e Nome10 M. (1992). Titolo del lavoro titolo del lavoro titolo del lavoro. *Altra rivista*. **1121**, 130-6.

Tnome W., Nome11 H., Nome12 M. e Nome13 M. (2012). Title of the paper title of the paper. *Name of the journal*. **182**, 97-105

**Comitato di Redazione del Rendiconto
dell'Accademia delle Scienze Fisiche e Matematiche**

Scienze Biologiche: F. Angelini, E. Boncinelli, G. D'Alessio, J.M. Denucé, A. Di Donato, G. Geraci, A. Giuditta, M. Iaccarino, G. La Mantia, M. Lorito, M. Moracci, C. Polito, R.K. Rastogi, C. Rigano, M. Rossi, C. Saccone, G. Sannia, A. Virzo De Santo

Scienze Chimiche: V. Balzani, S. Califano, D. Caputo, C. Colella, R. Lanzetta, G. Marino, G. Marrucci, L. Mayol, L. Mazzarella, L. Nicolais, L. Paduano, A. Panunzi, C. Pedone, O. Schettino, V. Vitagliano

Scienze Fisiche: F. Ambrosino, M. Capaccioli, A. Coniglio, G. Franceschetti, G. Marmo, L. Marrucci, L. Merola, M. Napolitano, M. Rigutti, M.V. Sazhin, G. Scarpetta, G. Sedmak, V. Silvestrini, S. Solimeno

Scienze Geomineralogiche: L. Brancaccio, R. Catalano, G. Dal Piaz, B. D'Argenio, P. De Castro, G. Luongo, A. Mottana, A. Rapolla, L. Simon

Scienze Matematiche: A. Alvino, A. Avantaggiati, A. Basile, H. Brezis, S. Buoncristiano, A. Canfora, L. Carbone, C. Ciliberto, A. Corbo Esposito, E. Cosenza, V. Coti Zelati, F. De Giovanni, P. De Lucia, V. Ferone, A. Fiorenza, R. Fiorenza, N. Fusco, R. Grassini, M.G. Graziano, L. Greco, T. Iwaniec, P.L. Lions, G. Manfredi, F. Mazzocca, A. Mercaldo, A. Murli, A. Romano, G. Romano, T. Ruggeri, R. Russo, C. Sbordone, B. Straughan, G. Talenti, M. Troisi, C. Trombetti, G. Trombetti, J.D.M. Wright

ISSN: 0370-3568

